UNIVERSITÀ DEGLI STUDI DI TORINO

University of Turin

DIPARTIMENTO DI SCIENZE DELLA TERRA

Department of Earth Sciences

PHD PROGRAMME IN EARTH SCIENCES

XXXV CYCLE

TECTONO-STRATIGRAPHIC SETTING AND METAMORPHIC EVOLUTION OF LIGURIAN-PIEDMONT UNITS IN THE UPPER SUSA AND CHISONE VALLEYS (WESTERN ALPS)

Phd student: **ALBERTO CORNO**

Supervisors: Prof. Marco GATTIGLIO[1]
Dott. Pietro MOSCA[2]
Prof. Alessandro BORGHI[1]
Prof. Chiara GROPPO[1]

PhD Programme Co-ordinator: Prof. Francesco DELA PIERRE

1 Department of Earth Sciences, University of Torino, Via Valperga Caluso 35, 10125 Turin, Italy

2 Geosciences and Earth Resources - National Research Council of Italy, Via Valperga Caluso 35, 10125 Turin, Italy

Academic years of enrolment

2019-2023

Code of scientific discipline **GEO-03**

PhD defense 31st January 2023

The research reported in this Thesis was carried out at:

Dipartimento di Scienze della Terra - University of Turin

Via Valperga Caluso 35,

10125 Torino

Italy

Financial support was provided by the Ministero dell'Università e della Ricerca Scientifica e Tecnologica (M.I.U.R.).

Reading committee:

Prof. Gianreto MANATSCHAL (Università di Strasburgo, France)

Prof. Paola TARTAROTTI (Università degli Studi di Milano)

Prof. Andrea FESTA (Dipartimento di Scienze della Terra, Università di Torino)

Cover photo: the upper Susa valley seen from the summit of M. Chaberton.

CONTENTS

CHAPTER 5
The oceanic succession of the BRU

CHAPTER 6
The continental succession of the BRU

CHAPTER 7
The Albergian unit

CHAPTER 8
The lawsonite-bearing rocks and tectono-metamorphic evolution of the Albergian unit

First of all, I'd like to thank my tutors.

Marco Gattiglio for the opportunity of this PhD project: he took me as a naïve Master student and brought me up to this PhD.

Alessandro Borghi is thanked for his omnipresent participation, for the endless hours at the SEM and his always joyful and enthusiastic approach.

I'm partly sorry to have "obliged" Chiara to take part in this PhD project, but without her I probably would have done only half the things I achieved in these 3 years. I sincerely appreciated her kind guidance in the treacherous paths of thermodynamics, much more difficult than the steep slopes of the Monte Banchetta.

My most heartfelt thanks go to Pietro, with whom I shared joys and pains of this PhD, he has been a true guide for these 3 years. I'm indebted to him for his continuous support and constructive guidance, the 5 a.m. e-mails, the luxurious lunches at the Prof. Bonetto's house and the devastating revisions, always brought forward with extreme kindness and respect. Grazie davvero.

Special thanks go to Gianreto Manatschal and Paola Tartarotti, whose Christmas holidays were spoiled by reading this Thesis. I hope they found it appealing and interesting, on the other hand I surely benefited from their comments. Also Andrea Festa is acknowledged for the acceptance to be Internal Member of the PhD defense and for various insightful discussions over the years.

I wish to thank all the professors that trained me as a student and have let me something, not only under a professional but also under a personal point of view.

Domenico Rosselli of the Parco Naturale Val Troncea is acknowledged for his support in some of the field activities.

The waste of time during this PhD project is the fault of the "Gang del Bosco", to which I'm truthfully grateful: my "roommate" Ale for his useful suggestions and the immortal coffee machine, and Maffo, for his help throughout the PhD and the most exquisite *salamelle*; a special thanks to Davidino, my "acquired" brother who's unfortunately always right and with whom I shared a lot.

I'd like to thank Marco Giovo for the numerous "weekly breaks" during this PhD, our climbs through the Western Alps permitted me to visit so many places and discover some beautiful mountains.

To my Family, mamma, papa, Tetè: you know I'm not a chatterer, I don't need to say anything. You've always been there for me, I just hope I can return the favor.

I wish to thank my Fra, who's entered my life with the impetus of a wolf on a prey and has taken care of me with love and kindness of an otter.

Abstract

The Alps are a collisional belt, developed after the closure of the Ligurian-Piedmont ocean, opened in Jurassic times between the Adriatic and European continental paleo-margins. The challenge of this PhD Thesis is to provide new data to constrain the lithostratigraphic setting and metamorphic evolution of four tectonic units from the Ligurian-Piedmont zone, exposed in the upper Susa and Chisone valleys (Western Alps). With the intent to constrain their relative pre-collisional position in the Alpine Tethys and their Alpine tectono-metamorphic evolution, the investigated units are: the Banchetta-Rognosa tectonic unit, the Albergian unit, the Lago Nero unit and the Chenaillet ophiolite.

To achieve this aim, this PhD project was based on a multidisciplinary approach including field investigations, petrographic observations, mineral chemistry analysis, and thermodynamic modeling.

The lithostratigraphic study of the Banchetta-Rognosa tectonic unit, made of both continental and oceanic successions, allowed proposing for it a pre-collisional position at the ocean-continent transition zone (Chapters 4 and 5). Thermodynamic modeling on this unit constrained peak P-T Alpine conditions at 20-23 kbar and 440-500 °C, implying that the Banchetta-Rognosa unit could represent one of the westernmost eclogitic units of the Alps (Chapter 6).

The Albergian and Lago Nero units consist of thick meta-sedimentary sequences embedding different (meta-)mafic bodies of the Alpine Tethys. Based on lithostratigraphic constraints, the Albergian unit sampled a sector resting in the hanging-wall of an oceanic core complex (Chapter 7). Thermodynamic modeling performed on this unit, tectonically embedding the Banchetta-Rognosa unit, constrained peak P-T conditions at 18-20 kbar and 380-420 °C (Chapter 8). Conversely, the Lago Nero unit has been restored close to an active spreading ridge, relatively closer to the continental margin than the Albergian unit and characterized by a very complex and articulate paleo-topography (Chapter 9). Conventional thermobarometry on this unit indicated peak P-T conditions higher than 17 kbar and lower than 450 °C.

Thermodynamic modeling provided new and surprising results on the Alpine evolution of the Chenaillet ophiolite. This unit is a full section of the Ligurian-Piedmont oceanic lithosphere, spectacularly preserving primary contacts between oceanic mantle and both mafic instrusives and basalts. Intra-oceanic, HT metamorphism and ductile deformation are also well recorded. Literature data proposed for this ophiolite a very weak Alpine overprint. Differently, the isochemical phase diagram approach used in this PhD constrained the Alpine event for this unit at $P > 9$ kbar and T ranging between 300 °C and 400 °C. These P-T conditions suggest that also the Chenaillet ophiolite may have been involved in subduction-related processes (Chapter 10).

Riassunto

Le Alpi sono una catena collisionale sviluppatasi dopo la chiusura dell'oceano Ligure-Piemontese, apertosi nel Giurassico e interposto tra i paleo-margini Europeo e Adriatico. L'obiettivo di questa Tesi di Dottorato è di fornire nuovi dati per caratterizzare l'assetto litostratigrafico e l'evoluzione metamorfica di quattro unità tettoniche della Zona Ligure-Piemontese, affioranti nelle alte valli Susa e Chisone (Alpi Occidentali). Con l'intento di vincolare la posizione pre-collisionale di queste unità all'interno della Tetide Alpina e la loro evoluzione metamorfica, le unità investigate sono: Unità tettonica Banchetta-Rognosa, Unità dell'Albergian, Unità del Lago Nero e ofiolite dello Chenaillet.

Per perseguire questi obiettivi, questo progetto di Dottorato si è basato su di un approccio multidisciplinare che ha incluso l'attività di terreno, osservazioni petrografiche, analisi della *mineral chemistry* e modellizzazione termodinamica.

Lo studio litostratigrafico dell'Unità tettonica Banchetta-Rognosa, costituita da una successione continentale e una oceanica, ha permesso di proporre per questa Unità una posizione paleo-geografica nella zona di transizione oceano-continente (Capitoli 4 e 5). La modellizzazione termodinamica su questa Unità ha vincolato le condizioni P-T di picco Alpino a 20-23 kbar e 440-500 °C, suggerendo che l'Unità Banchetta-Rognosa possa rappresentare una delle unità eclogitiche più a Ovest delle Alpi Occidentali (Capitolo 6).

Le unità Albergian e Lago Nero sono costituite da potenti sequenze meta-sedimentarie, che includono differenti corpi (meta-)mafici della Tetide Alpina. Sulla base di vincoli litostratigrafici, si può supporre che l'Unità Albergian abbia campionato una porzione del blocco di tetto di un *core complex* oceanico (Capitolo 7). La modellizzazione termodinamica effettuata su questa Unità, che avvolge tettonicamente l'Unità Banchetta-Rognosa, vincola delle condizioni P-T di 18-20 kbar e 380-420 °C (Capitolo 8). L'Unità Lago Nero è stata invece ricollocata in una zona di dorsale attiva, relativamente più vicina al margine continentale rispetto all'Unità Albergian e caratterizzata da una paleo-topografia complessa e articolata (Capitolo 9). La termobarometria convenzionale su questa Unità ha indicato pressioni maggiori di 17 kbar e temperature minori di 450 °C.

Per quanto riguarda l'ofiolite dello Chenaillet, la modellizzazione termodinamica ha fornito nuovi e sorprendenti dati sulla sua evoluzione Alpina. Questa unità campiona una sezione completa dell'Oceano Ligure-Piemontese e preserva in modo spettacolare i rapporti tra mantello oceanico, intrusivi mafici e basalti. Sono ben preservati anche il metamorfismo intra-oceanico di alta temperatura e la deformazione duttile, ad esso associata. I dati di letteratura propongono per questa unità un sovra-impronta Alpina molto debole. Al contrario, la modellizzazione basata su diagrammi di fase isochimici, utilizzata nell'ambito di questo Dottorato, indica per questa Unità pressioni maggiori di 9 kbar e temperature comprese tra 300 °C e 400 °C. Queste condizioni P-T suggeriscono che anche l'ofiolite dello Chenaillet sia stata quindi coinvolta in processi legati alla subduzione (Capitolo 10).

This dissertation is submitted for the degree of Doctor of Philosophy at the Università di Torino. The manuscript is an original contribution by the Author, except where references are made to previous studies. This work has been carried out during the 2019-2022 period. Part of this work has been presented in already published papers (listed below) and congress presentations.

- Corno, A., Borghi, A., Gattiglio, M., & Mosca*, P. (2019). Lithostratigraphy and petrography of the Monte Banchetta-Punta Rognosa oceanic succession (Troncea and Chisonetto Valleys, Western Alps). Ofioliti, 44, 83-95. https://doi.org/10.4454/ofioliti.v44i2.526
- Corno*, A., Mosca, P., Borghi, A., & Gattiglio, M. (2021a). Geology of the Monte Banchetta–Punta Rognosa area (Troncea valley, Western Alps). Journal of Maps, 17(2), 150-160. https://doi.org/10.1080/17445647.2021.1894996
- Corno*, A., Groppo, C., Mosca, P., Borghi, A., & Gattiglio, M. (2021b). Eclogitic metamorphism in the Alpine far-west: petrological constraints on the Banchetta-Rognosa tectonic unit (Val Troncea, Western Alps). Swiss Journal of Geosciences, 114(1), 1-20. https://doi.org/10.1186/s00015-021-00393-7
- Fioraso, G., Mosca, P., Corno, A., Bonadeo, L., Brunamonte, F., Baggio, P., Raco, B., Doveri M., Lelli, M., & Giacometti, F. (2021). Note Illustrative della Carta Geologica d'Italia alla scala 1:50.000. Foglio 171, Cesana Torinese. https://www.isprambiente.gov.it/Media/carg/note_illustrative/171_Cesana_Torinese.pdf
- Corno*, A., Mosca, P., Groppo, C., Borghi, A., & Gattiglio, M. (2022). More widespread than supposed: preserved lawsonite in the blueschist-facies ophiolitic bodies from the Albergian unit (Liguria-Piemonte zone, Western Alps). Ofioliti, 47(2), 137-154. https://doi.org/10.4454/ofioliti.v47i2.556
- Barale*, L., Console, F., Corno, A., Frasca, G., Mosca, P., & Pantaloni, M. (2022). The geology of the Western Alps through the field notebooks of Secondo Franchi (1859-1932). Italian Journal of Geosciences, 141(1), 120-143. https://doi.org/10.3301/IJG.2022.05
- Gambino*, F., Agostoni, A., Barale, L., Bonetto, S., Borghi, A., Corno, A., & Mosca, P. (2022, in press). Il Verde Cesana: una storica pietra ornamentale delle Alpi Occidentali. In: Bove, A., Masciocco, L., & Sassone, P. (in press) Geologia Ambientale in Piemonte e Valle d'Aosta.
- Guide Geologiche Regionali – Piemonte, dalle Alpi Graie alle Alpi Liguri, dal Monferrato alle Langhe (final editing). A cura di CNR-IGG and DST-UNITO. Contributions to the following sections: Itinerario 3 - La Valle di Susa: una sezione completa del settore assiale delle Alpi Occidentali. Itinerario 4 - Val Chisone e Val Germanasca, dalla pianura pinerolese al colle del Sestriere.

- Corno*, A., Groppo, C., Mosca, P., Borghi, A., & Gattiglio, M. (under review). To be or not to be Alpine: constraints on the metamorphism of the Chenaillet ophiolite (Western Alps). Submitted to the Journal of Metamorphic Geology.
- Corno, A. & Mosca*, P. New lithostratigraphic insights on the "boring" units of the Calcescisti con Pietre Verdi zone in the Western Alps (External Ligurian-Piedmont Zone, upper Susa and Chisone valleys). In preparation for Geosystems and Geoenvironment.

CHAPTER 1

Introduction

1.1. Aims

The aim of this PhD Thesis is to investigate several units of the Ligurian-Piedmont Zone in the upper Susa and Chisone valleys (Western Alps; Figure 1 and Figure 2), with the challenge to provide new data useful to constrain the location of these units within the pre-collisional paleogeographic setting as well as their Alpine tectono-metamorphic evolution.

A multidisciplinary approach was paramount to unravel the tectono-stratigraphic and tectono-metamorphic evolution of four studied units in the Axial sector of the Alpine belt.

This project was hence based on combined field survey, petrographic observations and thermodynamic modeling. Field investigations were carried out in order to study the stratigraphic relationships and the present-day juxtaposition among different rock bodies. Petrographic observations (combined with mineral chemistry analyses) were carried out in order to define the blastesis/deformation relationships and constrain tectono-metamorphic events in the different tectonic units, correlating mesoscale and microscale data. Thermodynamic modeling allowed to reconstruct the P-T paths followed by each unit during the Alpine metamorphic evolution.

The overall intent of this PhD project was to propose a reconstruction of the tectono-metamorphic evolution of the axial sector of the Alpine chain in the Cottian Alps, considering the new lithostratigraphic and metamorphic data. The hope is to lead to a better interpretation of the geological features and geometric relationships of four tectonic units, to unravel their syn-rift tectonic history and their following Alpine evolution.

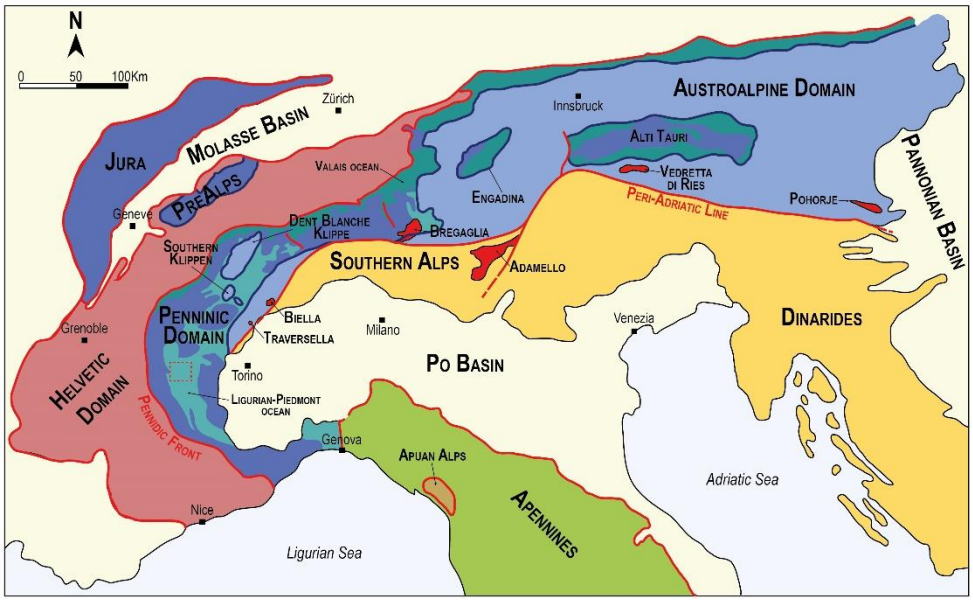

Figure 1 Simplified tectonic map of Northern Italy (redrawn from Schmid et al., 2004 and Dal Piaz, 2003). Red dashed polygon for the studied area.

1.2. Outlines of the Thesis

This Thesis is organized into 11 different chapters. Chapters from 4 to 10 present the results reported in manuscripts submitted/accepted by ISI Journals. Below, it is provided a summary of the main subject of each chapter.

Chapter 1 is the present general introduction to the aims and objectives of this research. In addition, it provides a description of the present-day morphology of the investigated area.

Chapter 2 provides the major traits of the geological setting of the Western Alps, from Alpine belt- to unit-scale. Scope of the chapter is to provide the basic knowledge on the subjects dealt with in this Thesis, for further debated questions and discussion.

Chapter 3 describes the methodologies used in this Thesis.

Chapter 4 focuses on the lithostratigraphic and structural setting of the Banchetta-Rognosa teconic unit, with particular emphasis on the Mesozoic evolution of the unit and the geometric relationships between the two occurring successions.

Chapter 5 focuses on the oceanic succession of the Banchetta-Rognosa tectonic unit, taking into account its lithostratigraphic, structural and petrographic features.

Chapter 6 focuses on the continental succession of the Banchetta-Rognosa unit, reporting its lithostratigraphy and petrographic features. Moreover, in this chapter the isochemical phase diagram approach is used to constrain the Alpine metamorphic peak recorded by this unit.

Chapter 7 presents the lithostratigraphic features of the Albergian unit, with particular focus on its Mesozoic evolution.

Chapter 8 presents the petrographic and petrological features of the Albergian unit, with particular focus on widespread (fresh) lawsonite occurrence in the meta-mafic rocks of this unit.

Chapter 9 introduces the lithostratigraphic features of the Lago Nero unit, taken into account the variations among the different outcrops and their implications on the Mesozoic evolution of this unit.

Chapter 10 focuses on the petrographic and petrological features of gabbro and albitite from the Chenaillet ophiolite, with particular emphasis on the difference between oceanic HT- and Alpine metamorphism, constraining its peak conditions.

Chapter 11 discusses the lithostratigraphic and tectono-metamorphic evolution of this sector of the Western Alps, based on the inferred considerations and achieved results in this Thesis.

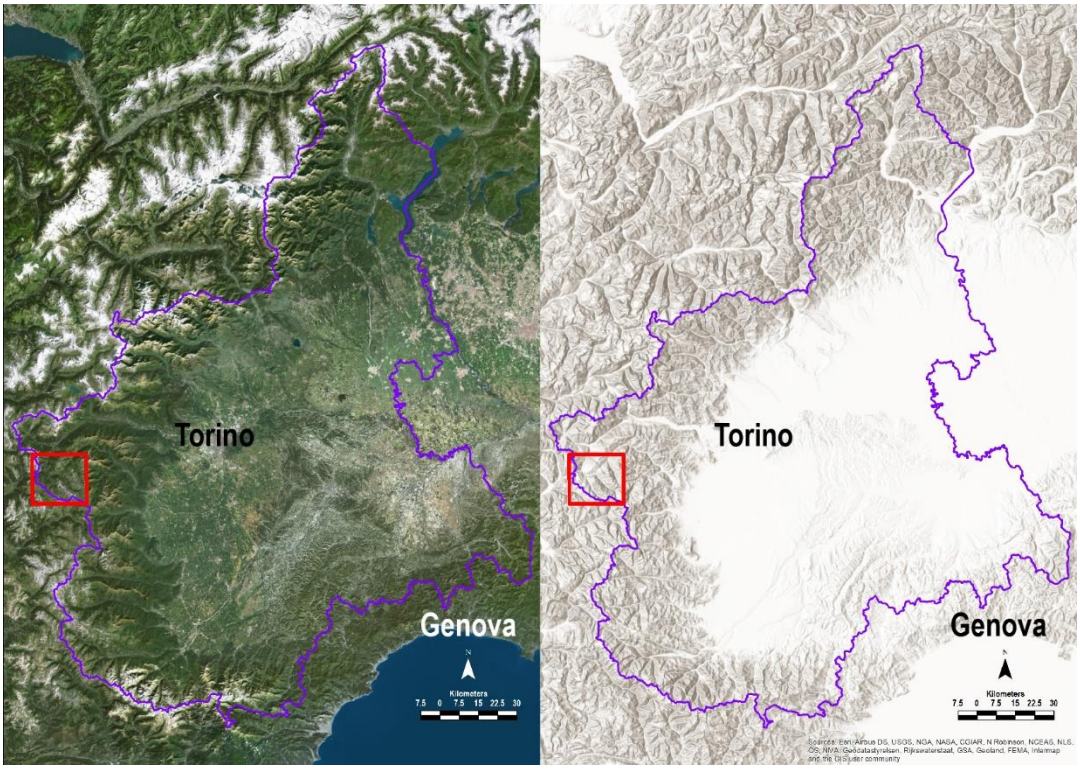

Figure 2 Position of the studied area in the Western Alps, close to the Italian-French border.

1.3. Geographic setting

The area investigated for this PhD thesis is located in the Western Alps, along the Italian and French border (Figure 2). More in detail, the area of interest is located in the central Cottian Alps, comprising the upper Susa valley and the upper Chisone valley (Figure 3). The area is located in the drainage basin of the Dora Riparia river (in the territory of the Cesana Torinese and Claviere villages, and partially around the Montgenèvre pass) and of the Chisone river (in territory of the Pragelato and Sestriere villages). The area taken into account comprises the Troncea (prosecution of the Chisone valley), Argentera (to the South with respect to the village of Sestriere), and Thuras (to the South with respect to the village of Cesana Torinese) secondary valleys.

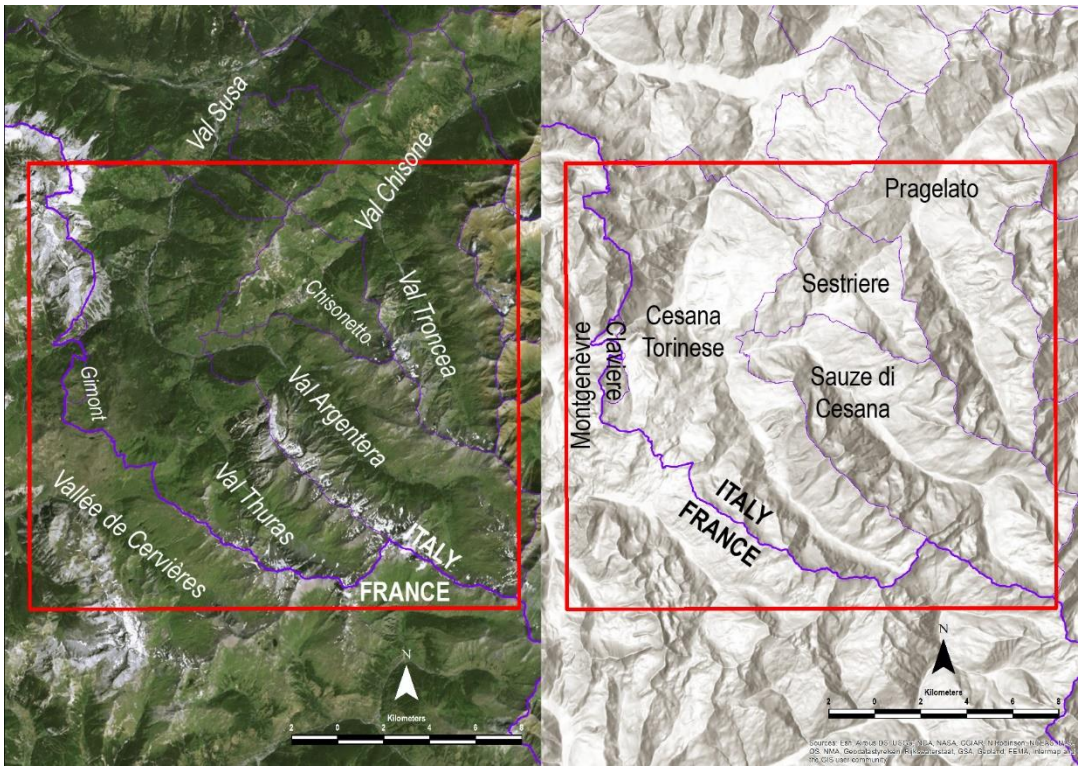

Figure 3 Main valleys and villages in the studied area, in the upper Susa and Chisone valleys.

This area (Figure 4) ranges between valley floors at around 1300-1500 m a.s.l. up to mountain tops at around 3200-3300 m a.s.l. The highest mountains are distributed on the drainage divides: M. Albergian (3041 m a.s.l.), Bric Ghinivert (3037 m a.s.l.), M. Barifreddo (3028 m a.s.l.), and P. Rognosa (3280 m a.s.l.) are located on the Susa-Chisone watershed, while M. Furgon (2816 m a.s.l.), Gran Roc (3121 m a.s.l.), Roc de Boucher (3285 m a.s.l.), P. Ciatagnera (3294 m a.s.l.), P. Ramiere (3303 m a.s.l.) are located on the secondary Argentera-Thuras watershed. Also M. Dormillouse (2908 m a.s.l.), P. Terra Nera (3100 m a.s.l.), M. Merciantaira (3293 m a.s.l.) and

again P. Ramiere are located on the watershed between Thuras valley (Italy) and Cervières valley (France). The sector comprised on the watershed between Italy and France South of the Montgenèvre pass is known as "monts de la lune". It is characterized by a gentle morphology from which the sharpest peaks (such as the M. Gimont, 2648 m a.s.l., and Le Chenaillet, 2650 m a.s.l.) stand out.

In this sector of the Western Alps, two important Alpine pass occur: the Montgenèvre pass (connecting the Susa and the Briançon valleys), and the Sestriere pass (connecting the Susa and Chisone valleys).

The main valleys (i.e. upper Susa and Chisone valleys) display a general NE-SW direction, while the secondary valleys display NNW-SSE directions. The main valleys display complex morphologies, while the secondary valleys display steep slopes and mountainsides on the hydrographic left and more gentle slopes on the hydrographic right. The ensemble of these characteristics reflects the regional litho-structural setting at a local scale, and has been strongly influenced by recent tectonics in this portion of the Alps.

The landform of the studied area is influenced by:

i) Occurrence of very hard lithologies (i.e. dolostone, meta-basalt, meta-gabbro etc.; Figure 5a), which give birth to high walls and steep slopes alternating with less steep slopes made of softer lithologies (i.e. calcschist);
ii) Pleistocene glacialism, responsible for noticeable glacial shaping of the valleys, and formation of moraines and kame terraces. In the studied area glaciers are extinct but where still present locally at the end of the '70s. However, Holocene rock glaciers are still widespread on the northern slopes of the highest peaks (e.g P. Rognosa, M. Barifreddo, Bric Ghinivert, Roc de Boucher, P. Ramiere, etc.; Figure 5b)

The high grade of erosion in several sectors witnesses the erosional deepening in the main valleys, directed NE-SW, which controls the trend of the watersheds.

Wide sectors of flat valley floors (e.g. Cesana T.se and Pragelato plains) allow significant sedimentation by major rivers, where were also tributary and secondary valleys converge. Landslides and especially deep-seated gravitational slope deformations are widespread in the investigated area involving large portions of the valley sides characterized by convex shapes and counter slopes (Figure 5c, Figure 6).

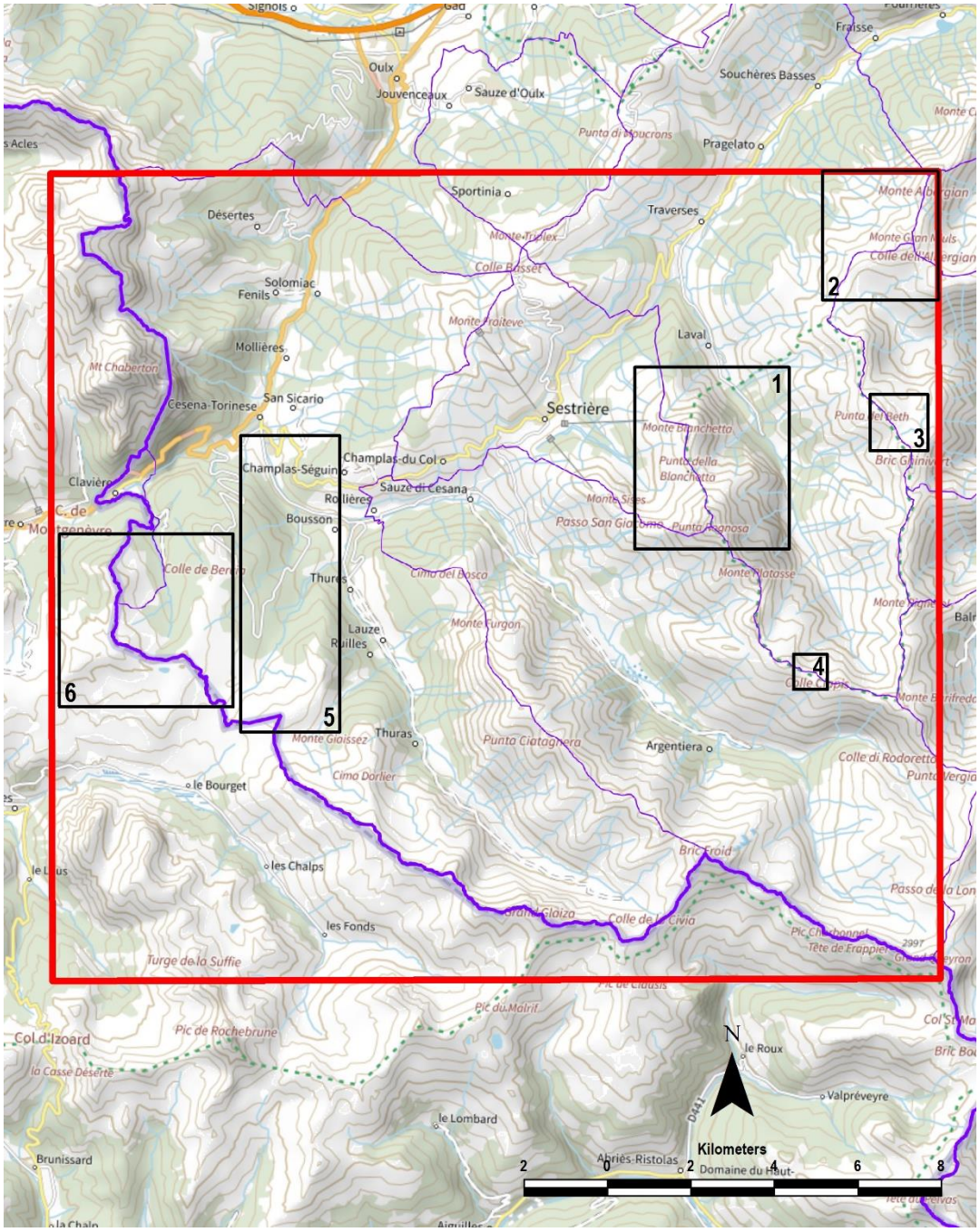

Figure 4 Detail on the upper Susa and Chisone valleys, black polygons show the locations of the areas cited in the text. 1: M. Banchetta - P. Rognosa area, 2: M. Albergian – M. Gran Mioul mountain ridge, 3: Colle del Beth – Bric Ghinivert area, 4: Col Clapis area, 5: Lago Nero area, 6: Chenaillet area.

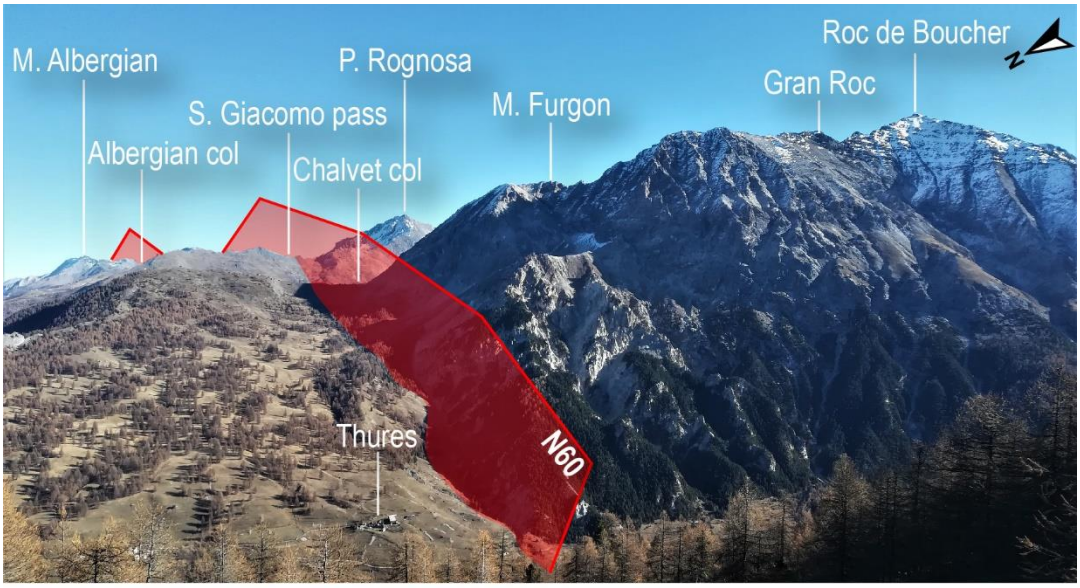
M. Albergian
P. Rognosa
Roc de Boucher
Gran Roc
M. Furgon
S. Giacomo pass
Albergian col
Chalvet col
Thures
N60

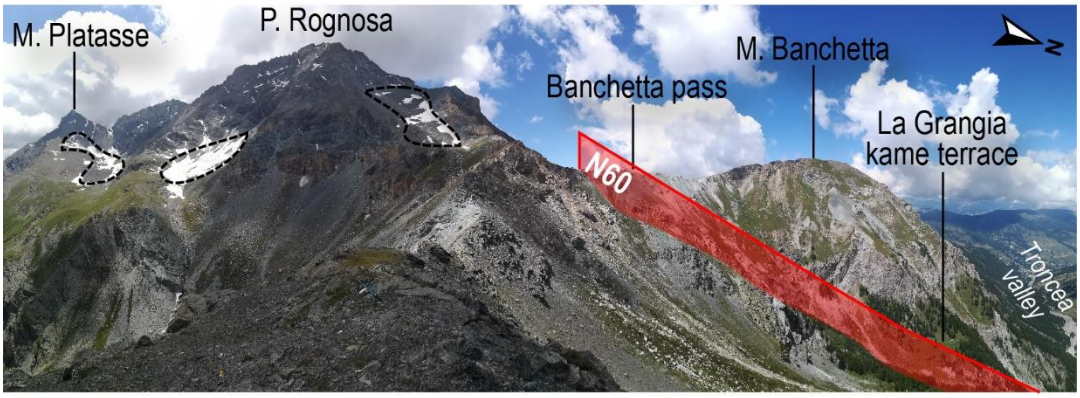
M. Platasse
P. Rognosa
M. Banchetta
Banchetta pass
La Grangia
kame terrace
N60
Troncea
valley

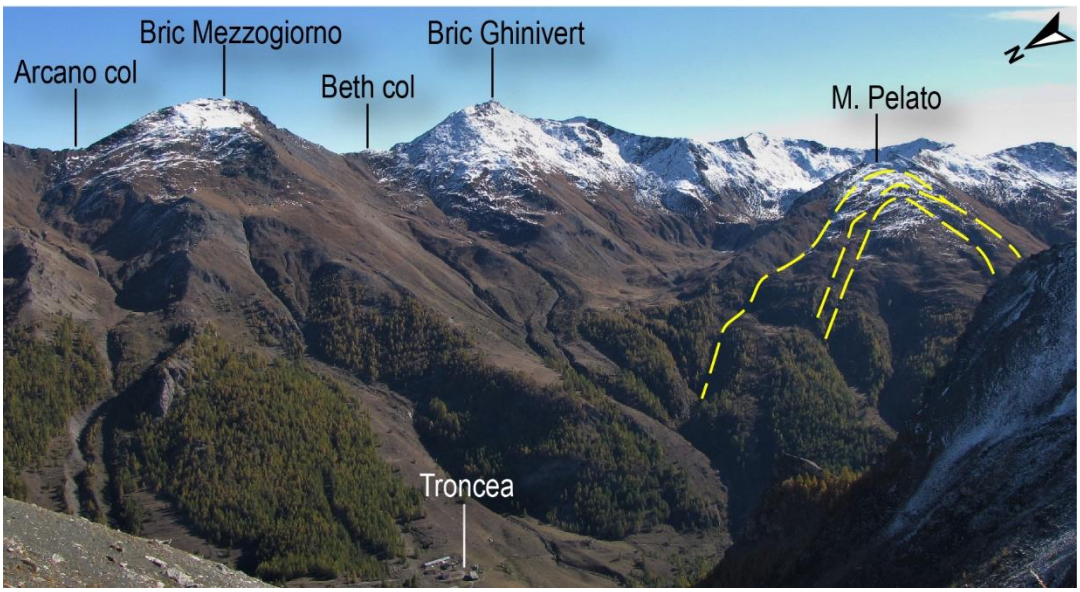
Bric Mezzogiorno
Bric Ghinivert
Arcano col
Beth col
M. Pelato
Troncea

Figure 5 (previous page) Landscape pictures of the studied areas. a. Upper Susa valley, South of the Cesana T.se village. Dolostone of the Gran Roc pre-piedmont unit, which give birth to high walls and steep slopes, are separated to the more gentle slopes made of calcschist from N60 trending faults ; b. Left side of the Troncea valley. Widespread rock glaciers occur on the upper slopes of the P. Rognosa di Sestriere. N60 trending faults are the dominant brittle feature in the area; c. Right side of the Troncea valley, characterized by calcschist of the Ligurian-Piedmont zone affected by widespread deep-seated gravitational slope deformation.

Figure 6 (next page) Landscape picture from the Begino Col (Lago Nero area, above the village of Cesana T.se). The Chenaillet ophiolite on the Italian side crops out as gentle slopes, wooded up to 2100m. On the background, the external portions of the Alpine belt is visible, from the Briançonnais domain up to the Pelvoux External Crystalline Massif.

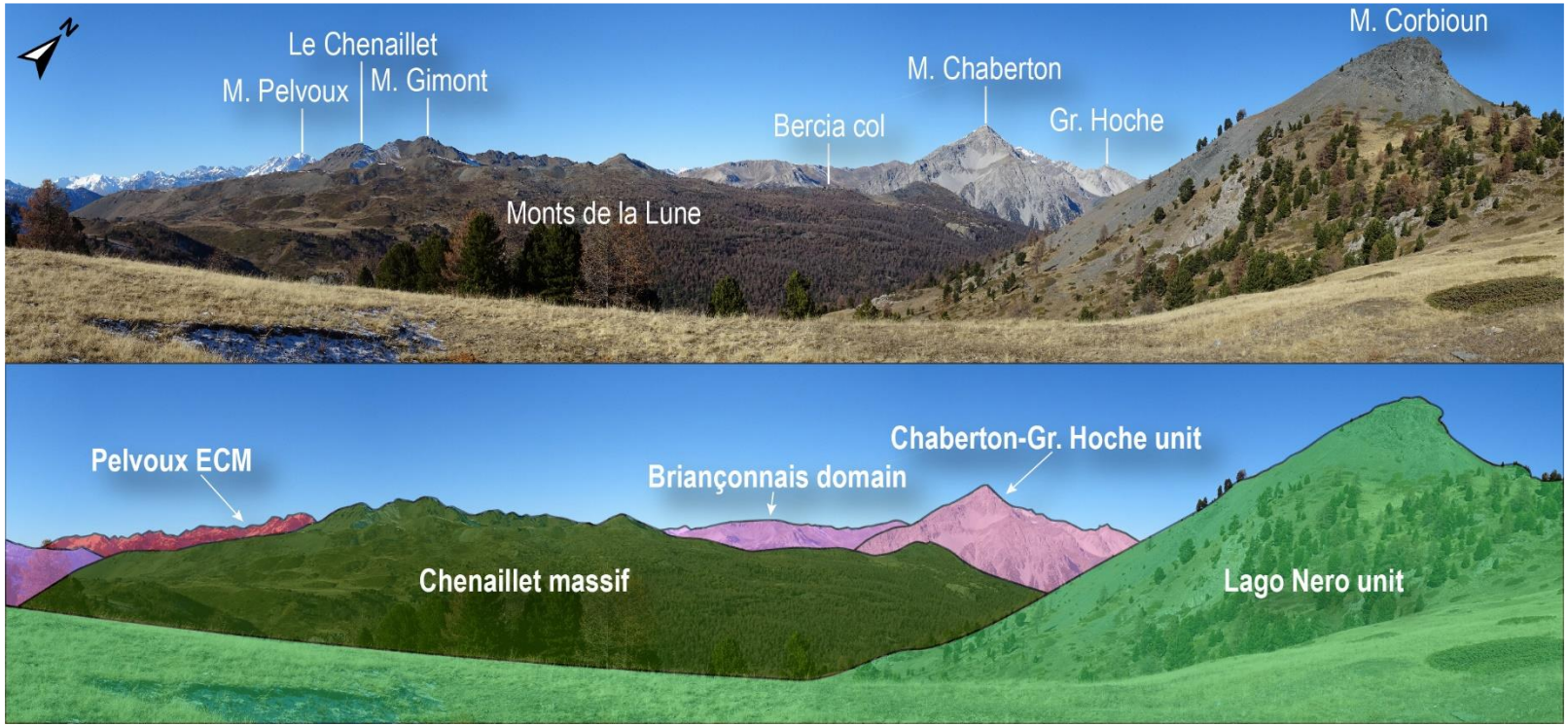
N
Le Chenaillet
M. Pelvoux
M. Gimont
Monts de la Lune
Bercia col
M. Chaberton
Gr. Hoche
M. Corbioun
Pelvoux ECM
Briançonnais domain
Chaberton-Gr. Hoche unit
Chenaillet massif
Lago Nero unit

CHAPTER 2

Geological setting of the Alps

2.1. The Alps

The Alps are the typical example of collisional belt, formed after the closure of the Ligurian-Piedmont Ocean (i.e. Alpine Tethys; Elter, 1971; Lemoine, 1971; Dal Piaz, 1974), interposed during the Mesozoic between the Adriatic and European paleo-margins (See Dal Piaz et al., 2003 for a review). A first stage of convergence was followed by the subduction of oceanic lithosphere and lower European plate underneath the upper Adriatic plate by Cretaceous times (see Dal Piaz, 2010 for a review; Figure 7). Complete closure of the ocean in Eocene times marked the onset of consequent collision of the two paleo-margins in Oligocene (see Dal Piaz, 2010 for a review). Hence, nowadays the Alpine accretionary wedge is characterized by double vergence and the occurrence of oceanic-related rocks (i.e. ophiolites) tectonically juxtaposed to successions belonging to the continental paleo-margins. In the Alpine belt, four different tectonic domains have been distinguished, each ones referring to different pre-collisional paleogeographic sectors: the Southern Alps, the Austroalpine, the Penninic and the Helvetic-Dauphinois domains. In the present setting of the Alps, these domains are juxtaposed by tectonic contacts.

Hereunder, the major features of these 4 domains will be described from the inner to the outer part of the chain (Figure 8).

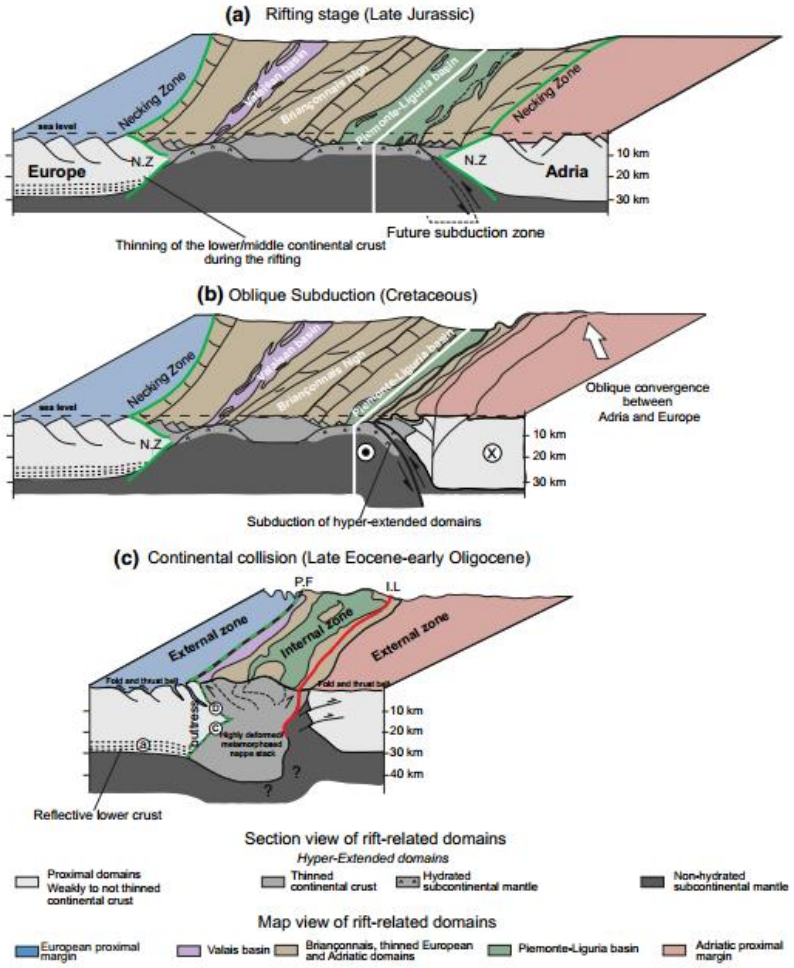

Figure 7 Conceptual model from Mohn et al. (2014) illustrating the role of Mesozoic rifting in the architecture of the Alps. (a) Rifting stage, (b) Subduction stage, (c) Continental collision stage. It is important to note that subduction of the Piemonte-Liguria basin, which probably consisted of hyper-extended rifted margins bounded by transform faults, took place within a setting characterized by highly oblique convergence (Beltrando et al., 2010).

Figure 8 (next page) General structural map of the Alpine belt from Agard (2021). a. General map showing the four Alpine domains (after Handy and Oberhänsli, 2004; Schmid et al., 2004). The two branches of the Alpine 'ocean', the Valais and Ligurian-Piedmont domains, are outlined in light and dark blue respectively. b) Highly schematic cross-section (along A-A'; after Agard & Lemoine, 2005) illustrating the structural organization of the major paleogeographic domains recognized in the belt, from the Adria units on top to the European units below. The sub-division into Western, Central and Eastern Alps corresponds to that adopted in the Thesis. Abbreviations: AM: Argentera-Mercantour; AG: Aar-Gotthard; BO: Belledonne-Oisans; DM: Dora Maira; GP: Gran Paradiso; MB: Mont Blanc; MR: Monte Rosa. c) Cartoon showing the simplified geodynamic subduction setting of the Alps, with emphasis on subduction interface processes. The respective location of the Valais and Ligurian-Piedmont oceans can be readily deduced from the structural relationships between the European, Penninic and Austro/Southalpine domains.

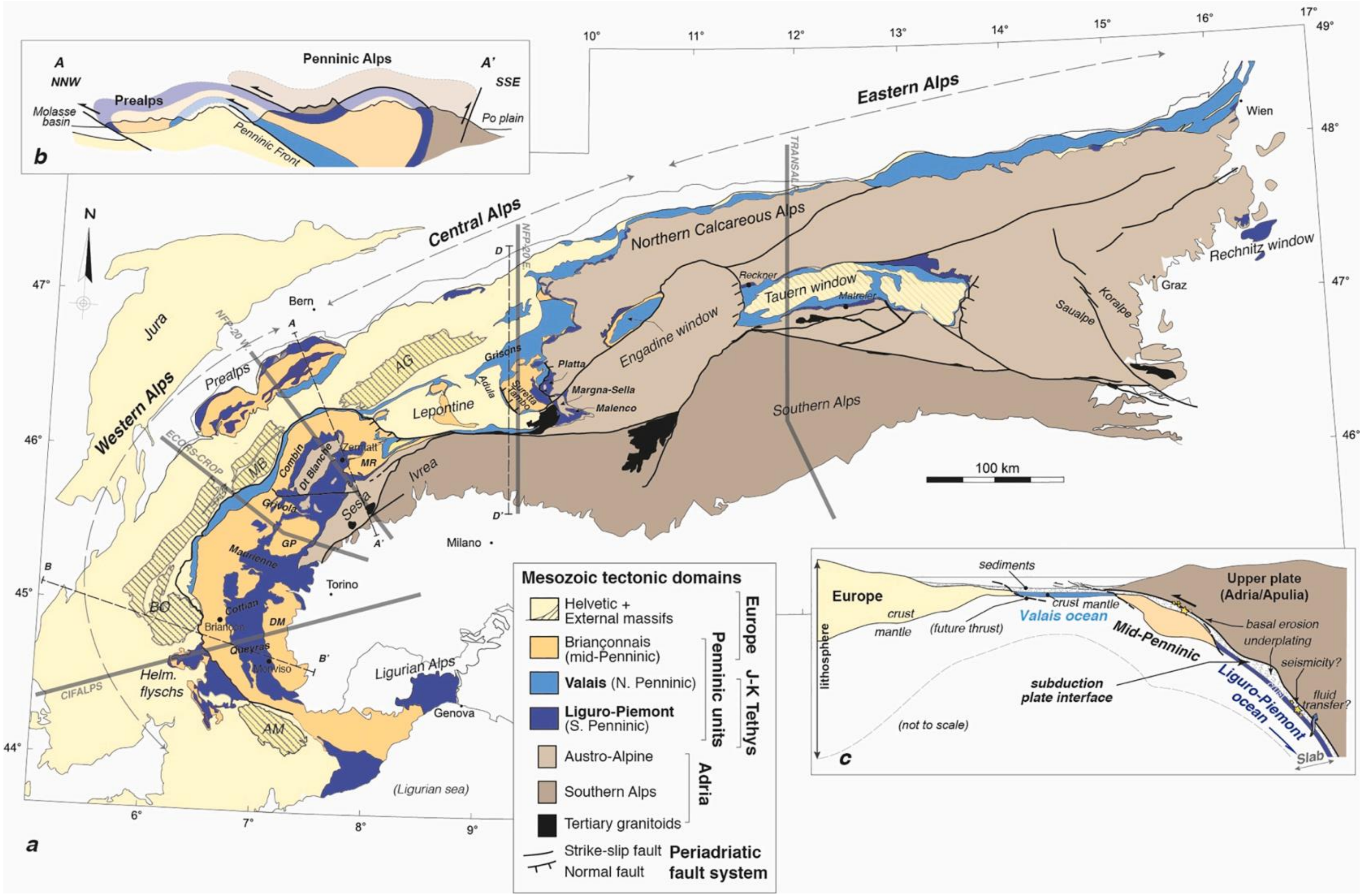
Penninic Alps
A
A'
NNW
SSE
Prealps
Molasse basin
Penninic Front
Po plain
b
Eastern Alps
Central Alps
Western Alps
Jura
Prealps
Bern
NFP-20 W.
NFP-20 E.
TRANSALP
ECORS-CROP
CIFALPS
AG
MB
BO
AM
GP
DM
MR
Lepontine
Grisons
Adula
Suretta
Tambo
Platta
Margna-Sella
Malenco
Engadine window
Northern Calcareous Alps
Reckner
Tauern window
Matreier
Southern Alps
Sausalpe
Koralpe
Graz
Wien
Rechnitz window
Combin
Dt Blanche
Zermatt
Grivola
Sesia
Ivrea
Maurienne
Cottian
Briançon
Queyras
Monviso
Helm. flyschs
Torino
Milano
Genova
Ligurian Alps
(Ligurian sea)
100 km
D
D'
B
B'
N
a
Mesozoic tectonic domains
Helvetic + External massifs
Briançonnais (mid-Penninic)
Valais (N. Penninic)
Liguro-Piemont (S. Penninic)
Austro-Alpine
Southern Alps
Tertiary granitoids
Strike-slip fault
Normal fault
Periadriatic fault system
Europe
Penninic units
J-K Tethys
Adria
Europe
crust
mantle
lithosphere
sediments
(future thrust)
crust mantle
Valais ocean
Mid-Penninic
subduction plate interface
Upper plate (Adria/Apulia)
basal erosion
underplating
seismicity?
fluid transfer?
Liguro-Piemont ocean
Slab
(not to scale)
c

Southern Alps domain

This domain is made of units belonging to the Adriatic paleo-margin, devoid of Alpine metamorphic overprint. It identifies a fold and thrust belt with a main vergence to the South, outcropping from the Biella region in Italy to Slovenia (e.g. Castellarin et al., 1992; Castellarin et al., 2006). This South-verging thrust system involves also Cenozoic sediments of the Po plain and tends to interfere with north-verging "appeninic" thrust system (e.g. Pieri & Groppi, 1981; Castellarin & Vai, 1986; Castellarin et al., 1992; Castellarin, 2001; Mosca et al., 2010). To the North, the Periadriatic Seam (or Insubric Line; Schmid et al., 2004) divides the Southern Alps domains to the others domain of the Alpine belt, variously involved in the Alpine tectono-metamorphic evolution. The Periadtriatic Seam is a system of faults (with different local names, e.g. Canavese Line, Insubric Line etc.) cropping out for more than 700 km from the Eastern to the Western Alps (e.g. Schimd et al., 1989; Dal Piaz et al., 2003), whose western prosecution is hidden beneath the Cenozoic sediments of the western Po plain (Castellarin & Vai, 1986; Mosca et al., 2010).

From a paleogeographic point of view, the Southern Alps domain represents a portion of the Adriatic paleo-margin, from its proximal to distal sectors. In the Western Alps, this domain can be further subdivided in two sectors (Mohn et al., 2012): i) the Laghi Series and the Ivrea-Verbano zone, bordered by the Periadriatic Seam and ii) the Canavese zone, comprised between the Periadriatic Seam and the Internal Canavese Line.

The Laghi Series and the Ivrea-Verbano zone comprise mono- and polymetamorphic metasedimentary rocks (variscan and pre-variscan metamorphism), scattered bodies of mantle peridotite, various mafic and felsic intrusions (generally Permian in age), and a Permian-Cretaceous cover made of volcanic rocks and minor carbonate rocks (Rivalenti et al., 1984; Boriani et a., 1990; Quick et al., 1995; Berra et al., 2009). These units have been interpreted as a portion of lower to upper crust, now overturned in vertical position with polarity to the NW.

On the other hand, the Canavese zone is made of variscan basement, intrusive and effusive Permian rocks, bodies of serpentinized mantle and a Mesozoic sedimentary cover. This Mesozoic cover is very similar to the one occurring in oceanic-derived units. Hence, the Canavese zone (representing the Adriatic hyper-extended margin) has been ascribed to an OCT (ocean-continent transition), with very weak Alpine metamorphism (Ferrando et al., 2004; Festa et al., 2020; Balestro et al., 2022).

Austroalpine domain

The Austroalpine domain represents a portion of the Adriatic paleo-margin, variously involved in the Alpine tectono-metamorphic evolution. In the Western Alps, this domain includes the Sesia Zone and the Dent Blanche system (e.g.

Compagnoni, 1977; Ridley, 1989; Dal Piaz, 2010; Manzotti et al., 2014). The Sesia zone comprises different portion of continental basement subdivided in: i) the Dioritic-Kinzigitic complex (with no Alpine metamorphism; e.g. Babist et al., 2006), ii) the Gneiss Minuti complex (with peak blueschist-facies Alpine metamorphism; e.g. Inger et al., 1996), and iii) the Micascisti Eclogitici complex (with peak eclogite-facies Alpine metamorphism; e.g. Compagnoni et al., 2014). These complexes are made of mono- and polymetamorphic metasedimentary rocks, various intrusive rocks (both mafic and felsic, and Permian in age) and scattered permo-mesozoic cover rocks (Regis et al., 2016). During the Oligocene, the Sesia Zone has been involved in the periadriatic magmatic event, which was responsible for the emplacement of small intrusive bodies along the Periadriatic Seam (e.g. Bigioggero et al., 1994; Zanoni, 2010; Berger et al., 2012).

The Dent Blanche system is made of polymetamorphic basement rocks, with post-variscan felsic intrusive rocks and scattered permo-mesozoic cover rocks. The Dent Blanche system has been subdivided on the base of the peak Alpine metamorphism in upper and lower units (Manzotti et al., 2014a; Manzotti et al., 20114b; Manzotti et al., 2018). Upper units display a weak to medium peak Alpine metamorphism, from greenschist- to blueschist-facies conditions (Manzotti et al., 2011; Manzotti et al., 2020); they crop out to the North of the Aosta-Ranzola fault and they are tectonically juxtaposed above the blueschist-facies units of the Piedmont Zone (see next paragraph). The lower units, on the other hand, display eclogite-facies peak metamorphism and crop out to the South with respect to the Aosta-Ranzola fault (Roda & Zucali, 2008; Ballevre et al., 2014). Preserving rare eclogite relicts, these unis tectonically rest above the eclogite-facies units of the Piedmont Zone (see next paragraph).

Penninic domain

The Penninic domain (more exhaustively investigated in the next Chapter) includes oceanic- and continental-derived units, i.e. from the Ligurian-Piedmont and the Valais oceans, and from the European paleo-margin respectively. The domain is subdivided into Upper, Middle and Lower nappes (e.g. Dal Piaz 2003, 2010 and references therein).

The Upper nappes comprise various oceanic-derived units from the Ligurian-Piedmont ocean (i.e. Alpine Tethys) and the three main Internal Crystalline Massifs (ICM hereafter, i.e. Dora-Maira, Gran Paradiso, and Monte Rosa). For these latter, the paleogeographic pertinence (European or Adriatic) is still strongly debated (see Agard & Handy, 2021, for a review). In their general features, the ICM are made of mono- and polymetamorphic basement rocks, Permian meta-intrusive rocks and minor Mesozoic cover rocks. The ICM record eclogite-facies conditions during the

Alpine metamorphic peak, with local UHP conditions in the southern Dora-Maira massif (e.g. Chopin, 1984).

The Piedmont Zone (detailed in the following section 2.2.4) consists of units made of ophiolites and their own sedimentary cover spanning from Jurassic to Cretaceous. These units, at the scale of the Alpine orogen, are subdivided in eclogite-facies units (Internal Piedmont Zone or Zermatt-Saas zone *Auct.*) and blueschist-facies units (External Piedmont Zone or Combin zone *Auct.*).

Locally and historically, sub-greenschist-facies conditions have been referred to the oceanic Chenaillet unit (e.g. Manatschal et al., 2011).

The Middle nappes comprise the Grand St Bernard-Briançonnais nappe system, consisting of European continental basement and its Mesozoic cover. The original paleogeographic position of this nappe system is still debated: according to some authors, it represents a spur of the European passive margin (Lemoine et al., 1986) while others relate it to a micro-continent/allochthonous terrane separated from the mainland of the European paleo-margin (Stampfli, 1993; Bertrand et al., 2000). The main units made of mono- and polymetamorphic basement rocks crop out in the Aosta valley and in the various small "massifs" of the Ligurian Alps in Italy, in the Ambin massif and the *écailles intermédiaires* across the Italian-French border, the Vanoise region in France, and in the Valais region in Switzerland. The Meso-Cenozoic cover units (generally described as Briançonnais s.s.) have been historically subdivided based on their assumed paleogeographic position: from near the Dauphinois domain (the sub-briançonnais units) to the distal part of the European paleomargin (pre-Piedmont units). The Alpine metamorphic peak recorded in the Middle nappe ranges from eclogite-blueschist-facies conditions to greenschist-facies and anchizone metamorphism.

The Lower nappes, cropping out in the Ossola-Ticino tectonic window and made of continental crust, represent the deepest element of the Alpine belt. These nappes are known as "Lepontine thermal dome" due to the extensive Alpine metamorphic requilibration at amphibolitic conditions (Dal Piaz & Gosso, 1984; Engi & Berger, 2003; Augenstein, 2012).

Helvetic-dauphinois domain

From a paleogeographic point of view, the Helvetic-Dauphinois domain represents the proximal European paleo-margin, made of Variscan continental crust cropping out in the five External Crystalline Massif (Aar-Gothard, Aiguilles Rouge-Mont Blanc, Belledonne, Pelvoux, Argentera-Mercantour). The domain is bounded to the NW by the Helvetic basal thrust, and to the SE by the Penninic thrust front. It is made of polymetamorphic (related to the Ordovician subduction cycle and the Variscan collision) and mono-metamorphic basement rocks (only related to the Variscan

collision), and Carbo-Permian intrusive rocks (Dal Piaz et al., 2003; Dal Piaz, 2010 and references therein). These basement rocks are unconformably covered by a thick sedimentary sequence, from the Late Carboniferous detrital and volcaniclastic successions up to a thick sequence of Meso-Cenozoic succession, characterized by asymmetric fault-bounded rift basins. The Helvetic-Dauphinois domain experienced only the last Alpine metamorphic events related to crustal deformation under sub-greenschist facies conditions (i.e. kilometer-scale folds; Egli & Mancktelow, 2013), followed by transpressive shearing especially in the Meso-Cenozoic cover (d'Atri et al., 2016).

2.2. The Alpine Frontal Wedge

Based on geophysical investigations (Roure et al., 1990, 1996; Pfiffner et al., 1997), the Western Alps can be subdivided in three sectors: i) the inner part of the chain, the Adriatic paleo-margin representing the upper plate of the collisional system, made of the Southern Alps domain with internal vergence; ii) the outer part of the chain, the European paleo-margin representing the lower plate, made of the Helvetic-Dauphinois with external vergence; iii) the axial sector, delimited by the Periadriatic Seam and the Frontal Penninic thrust, where units from the oceanic lithosphere, European and Adriatic crust are tectonically juxtaposed. This sector can be further subdivided (Malusà et al., 2011; Figure 9) in Cretaceous wedge (made of units from the Austroalpine domain), the Eocene Eclogite belt and the Frontal Wedge (both made of continental- and oceanic-derived Penninic units. The axial sector is characterized by a wide range of peak Alpine metamorphism (from UHP eclogite-facies to greenschist-facies conditions; Figure 10) and is characterized by a double vergence, towards the inner and outer part of the chain.

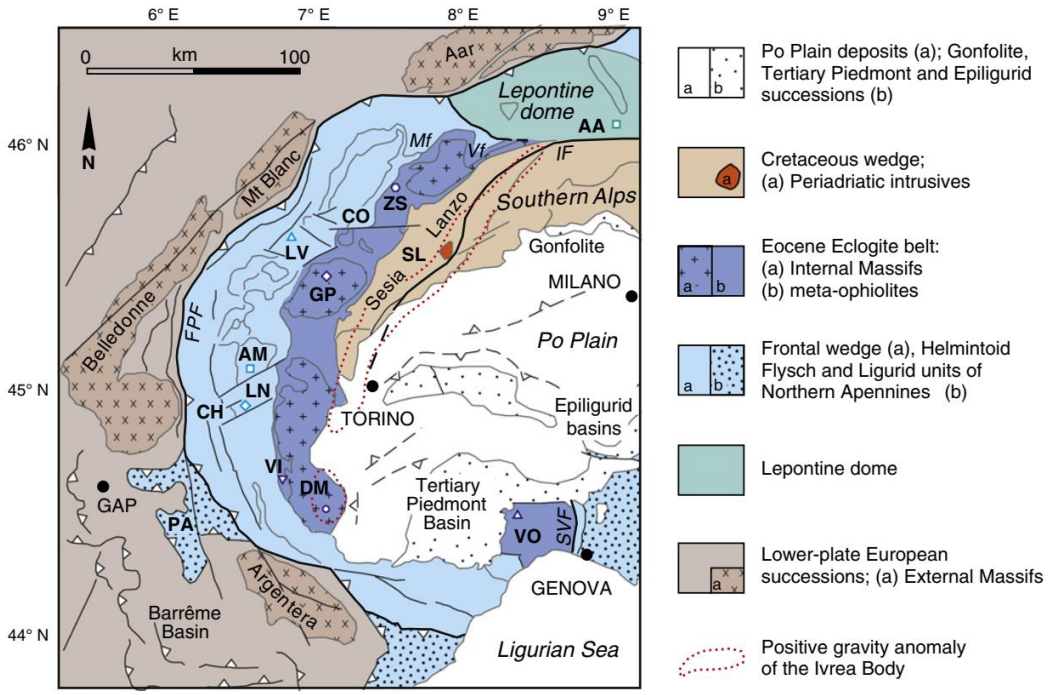

Figure 9 Tectonic sketch of the Western Alps from Malusà et al. (2011). The Eocene Eclogite belt (blue) is exposed on the upper-plate side of the orogen, between the Frontal wedge (light blue) and the remnants of a Late Cretaceous doubly-vergent wedge including the Sesia-Lanzo unit (brown). Major faults (acronyms in italics): FPF, Frontal Pennine; IF, Insubric; SVF, Sestri-Voltaggio. Tectonic units (acronyms in bold): AA, Alpe Arami; AM, Ambin; CH, Chenaillet; CO, Combin; DM, Dora-Maira; GP, Gran Paradiso; LN, Lago Nero; LV, Leverogne; PA, Parpaillon; SL, Sesia-Lanzo; VI, Viso; VO, Voltri; ZS, Zermatt-Saas. Mf, Mischabel backfold; Vf, Vanzone backfold. Open symbols indicate location of samples shown in the next Figure.

The tectonic units object of this Thesis belong to the Frontal Wedge, hence its main geological features will be summarized in this chapter. The Frontal Wedge of the Western Alps (*sensu* Malusà et al., 2011) corresponds to the accretionary wedge (well identified in seismic profiles) characterized by double vergence, delimited to the East by the Eocene Eclogite belt and to the West by the Frontal Pennine Thrust. The Frontal Wedge comprises tectonic units from eclogite-blueschist facies conditions to greenschist-facies conditions, made of pre-Mesozoic continental basement, oceanic lithosphere and Mesozoic meta-sedimentary cover sequences (Figure 10).

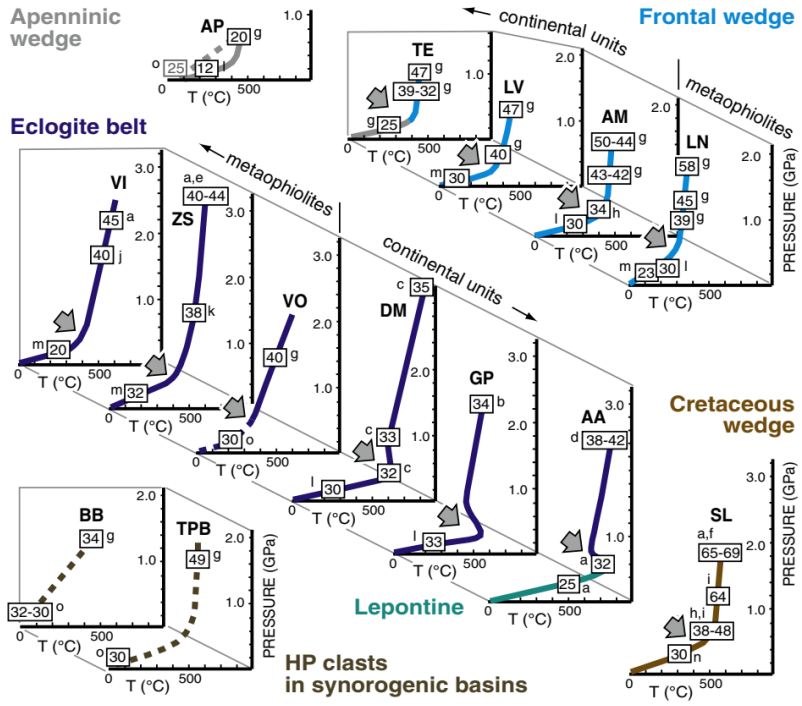

Figure 10 Pressure–temperature paths for the Western Alps, and selected geochronological ages unambiguously linked with petrological and structural data (boxes, in Ma), from Malusà et al., 2011. Exhumation paths in the Eclogite belt (blue), Frontal wedge (light blue) and Cretaceous wedge (brown) are compared with paths related to Apenninic subduction (gray) and late indentation of Adria beneath the axial belt (green). Dashed lines indicate paths inferred from HP clasts in synorogenic basins. Arrows mark the inflection point in pressure–temperature paths after isothermal decompression. AA, Alpe Arami; AM, Ambin unit; AP, Massa unit, Northern Apennine; BB, Barrême Basin HP clast, European foreland; DM, Brossasco-Isasca UHP slice inside the Dora-Maira unit; GP, Gran Paradiso unit near Cogne; LN, Lago Nero unit, Schistes lustrés; LV, Leverogne unit, Gran San Bernardo nappe; SL, Sesia-Lanzo unit, Cretaceous wedge; TE, Tenda unit, Corsica; TPB, Tertiary Piedmont HP clast; VI, Viso unit; VO, Voltri unit at Cascine Parasi; ZS, Cignana UHP slice on top of Zermatt-Saas unit. Geochronological constraints: U–Pb SHRIMP on zircon (a), allanite (b), titanite (c); Sm–Nd on garnet–clinopyroxene (d), or garnet–omphacite–paragonite–clinozoisite–glaucophane (e); Hf–Lu on garnet–phengite (f); 40Ar–39Ar on white mica (g); Rb–Sr on phengite–calcite (h), phengite–feldspar (i), phengite–omphacite (j), phengite–whole rock (k); fission tracks on zircon (l), or apatite (m); age of undeformed magmatic bodies (n); biostratigraphic age of sediments (o). Sample location in previous Figure.

These units derived from different sectors of the pre-collisional paleogeographic scenario and, from the external to the inner sectors, are (Figure 11): i) the Grand St Bernard-Briançonnais nappe system; ii) the écailles intermédiaires (or Externl Piedmont zone; e.g. Acceglio zone); iii) the pre-Piedmont zone; and iv) the Ligurian-

Piedmont Zone, made of portions of oceanic lithosphere and its widespread meta-sedimentary cover.

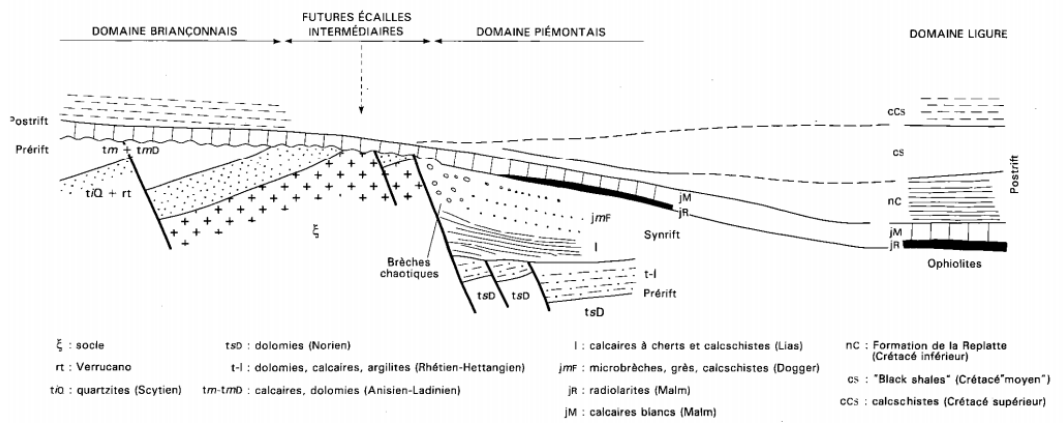

Figure 11 Simplified sketch of the relationship among the domains constituting the Alpine Frontal Wedge (i.e. Briançonnais domain, écailles intermédiaires, pre-Piemont zone,i.e. Piémontais, Ligurian-Piedmont ocean, i.e. Ligure (from Barféty et al., 1996).

2.2.1. The Briançonnais zone

The Briançonnais zone is classically subdivided into two sectors (Barféty et al., 2006a), separated by the Internal Houillere Front: to the West, the External Briançonnais zone consists of thick Mesozoic sedimentary series and Permo-Carboniferous basement rocks of the Houillere Zone, with low-grade Alpine peak metamorphism; to the East, the Internal Briançonnais zone occurs, characterized by a thinner Mesozoic sedimentary cover on top of polymetamorphic basement rocks (e.g. Ambin and South Vanois massifs), with eclogite-blueschist-facies Alpine peak metamorphism (Schwartz et al., 2000; Michard et al., 2004; Strzerzynski et al., 2012).

Basement rocks of the Houillere Zone (Lanari et al., 2012; Ballèvre et al., 2020) consist of siliciclastic successions (originally polygenetic conglomerate, sandstone and siltstone) intruded by volcanic sills and dykes (Mercier & Beaudoin, 1987; Barféty et al., 2006). The Alpine cycle of sedimentation in the area starts with quartzite and conglomeratic quartzite (Verrucano-like conglomerate) of Early Triassic, up to 300 m in thickness (Debelmas & Lemoine, 1966; Barféty et al., 1996). Up section, a thick Meso-Cenozoic cover is made of early Trias evaporites and middle-late Triassic dolostone and limestone, up to 1000m in thickness. The top of the Triassic calcareous platforms is characterized by an important depositional hiatus, covering in some cases the whole Jurassic-early Cretaceous interval (Barféty et al.,, 1972; Barféty et al., 1970; Baud, 1976; Baud & Mégard-Galli, 1975; Caby &

Galli, 1964; Mégard-Galli, 1972a, b, 1974; Mégard-Galli & Baud, 1977; Mégard-Galli & Faure, 1988; Schneegans, 1933). This hiatus (cropping out as hardground and lithified sediments), marks the emersion and erosion of local blocks of Briançonnais units, delimited by Jurassic listric faults. From re-start of sedimentation from the late Jurassic, the External Briançonnais units are characterized by the occurrence of syn-sedimentary breccia, related to intense tectonic processes linked to the opening of the Ligurian-Piedmont ocean. These breccias bodies are characterized by clasts sampling older lithologies, up to Permian Verrucano-like conglomerate (Graciansky & Mercier, 1976; Mercier, 1977; Pussenot, 1930). From the Cretaceous, sedimentation is characterized by pelagic limestone, historically known as *marmbres en plaquettes* (Termier, 1903). This period of time is also characterized by the emplacement of large olistostromes made of black shales, known as *black flysch* (Termier, 1903; Lemoine, 1960; Barféty et al., 1992).

The Internal Briançonnais zone is represented by the Ambin and South Vanoise massifs. They occur as dome-shaped basement windows, made of different lithological groups separated by tectonic discontinuities. From the deepest to the shallowest levels, the polymetamorphic Clarea and then Ambin units occur, followed by the Etache unit. The Clarea unit is mainly made of banded micaschist (with Variscan relicts; Borghi et al., 1999), locally embedding fine-grained metabasite and rare marble. The Ambin unit is made of several arenaceous sequences (comprising quartz meta-conglomerate, micaschist, and gneiss) and the Exilles-Ramats magmatic body (made of meta-rhyolite dated to 500 My; Bertrand et al., 2000). The Etache unit is made of Permo-Triassic siliciclastic rocks covered by meta-sediments from Triassic to Eocenic in age.

2.2.2. The écailles intermédiaires

The *écailles intermédiaires* comprise a zone, N-S striking, interposed between the Briançonnais zone and the pre-Piedmont Zone. This zone is made of a series of units, of which the most widespread and important is the Acceglio-Col Longet unit (Michard, 1959; Lefèvre & Michard, 1976; Schwart et al., 2000; Michard et al., 2004; Michard et al., 2022). These units are characterized by: i) a poly- and mono-metamorphic basement rocks, discontinuously covered by Verrucano-like meta-conglomerate and quartzite (upper Permian-Lower Triassic) ; ii) the (almost complete) absence of Triassic calcareous-dolomitic successions; iii) a very much condensed Jurassic-Cretaceous series. Under a paleogeographic point of view, the *écailles intermédiaires* have been interpreted as horst-like structures or structural highs, delimited by syn-rift listric faults, and the (almost complete) absence of Triassic meta-sediments has been linked to very high erosion ratios in the early to middle Jurassic (Michard et al., 2022 and references therein). This erosional event

justifies the widespread occurrence of Jurassic-Cretaceous meta-breccia, with dolostone, quartzite and micaschist clasts within an arkosic matrix, above Permo-Triassic quartzite and meta-conglomerate. This breccia, associated with pelagic sedimentation of calcschist, is known as "reconstituted rocks" (Lemoine, 1951, 1961), linked to dismantling and erosion of the carbonate Triassic platforms and of the underlying basement rocks.

Units ascribable to the *écailles intermédiaires* have been observed also to the North, in the Vallon the Baisses, between the pre-Piedmont Chaberton-Grand Hoche unit and the Briançonnais zone (Barfety et al., 1996).

2.2.3. The pre-Piedmont Zone

This zone comprises a series of units delimited to the West by the Briançonnais units or by the *écailles intermédiaires*, and to the East by the oceanic units of the Ligurian-Piedmont ocean (Caron, 1971; Dumont, 1983, 1984; Dumont et al., 1984a,b; Franchi, 1911; Lemoine et al., 1978; Polino et al., 1983; Tricart et al., 1985). The main pre-Piedmont units cropping out near the studied area are the Chaberton-Gran Hoche unit (Polino et al., 1983; Polino et al., 2002), the Rochebrune unit (Dumont, 1983; Barféty et al., 1996), and the Gran Roc unit (Caron, 1971). These units are characterized by a thick sequence of Noric dolostone (600-800 m), very similar to the dolostone of the Austroalpine units in the Central and Eastern Alps. A decollement surface, highlighted by gypsum and *cargneules*, separates these units from their original continental basement. In the late Triassic and early Jurassic times dolostone, limestone and shale sedimentation of various thickness (from 10 to 150 m) occur. This sedimentation testifies the various stages of the Jurassic rifting development. The first stage of rifting is characterized by the deposition of the so-called *Lias piemontese* or *Lias piémontais*, made of an alternance of limestone and calcschist (typical of a deeper, pelagic environment). The second stage of rifting (middle Jurassic) is responsible for the formation of a sequence of breccia, sandstone, black schsist and calcschist, interpreted as syn-rift turbidites (30-500 m in thickness). In the lower part, the syn-rift breccia is made of dolostone clasts, while in the upper part micaschist clasts become more abundant: this points out a "reverse stratigraphy" due to dismantling/erosion of progressively older lithologies exhumed by extensional tectonics linked to Tethyan rifting. Pre-Piedmont successions end with late Jurassic-early Cretaceous limestone with cherts levels of presumed detrital origin.

Due to stratigraphic similarities and the absence of clear stratigraphic contacts with their continental basement, the pre-Piedmont units have been ascribed by some authors to the Adriatic paleo-margin (i.e. Austroalpine units), instead of to the

European one (Barféty & Gidon, 1975; Caron et al., 1984; Mégard-Galli & Baud, 1977; Polino et al., 1983).

2.2.4. The Ligurian-Piedmont zone

This zone encompasses a series of units that witness the occurrence of the Mesozoic Ligurian-Piedmont ocean, interposed between the Adriatic and European paleo-margins (Elter, 1971; Lemoine, 1971; Dal Piaz, 1974; Figure 12). The units ascribed to this paleo-geographic realm have been widely investigated by Alpine geologists since the late XIX century (among the first Gastaldi, 1878, and Franchi, 1899) and inevitable contrasts of nomenclature have arisen through the Alps. At a regional scale, the units of this zone are ascribed to the Internal Piedmont Zone (IPZ) or the External Piedmont Zone (EPZ) on the basis of their alpine peak metamorphic conditions, resting respectively in lower and upper structural position. IPZ units (or Zermatt-Saas in literature, see Bearth, 1967) recorded eclogite-facies peak Alpine conditions and usually tectonically overlie the Internal Crystalline Massif (ICM). On the other hand, EPZ units (or Combin zone units, after Bearth) recorded blueschist-facies peak metamorphic conditions and tectonically overlie the IPZ units and the Grand St Bernard-Briançonnais nappes system. IPZ units are also known nowadays as ophiolites-dominated (OD hereafter) or mafic-ultramafic dominated units (see Agard, 2021). The EPZ units (or Combin or Tsaté) are characterized by large amounts of meta-sediments, mainly pelagic calcschists, and metric to kilometric bodies of ophiolites. These units are known nowadays as metasedimentary-dominated units (SD hereafter). Several units studied for this Thesis belong to the metasedimentary units of the Ligurian-Piedmont Zone.

OD units crop-out in the Monviso zone (e.g. Lombardo et al., 2002; Angiboust et al., 2012; Balestro et al., 2013; Festa et al., 2015; Locatelli et al., 2019), around the Dora-Maira (e.g. Assanelli et al., 2020; Ghignone et al., 2021; De Togni et al., 2020) and the Gran Paradiso crystalline massifs (e.g. Gasco & Gattiglio, 2011; Caso et al., 2020), north and south of the Aosta valley (e.g. Dal Piaz et al., 2001; Tartarotti et al., 2011, 2019) up to the Zermatt-Saas area in Switzerland (Bearth, 1967), in the Ligurian Alps (e.g. Scambelluri et al., 1995) and in the Alpine Corsica (e.g. Vitale Brovarone et al., 2013).

The SD units extensively crop out above the OD units in the Queyras and Maurienne region in France (Deville et al., 1992), in the Cottian Alps in Italy (Lagabrielle & Polino, 1988), in the southern and northern part of the Aosta valley, and in the Combin or Tsaté area in Switzerland (Marthaler & Stampfli, 1989).

A case of its own is represented by the Chenaillet ophiolite (Chalot-Prat, 2005, and Manatschal et al., 2011 for a review), in the Western Alps, outcropping near

Montgénevre and Claviere villages. This unit is made of oceanic lithosphere with a very thin, rare sedimentary cover (made only of breccia eroding the oceanic lithosphere). Differently by most of the other OD units, the Chenaillet ophiolite did not suffer eclogite-facies metamorphism.

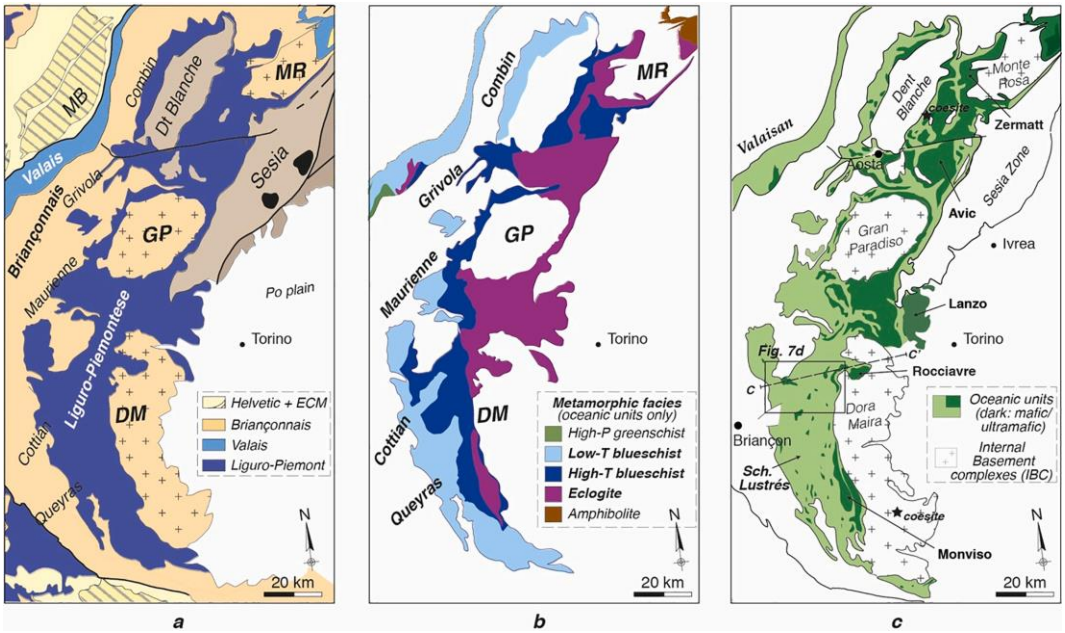

Figure 12 a) Close-up view of the axial sector of the Western Alps for comparison with b) and c), from Agard (2021). Abbreviations as for Figure 7. b) Distribution of metamorphic facies (as in Oberhansli & Goffé, 2004) within the ocean-derived units across the same area. c) Distribution of lithologies across the oceanic units separating the sedimentary-dominated (SD, light green) domains from those dominated by oceanic crust and serpentinized peridotites (i.e. mafic and ultramafic OD, dark green). Note the marked W-E zoning in b) and c). For the sake of convenience, the main sectors of the Western Alps are subddivided into the Combin, Grivola, Maurienne, Cottian and Queyras (b). The main mafic- and ultramafic-dominated OD massifs referred to in the text are shown in c).

2.3. The Ligurian-Piedmont units of the Cottian Alps

In their general traits, the upper Susa Valley and Chisone valleys (investigated during this PhD project) consist of Ligurian-Piedmont successions made of widespread calcschists embedding ophiolitic bodies, local sector of crystalline basement rocks with associated carbonate meta-sedimentary covers (i.e. the Ambin massif and the studied Banchetta-Rognosa tectonic unit). To the West, carbonate successions of the Briançonnais zone/pre-piedmont zone extensively occur.

The first Italian reference map for these area is that realized by Sismonda (1866), where large part of these successions have been mapped as *Giurassico metamorfosato* (i.e. metamorphosed Jurassic rocks). This interpretation differed from the one proposed by Lory (1863) for which *Schistes lustrés* (i.e. calcschist) are

Triassic in age and rest below liassic (i.e. early Jurassic) carbonate successions of the Briançonnais zone. The *Gran Carta di Gastaldi* (i.e. the Geological Map of the Piedmont Alps realized under the direction of B. Gastaldi between 1860-1879; see Mosca & Fioraso, 2016 for further details) mapped widespread calcschist and associated ophiolites with the name of *Zona delle Pietre Verdi* (i.e. greenstones zone), regarded as Huronian in age. Another mapping of the area was carried out during the realization of the Geological Map of the Western Alps at 1:400,000 scale, published in 1908 by the *Regio Ufficio Geologico* (i.e. Royal Geological Office). Then accurate mapping was carried out for the official Italian Geological Map for the sheets Oulx (1911) and Cesana Torinese (1911; Figure 13), during the realization of the geological map of Italy at 1:100,000 scale.

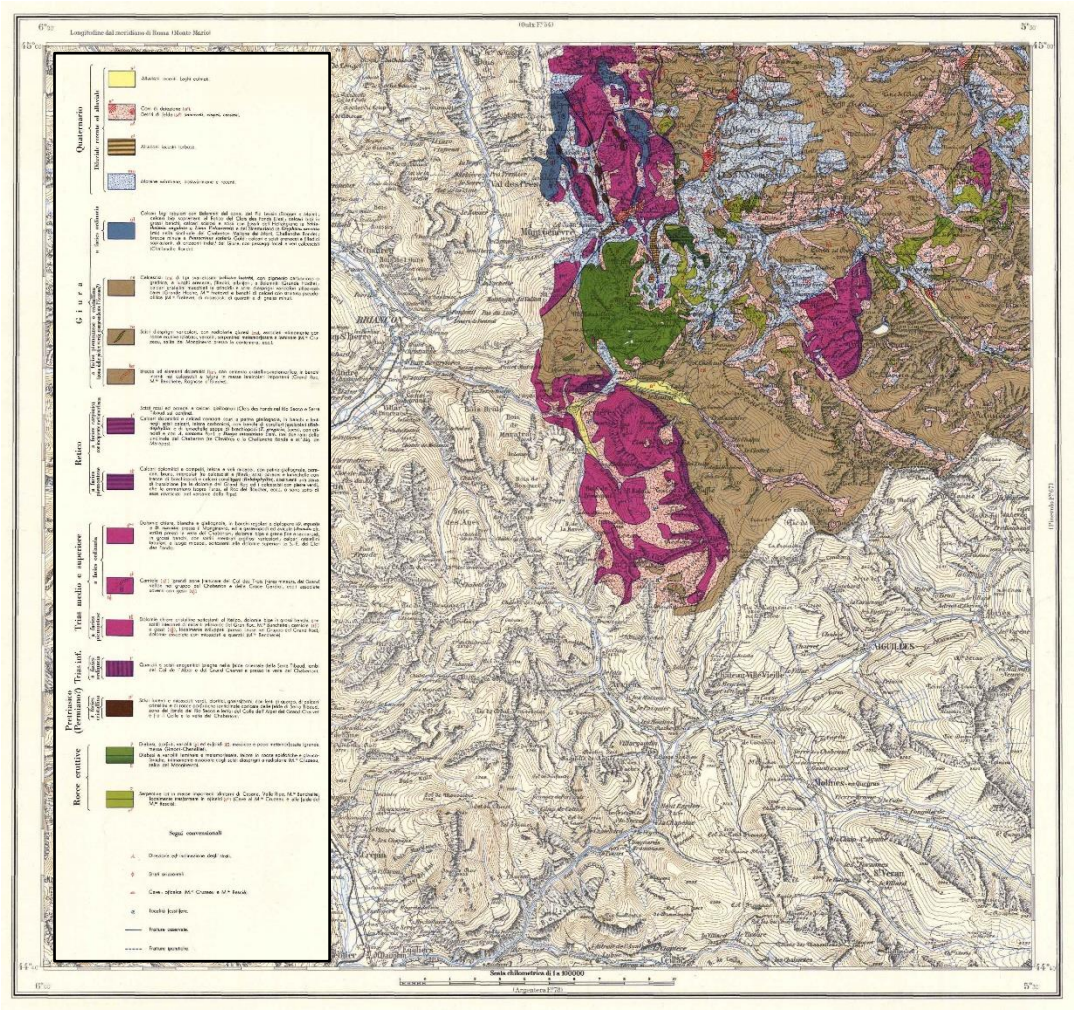

Figure 13 Official Geological map of Italy at 1:100.000 scale, Foglio 66 – Cesana Torinese (Servizio Geologico d'Italia, 1911).

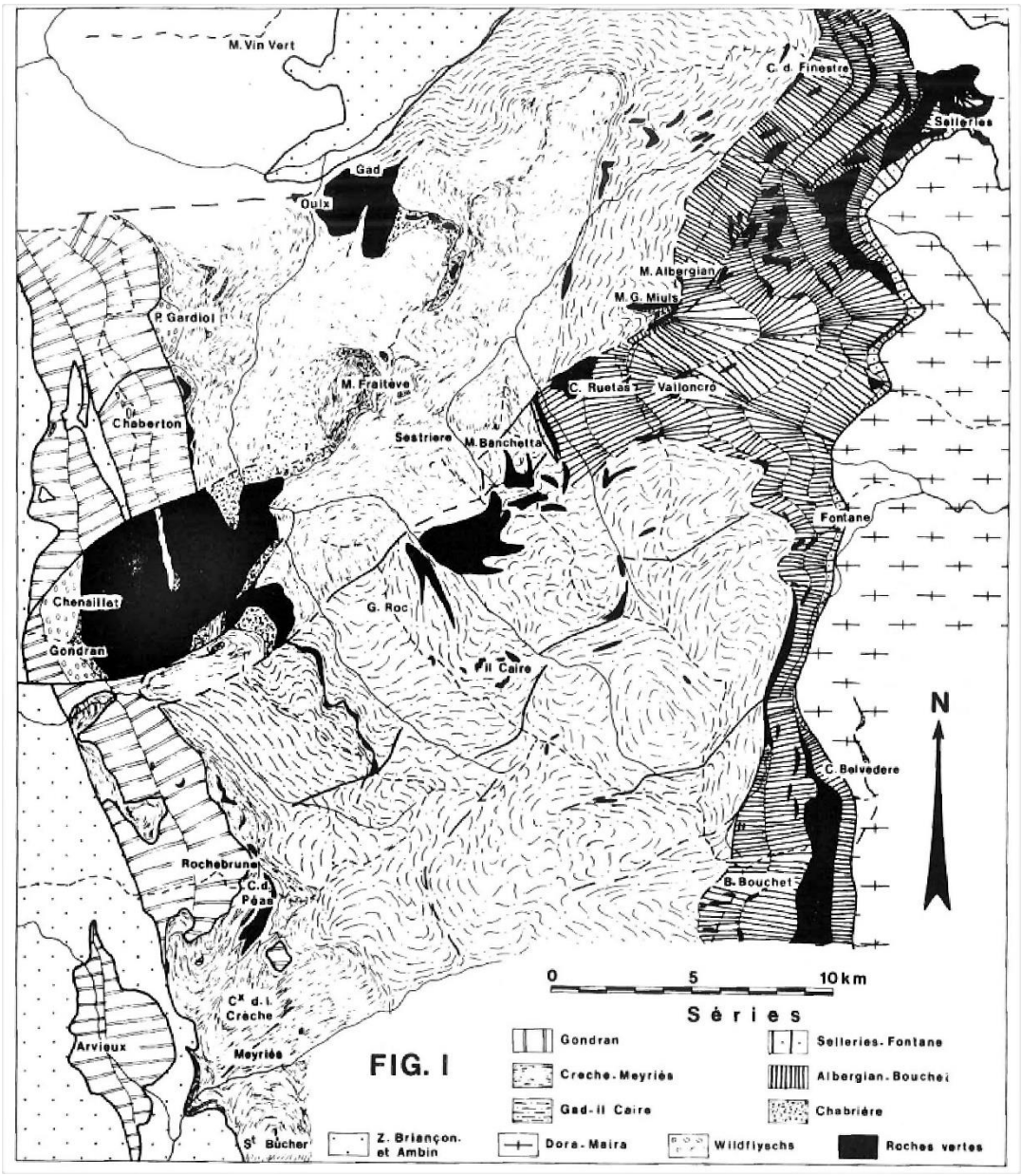

Figure 14 Distribution of the lithostratigraphic series distinguished by Caron (1977) in the Central Cottian Alps.

In the area investigated for this Thesis and in the neighboring areas, multiple subdivisions have been put forward, both regarding the lithostratigraphic features and the tectono-metamorphic evolution (Marthaler et al., 1986; Fudral et al., 1987; Dal Piaz & Polino, 1989; Deville et al., 1992; Lemoine et al., 1993; Cadoppi et al., 2002; Polino et al., 2002).

The first works on the area are from Franchi (1899; see Barale et al., 2022 for details), who attributed a Mesozoic age to the calcschist of the Piedmont Zone. Years later, Franchi (1911) examined the structural setting of this area, highlighting the

occurrence of high angle faults among Triassic carbonate successions (i.e. European paleo-margin) and calcschist-dominated successions (i.e. Ligurian-Piedmont oceanic units). Franchi (1911) also focused on the complex internal lithostratigraphy of the Banchetta-Rognosa area, in the Troncea valley. He reported the complexity of this small area "tectonically very important, and characterized by dolostone bodies intimately associated with serpentinite bodies". In his study, he distinguished Triassic dolostone, micaschist and quartzite, Jurassic calcschist with breccia made of dolostone clasts and blocks, serpentinite and ophicarbonate bodies.

Caron started to investigate the Banchetta-Rognosa area in the late '60s. Caron (1969) firstly detailed there the occurrence of three main kind of breccia and then reported the occurrence of jadeite in the micaschist of the continental basement of the Banchetta-Rognosa unit (1970). Eventually, he distinguished in the area (Caron 1971) three main stratigraphic ensembles: i) a lower one, made of Permian continental basement, with a reduced Mesozoic cover; ii) a middle one, made of Triassic and Jurassic carbonate rocks; and iii) an upper on, made of polygenic breccia, greenstone and thick sequence of undetermined calcschist.

Thanks to the skills and knowledge on the subject acquired in these previous works, Caron (1977) later focused on the meta-sedimentary rocks of a wider area in the central Cottian Alps (Figure 14, Figure 15 and Figure 16). He distinguished and recognized six main lithostratigraphic "series" (often used as references in other alpine studies) in the Schistes Lustrés of the upper Susa and Chisone valleys:

- *"series de type Chabrière"*, supra-ophiolitic and where the first meta-sedimentary terms are made of Jurassic (meta-)radiolarite. It is described above the Chenaillet massif, in the tectonic window of the Gimont valley, to the South of Cesana and Claviere villages, in the area around the Bousson and Chabaud passes in the left side of the Thuras valley; and in the area comprising M. Cruzore – M. Fraiteve – Sauze d'Oulx village;
- *"séries du Gondran"*, of continental pertinence and Triassic-Jurassic in age (now interpreted as pre-Piedmont zone). It is described in the Chaberton-Grand Hoche massif, the Gondran massif (to the East of Briançon), and the Rochebrune massif;
- *"séries de type Créche-Meyriès"*, apparently continuous between Noric dolostone and banded greenschist. To the north, it is described in the vicinity of the "Gondran series", to the East with respect to the Chaberton-Grand Hoche unit and on both sides of the Susa valley between Cesana T.se and Oulx and up to the village of Sestriere. To the South, it is described in the tectonic window of Cervières and to East (i.e. below) of the Rochebrune massif (referred to the pre-Piedmont zone);

- *"séries de type Gad- il Caire"*, similar to the one previously described but with differences at the level of singular layers. Also its location is not clear in Caron's work, but it is generically extended to those areas in the upper Susa-Chisone valleys between the Créche-Meyriès and the Albergian-Bouchet series, up to the Colle delle Finestre to the East. The two toponyms characterizing this series are in the Argentera valley, to the South of Sestriere, and to the East of Oulx;
- *"séries de type Albergian-Bouchet"*, more unknown and characterized mainly by massif calcschist, greenschist and abundant meta-ophiolites. It is described in a N-S trending band, from the M. Albergian (to the North) to the Bric Bouchet (or Bucie in Italian) to the South;
- *"séries de type Selleries-Fontane"*, reduced and transgressive above the crystalline basement rocks of the Dora-Maira massif, now interpreted as its continental meta-sedimentary cover more or less detached and sheared. It crops out discontinuously all around the Dora-Maira crystalline massif, from the middle Chisone valley to the Germanasca valley.

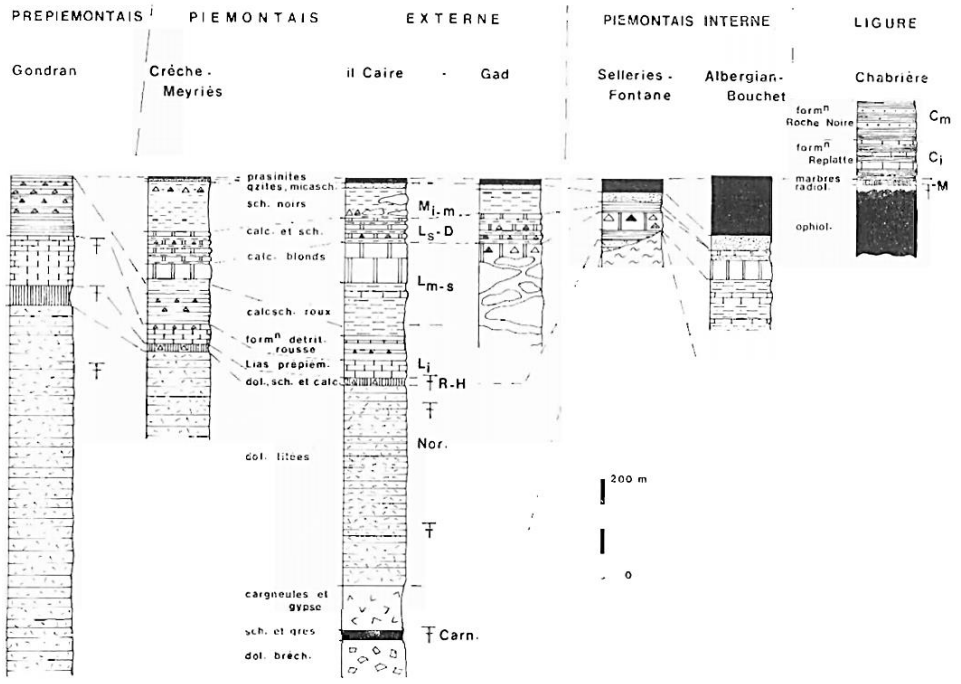

Figure 15 Main types of lithostratigraphic series recognized by Caron (1977) in the Central Cottian Alps.

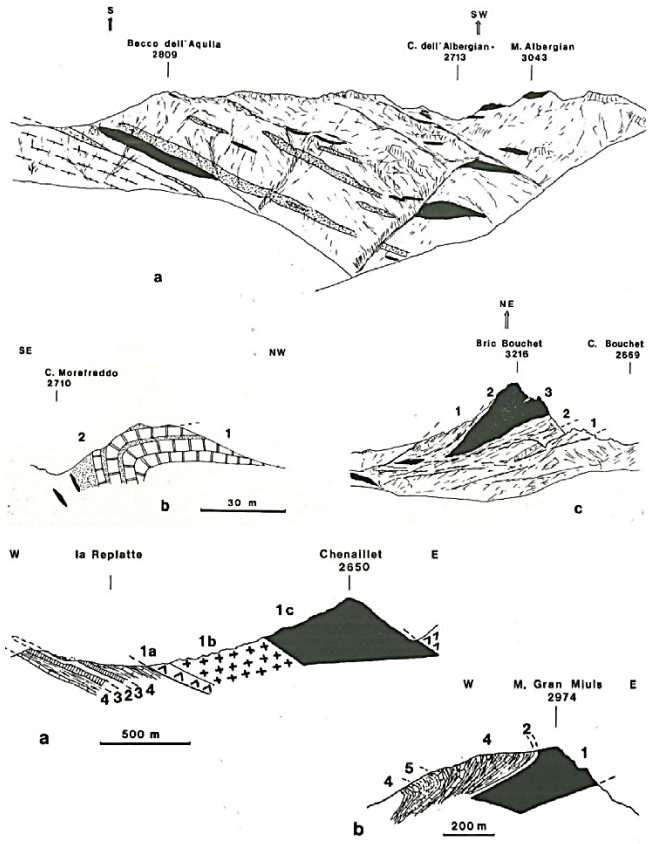

Figure 16 Cross-sections of the areas of the Cottian Alps investigated by Caron (1977).

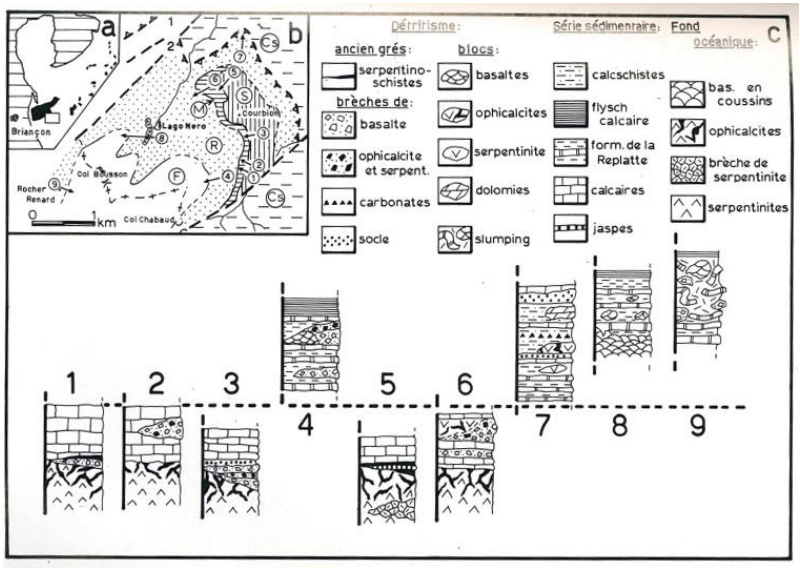

Figure 17 Sketch map of the Lago Nero area and lithostratigraphic logs from Polino & Lemoine (1984).

Lagabrielle (1982) and Polino (1984) carried out a thorough investigation on the lithostratigraphic successions occurring in the upper Susa valley. They focused on the Lago Nero unit and based on the several lithological associations between oceanic basement and meta-sedimentary cover, they distinguished four different sectors: i) the Lago Nero sector, ii) the Roccia Rossa sector, iii) the M. Cruzeau (or Cruzore) sector, and iv) the M. Sisnières sector.

Polino & Lemoine (1984) proposed a more thorough study on the relationships between the oceanic basement and the meta-sedimentary cover of the Lago Nero sector (Figure 17). They reported for the first time the occurrence of continental-derived detritus within the calcschist.

Recently, for the realization of the 154-Susa, 153-Bardonecchia and 171-Cesana T.se sheets (Servizio Geologico d'Italia, 2002a, 2002b, 2020) of the official Geological Italian cartography, a tectono-stratigraphic differentiation of units was made (Figure 18). This subdivision takes into account the occurrence of different tectono-stratigraphic units distinguished on the basis of their lithostratigraphic succession and, consequently, their original paleo-geographic position. Three main units were distinguished in the investigated areas (Figure 19): i) the Cerogne-Ciantiplagna unit; ii) the Albergian unit; iii) the Lago Nero unit.

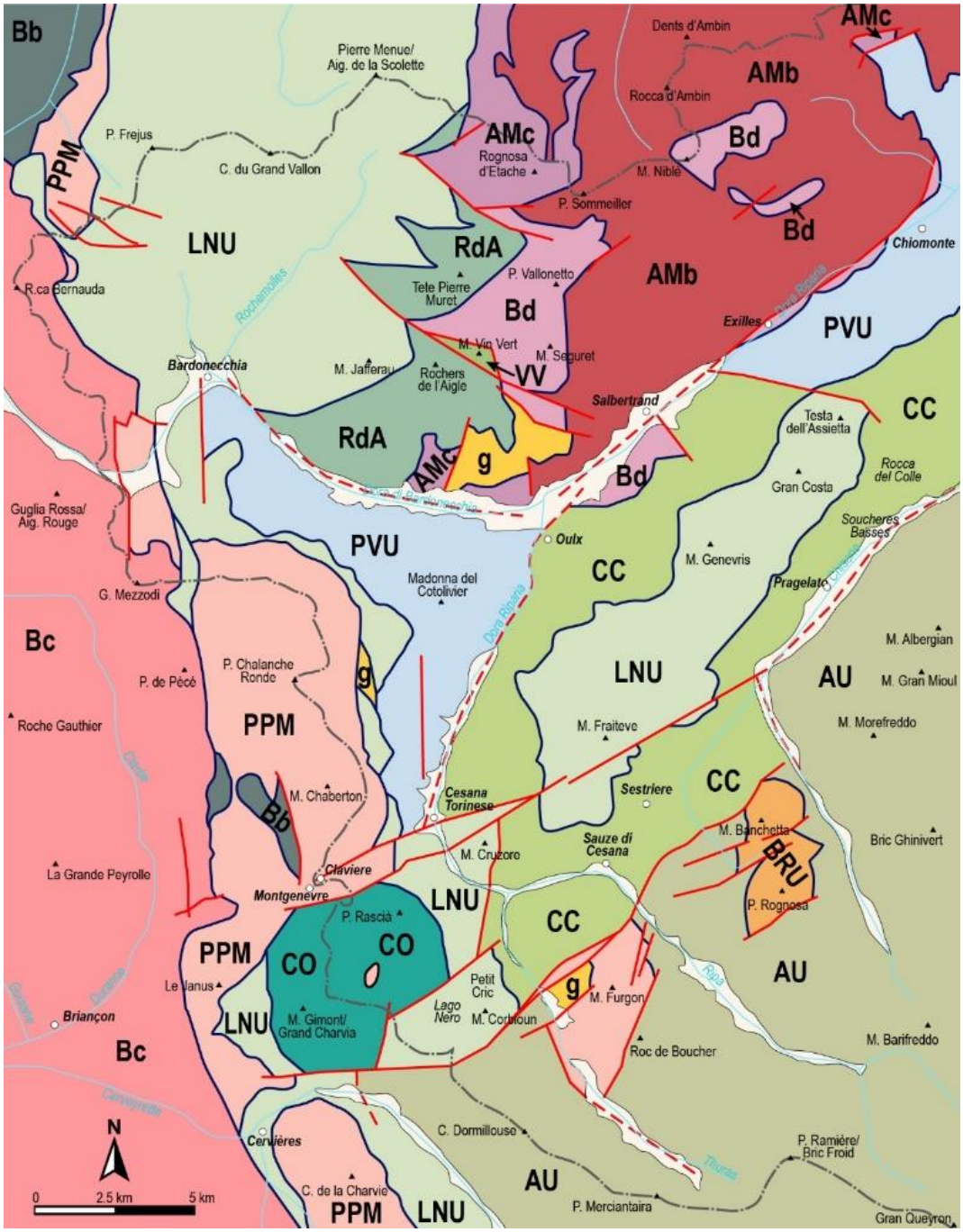

Figure 18 Tectonic sketch map of the studied area, redrawn from the Bardonecchia and Cesana T.se sheets of the Official Italian Geological map (Servizio Geologico d'Italia, 2002a, 2020). Abbreviations are: CC, Cerogne-Ciantiplagna unit; AU, Albergian unit; BRU, Banchetta-Rognosa tectonic unit; LNU, Lago Nero unit; CO, Chenaillet ophiolite; PVU, Puys-Venaus unit; PPM, pre-Piedmont units; Bc, Briançonnais cover units; Bb, Briançonnais basement units; RdA, Rochers de l'Aigle unit; VV, Vin Vert unit; Bd, Briançonnais detached units; AMc, Ambin massif cover; AMb, Ambin massif basement; g, main bodies and masses of gypsum and tectonic cargneules.

The Cerogne-Ciantiplagna unit is mainly made of a meta-sedimentary cover, embedding discontinuous bodies of oceanic lithosphere, it is characterized by epidote blueschist-facies Alpine metamorphism.

The Albergian unit, as well as the previous one, is mainly made of meta-sedimentary rocks embedding discontinuous bodies of oceanic lithosphere at various stratigraphic levels. It is characterized by lawsonite blueschist-facies Alpine metamorphism, recently constrained at 18-21 kbar and 380-430 °C (see Corno et al., 2022).

The Lago Nero unit is made of oceanic lithosphere covered by a thick meta-sedimentary cover. It is characterized by lawsonite- and/or Mg-carpholite blueschist facies Alpine metamorphism. Its interpretation and paleo-geographic position is still debated, although Burroni et al., 2003 locate it close to a continental margin in a more external position with respect to other units of the Ligurian-Piedmont ocean.

The following 4-5-6-7-8-9-10 chapters of this Thesis present new data on the lithostratigraphy and metamorphic evolution of these units.

The tectono-metamorphic differentiation of the Ligurian-Piedmont units has been recently summed up by Agard (2021; Figure 20), based on structural setting and metamorphic conditions (constrained with Si-in-Phe barometer and the RSCM thermometer; see Agard et al., 2001a,b, and Beyssac et al., 2002). This kind of subdivision of units has already been presented in the late ‘80s by Lagabrielle (1987) and Pognante (1991), and distinguishes three units, stacking above the OD units, in this area represented by the Orsiera-Rocciavré meta-ophiolitic complex (Pognante, 1979). From the lower to the upper nappe stack, above the OD units are located the Lower meta-sedimentary units (LSD hereafter), then the Middle meta-sedimentary units (MSD) and eventually the Upper meta-sedimentary units (USD).

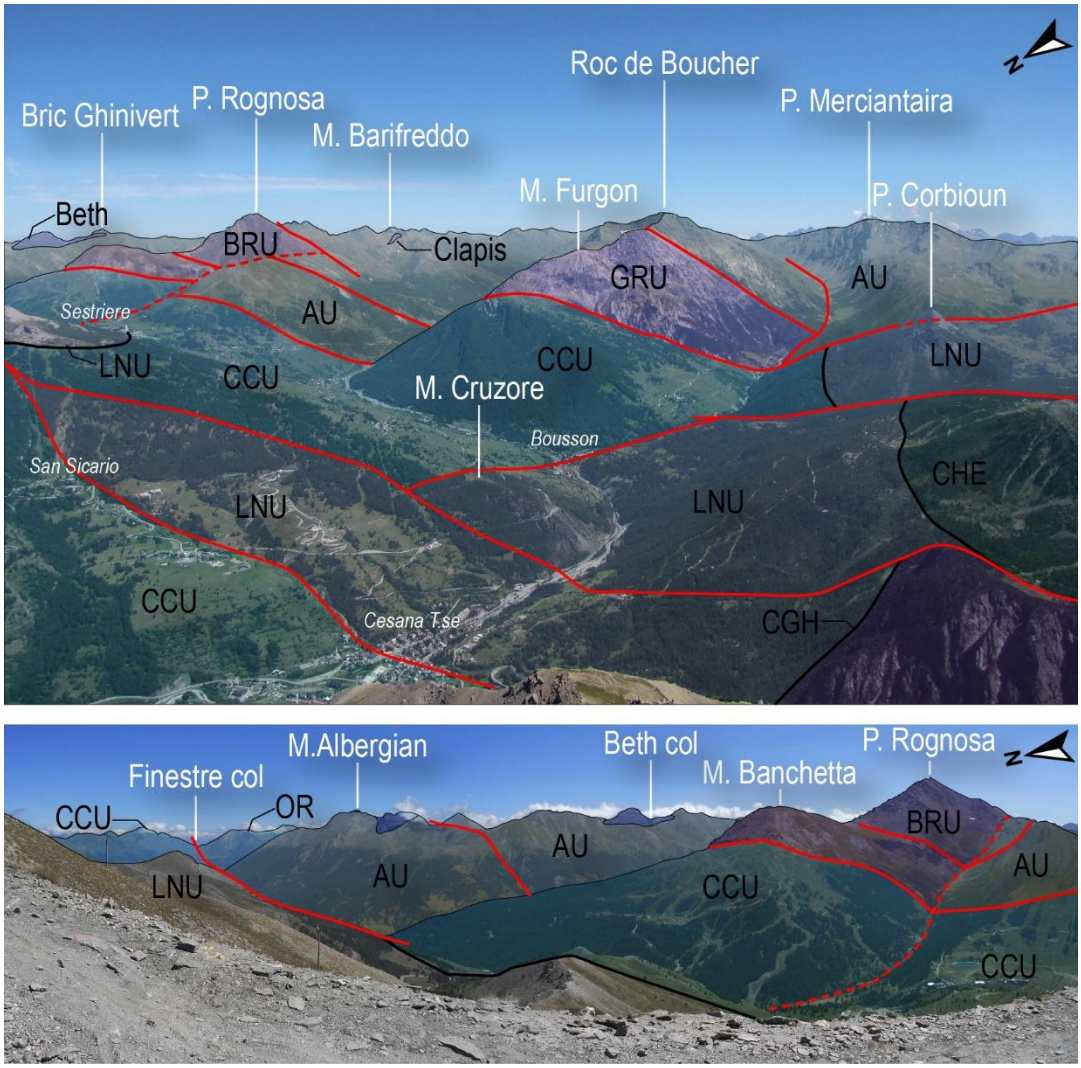

Figure 19 Landscape pictures of the studied area. a. Landscape from the summit of M. Chaberton on the area South of Cesana T.se. b. Landscape from the summit of M. Fraiteve on the upper Chisone valley. Abbreviations for both pictures are: CCU, Cerogne-Ciantiplagna unit; AU, Albergian unit; BRU, Banchetta-Rognosa tectonic unit; LNU, Lago Nero unit; GRU, Gran Roc unit (belonging to the pre-Piedmont Chaberton-Grand Hoche unit); OR, Orsiera-Rocciavré meta-ophiolitic complex; CHE, Chenaillet ophiolite.

Figure 20 (next page) Focus on the metasedimentary-dominated (S) units from the Maurienne to Northern Queyras, Western Alps from Agard (2021). a) Schematic crustal-scale section across the Western Alps along profile B-B′ of Figure 8, approximately at the latitude of Briançon (after Agard et al., 2009). b) Close-up, simplified section across the SD units along profile C-C′ (location in Figure 8). Note the fairly regular increase of P-T conditions from west to east. c) Structural map from the Maurienne to Cottian Alps showing the sub-division into three major units (lower, middle and upper SD units). In the Cottian Alps, three or four units are recognized depending on latitude and authors (the two upper S units are after Lagabrielle et al., 2015). Temperatures correspond to maximum temperature estimated using the irreversible transformation of organic matter in the rocks (data and calibration from Beyssac et al., 2002; data from Gabalda et al., 2009; Plunder et al., 2012; Schwartz et al., 2013). Figure modified after Plunder et al. (2012) and Vitale Brovarone et al. (2014). d) Simplified structural map of the area to the east of Sestriere, at the latitude between the Chenaillet and Orsiera-Rocciavré ophiolites. Mineral isograds outline the eastward increase in temperature. Phengite isopleths, which vary from 3.3 to 3.6 Si per formula unit, outline the eastward increase in pressure. Both are from Agard et al. (2001a, 2001b). e) Pressure-temperature estimates for the area shown in Figure 20d (plain ellipses; updated from

Agard et al., 2001a, 2001b, 2002). Dotted ellipses refer to studies further north in the Maurienne (Pl12: Plunder et al., 2012) or further south in the Monviso area (Locatelli et al., 2018 and references therein; AG20: Angiboust and Glodny, 2020). f) Boxplots capturing the range of maximum temperatures for the lower, middle and upper units across the area shown in Figure 20c.

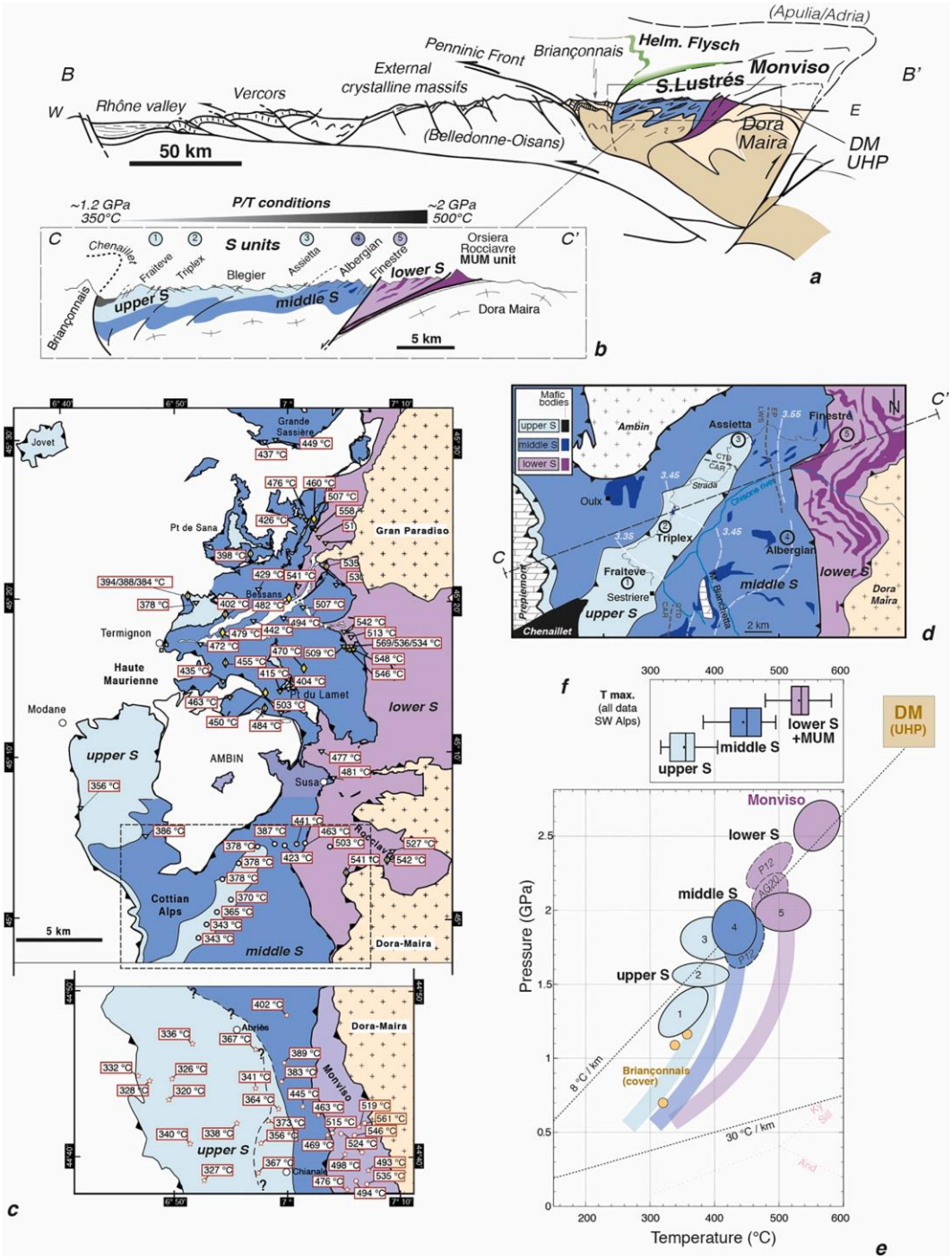

LSD units are generally made of a meta-sedimentary cover rich in volcanic debris and meta-cherts, overlying oceanic lithosphere or interleaved with meta-ophiolitic bodies. It is still unclear among authors whether these units represent units of their own or they represent the former ultra-/mafic cover of the OD units. P-T estimates for these units range in the eclogite-facies eclogite-blueschist-facies transition (P 20-23 kbar, T 470-550 °C; Agard et al., 2001a; Beyssac et al., 2002; Ghignone et al., 2021).

MSD units generally are mainly made of calcschist (i.e. carbonate micaschist), with local level of continental and oceanic detrital origin. Sheared ophiolitic bodies can be found widespread within the meta-sedimentary cover. MSD units usually rest above LSD units, however locally they can rest directly on top of basement rocks of the Internal Crystalline Massifs (e.g. Dora-Maira massif). P-T estimates for these units range between P of 15-20 kbar and T of 370-450 °C, hence in the lawsonite- to epidote-blueschist-facies fields (Agard et al., 2001a; Beyssac et al., 2002). MSD units can be further distinguished based on the occurrence of fresh lawsonite or equilibration in the epidote-stability field.

USD units are generally made of pelitic and organic-rich meta-sediments. The occurrence of large fragments of pre-Piedmont carbonate rocks, usually close to the Briançonnais domain, suggests that USD units originally were paleo-geographically close to OCT zones (Tricart et al., 1982). Another hypothesis is that USD units represent a dismembered unit on top of the nappe stack. Mafic and ultramafic bodies can be found embedded within the USD units along with meta-chert (Martin & Polino, 1984). P-T estimates for these units range between P of 11-15 kbar and T of 330-350 °C, in the lower blueschist-facies and HP-greenschist-facies (Agard et al., 2001a; Beyssac et al., 2002). Referring to the subdivision proposed in official Geological Italian cartography, the Cerogne-Ciantiplagna and Albergian units are ascribed to the MSD, while the Lago Nero is ascribed to the USD.

Under the point of view of the ophiolitic bodies and successions, the most studied unit is the Chenaillet ophiolite (Buffon, 1786; Delesse, 1848; Michel-Lévy, 1877; Vuagnat, 1949, 1966, 1975; Vuagnat & Pusztaszeri, 1965; Pusztaszeri, 1969; Kohen & Vuagnat, 1970; Mével, 1975; Mével et al., 1978; Bertrand et al., 1980, 1982; Lewis & Snewing, 1980). In a first stage it was interpreted as a single unit, while after the ‘80s it has been subdivided in the Chenaillet massif and Lago Nero unit. The former unit with very low Alpine metamorphism (Bertrand et al., 1987; Caby, 1995; Barféty et al., 1996; Costa & Caby, 2001; Chalot-Prat et al., 2003; Mantaschal et al., 2011; Tribuzio et al., 2019; Nicollet et al., 2022), and the latter unit, with blueschist-facies Alpine metamorphism (Mével & Kienast, 1980; Polino, 1984; Polino & Lemoine, 1984; Burroni et al., 2003). A recent and complete review on the

differences between the Chenaillet ophiolite and the Lago Nero unit is reported in De Graciansky et al., 2011 (Figure 21).

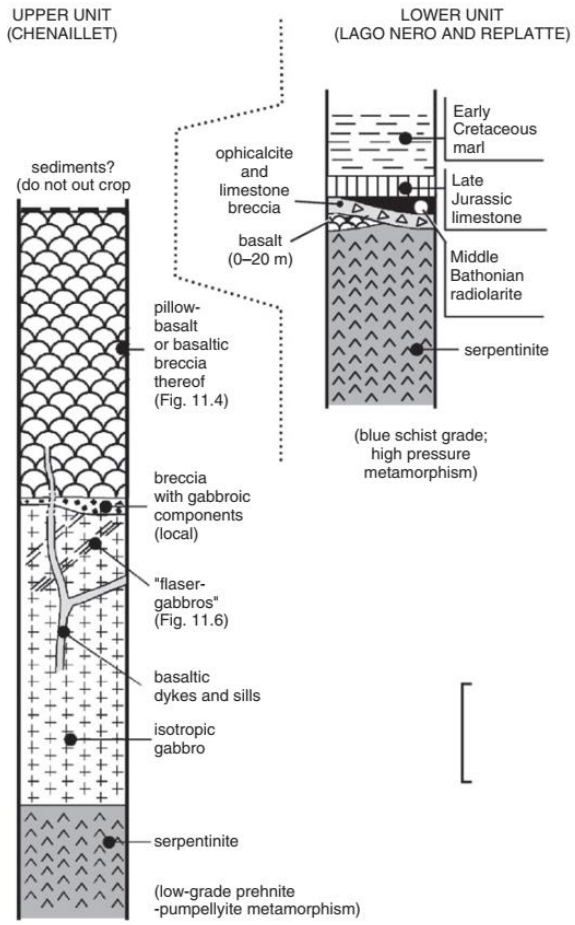

Figure 1 The ophiolite successions of the Chenaillet ophiolite and Lago Nero unit from De Graciansky et al. (2011). The Chenaillet massif consists of two stacked ophiolite nappes derived from different parts of the ocean and not subjected to the same history of subduction and collision. The lower unit was subjected to high-pressure, blue schist-grade metamorphism. The first sediments are represented by ophicalcites, which everywhere rest directly on the serpentinites. Locally, at Mt. Corbioun, a conglomeratic horizon with granite pebbles of continental origin is interbedded with the ophicalcites. Above, granitic and Triassic dolomite clasts are found locally in Early Cretaceous sediments. The lava pillows of the upper ophiolite unit of the Chenaillet were subjected only to low-grade prehnite–pumpellyite metamorphism, which took place on the floor of the actively spreading Liguro-piemontais Ocean. The unit is unaffected by Tertiary Alpine syn-metamorphic deformation. In particular, the pillow basalts are nearly undeformed unlike those of the lower unit. Adapted from Lemoine et al., 2000.

2.4. Mesozoic rifting

As introduced in the previous chapters, the Alps are the result of collision between the former continental rifted margins (respectively the Adriatic/African and the European). Collision involved also the oceanic basin (i.e. Alpine Tethys, made of Ligurian-Piedmont and Valaisan oceans) previously interposed between the two paleo-margins and then subducted. Modern studies emphasize that rift-related pre-orogenic architecture and crustal thickness can play a major role in the Alpine orogeny (Mohn et al., 2014). Starting from current studies of the architecture of distal rifted margins of Iberia-Newfounland (Pe´ron-Pinvidic & Manatschal, 2009; Brune et al., 2017), of the Atlantic (Contrucci et al., 2004; Aslanian et al., 2009; Brune et al., 2017), and of Australia (Karner and Driscoll, 1999), a new mind setting in studying lithospheric thinning and continental breakup (and their consequences on the stratigraphic record) has developed through the Alps. Nowadays, the rift system of the Alpine Tethys in the Alps has been related to an analog of the Atlantic type magma-poor rifted margin. This concept allowed for a major breakthrough in understanding the Alpine rifting has come from the study of un-deformed domains in the Lower Austroalpine nappes of the Central Alps, in the South-East of Switzerland/Northern Italy area (Froitzheim & Eberli, 1990; Florineth & Froitzheim, 1994; Manatschal et al., 2007; Mohn et al., 2010).

In the Alpine Tethys, fossil evidence of rift-related hyper-extension has been reported since the early 1990s (Lemoine & Trümpy, 1987; Froitzheim & Eberli, 1990: Marroni et al., 1998; see Masini et al., 2013 for a review).

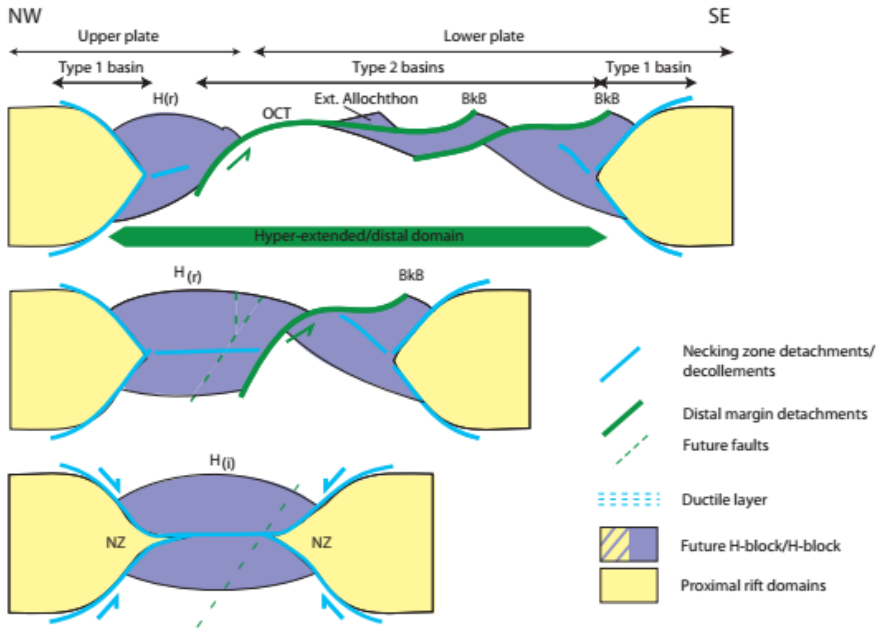

Figure 22 (previous page) Conceptual kinematic model from Masini et al. (2013) showing the creation of the initial H-block, also referred to as H(i) and the following creation of a hyper-extended distal margin using low-angle detachment faulting. Step I: development of the conjugate necking zones (NZ) defining the 'keystone block' or H(i) (see Mohn et al., 2012 for more details). Steps II and III delamination of the H(i) by the onset of low-angle detachment faulting. This defines the upper plate from the lower plate and their respective architecture. Note that the lower plate is made up of exhumed footwall as detached and delaminated blocks (i.e. allochthons or breakaway blocks), whereas the upper plate preserves the residual H-block [i.e. H(r)]. 'BkB': breakaway block; 'H(i)': initial H-block; 'H(r)': residual H-block; 'NZ': crustal necking zone; 'OCT': ocean continent transition.

The production of a hyper-extended margin has been summarized by various authors (Froitzheim & Manatschal, 1996; Desmurs et al., 2002; Manatschal & Müntener, 2009; Mohn et al., 2011; Masini et al., 2013; Beltrando et al., 2014; Mohn et al., 2014; Decarlis et al., 2015; Ribes et al., 2019) in a 3 steps scenario (Figure 22). The starting point of this evolution foresees a first step crustal thinning along low-angle detachments (from late Permian to late Triassic). The following development of (conjugate) necking zone defines the H-block (or key-stone block) in Jurassic times, a hanging block comprised between the two paleo-margins and in the Alps made of the Alpine Tethys and Briançonnais block. Then, the last step foresees the delamination of the H-block due to the developments of low-angle detachment faults. This asymmetrical shearing defines an upper (European) and a lower plate (Adriatic). The lower plate in the footwall is made of exhumed footwall (in the case of the Alps made of continental crust and exhumed mantle), while the upper plate preserves portions of the dismantled H-block (i.e. the Briançonnais domain). In this scenario (Figure 23), in late Jurassic / early Cretaceous times the (future) Alpine area was characterized by an oceanic domain (comprised between the two continental margins), characterized by oceanic mantle and poor magma production. Laterally, the oceanic domain passed towards areas of exhumed mantle (previously sub-continental mantle), covered by local pieces of detached continental crust and/or pre-rift covers (i.e. extensional allochthons or breakaway blocks), known as ocean-continent transition (OCT hereafter). Moving towards the continent, the hyper-extended domain of the distal margins occurred, made of continental crust characterized by intense listric faulting, responsible for the development of tilted basins. The transition from this sector to the proximal margin (characterized by the full sequence of lower, middle and upper crust) is defined by the necking zone (Mohn et al., 2012 for a review). In this sector the major delamination of the crust occurs, from more than 30km to less than 10km, well identified in current hyper-extended margins thanks to refraction and reflection seismic sections (Minshull, 2009; Gillard et al., 2016).

Figure 23 (next page) Idealized cross-section across a magma-poor rifted margin showing the different domains, crustal architecture and terminology, from Mohn et al. (2012).

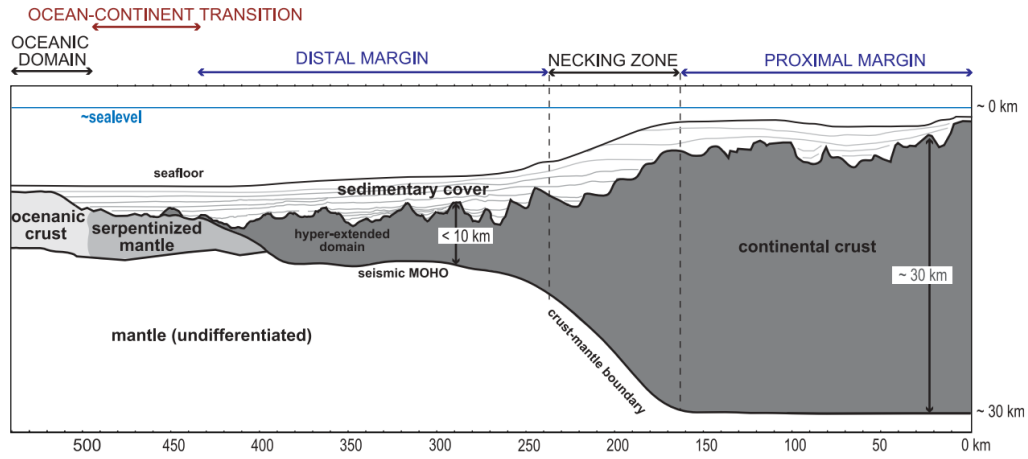

Based on mapping and petro-structural investigations, Mohn et al. (2011, 2012) suggested the existence of necking zones in the Alpine Tethys margins separating the proximal from the distal parts of the margin. Hence, the Frontal Penninc thrust and in the Insubric Line have been inferred as possible location of the fossil necking zones of the European and Adriatic distal margins (respectively).

In this framework, these different sectors displayed also different, diagnostic stratigraphic record (Figure 24). Only post-rift sediments characterize sectors from the oceanic domain, while syn- and post-rift sediments, in structural lows and pre- and post-rift covers in structural highs, characterize hyper-extended distal margins. Necking zones and proximal margins are usually characterized by a complete sequence of pre-, syn- and post-rift sediments, in variable amounts and ratios.

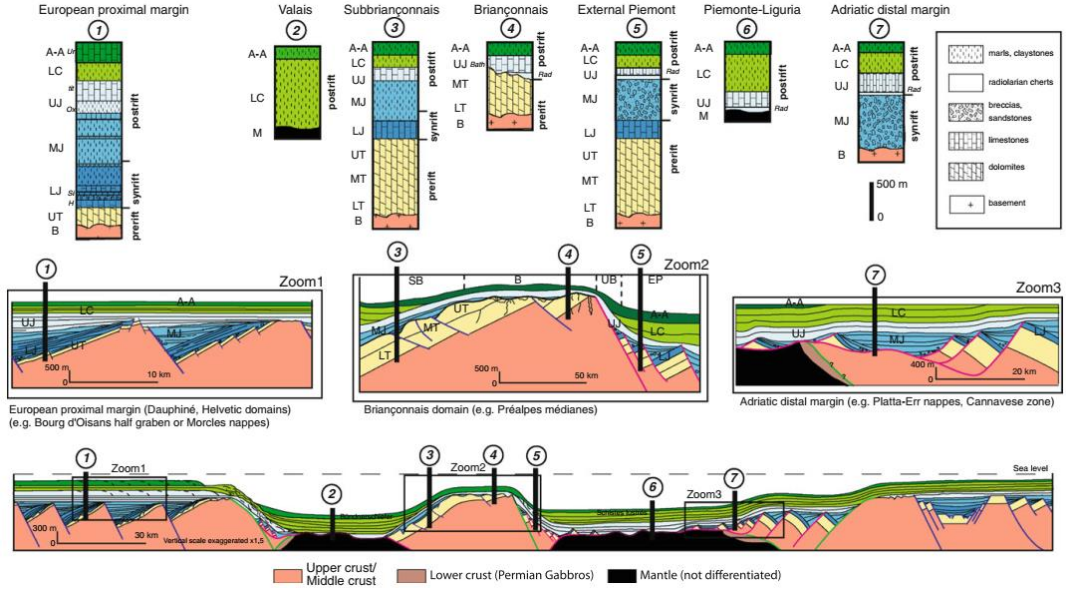

Figure 24 (previous page) Section across the Alpine Tethys margin (from Mohn et al., 2010) showing the stratigraphic record documented in the major paleogeographic domains. Zooms show the detailed sediment-architecture of the proximal European margin (modified from Lemoine et al. 1986), the Valais (modified from Steinmann 1994), the Briaçonnais (modified after Baud and Stepfontaine 1980) and the distal Adriatic margin. The simplified composite stratigraphic logs above show typical logs for the different paleogeographic domains. Abbreviations: M, Mantle; B, basement; LT, MT, UT, Lower, Middle, Upper Triassic; LJ, MJ, UJ, Lower, Middle, Upper Jurassic; (H, Hettangian; Si, Sinemurian; Bath, Bathonian; Ox, Oxfordian; Tit, Tithonian), LC, Lower Creatceous; A-A, Aptian-Albian (Ur, Urgonian).

These rock assemblages have been extensively recognized and studied in the less deformed portion of the Alpine belt (i.e. Central Alps and Ligurian Alps; e.g. Manatschal, 2004; Mohn et al., 2014; Decarlis et al., 2017). Nevertheless, some studies have tried to recognize and study the distinctive features of hyper-extended magma-poor rifted margins in the Western Alps (e.g. Beltrando et al., 2012, 2014). Furthermore, some studies have underlined that relict major structures played a fundamental role in the current setting of the chain, controlling the development of the main tectonic lines (Figure 25).

Regarding current knowledge about the tectonic and paleogeographic setting of the Alps, various authors (Masini et al., 2013; Decarlis et al., 2015; Haupert et al., 2016) have inferred that external domains (i.e. Helvetic-Dauphinois and Southern Alps) represent the original proximal margins, while the Austroalpine domain represents the Adriatic distal margin. As said before, these paleogeographic restorations have been carried out widely in the external domains (lacking Alpine metamorphism) and in the Australpine domain cropping out in the Central Alps (Mohn et al., 2011; Incerpi et al., 2017; Ribes et al., 2019) while much more doubts exist on the precise paleogeographic positions of the units of the Penninic domain.

The evolution of the Briançonnais domain, during Pliensbachian age, was influenced by high rates of uplift and erosion (as witnessed by the well-known “Liassic hiatus” at the top of Triassic dolostone) and is now interpreted as the H- (delaminated) block. This area would currently correspond to the units of the Frontal Wedge. In the same period (early Jurassic), on the other hand the pre-Piedmont units were presumably submerged. From this point of view, units belonging to the Ligurian-Piedmont ocean, to the European distal margin and to the lower Austroalpine domain developed from middle Jurassic after exhumation along different detachment faults. This kind of units comprises relicts of hyper-extended continental crust and serpentinized mantle, coupled by systems of extensional detachments, variously preserved according to different peak Alpine metamorphism and deformation. Generally, these units are covered by syn-and post-rift (meta-)sediments. Usually, units ascribed to the OCT and the distal margins, display rock assemblages characterized by local exhumation of mantle rocks with delamination of continental crust, associated with pre-rift (meta-)sedimentary covers (i.e. extensional allochthons). Detachment surfaces along

the oceanic – continental boundaries in the Alps (where geophysics methods cannot be used), have been recognized thanks to systematic changes in mineralogy, and peculiar textures and structures along the detachments. Detachment-related fault rocks are usually cataclasites or gauges, interested by continuous and pervasive circulation of fluids of mantle origin. In fact, serpentinized mantle usually occurs deprived in those elements (such as Cr, V and Ni) of which the continental rocks above are enriched (see Pinto et al., 2015 for further details; Figure 26). However, recognition of fossil detachment-related fault rocks in Alps remains a very difficult task due to the intense deformation. On the other hand, units ascribed to the oceanic domain display heterogeneous rock assemblages characterized by oceanic lithosphere and a complex post-rift (meta-)sedimentary cover.

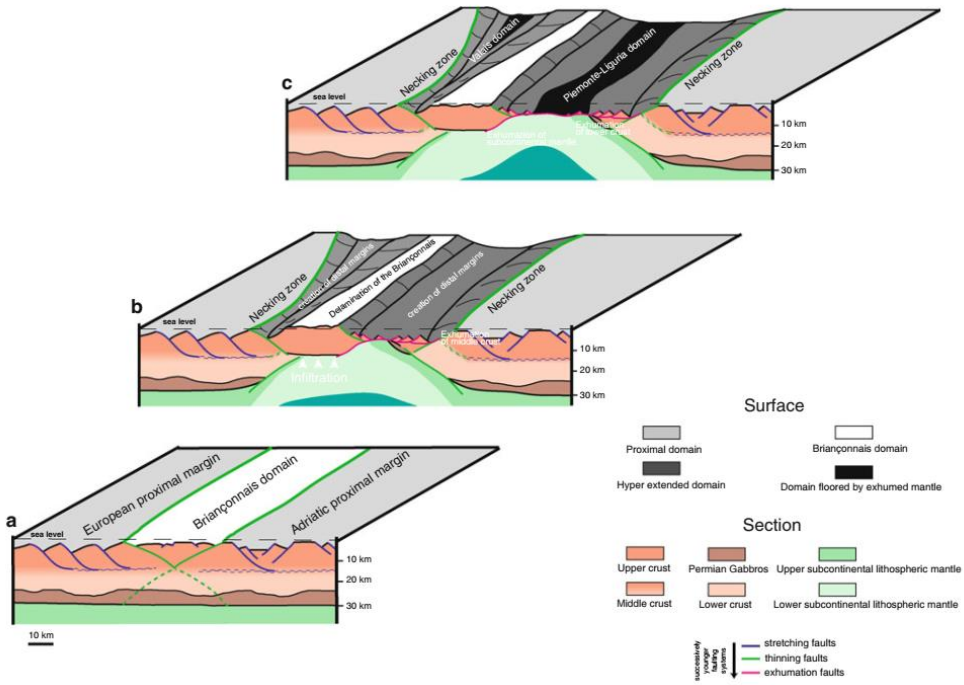

Figure 25 Conceptual 3D model showing the temporal and spatial evolution of the Alpine domain from onset of rifting to final rifting (from Mohn et al., 2010). a) Early rifting (stretching) phase characterized by distributed faultbounded basins that can be found across the whole future margin. b) Late rifting (thinning) phase during which the extension is localized in the Proto Valais and Piedmont-Liguria domains. Note that during this stage, the distal margin is undergoing extreme crustal thinning. Note also that the Briançonnais domain is delaminated and uplifted during this stage. c) Onset of mantle exhumation in the Valais and Piedmont-Liguria Basins. Note that the Valais is interpreted to die out laterally, whereas the Piedmont-Liguria basin is evolving into an embryonic oceanic domain.

Figure 26 (next page) Conceptual processes of fluid migration from Pinto et al. (2015). (a) Flow of mantle-reacted fluids along the active segment of the detachment fault. At the point x, the detachment is active and probably with undeveloped gouges. At the point y, the detachment is active and gouge are well-developed. At the point z, the detachment is inactive. Fluid migration is recorded at the points x and y but not at z. (b) Maximum depth for serpentinization is limited around the 400°C isotherm. The high geothermal gradient may play an important role in the remobilization of elements by controlling convective cells. (c) Direct migration of mantle-reacted fluids toward syn-tectonic sediments in the supra-detachment basin. (d) Seawater Pollution by the rising

plume of mantle-reacted fluids spreading in the seawater and interacting with the post tectonic sediments, which is contemporaneous with serpentinization and mantle-exhumation. Note that the segment of detachment fault is active in the zone of exhumed continental mantle but inactive below the supra-detachment basin (Saluver C).

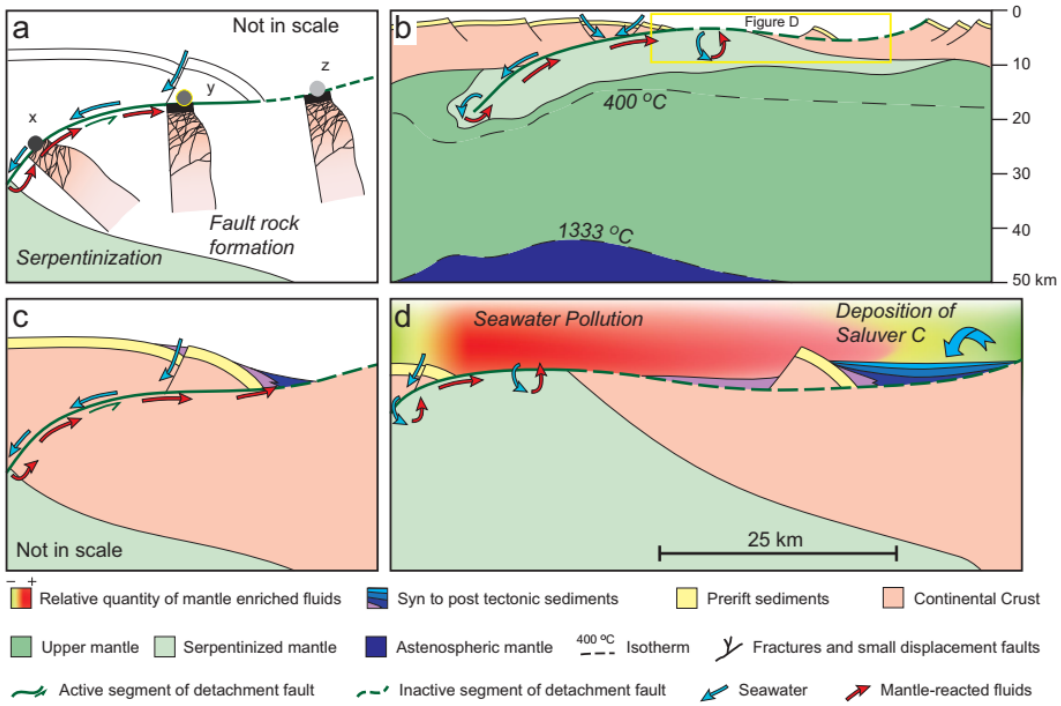

Regarding oceanic lithosphere, it is generally exhumed along features known as oceanic core complexes (OCCs). OCCs are geological features well-recognized along both modern and fossil slow-spreading mid-oceanic ridges (Ildefonse et al., 2007; Miranda et al., 2010; Balestro et al., 2015; Festa et al., 2015; Lagabrielle et al., 2015; Festa et al., 2021). OCCs are characterized by dome-shaped bodies of gabbroic rocks as well as serpentinized mantle, embedded in predominantly volcanic rocks and covered with (meta-)sedimentary clastic rocks (Figure 27). Locally, wedges of volcanic rocks occur at the serpentinized mantle-mafic extrusives transition and are known as “rider blocks” or “rafts” (Karson and Winters, 1992; Cann et al., 1997; Karson et al., 2006; Choi & Buck, 2012).

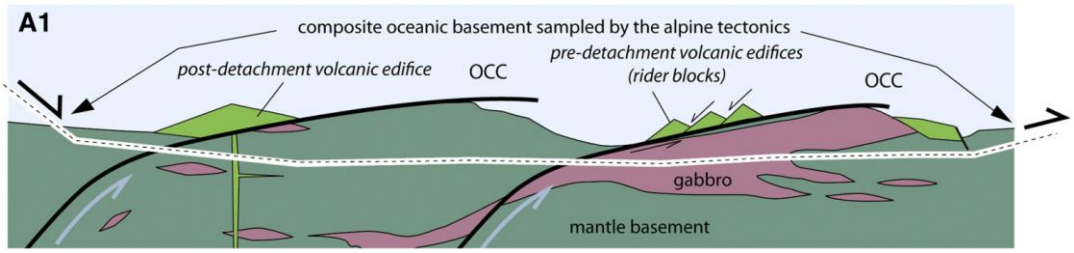

Figure 27 (next page) Reconstruction of the Tethyan oceanic basement from Lagabrielle et al. (2015) involving exhumation of deep rocks along two detachment faults with similar orientation (A1). One detachment leads to a

mantle osted OCC (left), the other one to a gabbro-hosted OCC (right). Note the particular position for the formation of rider blocks in the hanging wall of a gabbro OCC.

These fault-bounded blocks of hanging wall can correspond to the detachment itself, and can possibly form isolated extensional allochthons (Coltat et al., 2020). In the internal evolution of the Alpine Tethys, four main stages can be recognized (Balestro et al., 2019; Figure 28). A first magmatic event is responsible for the emplacement of large gabbroic bodies in Middle Jurassic. This event is followed by a second stage of upper mantle peridotite and gabbro exhumation on the seafloor, and extensive serpentinization. In this context, serpentinized mantle and gabbro in the footwall of detachment faults become oceanic core complexes. This extension is then sealed by basaltic lava flows and emplacement of several ophiolitic breccias, representing the syn-rift volcano-sedimentary sequence. The last stage is related to the deposition of the post-rift sequence, made of discontinuous radiolarian meta-chert, minor marble and widespread calcschist.

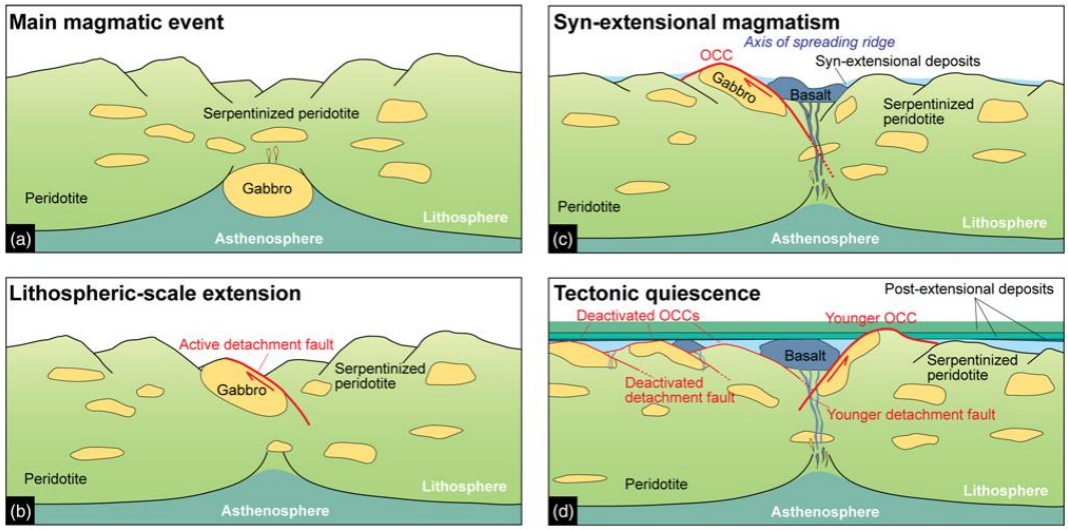

Figure 28 Sequential tectonic diagrams from Balestro et al. (2019) depicting the four main stages of the evolution of the Western Alps ophiolites emplacement (modified from Ildefonse et al. 2007). (a) Main magmatic event (Stage 1). (b) Lithospheric-scale extension and upper mantle exhumation controlled by detachment faulting (Stage 2). (c) Syn-extensional volcanism and sedimentation on the exhumed detachment fault and upper mantle peridotites (Stage 3). This stage corresponds to the seafloor spreading and oceanic core complex (OCC) development episode along a slow-spreading ridge system within the Ligurian–Piedmont Ocean. (d) Tectonic quiescence phase and deposition of the post-extensional sedimentary sequence (Stage 4).

Regarding the internal composition of the post-rift cover, its detailed lithostratigraphic features are very much sensible to the original paleogeographic setting and different successions of reference have been reported (see Tartarotti et al., 2021 and Festa et al., 2021 for a review). In general, two main kinds of supra-

ophiolitic cover sequence can be found (see Tartarotti et al., 2021; Figure 29): i) complete successions, generally related to structural lows, and ii) reduced successions, related to structural highs. Moreover, at different lithostratigraphic levels, mass-transport and chaotic deposits occur widespread through the oceanic units of the Alps (Festa et al., 2021). These kind of deposits have been variably ascribed to seafloor spreading or subduction zone tectonics (Figure 30).

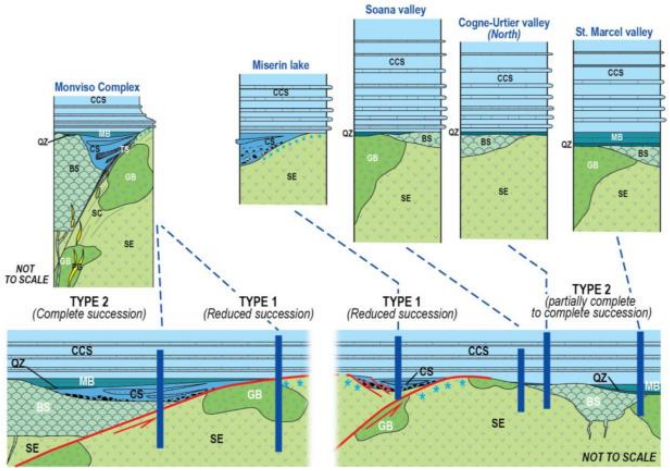

Figure 29 Conceptual model modified from Tartarotti et al. (2021) illustrating interpretative reconstructions of the Jurassic Ligurian-Piedmont paleo-structure as deduced from the metasedimentary successions of the Aosta Valley and Monviso areas. The stratigraphic columnar sections of the studied areas (above) are tentatively projected to the inferred location within the reconstructed Jurassic ocean (middle).

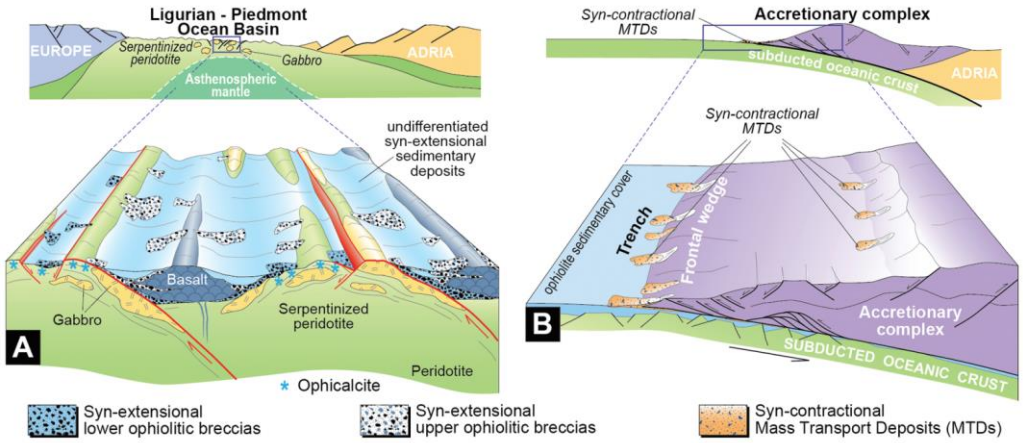

Figure 30 Interpretative block diagrams from Festa et al. (2021) depicting the geodynamic and tectonostratigraphic depositional setting for syn-extensional, lower and upper ophiolitic breccias, and syn-contractional mass-transport deposits during (A) the Middle–Late Jurassic seafloor spreading and (B) Late Cretaceous–Paleocene convergence tectonic stages of the evolution of the Western Tethyan realm (Ligurian-Piedmont Ocean Basin), respectively.

CHAPTER 3

Common methodologies

For the production of this Thesis, the same analytical routine was followed for all the investigated units, changing only in same cases the mode of operation, based on the amount of previous works and data available for each unit.

The research applied the following methodologies: i) field mapping, ii) optical microscope analyses and observations, iii) SEM-EDS analysis and, in most cases, iv) acquisition of high-resolution multispectral maps, used to derive effective bulk compositions of various samples and, eventually, thermodynamic modeling of Alpine metamorphic conditions.

- Field mapping, carried out in some areas already since 2016 (for my Master degree Thesis), permitted to define the geometric relationships among different lithologies and among different rock volumes, in order to organize and constrain the various lithostratigraphic successions; field mapping led to the production of several geological maps reported in this Thesis and in the cited published papers. Symbols used for structural elements are S for schistosity, D for deformation event, A for folds axis, and L for stretching lineation;
- Optical microscope observations were fundamental in order to constrain the tectono-metamorphic evolution and internal history of each collected sample and its correlation to field geometries and structural evolution. For every analyzed unit, more than 50 thin sections have been analyzed and studied. Optical microscopy was essential in order to determine the most interesting rock samples to analyze with SEM-EDS;
- For mineral chemistry and petrography, a Scanning Electron Microscope (i.e. SEM, JEOL JSM-IT300LV) equipped with an energy-dispersive X-ray spectrometer (EDX), with an SDD (a silicon drift detector from Oxford Instruments), hosted at the Dipartimento di Scienze della Terra of the Università degli Studi di Torino, was used for the determination of major elements. The experimental conditions include: accelerating voltage 15 kV, 1 nA probe current, counting time 50 s, process time 5 μs, and a working distance of 10 mm. The measurements were conducted in high vacuum conditions. The EDX acquired spectra were corrected and calibrated both in energy and in intensity thanks to measurements performed on cobalt standard introduced in the vacuum chamber with the samples. The Microanalysis Suite Oxford INCA Energy 300, which enables spectra visualization and elements recognition, was employed. A ZAF data reduction program was used for spectra quantification. The resulting full quantitative analyses were performed, using natural oxides and silicates from Astimex Scientific

Limited, as standards. All the analyses were recalculated using the MINSORT computer software (Petrakakis and Dietrich, 1985); structural formulae for the mineral phases from the Chenaillet ophiolite were calculated using 190 algorithms in XMapTools (Lanari et al., 2019 and references therein). Potassic white micas have been classified as muscovite or phengite according to their Al_{tot}/Si ratio (i.e. muscovite: Al_{tot}>5.00, Si<3.30; phengite: Al_{tot}<5.00, Si>3.30). X_{Mg} of amphiboles, chloritoid, chlorite, white mica, and pumpellyite is defined as $Mg/(Mg+Fe^{2+})$. X_{Zo} in epidote-group minerals is defined as $Al/(Al+Fe^{3+})$. Mineral abbreviations are according to Whitney & Evans (2010), with the exception of Wm (potassic white mica), LT-amp (general low T, Ca-amphibole), and HT-amp (general high T, Ca-amphibole);

- High-resolution multispectral maps of the thin sections used for deriving the effective bulk compositions of the investigated samples were obtained using the same SEM-EDS instrument. Operative conditions used for mapping the entire thin sections were: 15 kV accelerating voltage, 5 nA probe current, 1 µs EDS process time, 10^5 cnts/s, 2.5 µm point step, 1 msec dwell time. The raw data were processed using the MultiSpec© software to obtain the modal compositions (vol% of all the minerals). Bulk rock compositions, were then calculated by combining the mineral proportions obtained from the quantitative modal estimates of SEM-EDS multispectral maps with mineral chemistry acquired at SEM-EDS. Isochemical phase diagrams were all carried out with the Perple_X software package. However, reader should refer to single chapter/unit for a complete discussion, since different versions of the software were used and different chemical systems were taken into account.

CHAPTER 4

The M. Banchetta – P. Rognosa tectonic unit

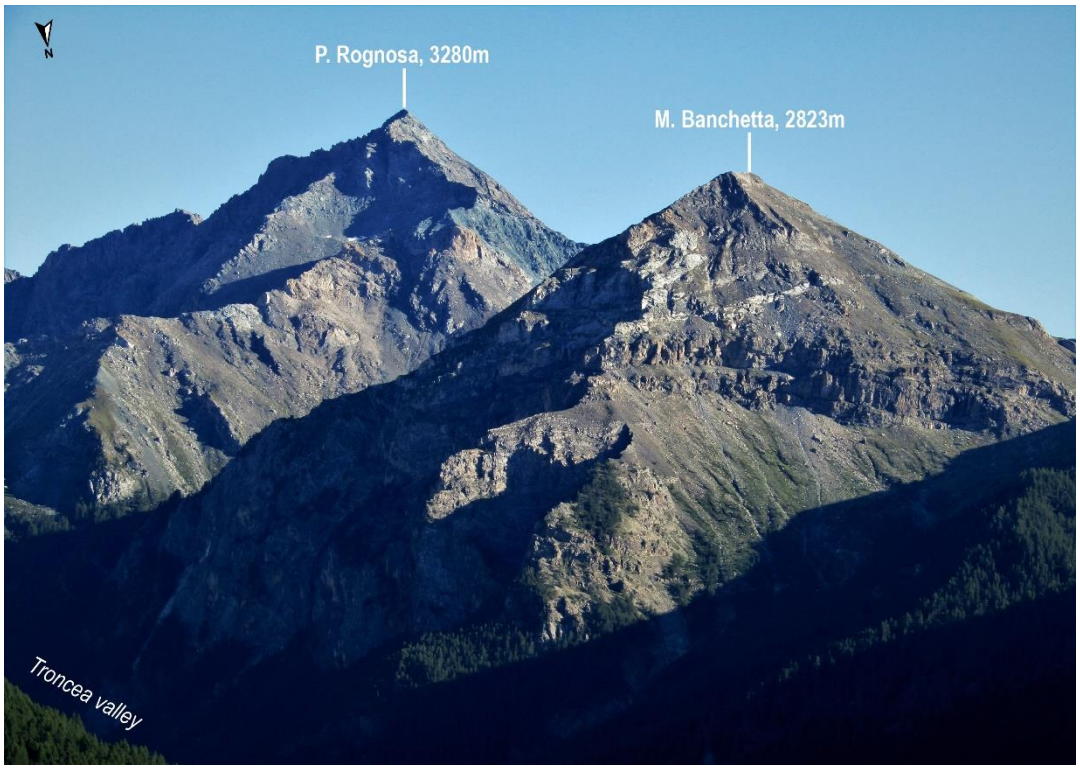

Figure 31 Landscape of the M. Banchetta (on the right) and P. Rognosa (on the left), on the left side of the Troncea valley (lower left of the picture).

4.1. Introduction

The Banchetta-Rognosa tectonic unit (BRU hereafter) crops out within an area of 10 km^2 on the mountain ridge between Troncea and Chisonetto valleys (upper Chisone valley; Figure 31), where it is tectonically juxtaposed to several oceanic units (Servizio Geologico d'Italia, 2020). This unit consists of two successions respectively recording the Mesozoic tectono-depositional evolution of (i) a continental margin, i.e. Monte Banchetta succession, and (ii) a neighboring oceanic sector, i.e. Punta Rognosa succession.

Based on Corno et al. (2021a), this chapter deals with the lithostratigraphy and structural evolution of these continental and oceanic successions forming the BRU. The result of new, extensive and detailed lithostratigraphic and structural field studies (supported by petrographic analyses) are reported in the 1:6,500 scale "Geological map of the Monte Banchetta – Punta Rognosa area (Troncea valley, Western Alps)", attached at the end of this Thesis in Appendix I.

In general, field mapping, stratigraphic and sedimentological analyses, also supported by petrological studies, are the starting point to define which geological process is responsible for the present juxtaposition of continental crust, mantle and sediments in the Alpine belt. The following processes can be taken into: i) subduction and/or exhumation tectonics, ii) rift-related extension, or iii) sedimentary mélanges (e.g. Beltrando et al., 2014 and references therein for detailed review). This allows to define the architecture of the pre-orogenic paleogeography (from proximal-distal margin to oceanic domain) involved in the Alpine Orogeny. Numerous researches are devoted to better improve the knowledge of the Alpine pre-orogenic paleogeography in terms of structural domains and dominant processes (e.g. Mohn et al., 2010, 2014; Masini et al., 2013; Beltrando et al., 2014; Decarlis et al., 2015; Balestro et al., 2022). The pre-orogenic setting may have played a fundamental control since the earliest stages of convergence in the Alpine orogeny (Mohn et al., 2010, 2014; Beltrando et al., 2014).

Whilst the pre-orogenic relationships are best recognizable in those sectors that escaped the pervasive Alpine deformation (such as the Central Alps), they are very difficult to decipher in the Alpine axial sector. In this sector, the Tertiary orogenic-related tectono-metamorphic evolution (e.g. Dal Piaz et al., 2001; Beltrando et al., 2010a; Dal Piaz, 2010; Villa et al., 2014) may have modified and/or reworked primary stratigraphic relationships between syn-to-post rift sediments and adjacent continental crust or ophiolites.

Based on accurate field studies supported by petrological and petrographic analyses, the main purposes of the ‘Geology of the Monte Banchetta – Punta Rognosa area (Troncea valley, Western Alps)’ (see enclosed Main Map of Corno et al., 2021a) are i) to propose a much more detailed geological map of this area than previously documented, and ii) to illustrate new details on the lithostratigraphy of the continental and oceanic related rock successions despite late overprinting deformation. Therefore, the map gives significant contributions to interpret pre-orogenic relationship between continental and oceanic successions, today outcropping in the highly imbricated tectonic setting of the Alpine axial belt.

4.1.1 Map design

The main map (Appendix I) covers an area of about 10 km2 at an altitude between 1800m and 3280m a.s.l and the map scale is 1: 6,500 (even if the complexity of the area imposed a few auxiliary maps and more detailed investigations in some areas). Lithological and structural data were stored in a GIS database using the UMT WGS84 reference system, and all topographic elements (contour lines, hydrography, buildings and roads) have been derived from the vector map “Carta Tecnica Regionale Vettoriale at 1: 10,000 scale of the Regione Piemonte (vector_10 series, Edition 1991 – 2005)”.

The structural architecture and geological setting are illustrated in six cross sections and in a tectonic sketch map, where geological interpretation and generalization of outcrops and structures are provided. Overprinting relationships of structural elements (from outcrop to thin-section scale) and their relative metamorphic conditions have been considered for the identification of deformation phases (labelled D with subscript numbers on the basis of their chronological order). Symbols used for structural elements are S for schistosity, A for folds axis and L for stretching lineation.

The most penetrative schistosity at the outcrop scale is S2, which represented during the geological mapping the main foliation for the identification and correlation of tectonic features at map scale. Structural elements (S, A and L) are plotted in eighteen equal-area lower hemisphere stereographic projections, referred to ten sub-areas.

Minerals abbreviations in the map and in the figures of the following text are from Whitney & Evans (2010), integrated with the acronym Wm used for white mica.

No paleontological data exist for the successions exposed in the mapped area. Therefore, the ages of the distinguished lithologies are inferred by published papers and/or geological maps (e.g. Caron, 1971; Barfety et al. 1995; Polino et al., 2002; Mohn et al., 2010; Piana et al., 2017 and references therein) or on the basis of their stratigraphic positions.

The geological map was digitalized using ESRI ArcGIS v. 10.3, its final layout has been edited using Adobe Illustrator®. Structural data have been projected with the software StereoNet®. The cross sections presented in the geological map and the photographs were edited with Adobe Illustrator®.

Figure 32 (next page) from Corno et al., 2021a. (a) tectonic sketch map of the Western Alps. Red box is the location of *Figure 32*(b). (b) tectonic sketch map of the investigated region (from Corno et al., 2019; Servizio Geologico d'Italia, 2020). (c) line drawing on photograph of the Monte Banchetta east face and Punta Rognosa north-east face. Acronyms are: CB – continental basement rocks, CC – continental metasedimentary cover, OB – serpentinized mantle, OC – oceanic metasedimentary cover, LP – Liguria-PiemonteTectonic Units, IS – La Tuccia Incertae Sedis and Q-undifferentiated Quaternary deposits. The legend of the lines drawn in the picture is reported in the Geological Map attached at the end of this Thesis.

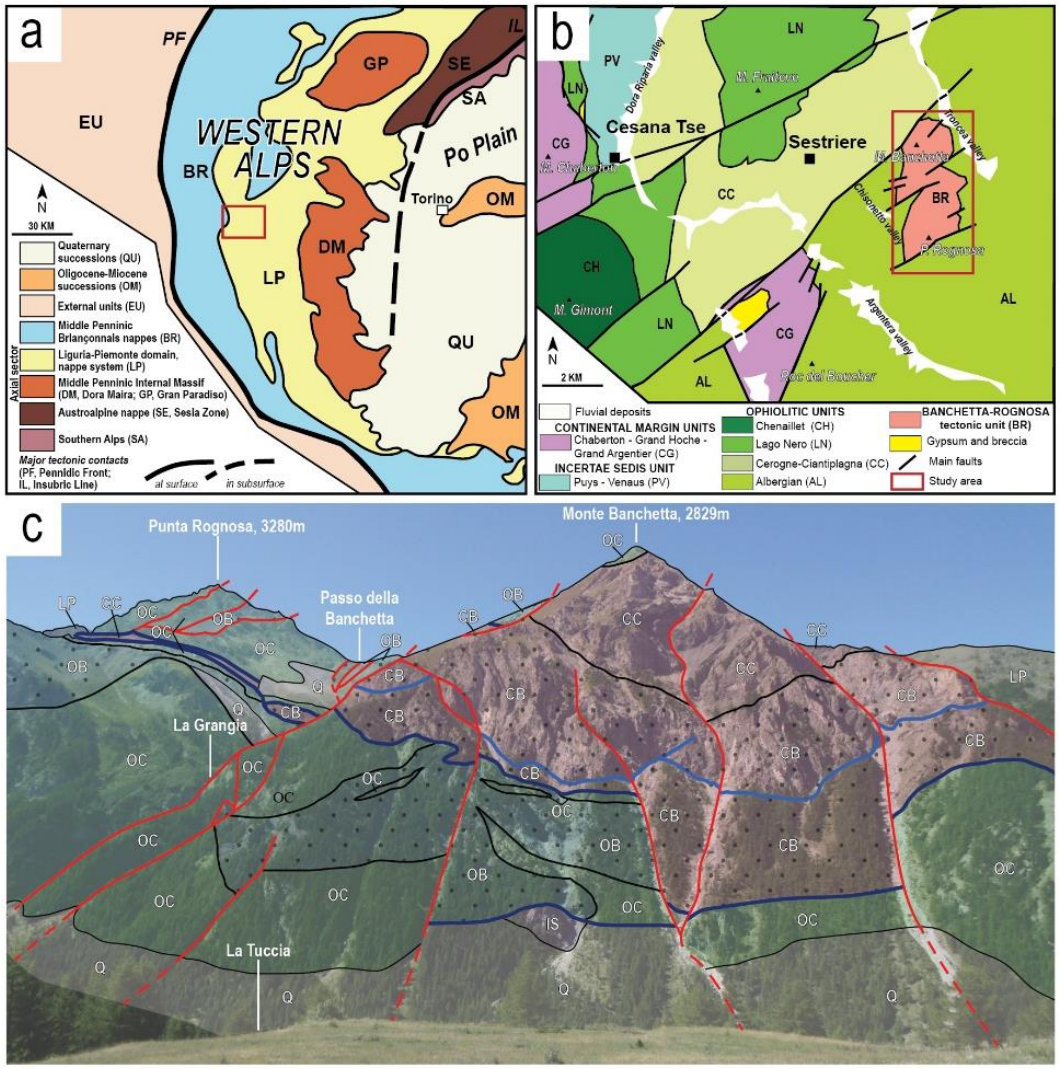

4.2 Relationships between oceanic and continental successions

4.2.1 The Monte Banchetta – Punta Rognosa tectonic unit

4.2.1.1 The Punta Rognosa succession (Ligurian-Piedmont oceanic domain)

The Punta Rognosa succession consists of oceanic basement and its own stratigraphic cover. The serpentinized mantle (OCs), locally preserving pyroxene relics (cm in size) of the original peridotite, grades upwards to meta-ophicarbonate rocks (OCof) characterized by serpentinite fragments (up to 50cm) within a matrix of serpentine + chlorite + amphibole and displaying an irregular network of calcite veins.

Serpentinite and meta-ophicarbonate rocks are often directly overlain by a polymictic meta-breccia (OCbr), reaching a thickness up to 30m, characterized by clasts of oceanic and continental origin. The matrix of the meta-breccia is made of carbonate+ chlorite + Ca-amphibole and widespread fine-grained Fe-oxides, and the embedded clasts and blocks (Figure 33a-b) consist of serpentinite and meta-ophicarbonate rocks (of), micaschist and gneiss (co), and dolostone and dolomitic breccia (bl1). Locally (e.g. gorge north of La Grangia, Monte Banchetta eastern side), blocks of dolostone (bl1) lie directly on the serpentinized mantle. On the western side of Monte Banchetta (east of the upper chairlift departure station) the polymictic meta-breccia contains a metric block of meta-gabbro (g), characterized by large pseudomorphs after magmatic plagioclase consisting of epidote + white mica + albite and a recrystallized fine-grained matrix made of omphacite ± aegirine augite + Mg-chlorite + epidote + phengite (Corno et al., 2019). Up section, the polymictic metabreccia grades into a fine-grained impure marble (~10m thick) defining then a broad fining upward sequence. The observed stratigraphic relationships suggest a Middle to Late Jurassic age for the polymictic meta-breccia.

Laterally discontinuous bodies of metasandstone (OCq; Figure 33c), up to 15m thick and 50-60m long, are usually observed on the top of the polymictic meta-breccia or locally directly above serpentinite and meta-ophicarbonate rocks. This lithology consists of quartz + phengite + muscovite + chlorite + Fe-oxides aggregates (up to cm in size), and has a few (<50cm thick) green to blueish metabasic levels made of chlorite + glaucophane ± detrital allanite. In its uppermost part, the metasandstone contains bodies of dolostone and dolomitic breccias (bl2), centimetric (Figure 33c) to plurimetric in size. The supposed age of the metasandstone is Middle to Upper Jurassic.

Serpentinized mantle and the overlying sediments are unconformable covered by ophiolite-bearing carbonate-micaschist (csO; Figure 33d) of Upper Jurassic-Cretaceous age. It consists of carbonates + quartz + muscovite + phengite + chlorite, and preserve pseudomorphs after lawsonite. The csO presents intercalations of black and green schists with garnet + stilpnomelane + opaque minerals + Mn and Fe carbonate minerals.

The carbonate-micaschists embed isolated sheared bodies of serpentinite (s) and metabasite (m; Figure 33d) from metric to pluri-decametric in size (eastern side of M. Banchetta, just above the valley floor in front of Seytes village). The metabasite is made of glaucophane + tremolite ± aegirine-augite + chlorite + epidote + rutile + phengite + muscovite + pumpellyite assemblage.

As observed south of Passo della Banchetta, the carbonate-micaschist (csO) overlays blocks of dolomitic breccia (bl1), up to hectometric in size, resting directly on the serpentinized mantle.

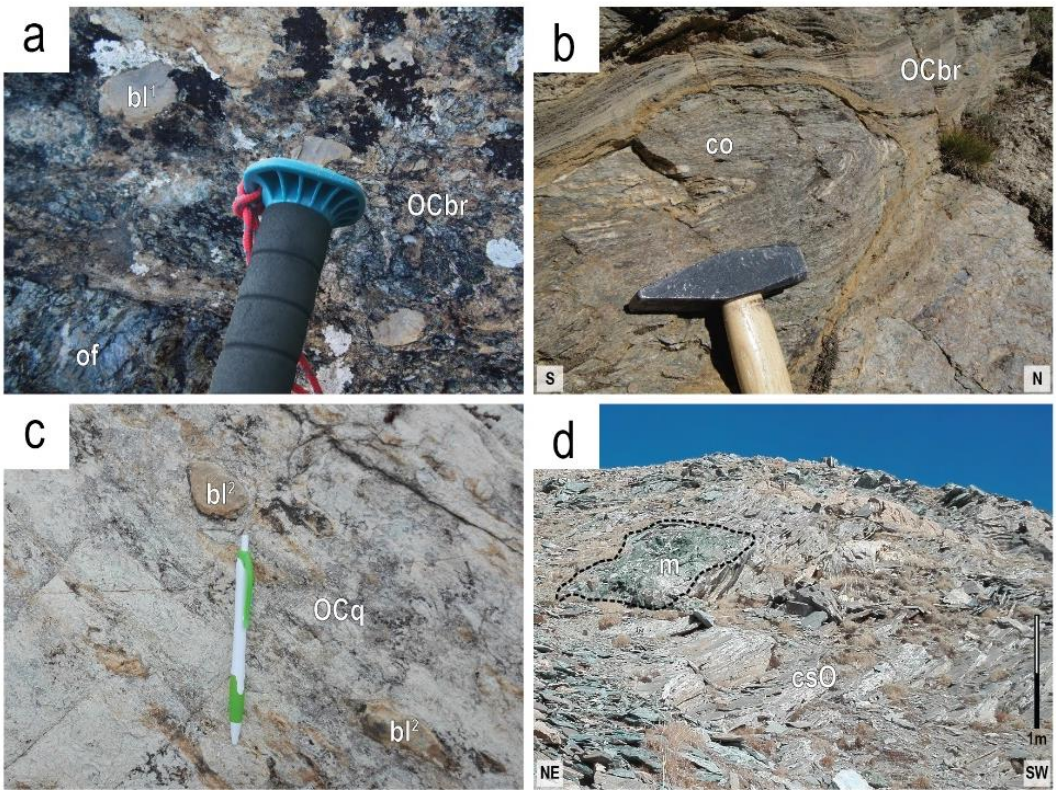

Figure 33 Representative lithologies of the Punta Rognosa succession from Corno et al., 2021a: (a) clasts of meta-ophicarbonate rock (of) and dolostone (bl1) in the polymictic meta-breccia (OCbr; Monte Banchetta south-western side, 2400 m); (b) continental clast (co – gneissic micaschist) in the polymictic meta-breccia (OCbr; Monte Banchetta summit, 2823 m); (c) dolomitic clasts (bl2) in the upper part of a discontinuous body of metasandstone (OCq; south-east of Passo della Banchetta, 2710 m); (d) metabasite (m) in carbonate-micaschist (csO; south-west of Monte Banchetta, 2750 m).

4.2.1.2 The Monte Banchetta succession (continental margin)

Two main associations of continental basement rocks, here considered as Paleozoic in age, have been identified.

Dark grey gneiss with minor occurrence of micaschists (CBpm; Figure 34a) crop out south of La Grangia (in the southern-central sector of the map). These rocks consist of quartz + muscovite + phengite + paragonite + jadeite + chloritoid + chlorite + allanite assemblages, and at the outcrop scale they have several intercalations (thickness < 1-2m) of graphite bearing dark schist, marble and metabasite.

Along the eastern slope of the Monte Banchetta, the continental basement outcrops are widely represented by white-greyish micaschists (CBm; Figure 34b) made of quartz + muscovite + phengite + paragonite + chlorite + albite + epidote ± glaucophane, and containing levels, up to plurimetric in size, of fine-grained gneiss

(gn), glaucophane + chloritoid-bearing micaschist (cld; Figure 34b), and white quartzite (mq). In the southern part of the map, south-west of La Grangia, a pluridecametric glaucophane + garnet meta-diorite (md), preserving magmatic K-feldspar, has been observed embedded within the micaschist.

The basement rocks are unconformable overlain by siliciclastic deposits (CBq; Figure 34c-d), reaching maximum thickness of about ten meters. These are quartzite and quartz metaconglomerate (locally characterized by mm to cm-sized clasts of pink quartz) upward passing to massive phengite-bearing quartzite. These deposits are correlated with the Upper Permian (?) to Lower Triassic quartzitic deposits extensively occurring through the Western Alps.

Up section, a Middle to Upper Triassic dolomitic sequence, reaching a thickness up to 200m, consists of well-stratified dolostone (locally exposed west of La Tuccia) overlain by clast-supported monomictic meta-breccia (CBd; FFigure 34d). The dolomitic meta-breccia is made of poly-dolomitic clasts (up to dm in size) within a dolomitic matrix. Locally, discontinuous plurimetric-thick levels of black shale, carbonate schist and phyllite occur through the sequence.

The dolomitic sequence is unconformable overlain by a detrital sequence (up to 200m thick) including carbonate-bearing quartzite (CBsq), black micaschist (CBbs) and polymictic meta-breccia (Cbdq).

The lower part of the detrital sequence consists of carbonate-bearing quartzite (CBsq), composed of quartz + muscovite + phengite and variable amount of calcite and ankerite. Up section it passes to a black micaschist (CBbs) consisting of graphite + muscovite + phengite + chlorite + calcite + dolomite + quartz and has pseudomorphs after lawsonite. This black micaschist is interleaved with polymictic meta-breccia (Cbdq; Figure 34e) and seems to embed a few portions of this lithology. The polymictic meta-breccia is composed of dolostone and quartzite clasts (Figure 34f) in a carbonate matrix containing minor fuchsite, talc and detrital K-feldspar. In the uppermost part of the polymictic meta-breccia (exposed on the western side of Monte Banchetta, north of the upper chairlift departure station), a level of impure quartzite (qr) contains dolostone clasts up to decimetric in size.

The uppermost lithostratigraphic levels of the Monte Banchetta succession consist of a carbonate-micaschist (csC), laterally passing to that (CsO) resting on the Punta Rognosa succession.

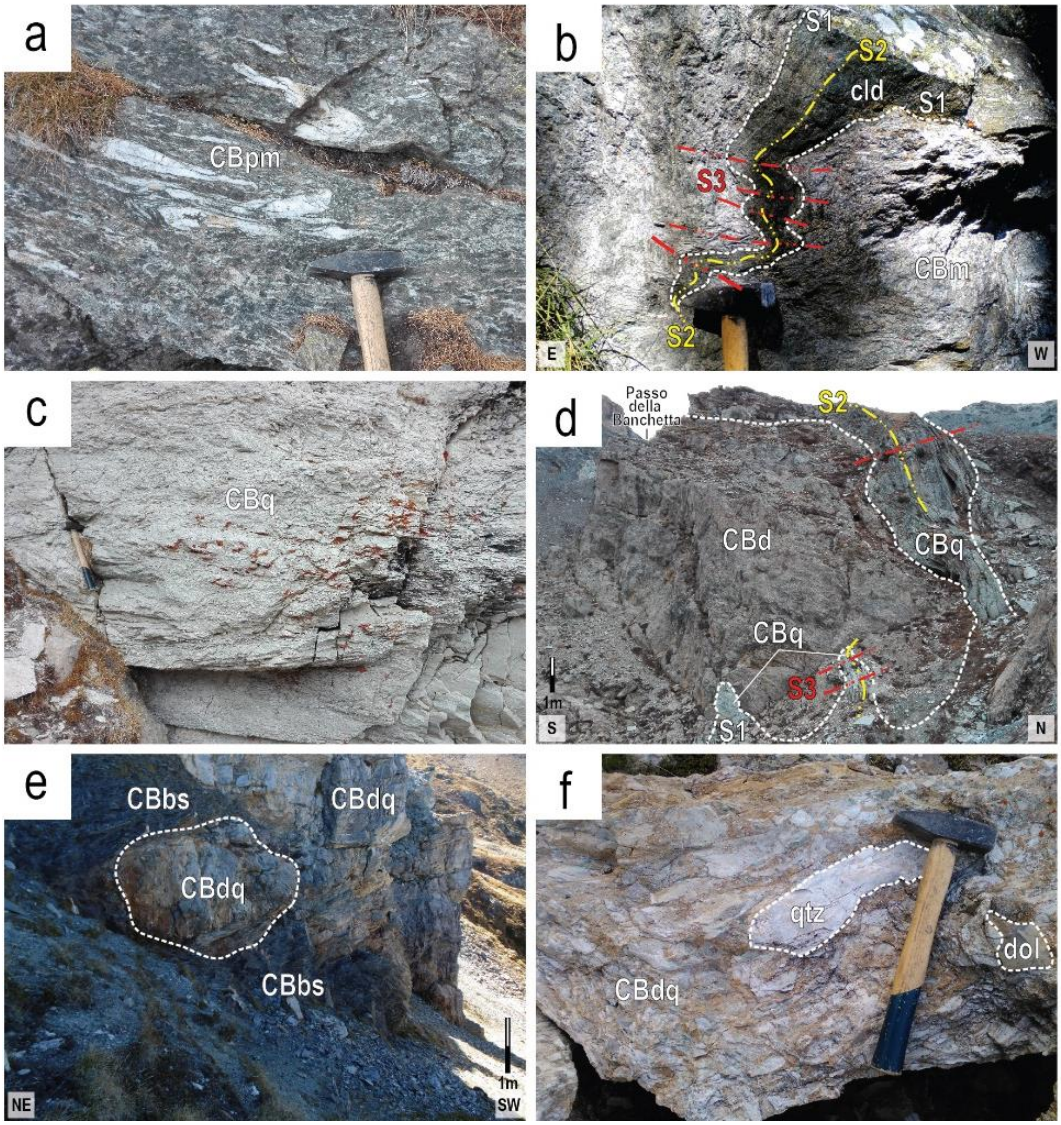

Figure 34 Representative lithologies of the Monte Banchetta succession from Corno et al., 2021a: (a) polydeformed Jd-bearing gneiss (CBpm; south of La Grangia, 2300 m); (b) Gln + Cld-bearing micaschist level (cld) folded together with micaschist (CBm), D3 folds (with incipient S3 axial plane schistosity) overprint a D2 fold hinge (Monte Banchetta eastern side, 2020 m); (c) white-greenish Phe-bearing quartzite (CBq; west of Passo della Banchetta, 2400 m); (d) Phengite-bearing quartzite (CBq) folded together with dolomitic meta-breccia (CBd), a major overturned D2 fold is overprinted by minor D3 folds (east of Passo della Banchetta, 2400 m); (e) heteropic relationship between black micaschist (CBbm) and meta-breccia with dolostone and quartzite clast (CBdq; south-west of Clot della Mutta, 2450 m); (f) detail of dolostone (dol) and quartzite (qtz) clasts within clast-supported carbonate meta-breccia (CBdq; north of Monte Banchetta, 2400 m).

4.2.2 Ligurian-Piedmont tectonic units

The BRU is tectonically bounded by the Albergian Unit (LPa) to the south and the Cerogne-Ciantiplagna Unit (LPcc) to the north. These units consist of Cretaceous carbonate-micaschist made of carbonate minerals + quartz + white mica + chlorite +

graphite, embedding locally pluri-decimetric meta-ophiolitic bodies (not reported in the map).

4.2.3 La Tuccia *incertae sedis* tectonic unit

On the eastern side of Monte Banchetta, just above the valley floor close to La Tuccia, the Punta Rognosa succession is tectonically juxtaposed to a pluri-decametric body of mica-bearing dolomitic marble and clast-supported dolomitic meta-breccia. Due to the complicate tectonic relationships with neighboring rocks, these dolomitic rocks are referred to as an Incertae Sedis unit. A Triassic age can be supposed for these dolomitic rocks.

4.3 Structural evolution of the Banchetta –Rognosa tectonic unit

Structural and petrographic data reveal for the Monte Banchetta and the Punta Rognosa successions a common structural evolution consisting of three tectono-metamorphic deformation phases, labelled from D1 to D3, and a late D4 deformation phase.

The D1 is the first tectono-metamorphic deformation phase observed. At the outcrop scale, the S1 is well recognizable only in quartzitic and dolomitic rocks (see cross-section F-F' in the map), while at the microscale it is usually preserved as microlithons and/or intrafolial folds. The S1, resulting parallel to the original compositional banding of the rocks (Figure 34b-d), is characterized by assemblages developed at the transition between lawsonite- and epidote- blueschist facies conditions (see Chapter 5 form Corno et al., 2019): this is constrained by omphacite + zoisite + glaucophane + rutile paragenesis in the basic system, quartz + phengite + chloritoid + jadeite + rutile paragenesis in the quartz-feldspatic system and quartz + phengite + chloritoid + glaucophane + graphite + rutile paragenesis in the pelitic system. A pre-D1 metamorphic event has been only locally recorded by growth of lawsonite, now completely pseudomorphosed, in carbonate-micaschist mapped as csC and CBbs of the Monte Banchetta succession and csO of the Punta Rognosa succession respectively (see Chapter 5 from Corno et al., 2019). The D2 tectono-metamorphic deformation phase led to the development of tight to isoclinal folds, from outcrop to thin section scale (Figure 34b-d and Figure 35a), whose axial plain schistosity (S2) is usually the most penetrative planar fabrics in the field. The S2, developed under epidote-blueschist facies conditions, is characterized by glaucophane + epidote + phengite paragenesis in the basic system (Figure 35b), and quartz + phengite + paragonite + chloritoid paragenesis in the pelitic system. At the map scale, the S2 generally dips to the W-NW and contains a L2 stretching lineation

marked by alignment of phengite, glaucophane and chloritoid. At the outcrop scale, the L2 has been observed to be sub-parallel to A2 fold axis, highlighting non-cylindrical folding during D2 deformation (see cross-section D-D'). A2 fold axes are NE-SW trending.

Major tectonic contacts between the Monte Banchetta and the Punta Rognosa successions, as well as their minor intra-succession tectonic contacts, were deformed since the earliest deformation phases (D1-D2). The D3 tectono-metamorphic deformation phase overprints previous D1 and D2 planar and linear tectonic features. It is characterized by meso- to large-scale folds with generally sub-horizontal ENE-WSW trending A3 axes and axial planes dipping towards SSE at high angle (see cross-section C-C'''). Locally, the D3 develops an incipient S3 crenulation cleavage in the micaschist and carbonate-micaschist (Figure 35c) defined by chlorite ± stilpnomelane occurrence. The D3 is associated with blastesis typical of greenschist facies conditions, replacing D2 mineral assemblages (Figure 35d): muscovite + tremolite + chlorite + albite + stilpnomelane ± epidote in the basic system and of quartz + muscovite + chlorite + albite in the pelitic system. The late D4 deformation phase is responsible for gentle km-scale folding recognizable at the map scale, characterized by N-S trending axes and high-angle dipping axial planes. During D4, major and minor tectonic contacts often show evidences of S-SW extensional reactivation.

The post-D4 faulting is characterized by three major systems oriented ENE-WSW, N-S and NNW-SSE, all revealing often close relationship with morphology. The most relevant systems are ENE-WSW trending right-lateral strike-slip faults and two of these faults separate the BRU to the north and south from the adjacent ophiolitic units. The N-S and NNW-SSE trending systems are high-angle normal to transtensional faults.

Figure 35(next page) Representative meso – and microstructures from Corno et al., 2021a: (a) D2 folds with S2 axial plane foliation in carbonate-micaschist (csO; west of Clot della Mutta, 2400 m); (b) metabasite embedded in the micaschist (CBpm) of the Monte Banchetta succession, displaying S2 pervasive foliation defined by Gln partially replaced by Chl (Plane Polarized Light, PPL); (c) S3 crenulation cleavage growing in carbonate-micaschist (csO) of the Punta Rognosa succession (west of Clot della Mutta, 2350 m); (d) photomicrograph from a level of Gln + Cld micaschist with D2-Gln crystals partially (right) and completely (upper left) replaced by D3 Chl + Ab. Note that Wm + Ep grow both in D2 mineral assemblage and recrystallize during the D3 phase (PPL).

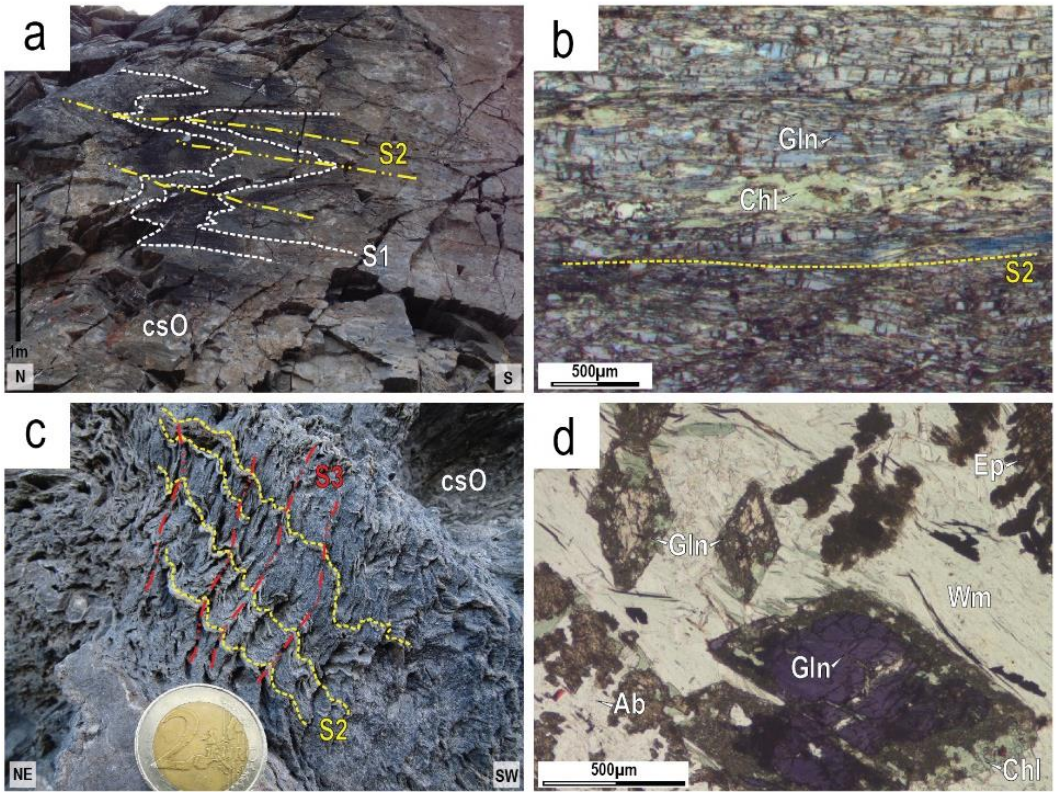

4.4 Main remarks

The 1:6,500 scale "Geological map of the Monte Banchetta – Punta Rognosa area (Troncea valley, Western Alps)" is the result of new, extensive and detailed lithostratigraphic and structural field studies supported by petrographic analyses.

The geology of the mapped area is characterized by the complex juxtaposition of different lithological associations ascribed to the Punta Rognosa succession of oceanic origin and to the Monte Banchetta succession of (European) continental margin origin.

Serpentinite of the Punta Rognosa succession is covered by meta-ophicarbonate rocks followed up section by polymictic metabreccia with continental and oceanic-derived clasts and by siliciclastic deposits (quartz-rich sands). This lithostratigraphy suggests that the BRU includes a segment of exhumed mantle adjacent to continental crust source areas.

In the Monte Banchetta succession, pre-rift rocks (continental basement with dolostone) are covered by syn-rift middle-late Jurassic (?) polymictic metabreccias whose fuchsite (chrome mica) in the matrix can be interpreted as signature of

deposition in sectors proximal to areas floored by mantle exhumation (where pervasive Cr-enriched fluids derive from chromite related to exhumed serpentinites or Mg-Cr gabbros).

The Monte Banchetta and the Punta Rognosa successions share the upper stratigraphic levels consisting of late Jurassic?-Cretaceous post-rift deposits (carbonate-micaschist), distinguished in the map taking into account their deposition on continental or oceanic substratum.

Based on these considerations, the BRU can be inferred as a lithospheric portion where thinned continental crust was adjacent to exhumed mantle, both covered by the same post-rift sediments. This setting can be referred to a distal continental margin that underwent rift-related hyperextension: hence, the BRU represents a remnant of the pre-orogenic setting preserved in the axial sector of the Alpine chain. However, alternative possible processes (syn-orogenic mélanges, possibly reworked) should not be excluded.

The two continental and oceanic successions included in the BRU recorded a common orogenic tectono-metamorphic evolution at least since the D1 deformation phase, therefore from HP/LT to greenschist facies conditions, during which the primary contacts were variably reworked. According to the available literature, the HP-LT D1 and D2 phases can be related to the Eocene subduction history (Dal Piaz et al., 2001; Beltrando et al., 2010a and references therein).

The post-D4 brittle deformation is represented by a fault network characterized by ENE-WSW right-lateral strike-slip faults and N-S and NNW-SSE high-angle normal to transtensional faults that contribute to the shaping of the present-day landscape.

In conclusion, the study of the BRU places emphasis on the role exerted by hyperextension in the development of the pre-collisional Alpine paleogeography, later involved and modified by the complex tectono-metamorphic orogenic evolution. Furthermore, this study confirms that relationships among the different paleo-structural domains must be constrained by accurate field mapping including stratigraphic and sedimentological analyses, and reconstruction of the structural evolution of the different rock volumes supported by petrological studies.

CHAPTER 5

The oceanic succession of the BRU

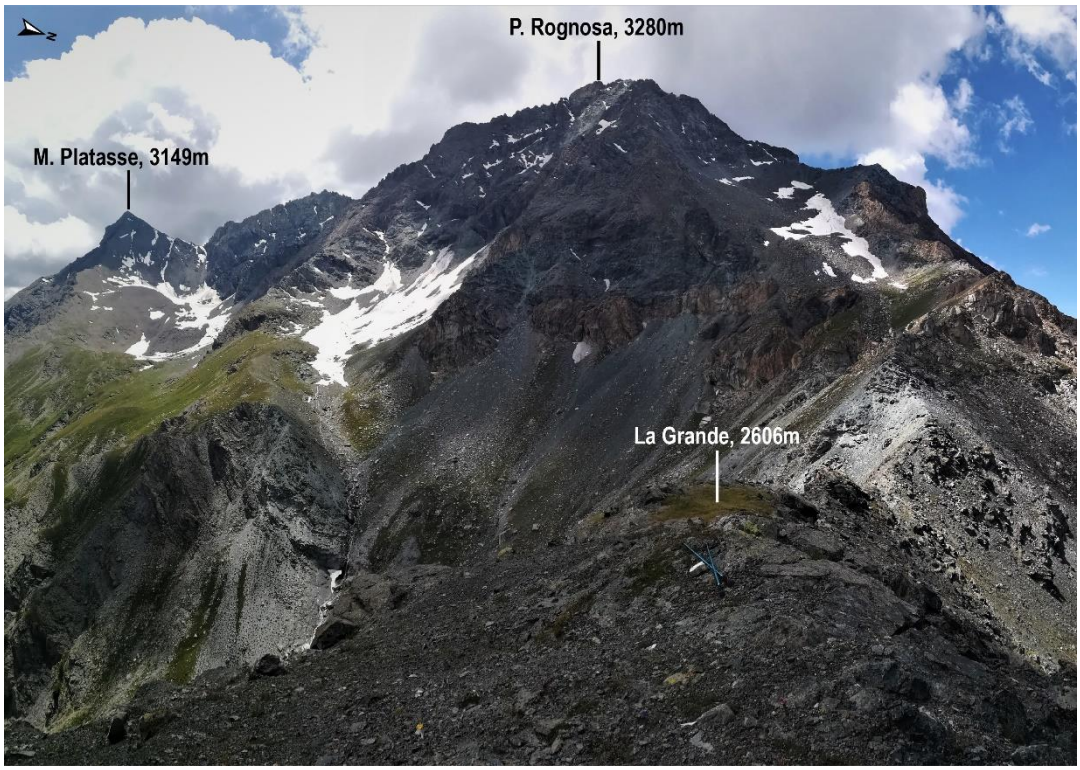

Figure 36 Landscape view of the eastern slopes of the P. Rognosa, made of oceanic-derived rocks of the Banchetta-Rognosa tectonic unit.

5.1. Introduction

As illustrated in the previous Chapter 4, the Banchetta-Rognosa tectonic unit consists of two juxtaposed successions respectively recording the Mesozoic tectono-depositional evolution of (i) a continental margin, i.e. Monte Banchetta succession, and (ii) a neighboring oceanic sector, i.e. Punta Rognosa succession (Figure 36), both covered by the same post-rift sediments consisting of Upper Jurassic?-Cretaceous carbonate micaschist. Based on the published paper Corno et al. (2019), this Chapter 5 focuses on the oceanic succession detailing its lithostratigraphy, petrography and metamorphic evolution.

Figure 37(next page) Lithostratigraphy of the oceanic succession from Corno et al., 2019.

5.2 Lithostratigraphic and petrographic features of the oceanic succession

5.2.1 Lithostratigraphy

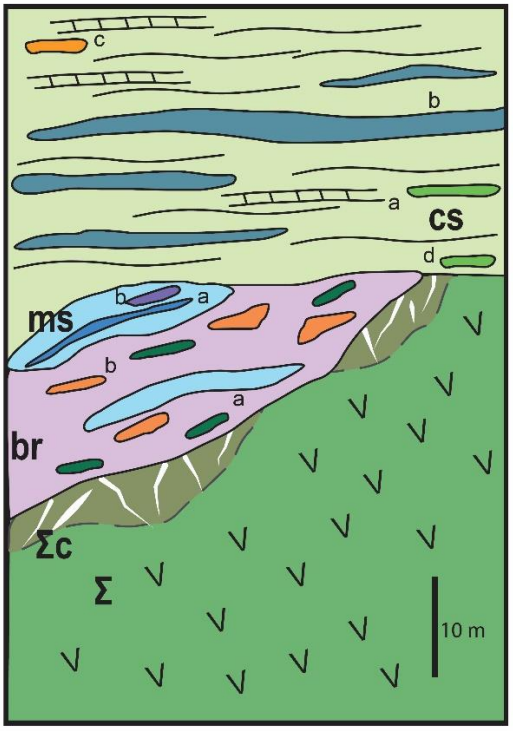

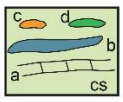

Calcschist (cs) with impure marble (a), black and dark green schist (b), dolomite (c) and metabasite (d) olistoliths.

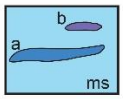

Metasandstone (ms) with horizon of mafic composition (a) and dolomitic detritus (b)

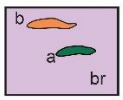

Polymictic meta-breccia (br) with oceanic (a) and continental (b) clasts and blocks

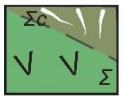

Serpentinite (Σ) and ophicarbonate (Σc)

Figure 37 is the schematic reconstruction of the oceanic succession of the Monte Banchetta-Punta Rognosa tectonic unit as obtained by correlation and interpretation of several lithostratigraphic logs during field investigations.

Serpentinite forms outcrops up to 100-m thick. It is both massive and coarse-grained, well preserving crystals (a few cm in size) of the pyroxene of the original peridotite (Figure 38a), and intensively foliated with fibrous serpentine along the foliation planes. In many outcrops, serpentinite has a brecciated texture, from 1 to 5 m thick, towards the overlying sediments, with 1-50 cm large serpentinite clasts bounded by an irregular network of veins (<1-3 cm thick) filled by calcite, dolomite and locally talc. This breccia can be referred to as ophicarbonate.

The overlying sedimentary succession starts with a polymictic metabreccia, ranging in thickness from few meters to 30 m, extensively exposed along the western and eastern sides of the Monte Banchetta. However, Caron (1971) has reported also a thin level of (probable) radiolarian chert directly on the serpentinite. The metabreccia has a block-in-matrix fabric: the matrix is an impure marble, often containing abundant Fe-oxides. The clasts, wrapped by the pervasive foliation and locally up to a few meters in size, consist of serpentinite, ophicarbonate (Figure 38b), and subordinate gneiss, micaschist (Figure 38c) and dolomitic marble. At the western side of the Monte Banchetta, a block of metagabbro with a well-preserved magmatic texture has been found (Figure 38d). In the south-eastern sector of the Monte Banchetta, the polymictic metabreccia displays a decrease of clast size from the

underlying serpentinite, and progressively passes upward into a fine-grained impure marble (showing a maximum thickness of ~10 m), defining then a broad fining upward sequence.

Bodies of white-greenish metasandstone (Figure 38e-f-g), with maximum thickness of ~15 m and 50-60 m long, have been variably observed with pinch-out terminations both intercalated and on the top of the polymictic metabreccia. Similar sediments have been locally observed also directly on serpentinites and ophicarbonate. The metasandstone is often characterized by the widespread occurrence of Fe-oxides aggregates (up to cm in size) and large white micas and chlorite flakes along the pervasive foliation planes. Locally, discontinuous micro-conglomerate (<50 cm thick) with mm to cm clasts of quartz and levels of white to gray impure quartzite have been observed associated with the metasandstone. The metasandstone has a few intercalations of green to bluish horizons (<50 cm thick) of mafic composition, rich in glaucophane and chlorite (Figure 38f). The metasandstone is capped by calcschist (described below) in its uppermost part, and it contains clasts and rare blocks up to a few meters in size of dolomitic marble and dolomitic metabreccia elongated between the foliation planes (Figure 38g).

The uppermost part of the sedimentary succession consists of calcschist, at least 100-200m thick and unconformably overlaying serpentinite-ophicarbonate and related sediments (Figure 38e). In the calcschist, primary compositional features are suggested by alternating cm to dm thick carbonate- and silica-rich domains, by discontinuous intercalations of impure marble, black and dark green schist (10 cm to 2 m tick). In addition, scattered blocks of serpentinite, metabasite and dolomitic metabreccia are embedded in the calcschist, generally stretched between the foliation planes.

Figure 38 (next page) Representative lithologies at the mesoscale from Corno et al., 2019. a) detail of massive serpentinites with magmatic pyroxene relics (Px) (sample AC82); b) serpentinite clasts (Σ) in the lower part of the polymictic metabreccias (Monte Banchetta south-eastern side, 1940 m); c) continental clast (mcs-micaschists) in the polymictic metabreccias (Monte Banchetta summit, 2823 m); d) metagabbro block in the polymictic metabreccias (Monte Banchetta western side, 2573 m); e) metasandtones (ms) intercalated in the polymictic metabreccias (br) between Passo della Banchetta and Monte Banchetta summit (cs- calcschists; Σ-serpentinites); f) bluish horizons of mafic composition (mh) in the metasandstones (ms), deformed by D2 folding and D3 crenulation (PaxF: axial plane; north of La Grangia, 2040 m); g) upper part of the metasandstones containing dolomitic clasts (dol) (south-east of Passo della Banchetta, 2710 m); h) non-cylindrical D2 fold in calcschists (Lest2, stretching lineation; F2, fold axis) (Monte Banchetta north-western side, 2570 m).

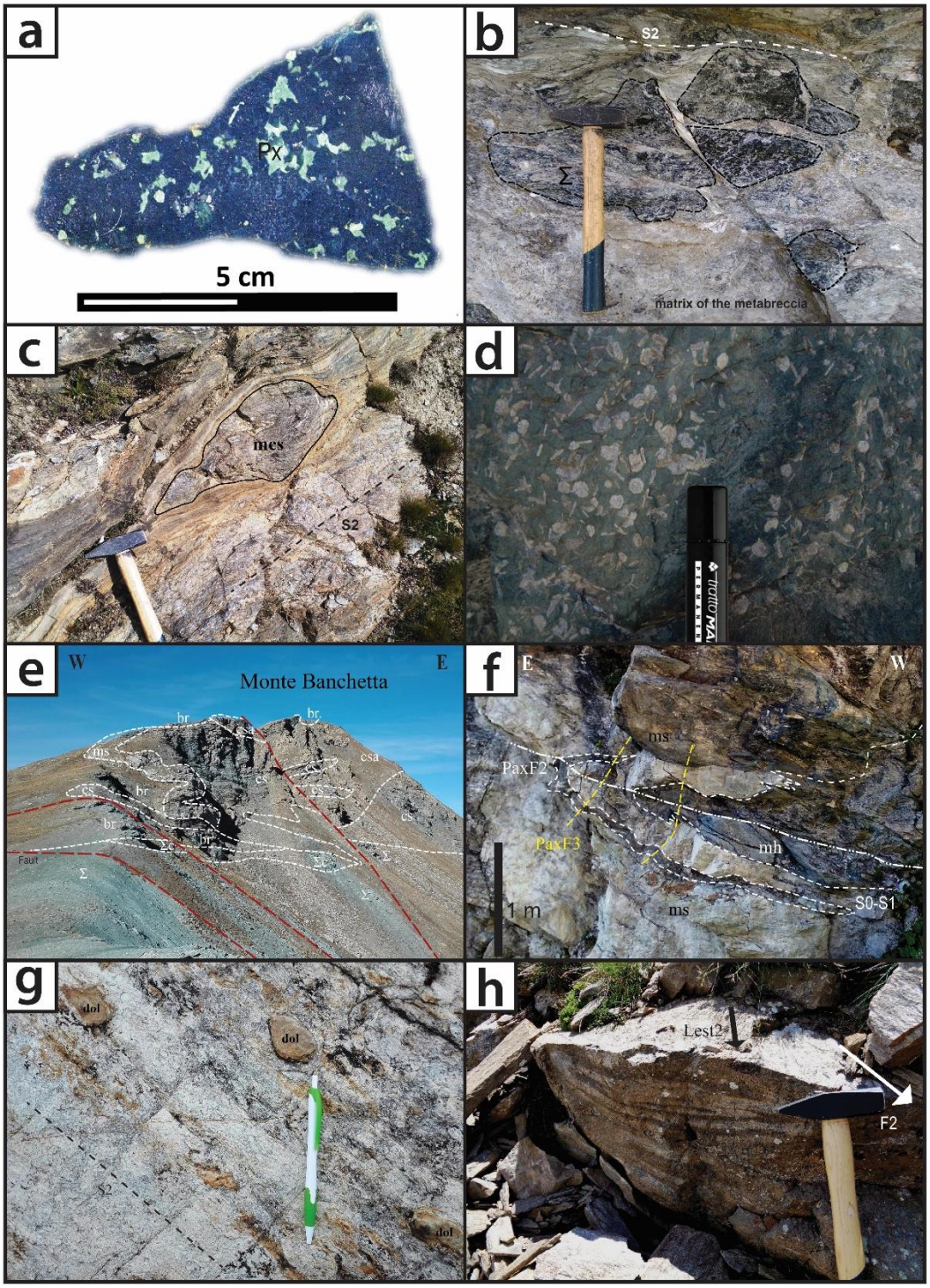
a
Px
5 cm
b
S2
Σ
matrix of the metabreccia
c
mes
S2
d
e
W
E
Monte Banchetta
br
ms
csa
cs
Σc
Σ
Faut
f
E
W
ms
PaxF2
PaxF3
mh
1 m
ms
S0-S1
g
dol
S2
h
Lest2
F2

5.2.2 Structural setting

Four main deformation events (D1-D4) can be identified in the oceanic succession. Petrographic description of the different planar fabrics related to these events are detailed in the following section. The oldest event D1 is recorded by the foliation S1, preserved in microlithons, intrafolial folds and isolated fold hinges. S1 results sub-parallel to primary compositional banding/ lithological contacts (Figure 38e and f) and is defined by Na-pyroxene + serpentine ± magnetite ± amphibole in ultrabasic rocks, Na-pyroxene + Na-amphibole ± quartz in basic rocks and quartz + phengite + Na-amphibole + chloritoid in pelitic rocks. S1 foliation (together with lithological contacts) is deformed and transposed during D2 into tight to isoclinal folds (Figure 38f). The axial plain schistosity S2 is usually the most penetrative planar fabrics in the outcrops. S2 is mainly defined by aegerin-augite + serpentine + amphibole in ultrabasic rocks, aegerin-augite +phengite + epidote in basic rocks and quartz + phengite + garnet ± chlorithoid + chlorite in pelitic rocks. A L2 stretching lineation is marked by alignment of phengite, amphibole, chloritoid or locally tourmaline on the S2. Kinematic indicators and relationships between L2 on S2 and fold geometries suggest an E- to SE verging non-cylindrical folding during D2 (Figure 38h). D3 is recorded by folds and crenulations with ENE-WSW trending sub-horizontal axes and axial planes usually dipping at high angle to SSE (Figure 38f). Chlorite + tremolite + muscovite + stilpnomelane assemblage defines a locally pervasive S3. A late D4 led to the development of gentle kilometer-scale folds with N-S trending axes and with axial planes dipping at high angle.

5.2.3 Petrology and mineral chemistry

This section deals with main textural relationships and mineral chemistry of rocks forming the oceanic succession. Representative selection of mineral composition is reported in Supplementary Material (Appendix II).

Figure 39 and Figure 40 show representative microstructures and Figure 41 reports chemical composition and classification diagrams of representative minerals. Figure 42 summarizes the parageneses developed during the different deformation stages.

Figure 39 (next page) Representative microstructures from Corno et al., 2019. a) massive serpentinites consisting of serpentine (Srp) and large pyroxene relics (Di, diopside) (sample AC82); b) aegerine-augite pyroxene grown after magmatic diopside and replaced by tremolite and chlorite in the serpentinites (sample AC82); c) ophicarbonates made of serpentine (Srp) and magnetite relics (Mag), with multiple sets of carbonate veins (Cb) (sample AC67); d) carbonatic matrix (cc) of the polymictic metabreccias with Na-amphiboles (Amp) isoriented to define S2 foliation and partially replaced by chlorite (Chl). Note widespread occurrence of Fe-oxides (Ox Fe) (sample AC2); e) metagabbro with muscovite (Ms) + epidote (Ep) + albite (Ab) pseudomorphosis after plagioclase and fine-grained matrix made of omphacite (Omp) + chlorite (Chl) ± epidote (Ep) replacing magmatic pyroxene (sample AC12); f) Na-Ca pyroxene with omphacitic (Omp) core and aegerine-augite (Aeg)

rim, in the metagabbro (sample AC12). Chl, chlorite; g) Clasts of gneiss in the polymictic metabreccias characterized by aggregates of chlorite (Chl) + muscovite (Mus) + opaque (Opq) after pyroxene (Px); h) mafic horizons within the metasandstones, showing a foliation defined by glaucophane (Amp) + phengite (Phe) + quartz (Qz). Note chlorite (Chl) replacing Amp, and isolated Apatite (Ap) grains (SEM image; sample AC57).

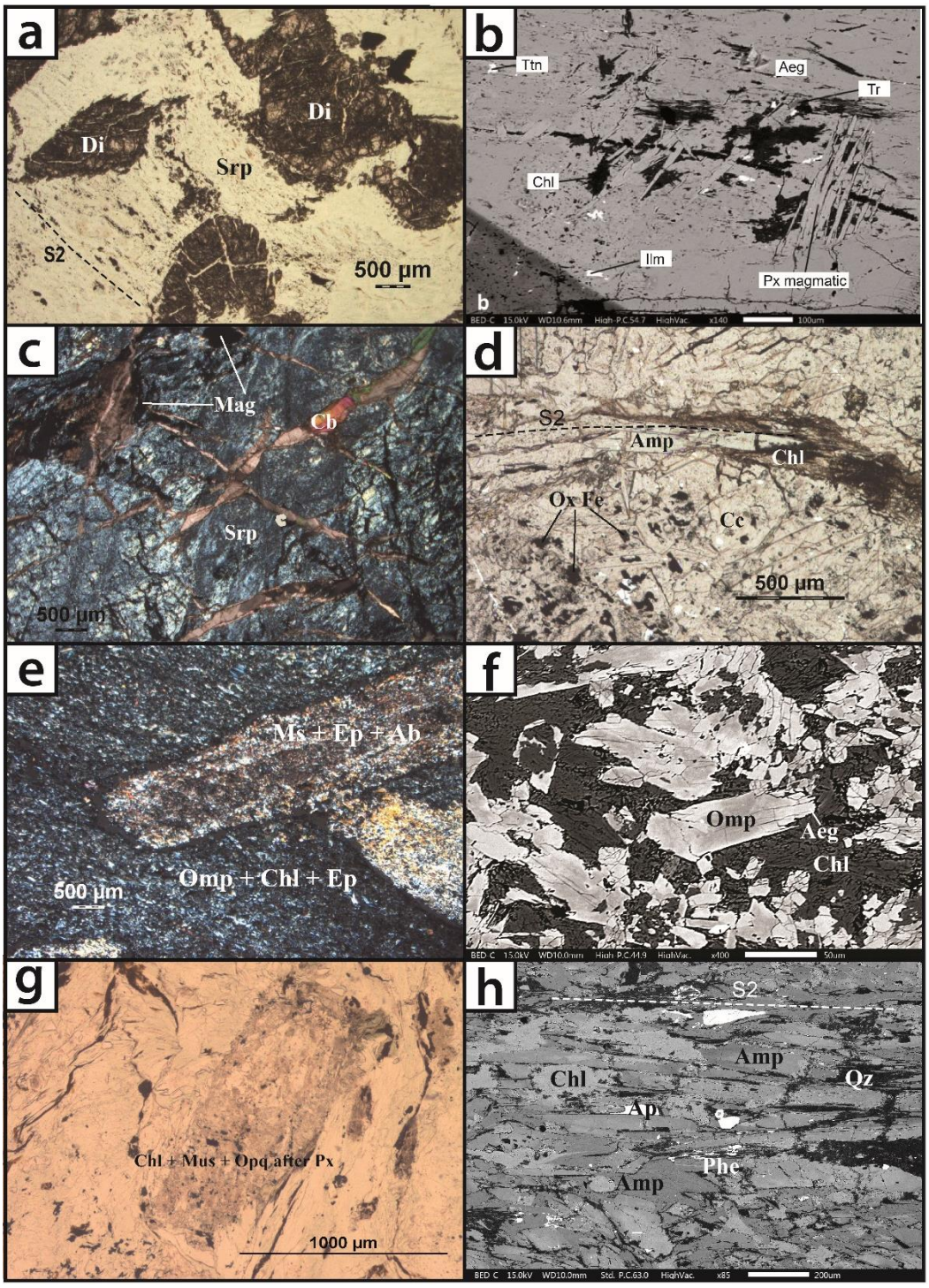

Serpentinite

The serpentinite consists of serpentine + pyroxene + amphibole + chlorite ± magnetite ± carbonate with variable occurrence of pyrite, calcopyrite, ilmenite and titanite. Coarse grained serpentinite preserves crystals (up to a few cm in size) of diopside (Na < 10 wt% and XMg> 0.9, showing very low content in Cr ranging between 0.4 and 0.7 wt%) and magnetite of the original peridotite (Figure 39a and Figure 41a). S1/S2 foliations are defined by serpentine and aegerine-augite, grown after magmatic pyroxene and in turn replaced by tremolitic amphibole and chlorite weakly isoriented (Figure 39b). The associated ophicarbonate shows large magnetite and serpentinite fragments separated by different sets of carbonate-bearing veins (Figure 39c).

Polymictic metabreccia

The matrix of the metabreccia (Figure 39d) is an impure marble consisting of calcite + quartz + Fe-chlorite + glaucophane + tremolite. S1/S2 foliation is defined by isoriented glaucophane within a calcite matrix. Fe-chlorite (Cr2O3 ~3 wt% and MnO ~1,57 wt%) and tremolite (Amph D3, Figure 41b) mark the S3 foliation.

The clast of metagabbro preserves evidences of an original coarse-grained magmatic texture (Figure 38d, Figure 39e-f). Large aggregates, up to few cm in size, of epidote + white mica + albite replaced magmatic plagioclase. They are dispersed within a fine-grained assemblage of Na-Ca pyroxene + Mg-chlorite + epidote replacing original magmatic pyroxenes. The Na-Ca pyroxene displays omphacitic core (recoding D1 event) and aegirine-augite rim (D2 event), and have acmitic content up to 30% (Figure 39f and Figure 41a). The S2 foliation is defined by Na-Ca pyroxene + phengite (Si~3.30-3.40 a.p.f.u., Figure 41d). The later S3 foliation is marked by Mg-chlorite + muscovite (after phengite, Si<3.30 a.p.f.u., Figure 41d) + zoisite (with contents <1% of Cr2O3 e MnO) ± allanite (epidote rich in Ce, La and Nd). Late pumpellyte crystals are also present. The clasts of gneiss (stretched along the S2) contains assemblage of chlorite + muscovite+ opaque after presumed clinopyroxene enveloped by a foliation defined by chlorite + albite + fine-grained sericite (Figure 41g).

Figure 40 (next page) Representative microstructures. a) Pseudomorphs after lawsonite defined by white mica (Wm) + Quartz (Qz) + graphite (Graph) ± zoisite (Ep) relicts of the S1 foliationin calcschist; b) Pyroxene-bearing metabasite embedded in the calcschists showing pyroxene of aegerine-augite composition partially replaced by Na- amphibole; c) spessartinic garnet (Grt) in the black schists; garnet is rimmed by ankerite rims (Ank) and wrapped by stilpnomelane (Stp) and quartz (Qz) (SEM image; sample AC15); d) spessartinic garnet (Grt) related

to D2 event in the black schists preserves an internal S1 foliation defined by quartz and white mica (sample AC15). Late stilpnomelane is statically growing.

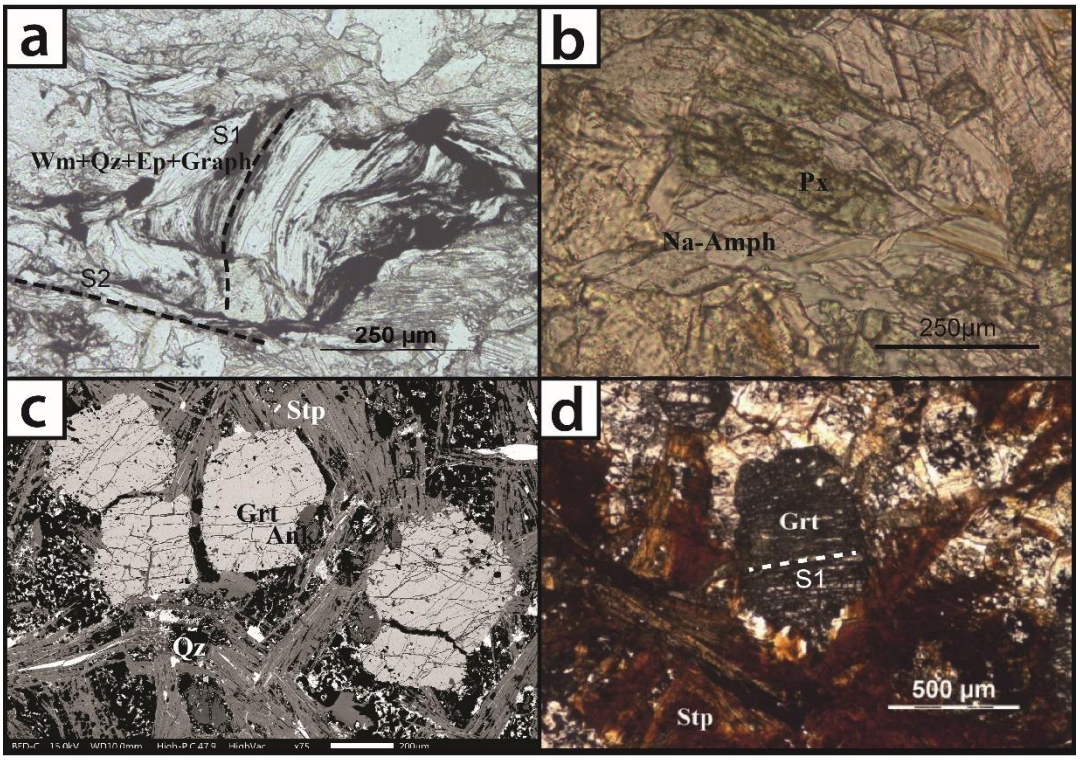

Metasandstone

The metasandstone consists of quartz (ranging from 70-90% in volume of total rock) + white mica + Fe-chlorite +chloritoid + glaucophane with variable amounts of stilpnomelane, tourmaline, calcite, apatite and rutile. This rock usually displays a lepidoblastic texture with the pervasive S2 foliation defined by quartz + chloritoid + white mica (generally zoned, with phengite at the core and muscovite at the rim, Figure 41d), transposing an earlier S1 foliation of quartz + phengite + glaucophane+ chloritoid + rutile. The late S3 foliation is marked by isoriented Fe-chlorite + muscovite + stilpnomelane. A primary micro-conglomeratic fabric is recorded by elongated and sub-rounded quartz grains wrapped by the S2 foliation. The white to gray impure quartzite shows fine-grained assemblages of quartz (more than 90% of the total rock) ± white mica ± calcite.

The mafic horizons intercalated in the metasandstone (Figure 39h) consist of abundant glaucophane (Figure 41b), white mica and quartz with minor and variable amount of calcite, pyrite, zircon, apatite and detrital allanite. In these horizons, nematoblasts of medium-grained glaucophane + phengite (Si<3.50, Figure 41d) + quartz define the S2 foliation, while assemblage of quartz + glaucophane + phengite (Si>3.50, up to 3.72 a.p.f.u., Figure 41d) rutile marks a S1 foliation in microlithons.

A locally very pervasive S3 crenulation cleavage is defined by muscovite + chlorite + albite (An<5%) + quartz.

Calcschist

The calcschist consists of carbonate, ± quartz, white mica, chlorite and graphite, with minor tourmaline and apatite. Monocrystalline quartz is irregularly distributed within the carbonate matrix, ranging from 10% to 30% of the rock. White mica is oriented along S1 and the main S2 foliation. Aggregates containing white mica + graphite ± zoisite relics within the S1 foliation can be interpreted as pseudomorphs after lawsonite (Figure 40a). Calcite + white mica + quartz define S2 foliation.

Pyroxene-bearing metabasite (Figure 40b) embedded in the calcschist consists of Na-amphibole + tremolite + chlorite + epidote + titanite + pumpellyite ± albite. It shows a nematoblastic texture with pyroxene of aegirine-augite (Figure 41a) composition partially replaced by glaucophane (Amphibole D2 in Figure 41b), that with epidote, white mica, chlorite and titanite defines the S2 foliation. Amphibole of tremolitic composition (Amphibole D3 in Figure 41b) has been observed in paragenesis with green chlorite and Cr-rich pumpellyite (Cr_2O_3content is ~4.5-5.5 wt%) to define S3.

The intercalations of black schist (Figure 40c-d) are mainly composed of quartz + garnet + stilpnomelane + chlorite + calcite + pyrite and have high contents of ankerite and Fe-Mn oxides. Usually, in this rock the S2 foliation is marked by white mica and chlorite films.

Garnet subhedral to euhedral porphyroblasts are syn-kinematic with respect to S2 and include an earlier S1 foliation consisting of white mica + quartz + graphite. This garnet is usually Mn-rich (Figure 41c) with spessartinic end-member up to 40-50%, and has a Mg content <0.30wt% (see Table 2 of the supplementary material in Appendix II). Grossular content is usually around 15% while almandine can reach 40%. Although a compositional cross-section has been carried out, no chemical zoning has been identified. The anomalous enrichment in Mn can be due to the original chemical composition of the protolith. Often, largest crystals of garnet are rimmed by late Mn-rich ankerite (Figure 40c). Stilpnomelane (from yellowish bronze to dark brown in colour) grows both after garnet and in fractures (Figure 40d).

The dark green schist, forming discontinuous levels in the calcschist, consists of white mica + stilpnomelane + chlorite+ quartz + calcite/dolomite with variable quantities of Fe-Mn ankerite, ilmenite and titanite. Relics of the S1 foliation are defined by amphibole (in turn replaced by chlorite) and white mica. White mica is typically zoned showing phengitic core with high content (up to 3.75 Si a.p.f.u., Figure 41d) and has a content of Cr_2O_3 of ~3 wt%. White mica-rich layers are often

strongly crenulated with development of S3 axial plane foliation defined by chlorite and stilpnomelane.

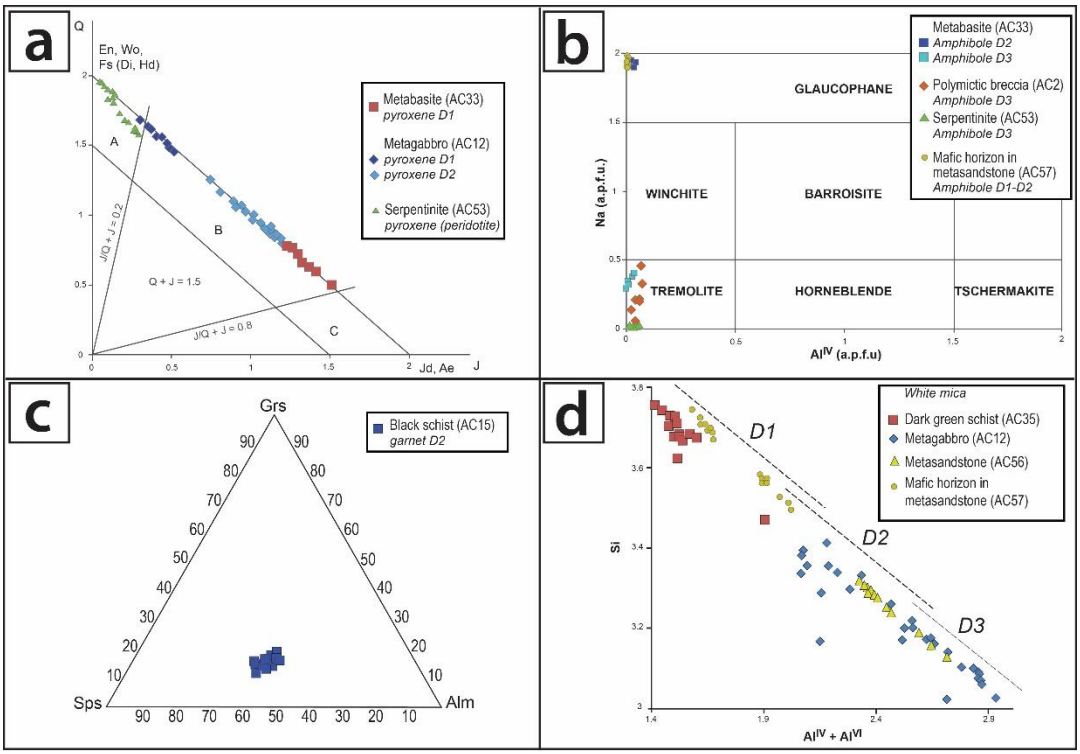

Figure 41 Chemical composition and classification diagrams from Corno et al., 2019. a) Morimoto (1988) pyroxene diagram A: Ca-Mg-Fe pyroxenes, B: Na-Ca pyroxenes, C: Na pyroxenes. En: enstatite, Wo: wollastonite, Fs: ferrosilite, Di: diopside, Hd: hedembergite, Jd: jadeite, Ae: aegerine-augite. b) Amphibole composition in the Hawthorne et al. (2012) diagram Na vs AlIV. c) Garnet composition in almandine (Alm) - spessartine (Sps) -grossular (Grs) diagram. d) White mica composition in the Si vs AlIV + AlVI diagram. Note that the shifting shown in *Figure 41*d by the analyses of white mica from different samples is due to the different content of iron present in the micas (see Table 3 of the supplementary material in Appendix II). In particular, the micas of mafic horizon are characterized by a lower iron content, while metagabbros and greenschists show higher iron values. In these last micas a greater amount of trivalent iron replaced the octahedral aluminium, while in the micas of mafic horizon this substitution is found to be smaller.

5.2.3 Metamorphic evolution

Metamorphic conditions of the oceanic succession have been reconstructed by combining microstructural observations, chemical analyses and conventional P-T thermobarometric estimates (Figure 43).

The recognition of pseudomorphs after lawsonite, observed as structural relict within the calcschist, constrains the burial path in the stability field of lawsonite bearing blueschist facies, characterized by low metamorphic gradient (Chen et al., 2013).

During the first tectono-metamorphic event D1, the metamorphic peak is defined by the omphacite + lawsonite + glaucophane + rutile paragenesis developed in the basic system.

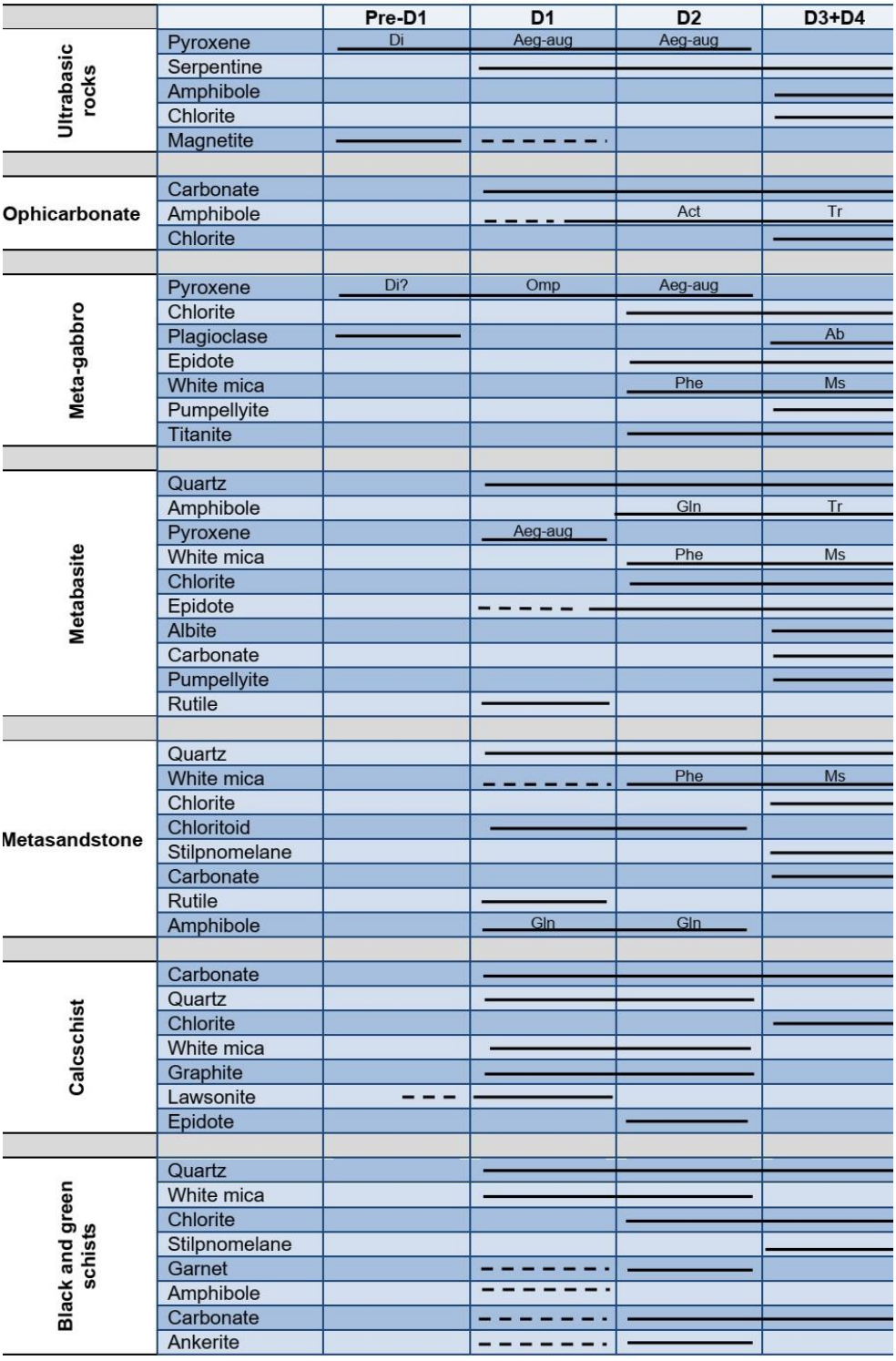

Figure 42 Mineral assemblages developed during the different deformation stages from Corno et al., 2019.

The occurrence of Na-amphibole in the metabasites implies P conditions lower than those of the amphibole vs chloritoid transition (Poli and Schmidt, 1995). Evidences of the HP metamorphism are also represented by the occurrence of the chloritoid + glaucophane assemblage in the metasandstone.

The maximum extension of the stability field of the chloritoid-glaucophane association, calculated for the NKFMASH system (Proyer, 2003), partly overlaps with the lawsonite blueschist facies and is indicative of temperatures between 420 ° C and 600 ° C and pressures of ~1.9 GPa. The aforesaid stability field, however, can sensibly expand as a function of the increase of Fe^{3+} in these two minerals, up to partially overlap with the field of the epidote blueschist facies (Guiraud et al., 1990). The results of the analyses indicated a XFe^{3+} content ranging from 0.1 to 0.2 in chloritoid and 0.4 - 0.5 for amphibole, and then a range of P-T conditions near the transition between the lawsonite - epidote blueschist facies can be inferred (Figure 43). The P-T peak conditions can therefore be estimated at approximately 470-520 ° C, at 1.7-1.9 GPa. These conditions are in agreement with the high Si content of phengite occurring in the mafic horizons in the metasandstone (Si ≈3.50-3.75 a.p.f.u., Figure 41d) and in the levels of dark green schist within calcschist (Si ≈3.60- 3.75 a.p.f.u., Figure 41d), that, according to phengite geobarometry of Massonne and Schreyer (1987), implies minimum P values of 1.7 - 1.9 GPa for T of around 500°C.

The second metamorphic stage (D2) is generally identifiable as the main tectonic-metamorphic event. The mineral assemblage (epidote, aegirine-augite, Na-Ca-amphibole and chlorite in metabasite) indicates that, according to Palin and White (2016), this second metamorphic stage developed under epidote-blueschist to epidote-amphibolite-facies transition. The occurrence of chlorite in the basic system points out that the upper limit of chlorite + quartz stability field calculated by Poli and Schmidt (1995) was not exceeded. These conditions are in agreement with the Si content (≤3.40 a.p.f.u) of phengite growth in the metagabbro and in the metasandstone (Fig. Figure 41d), that, according to phengite geobarometry of Massonne and Schreyer (1987), implies minimum P values of 0.9-1.1 GPa for T around 500°C. In addition, syn-cinematic D2 garnet (characterized by high Mn content) suggests that the temperature reached during its grown has never exceeded 500 ° C (Spear and Cheney, 1989).

The subsequent D3 event is characterized by typical parageneses of the greenschist facies conditions. In the metagabbro, zoisite is replaced by clinozoisite and Ca-amphibole. Chlorite and albite pervasively grew after omphacite. In metabasite, Na-amphibole is replaced by Ca-amphibole (Figure 41b) and albite, whereas garnet and rutile are replaced by chlorite and titanite, respectively. The white mica related to D3 event is characterized by a low Si content (<3.30 a.p.f.u., Figure 41d). The

stilpnomelane + chlorite assemblage in metasandstone and black and dark green schists implies temperature lower than 400 °C.

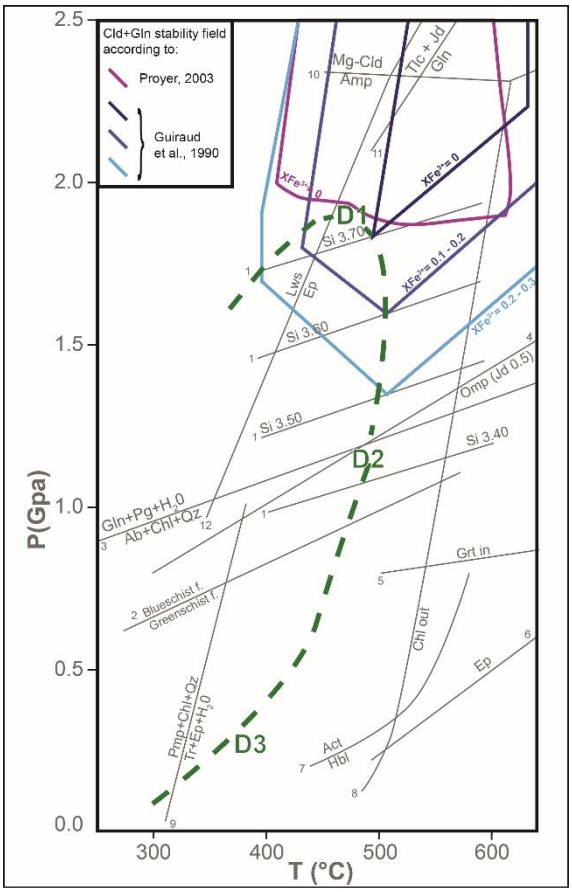

Figure 2 Petrogenetic grid from Corno et al., 2019. The dashed line shows average P-T conditions for the lawsonite-epidote blueschist peak (D1), blueschist facies (D2) and greenschist facies (D3) metamorphic events, respectively. The garnet, chlorite, epidote and lawsonite stability curves (5, 6, 8, 10, 12) were taken from Poli and Schmidt (1995), the chloritoid-glaucophane stability fields from Guiraud et al. (1990), and Proyer (2003). Other curves: 1) isopleths of Si4+ content in phengite (Massonne and Schreyer, 1987); 2) transition of blueschist/greenschist facies (Maruyama et al., 1986); 3) Guiraud et al. (1990); 4) Holland (1983); 7) Ernst (1979); 9) Evans (1990); 11) Corona et al. (2013).

5.3 Main remarks

Data discussed in this Chapter allow i) to propose a detailed model for the depositional history of the oceanic segment of the Monte Banchetta-Punta Rognosa unit and ii) to trace its Alpine tectono-metamorphic evolution.

The presence of serpentinised peridotite covered at their top by ophicarbonate generally records exhumation and exposure of the upper mantle at the seafloor in Jurassic times. Then, after discontinuous deposition of Middle-Upper Jurassic radiolarian chert (Caron 1971), the exposed mantle has been directly covered by the polymictic breccia (metabreccia) and intercalated siliciclastic sediments (metasandstone), both representing mass-flow deposits on sea floor and characterized by oceanic and continental clasts and blocks. The upper part of the sedimentary cover records the unconformable deposition of pelagic carbonate-rich sediments (calcschist), poor of oceanic and continental detritus. The largely accepted Cretaceous age for the calcschist deposition suggests to refer the underlying polymictic breccia and intercalated sandstones to the Late Jurassic - Early Cretaceous.

The polymictic breccia and intercalated sandstones indicate the close presence of structural highs made of oceanic and continental rocks in response to the Jurassic

rifting (e.g. Beltrando et al., 2014). Source areas for serpentinite, ophicarbonate and gabbro clasts (mainly prevailing in the lowermost stratigraphic parts) can be envisaged on a paleo-topography of exhumed mantle, probably controlled by extensional faults. The continental detritus in the polymictic breccia, represented by platform deposits (dolostone and dolomitic breccia) usually considered Triassic(-Early Jurassic?) in age (e.g. Dal Piaz, 2010 and therein references) and pre-Triassic rocks (gneiss and micaschist), suggests that this oceanic segment was in a proximal position to the rifted European margin. In a general context of the ocean-continent transition, continental source areas can be envisaged on the hyperextended part of the European margin or on its more proximal part. The observed enrichment in Mn and Cr contents and widespread occurrence of Fe-oxides in these mass-flow deposits document presence of exposed mantle.

Close association of continental and oceanic detritus in the supra-ophiolite sedimentary cover were described in several oceanic sections in these regions of the Western Alps (e.g. Caby et al., 1971; Lagabrielle, 1981; Lagabrielle et al., 1984; Polino and Lemoine, 1984; Balestro et al., 2015 and Tartarotti et al 2017). In the investigated region, mixed detritus typically characterizes the Jurassic-Cretaceous sediments of the Lago Nero unit (Polino and Lemoine, 1984; Servizio Geologico di Italia, 2002 and in press), resting to the west of Monte Banchetta-Punta Rognosa unit in an upper structural position (Figure 32). On the basis of this stratigraphic feature, a proximal position with respect to the European margin has been usually proposed in literature for this unit. Therefore, according to this interpretation, the oceanic segments of the Lago Nero and Monte Banchetta- Punta Rognosa units could be tentatively restored in a similar place.

However, Burroni et al. (2003) suggested that Upper Cretaceous calcschists (Gondran flysch) of the Lago Nero unit are covered by mass-gravity deposits (the Rocher Renard complex made up of dark schist with oceanic blocks). Due to this setting, Burroni et al. (2003) proposed that the upper mass-gravity deposits derived from erosion of the accretionary wedge during converging processes and then, in an alternative view, placed the Lago Nero oceanic segment in an internal position of the Piemonte-Liguria realm. Therefore, taking into account this alternative interpretation, the Lago Nero unit and the Monte Banchetta-Punta Rognosa unit would identify two different oceanic segments, in internal and external (peri-continental) position respectively.

Petrological and minero-chemical analyses constrain a metamorphic peak (D1) at the transition between lawsonite- and epidote- blueschist facies conditions, followed by a first decompression event (D2) always inside the blueschist facies conditions for the oceanic succession of the Monte Banchetta-Punta Rognosa unit. Then a third event (D3) under green schist facies conditions occurred. Considering the limited

reduction of temperature identified by the transition from D1 to D2, the trajectory of exhumation of the investigated succession seems to be characterized by a rather rapid exhumation.

As a general conclusion, this study documented primary stratigraphic relationships, related and following the Jurassic rifting, in a poorly known unit highly deformed by tectono-metamorphic events. However, data presented must be considered as a starting point for further multidisciplinary studies, aimed in particular to give constrains to the Jurassic paleogeographic scenario of this sector of the Alps, still variously debated and interpreted in literature.

CHAPTER 6

The continental succession of the BRU

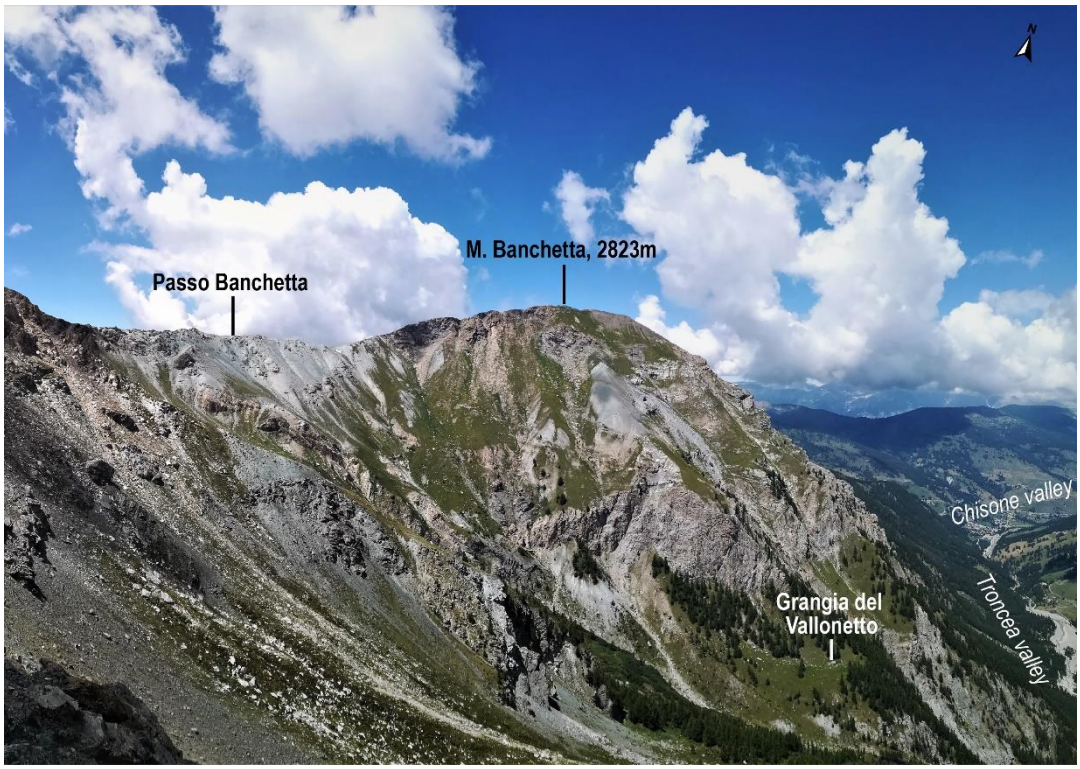

Figure 44 Landscape view on the eastern slopes of the M. Banchetta, made of the juxtaposition of continental- and oceanic-related rocks.

6.1. Introduction

As illustrated in the previous Chapter 5, the Banchetta-Rognosa tectonic unit consists of two juxtaposed successions respectively recording the Mesozoic tectono-depositional evolution of (i) a continental margin, i.e. Monte Banchetta succession (Figure 44), and (ii) a neighboring oceanic sector, i.e. Punta Rognosa succession, both covered by the same post-rift sediments consisting of Upper Jurassic?-Cretaceous carbonate micaschist. Based on the paper Corno et al. (2021b), this Chapter 6 focuses on the pre-Triassic continental basament of Monte Banchetta succession, detailing its lithological features, petrography and mineral chemistry, and estimating its alpine peak P–T conditions using the isochemical phase diagram approach.

According to the available, large-scale, metamorphic maps of the Western Alps (e.g. Bousquet et al., 2008; Beltrando et al., 2010; Ballèvre et al., 2020), the BRU is located in the external part of the belt, characterized by low temperature, high pressure (LT/HP) metamorphism with peak conditions at the blueschist-eclogite-

facies transition. However, at present, quantitative studies aimed at estimating the metamorphic peak conditions of the BRU are lacking. Corno et al. (2021b) aims at filling this gap: the metamorphic peak conditions registered by the BRU continental basement were quantified using a petrologic approach based on phase equilibria modeling, and the metamorphic evolution of this poorly investigated sector of the Western Alps was constrained for the first time. Finally, the peak P-T conditions recorded in the BRU are compared with peak P-T estimates published for other HP oceanic- and continental-derived units exposed in the proximity of the BRU.

6.2. Lithostratigraphic, petrographic and petrological features of the continental succession

The main features the Monte Banchetta continental succession (Figure 45) can be observed between the Banchetta gorge and the Vallonetto stream (hereafter named North La Grangia section; Figure 46a) and to the south of the Vallonetto stream (hereafter named Vallonetto section; Figure 46c).

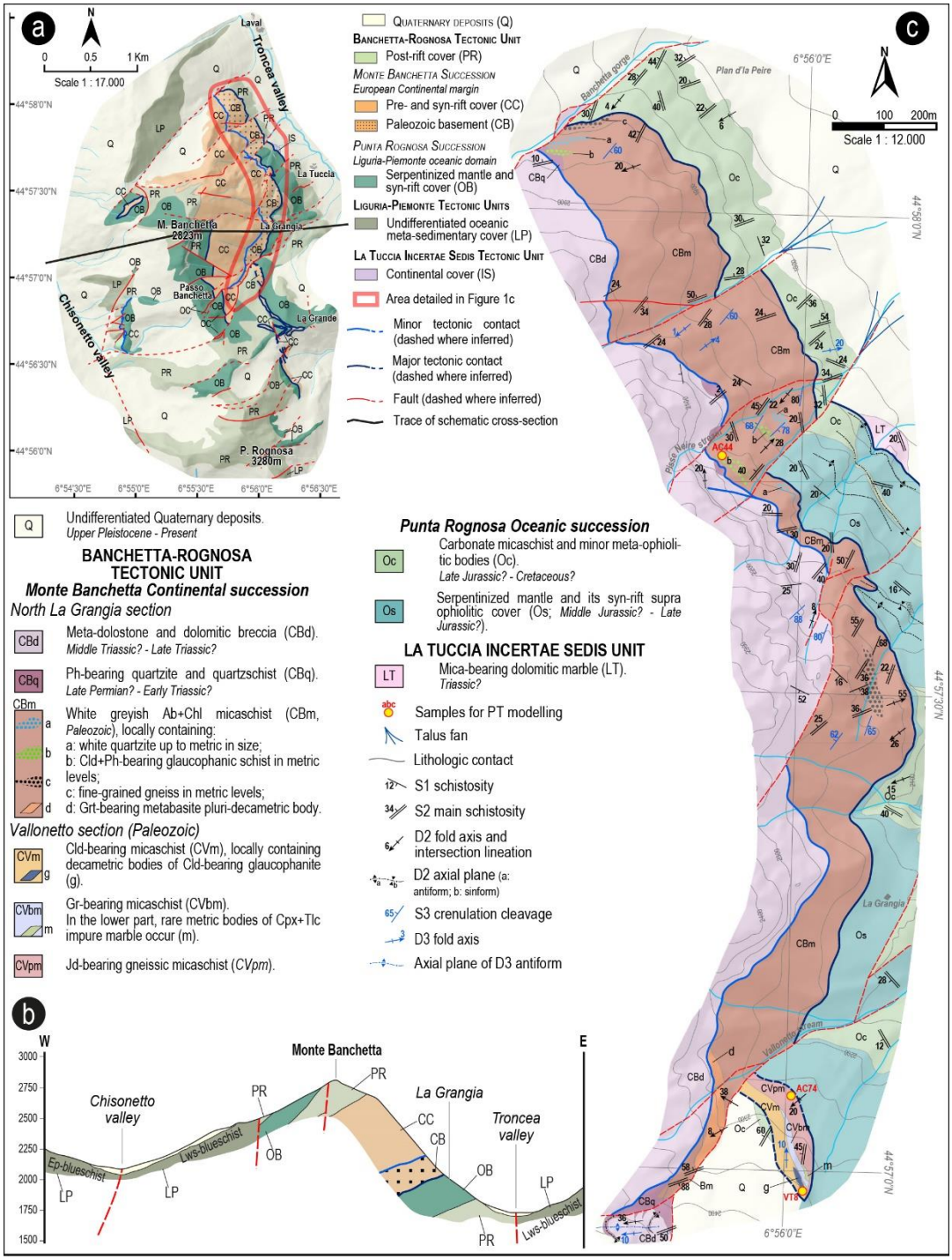

Figure 45 a) Tectonic sketch map of the Banchetta-Rognosa tectonic unit from Corno et al., 2021b; b) Schematic cross-section of the Banchetta-Rognosa tectonic unit and neighboring units, lines and colors are according a); c) Detailed geological map of the continental succession of the Banchetta-Rognosa tectonic unit, cropping out on the left side of Troncea valley, near Sestriere (Piemonte).

6.2.1 General features and lithostratigraphy

In the North La Grangia section, the continental basement mainly consists of a white-greyish strongly foliated micaschist sequence (CBm in Figure 46a) hosting layers and bodies of different lithologies. The medium- to fine-grained micaschist consists of quartz, white mica, chlorite, albite, epidote and graphite. The main lithological bodies embedded within the micaschist include: (i) chloritoid+phengite-bearing glaucophanic schist (b in Figure 46a and Figure 47), up to 2 m in thickness, mostly located in the central portion of the tectonic slice; (ii) white quartzite layers (a in Figure 46a), usually occurring in the upper portion of the micaschist; (iii) fine-grained gneiss (c in Figure 46a), consisting of quartz, white mica, chlorite, albite widely occurring along the whole Banchetta eastern side, in decametric-thick levels; (iv) a pluri-decametric body of metabasite is exposed in the southernmost part of the North La Grangia section (d in Figure 46a-b), including discontinuous white meta-aplites (1-2 m in length and up to 30 cm in thickness). This metabasite is a medium-grained massive rock consisting of glaucophane, garnet, chlorite, epidote, albite, titanite and minor paragonite, rutile, K-feldspar and quartz (Figure 48a). The main foliation is defined by the alignment of glaucophane and epidote. Garnet porphyroblasts (up to 1 mm in diameter and pale yellow in color) occur in discontinuous domains wrapped by the main foliation. A sharp discontinuity in their composition suggests the existence of two different generations of garnet (Figure 48b): a locally embayed Ca+Fe-rich core (Grt1), likely pre-Alpine in age, is surrounded by a Mn-rich Alpine rim (Grt2; see supplementary material in Appendix III for compositional diagrams). K-feldspar, interpreted as a relict phase, occurs in small crystals (up to 15 μm) in sub-mm patches with chlorite, epidote and rare muscovite (Figure 48c). The whole micaschist sequence is unconformably covered by Upper Permian-Lower Triassic siliciclastic deposits (CBq in Figure 46a), represented by white-greenish massive quartzite, locally micro-conglomeratic in the lower part (with detrital pink quartz clasts) and with phengite-bearing quartzite schists in the upper part. Up-section, Triassic meta-dolostone (up to 20-30 m-thick) and monomictic, clast-supported, meta-breccia occur (CBd in Figure 45c). The dolomitic clasts of the meta-breccia are polycrystalline, up to few decimeters in size, and are set within a dolomitic matrix with sporadic decametric levels of black shale, carbonatic micaschist and phyllite. Then, the overlying syn-rift cover (up to 200 m thick, see also Corno et al., 2021) consists of polymictic meta-breccia, black micaschist, and carbonate-bearing quartzite. The polymictic meta-breccia is composed of meta-dolostone and quartzite clasts in a carbonate matrix containing minor Cr-bearing white mica, talc and detrital K-feldspar. In the uppermost part of the polymictic meta-breccia, an impure quartzite contains meta-dolostone clasts up to decimetric in size.

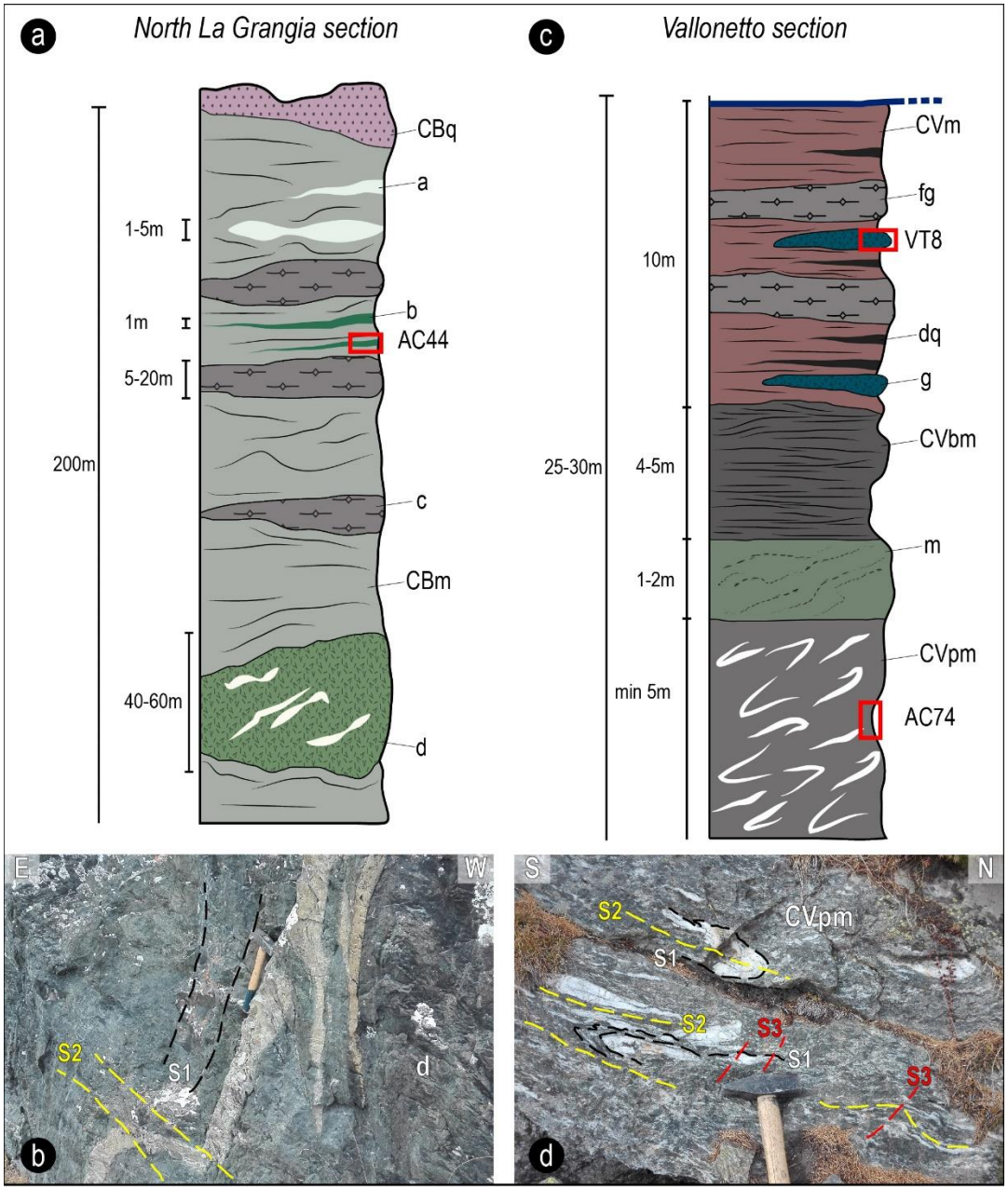

Figure 46 from Corno et al., 2021b. a) Lithostratigraphic succession of the North La Grangia section. Red polygon shows the location of the analyzed sample, used for P–T pseudosection modeling. Acronyms are: CBm, Ab+Chl micaschist; a, quartzite levels; b, Cld+Ph-bearing glaucophanic schist; c, fine-grained gneiss; d, metabasite body with meta-aplites (white bodies); CBq, Ph-bearing quartzite; b) Field photograph of the metabasite body (d) within the Ab+Chl micaschist of the North La Grangia section. The main foliation (S1) is highlighted by whitish meta-aplites layers and is sub-parallel to primary lithological surface, S2 grows in axial plane of D2 folds; c) Lithostratigraphic succession of the Vallonetto section. Red polygons show the location of analyzed samples, used for P–T pseudosection modeling. Acronyms are: CVpm, Jd-bearing gneissic micaschist; CVbm, Gr-bearing micaschist; m, Tlc+Aeg-bearing impure marble; CVm, Cld-bearing micaschist; g, Cld-bearing glaucophanite bodies; fg, fine-grained gneiss; dq, dark quartzites; d) Field photograph of Jd-bearing gneissic micaschist of the Vallonetto section (modified from Corno et al., 2021a); D2 folds transpose S1

compositional banding and develop S2 axial plane schistosity, D3 tectono-metamorphic event is expressed by S3 crenulation cleavage.

The Vallonetto section identifies a tectonic slice (only a few hundred meters long and 30 meters thick) of pre-Triassic basement rocks whose lower terms are made of dark grey jadeite-bearing gneissic micaschist (CVpm in Figure 46c-d and Figure 47). Locally, bodies (2-3m in size) of medium- to coarse-grained impure marble occur above the gneissic micaschist (m in Figure 45c). The marble consists of calcite, dolomite, talc, amphibole, epidote, aegirine, chlorite, hematite, and relict spinel. Due to the high oxygen fugacity in these marble bodies, all iron is ferric, stabilizing hematite and aegirine (see supplementary material in Appendix III). Due to the absence of ferrous iron, Mg-rich minerals like talc become stable. The matrix is mostly made of calcite while the main foliation is defined by discontinuous mm-thick layers of hematite + chlorite + talc (Figure 48d). A second, poorly developed, foliation is defined by the oriented growth of large crystals of zoned Mg-riebeckite amphibole (up to 250μm) + chlorite + epidote. Aegirine porphyroblasts, up to half a mm long, are wrapped by the main foliation and are concentrated in discontinuous domains, often in association with talc. Dolomite crystals, up to 300-400μm in diameter, are dispersed in the matrix and are partially replaced by calcite. They often include hematite flakes and are partially enveloped by talc (Figure 48e). Widespread through the rock, large relict crystals (up to 2mm) of Cr-bearing spinel occur, wrapped by the main foliation (Figure 48f). Late Ca-amphiboles overgrow talc and aegirine.

Up section, a graphitic micaschist follows (CVbm in Figure 46c), consisting of white micas (both phengite and muscovite), chlorite, albite, quartz, graphite and rare calcite. The tectonic slice ends upward with a ~ 10 m -thick reddish chloritoid-bearing micaschist (CVm in Figure 46c), with local levels of fine-grained gneiss (consisting of white micas, quartz, chloritoid, chlorite, albite and allanitic epidote; fg in Figure 46c) and dark quartzites (dq in Figure 46c). Especially in the upper part, this chloritoid-bearing micaschist embeds minor metric bodies of chloritoid-bearing glaucophanites (g in Figure 46c and Figure 47).

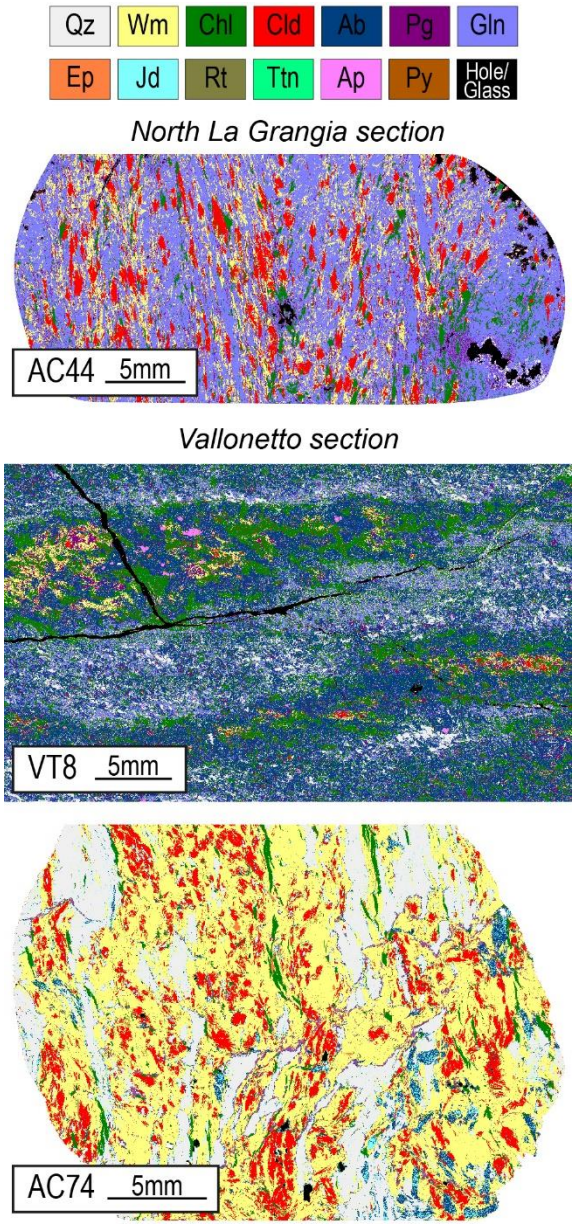

Figure 3 Processed X-ray maps of the modelled samples from the North La Grangia and Vallonetto sections from Corno et al., 2021b.

6.2.2 Structural evolution

A polyphasic evolution is recorded in the BRU, characterized by the overprinting of HP (D1 and D2 phases) and LP-LT deformation events (D3 phase), followed by a late folding (D4 phase) (Corno et al., 2019, 2021a).

The oldest D1 event is responsible for the development of the S1 schistosity sub-parallel to primary compositional surfaces (S0) (Figure 46b). S1 schistosity is deformed and transposed during D2 event into tight to isoclinal folds, whose axial plane schistosity S2 is usually the most penetrative planar fabric in the BRU (Figure 46d), defined by epidote + phengite/paragonite ± glaucophane ± chloritoid assemblage. S2 mainly dips to W-NW and contains a pervasive L2 stretching lineation. A2 NE-SW trending fold axis are sub-parallel to the L2 stretching lineation suggesting a likely non-cylindrical folding for the D2 event. Major contacts between continental- and oceanic-derived successions, as well as their minor intra-succession tectonic contacts, were deformed since the earliest deformation events (D1-D2). D3 event is recorded by mesoscopic folds and crenulations (Figure 46d) with sub-horizontal ENE-WSW-trending axes and axial planes usually dipping at high angle to SSE. Some rocks record an incipient S3 crenulation cleavage, widely associated with retrogression and development of LT-LP assemblages (chlorite + muscovite + albite ± stilpnomelane ± pumpellyite; Corno et al., 2019, 2021a). The late D4 event is responsible for the development of gentle km-scale folds, generally displaying sub-horizontal N-S trending axes and high-angle dipping axial planes. Tectonic contacts recorded a late top-to-S-SW extensional reactivation.

Table 1 Bulk compositions (mol%) of the modelled samples from Corno et al., 2021b.

	North La Grangia section	Vallonetto section	
	AC44	VT8	AC74
SiO_2	58.16	63.20	64.70
Al_2O_3	13.74	12.88	19.84
FeO	9.23	8.10	6.12
Fe_2O_3	0.52	0.90	0.11
MgO	11.00	7.68	2.00
MnO	0.24	–	0.06
Na_2O	5.60	6.41	3.82
K_2O	1.51	0.81	3.35
Total	100.00	99.98	100.00

6.2.3 Petrography and mineral chemistry of selected samples

Three samples have been selected from the pre-Triassic basement rocks of the Monte Banchetta succession out of a total of about 30 samples, based on their mineral assemblages, which are considered as the most suitable for constraining the HP tectono-metamorphic evolution of the BRU. Petrographic features and mineral chemical data are briefly summarized here for the three samples that have been selected for further petrological investigations: AC44 (Cld+Ph-bearing glaucophanic schist), VT8 (Cld-bearing glaucophanite) and AC74 (Jd-bearing gneissic micaschist). The blastesis-deformation relationships of the selected samples, as well as their mineral chemical data, are summarized in Table 2 and Table 3, respectively. Bulk rock compositions of these samples (Table 1) were calculated by combining the mineral proportions obtained from the quantitative modal estimate of SEM-EDS multispectral maps with mineral chemistry acquired at SEM-EDS. GPS coordinates of sampled locations are listed in the supplementary material in Appendix III.

6.2.3.1 North La Grangia section

Sample AC44: Cld+Ph-bearing glaucophanic schist

AC44 sample is a glaucophane + chloritoid- bearing schist, consisting of glaucophane (53%), chloritoid (11%), potassic white mica (18%), chlorite (9%), paragonite (7%) and rutile (2%). Its well-developed foliation (S2), defined by phengite, glaucophane, chloritoid and paragonite (Figure 47 and Figure 49a), is derived from the transposition of an earlier schistosity (S1; Figure 49a-b), preserved as polygonal arcs and intrafolial folds, highlighted by chloritoid and glaucophane crystals besides phengitic and paragonitic micas. Chlorite occurs as a late phase, statically overgrowing chloritoid and glaucophane (Figure 49b). Large flakes of muscovite statically overgrow S1- and S2-related phengite flakes.

Different white mica generations have different compositions, with highest Si content for phengite (Si from 3.30 up to 3.62 a.p.f.u.) and a strong decrease in Si content for the late muscovite flakes (Si < 3.25 a.p.f.u.) (Figure 50a). Both syn-D1

and syn-D2 Na-amphiboles are glaucophane according to the classifications of Hawthorne et al. (2012) and Leake (1978) (Figure 50b) and their X_{Mg} ranges from 0.56 to 0.67. Syn-D1 glaucophane crystals are usually zoned: lower X_{Mg} values (0.56-0.62) occur in prograde cores, while higher values (0.63-0.67) occur at peak syn-D1 rims. They generally display high Na(M4) values, close to theoretical value of 2.00 a.p.f.u. for glaucophane. Chloritoid of both generations (i.e. syn-D1 and syn-D2) has low X_{Mg}, in the range 0.15-0.18, and it locally contains low amounts of MnO, always lower than 2 wt%. Chlorite plots in the ripidolite field and has X_{Mg} between 0.47 and 0.54.

Figure 48 (next page) Representative microstructures of the Monte Banchetta continental succession from Corno et al., 2021b. (a, b, c) metabasite body. a) Garnet porphyroblasts partially retrogressed to chlorite and wrapped by S1 foliation, defined by glaucophane+epidote+quartz, partially retrogressed to poikiloblastic albite (Plane Polarized Light, PPL); b) Garnet porphyroblasts displaying an outer Mn-rich Alpine rim and an inner Ca+Fe-rich, likely pre-Alpine core (Back Scattered Electron image, BSE); c) Detail on a sub-mm patch made of relict K-feldspar+epidote+chlorite+white mica (BSE). (d, e, f) Tlc+Aeg-bearing impure marble; d) S1 hematite foliation transposed by S2 schistosity (BSE); e) Calcitic matrix with relict crystals of dolomite+hematite and talc flakes oriented along the S1 foliation (BSE); f) Large chromite crystals wrapped by chlorite, growing also along micro-fractures. Note aegirine partially retrogressed by Ca-amphiboles and talc flakes dispersed in the calcitic matrix (BSE).

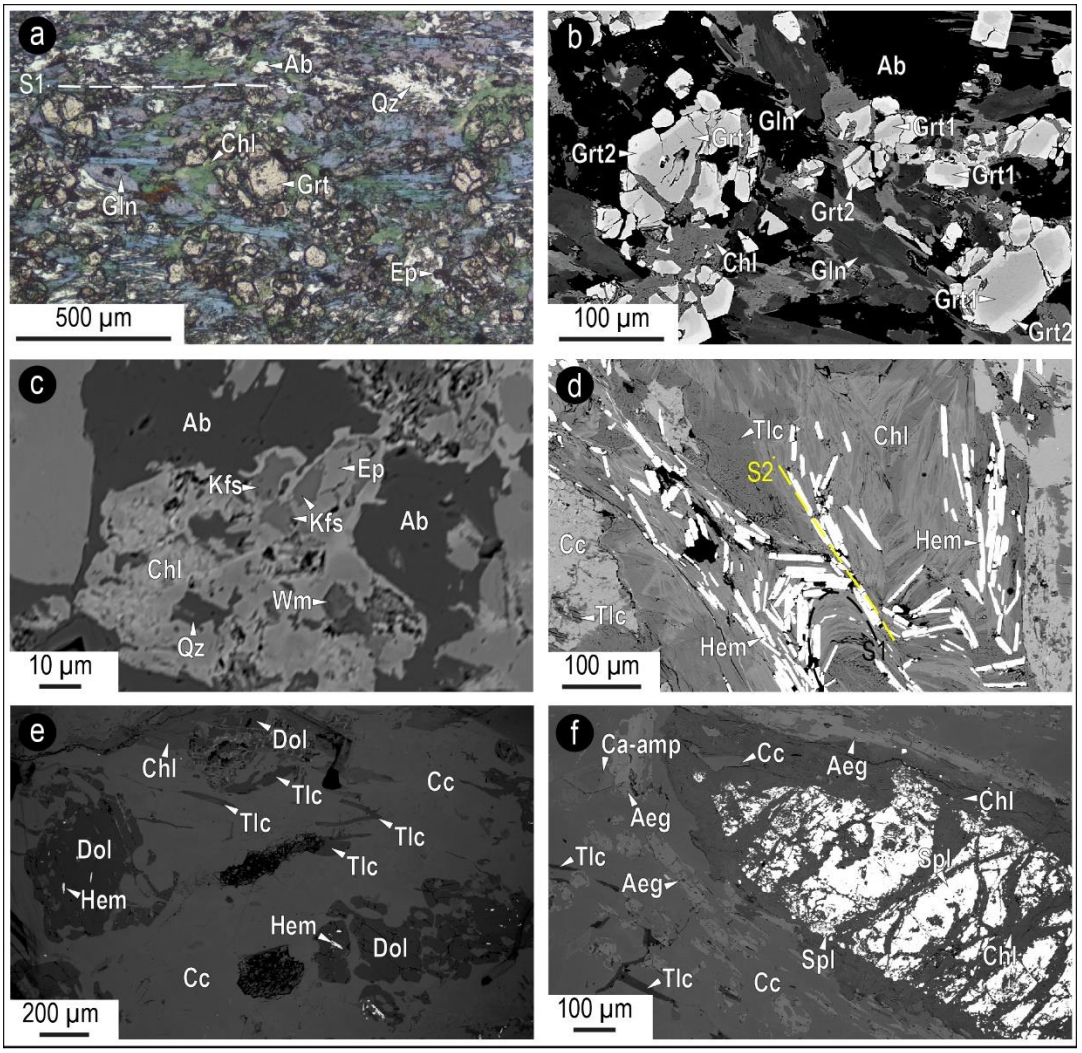

6.2.3.2 Vallonetto section

Sample VT8: Cld-bearing glaucophanite

This sample is a medium-grained, partially retrograded, glaucophanite consisting of chlorite (22%), glaucophane (18%), albite (38%), potassic white mica (6%), paragonite (4%), chloritoid (2%), quartz (8%), minor epidote (1%), and accessory rutile, zircon and apatite (~1% in total; Figure 47). Chloritoid, potassic white mica and paragonite are concentrated in lens-like discontinuous domains, whereas quartz only occurs in the matrix (Figure 47 and Figure 49c). The main foliation (S2) is defined by the alignment of white micas, glaucophane, chlorite and chloritoid, and it is derived from the transposition of an older schistosity (S1) defined by the preferred orientation of an earlier generation of glaucophane and chloritoid (Figure 49d), still

preserved in mm–sized microlithons wrapped by the main foliation (S2). White mica occurs as phengite and paragonite (Figure 49d), partially replaced by static growth of muscovite. Glaucophane crystals, up to 400 µm, are locally replaced at the rim by poikiloblastic albite or, along fractures, by fine-grained quartz + chlorite. Among accessory phases, abundant and large (up to 500 µm in length) rutile can be found together with zircon.

Phengite has Si content ranging from 3.30 to 3.40 a.p.f.u. and an X_{Mg} =0.31-0.54; muscovite overgrowing phengite flakes has Si < 3.25 a.p.f.u. (Figure 50a). Both syn-D1 and syn-D2 Na-amphiboles plot in the glaucophane field according to Hawthorne et al. (2012) and Leake (1978) classification criteria (Figure 49b) and have X_{Mg} ranging from 0.59 to 0.67. Both generations of chloritoid (i.e. syn-D1 and syn-D2) have similar low X_{Mg} values in the range 0.14-0.19, and low MnO contents, always lower than 2 wt%. Chlorite plots in the ripidolite and picnochlorite fields and have X_{Mg} values between 0.45 and 0.54.

Figure 49 (next page) Representative microstructures of the samples used for P–T modeling from Corno et al., 2021b. a, b AC44. a) Polygonal arc of chloritoid crystals, with S2 axial plane schistosity defined by phengite+glaucophane (PPL); b) S1 microlithon with chloritoid crystals (Cld1) wrapped by S2 main foliation, defined by a second generation chloritoid (Cld2)+glaucophane+phengite. Chlorite replaces both chloritoid and glaucophane (PPL). c, d Sample VT8. c) Boundary between matrix (lower part) and a lens-like domain (upper part), with relic S1 foliation almost completely replaced by white mica (=Wm)+chlorite+albite S2 axial plane schistosity (PPL); d) Intergrowth of white mica and paragonite close to syn-D2 chloritoid crystals (Cld2), almost completely replacing syn-D1 chloritoid (Cld1); note on the right a large rutile crystal (BSE). e–g Sample AC74. e) Syn-D1 chloritoid crystals (Cld1) preserved in a microlithon wrapped by S2 main foliation, defined by a second generation of chloritoid (Cld2)+phengite+quartz. Note the micro-scale expression of D3 tectono-metamorphic event, characterized by gentle folding (PPL); f) Partially retrogressed syn-D1 jadeite crystal, wrapped by the main foliation and locally replaced by albite+quartz intergrowth (PPL). The inset shows a detail of jadeite+quartz intergrowth (BSE); g) Schematic cartoon showing the most characteristic micro-structures and relationships of the three main tectono-metamorphic events.

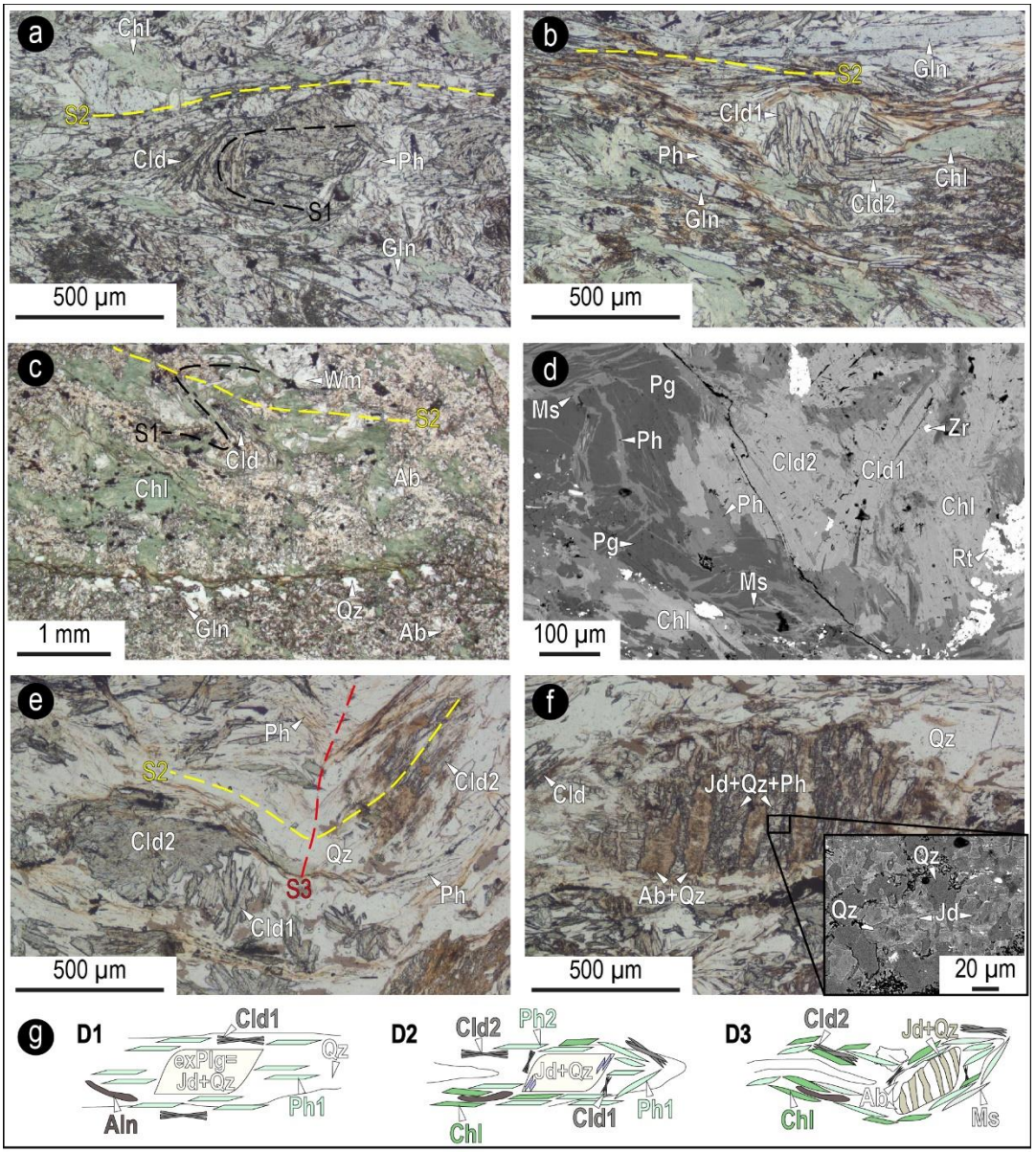

Sample AC74: Jd-bearing gneissic micaschist

This sample is a medium-grained gneissic micaschist consisting of quartz (21%), potassic white mica (49%), jadeite (3%), chloritoid (12%), chlorite (4%), albite (4%), paragonite (3%), and accessory allanite (3%) and rutile (1%). The main foliation (S2) is defined by the alignment of white micas, chlorite and chloritoid, concentrated in pluri-mm thick layers, alternated with discontinuous quartz-rich layers (Figure 47 and Figure 49e). A relic S1 foliation is defined by quartz + white micas + chloritoid + jadeite + rutile and is highlighted by polygonal arcs and intrafolial folds preserved

within micro-lithons (Figure 49e-f). Chloritoid occurs in two generations: an earlier syn-D1 generation, oriented at high angle with respect to the S2, and a syn-D2 generation (Figure 49e-f). Jadeite porphyroblasts, up to 1.3 mm in size, are enveloped by the main foliation and are partially and variably retrogressed (Figure 49f). The preserved portions of jadeite display intergrowth relationships with quartz and pre-kinematic white mica, while retrogressed portions are completely replaced by a fine-grained aggregate of quartz and albite. Late albite, chlorite and muscovite grow statically on the main foliation. Among accessory phases, mm-sized relicts of allanite are wrapped by the main foliation and include zircon and monazite. A schematic metamorphic evolution through the three main tectono-metamorphic event is reported in Figure 49g.

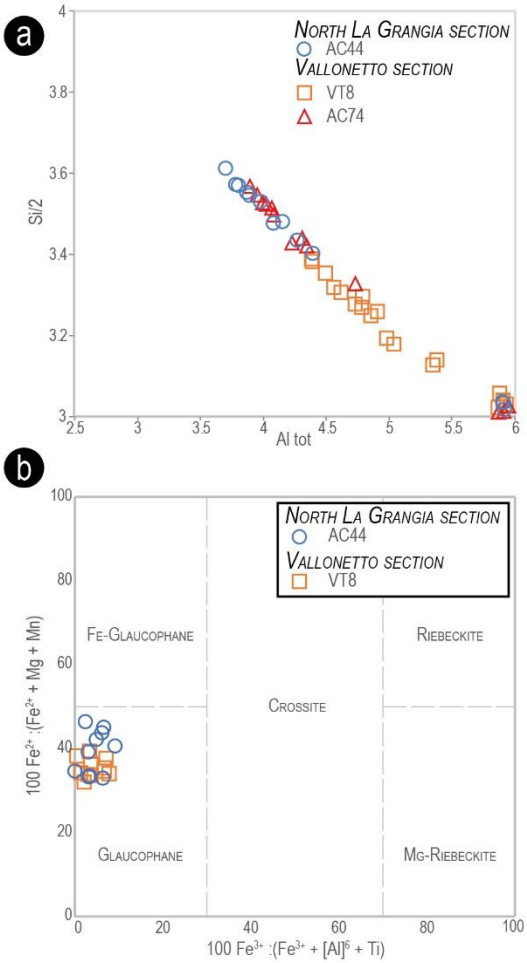

Figure 4 Compositional diagrams for potassic white mica (a) and Na-amphibole (b) in the three selected samples from Corno et al., 2021b.

White mica occurs as potassic white mica and paragonite. Phengite and paragonite are related to D1 and D2 tectono-metamorphic events, and are partially replaced by static growth of syn-D3 muscovite. Phengite flakes have the highest Si contents (Si from 3.30 up to 3.56 a.p.f.u; Figure 50a). X_{Mg} in phengite ranges between 0.48 and 0.75. Na-pyroxene is almost a pure jadeite according to Morimoto (1988), with Acmite < 15% (see supplementary material in Appendix III). Both chloritoid generations (i.e. syn-D1 and syn-D2) have low X_{Mg} values of 0.13-0.14, and low MnO contents, always lower than 1 wt%. Chlorite plots in the clinochlore field and has X_{Mg} ranging between 0.32 and 0.35.

Table 2 Blastesis-deformation relationships of selected samples from Corno et al., 2021b.

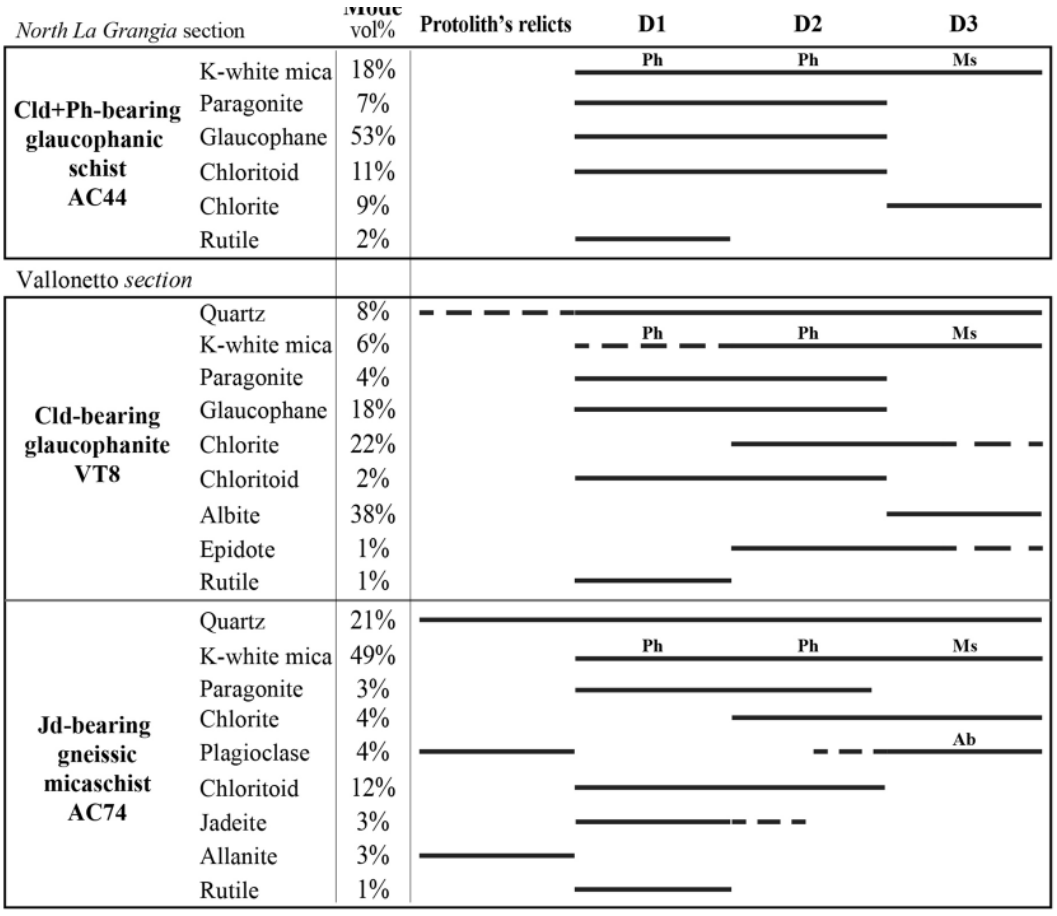

6.2.4 Thermodynamic modeling

The peak P-T conditions of the selected samples were constrained using the isochemical phase diagram approach, based on the predicted stability field of the observed assemblages, combined with the intersection of compositional isopleths modelled for chloritoid and glaucophane (samples AC44 and VT8). The isochemical phase diagrams were calculated in the system MnNKFMASOH (MnO-Na_2O-K_2O-FeO-MgO-Al_2O_3-SiO_2-$O2$-H_2O) for samples AC44 and AC74 and in the system NKFMASOH (Na_2O-K_2O-FeO-MgO-Al_2O_3-SiO_2-O_2-H_2O) for sample VT8,using Perple_X 6.9.0 (Connolly, 1990, 2005, 2009), the internally consistent thermodynamic database of Holland & Powell (2011) (ds62) and the equation of state for H2O of Holland & Powell (1998). Fluid saturated conditions were assumed, and the fluid was considered as pure H2O (a_{H2O}=1). This last assumption is realistic for the studied samples, because of the large occurrence of hydrous phases and the absence of primary carbonates and sulphides.

Table 2 Summary mineral compositions for the modelled samples from Corno et al., 2021b.

Wm	Ph	Si = 3.40–3.62	Si = 3.29–3.38	Si = 3.32–3.56
	Ms	Si = 3.01–3.03	Si = 3.13–3.28	Si = 3.01–3.03
Pg		Na = 1.90–1.95	Na = 1.72–1.86	Na = 1.80–1.90
Gln		Na(B) = 1.96–2.00 Ca(B) = 0.00 X_{Mg} = 0.56–0.67	Na(B) = 1.96–2 Ca(B) = 0.00 X_{Mg} = 0.59–0.67	
Jd				X_{Acm} = 0.05–0.11
Cld		X_{Mg} = 0.15–0.18	X_{Mg} = 0.14–0.19	X_{Mg} = 0.13–0.14
Chl		X_{Mg} = 0.47–0.54	X_{Mg} = 0.43–0.58	X_{Mg} = 0.32–0.35

CaO was neglected in all pseudosections, because Ca-bearing phases are lacking. TiO_2 was not included in the calculation because rutile is the only Ti-bearing phase stable at HP conditions in all the samples.

The following solid solution models were used: biotite, chlorite, chloritoid, garnet, staurolite, white mica (White et al., 2014), clinopyroxene (Green et al., 2007), amphibole (Green et al., 2016), feldspar (Fuhrman & Lindsley, 1988), carpholite (Smye et al., 2011) and epidote (Holland & Powell, 1998). Quartz, lawsonite and kyanite were considered as pure phases.

Phengite compositional isopleths have not been used, due to the difficulties in assigning each composition to a specific phengite generation (syn-D1 or syn-D2). The general topology of the calculated phase diagram sections is similar for all the samples: chloritoid is predicted to be stable up to 530-560°C and garnet appears in the temperature interval of 480-530°C, depending on samples. Glaucophane and paragonite are predicted to be stable in almost the whole P-T region of interest; exceptions are for sample AC74, where glaucophane is limited to P < 21-23 kbar and for sample AC44, where paragonite is absent in the P-T range of 400-520°C, 17.5-24 kbar.

6.2.4.1 North La Grangia section

Sample AC44

The modelled pseudosection is dominated mainly by quadri- and quini-variant fields (Figure 51a). The observed peak assemblage (Gln + Cld + Ph + Pg + Qz) is modelled at T < 450°C and P = 17-22 kbar; at T > 450°C, garnet is predicted to occur in addition to these phases, whereas at P > 21-22 Kbar, jadeite appears at the expenses of paragonite. The modelled chloritoid and glaucophane compositional isopleths allow further constraining the peak P-T conditions for this sample. The X_{Mg} measured in chloritoid (X_{Mg} = 0.15-0.18) defines a T range of 420-480 °C, whereas the X_{Mg} measured in the syn-D1 glaucophane (X_{Mg} = 0.63-0.67) constrains pressure

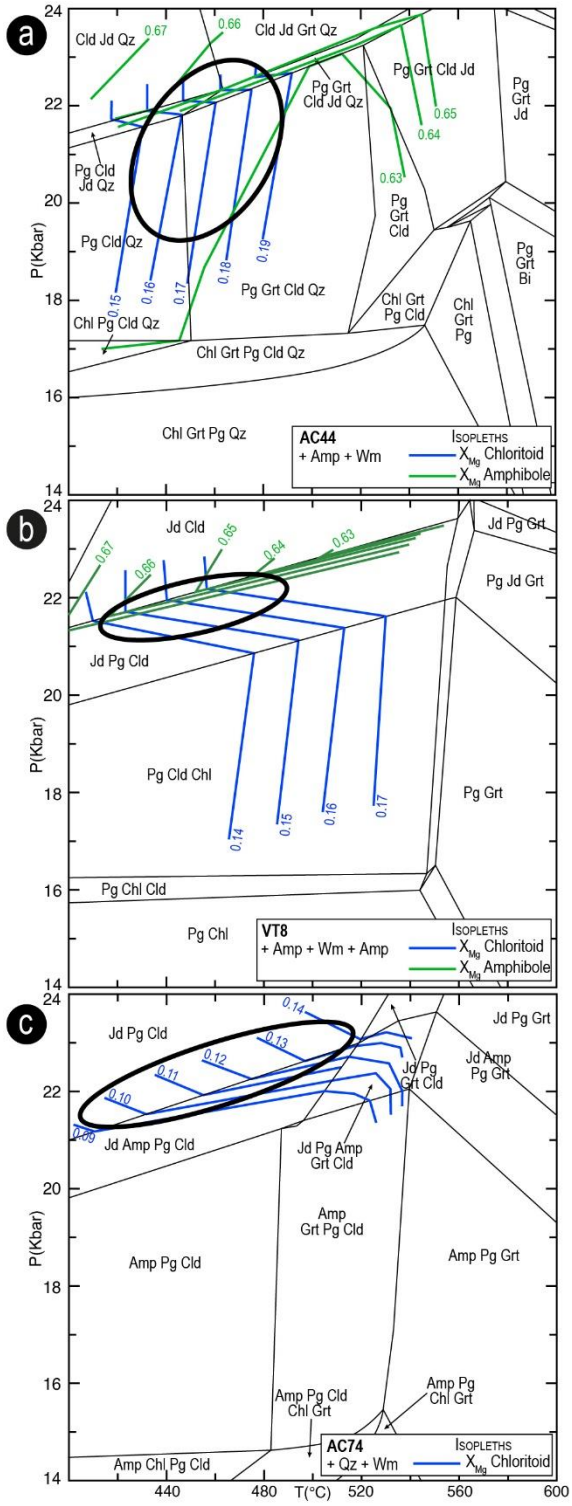

Figure 5 P–T pseudosections modelled for the selected samples from the North La Grangia and the Vallonetto sections using the measured bulk compositions of samples a AC44, b VT8 and c AC74 (from Corno et al., 2021b). The black ellipses show the constrained P–T conditions, based on the mineral assemblages and the intersection of compositional isopleths, as indicated in each legend. For clearness, all fields have been left white. Fields with five phases are quini-variant and those with six phases are quadri-variant, in all the pseudosections.

at 21-22 kbar, mostly in the narrow field where jadeite (< 0.15 vol%) coexists with paragonite. Very low modal amounts of garnet (<1 vol%) are predicted to occur at these P-T conditions, although it has not been observed in the sample. Such low modal amount of garnet could have been likely replaced by retrograde chlorite, which is widespread in the sample. Similarly, quartz is not observed in the sample but the modelled pseudosection predicts its stability over a wide P-T range. In this case, the predicted modal amount of quartz is extremely low (<0.2 vol%), and quartz could have been easily overlooked. Overall, peak P-T conditions of 21-22 kbar and 450 ±25 °C are constrained for this sample.

6.2.4.2 Vallonetto section

Sample VT8

The modelled pseudosection consists of large quadri-variant fields and smaller tri-variant fields (Figure 51b). The observed peak assemblage (Qz + Ph + Pg + Cld + Gln) is predicted to be stable in a large field ranging from 16 to 20-22 kbar and at T< 530 °C, limited by the garnet appearance at T > 530°C. At pressures higher than 20-22 kbar (depending on temperature), jadeite becomes stable

together with paragonite; this last disappears at P>22-23 kbar. The modeled compositional isopleths of chloritoid corresponding to its measured composition (X_{Mg} = 0.14-0.17) are nearly vertical in the jadeite-absent field, where they constrain temperatures in the range 460-520°C; however, in the paragonite + jadeite field, the chloritoid isopleths become P-dependent and constrain P in the interval 21-22 kbar (for T = 420-520°C). The X_{Mg} isopleths modeled for glaucophane and corresponding to its measured composition (X_{Mg} = 0.59-0.67) are concentrated in the paragonite + jadeite field and constrain P at 21-23 kbar. The intersection between chloritoid and glaucophane compositional isopleths further constrain peak P-T conditions at 450 ±20 °C and 21-22.5 kbar, in the Qz + Ph + Pg + Cld + Gln + Jd field. The amount of jadeite predicted at peak P-T conditions is about 15-17 vol%; although jadeite is not preserved, its former occurrence in the HP assemblage is compatible with the high amounts of retrograde albite (38 vol%) observed in the sample.

Sample AC74

The modelled pseudosection is characterized mainly by quadri- and quini-variant fields (Figure 51c). The observed peak assemblage (Qz + Jd + Ph + Pg + Cld) is predicted by a three-variant field at P > 22 kbar and T <480-520 °C, limited toward lower pressures by the appearance of glaucophane, and toward higher temperatures by the appearance of garnet. The modelled compositional isopleths of chloritoid corresponding to its measured composition (X_{Mg} = 0.09-0.14) plot both in this field and in the nearby glaucophane-bearing field (Jd + Gln + Pg + Cld + Qz + Ph), in which low modal amounts of glaucophane (<8 vol%) are predicted to occur. The former occurrence of low amounts of glaucophane in the peak assemblage, now completely replaced by retrograde chlorite + albite, cannot be excluded. Therefore, peak P-T conditions have been estimated at 21-23 kbar, 470 ± 50 °C, at the boundary between glaucophane-absent and glaucophane-bearing fields.

6.3. Main remarks

6.3.1 What the continental basement rocks of the BRU tell us: from the protoliths to eclogite-facies metamorphism

The detailed lithostratigraphic, structural, petrographic and petrologic analysis of the poorly investigated continental basement rocks of the BRU allowed us to make some hypothesis about the nature of their protoliths and to reconstruct their metamorphic evolution.

Protoliths

The North La Grangia section can be interpreted as a heterogeneous and composite Paleozoic basement derived from an original sedimentary sequence, mostly

consisting of pelites. These pelites had intercalation with different content and types of clay minerals (now transformed in Ab+Chl micaschist or Cld+Ph-bearing glaucophanic schist). They were also interbedded by arenaceous pelites (now fine-grained gneiss), and of minor quartz-arenite (now quartzite), with the arenaceous fraction increasing upward. In this setting, the photolith of the metabasite body embedded in this sedimentary sequence can be interpreted as a pre-Alpine metamorphic rock derived from a mafic protolith, either of magmatic or of sedimentary origin. The occurrence of relicts of unzoned garnet cores and of few relict K-feldspars, suggests that relatively high-T conditions were reached during the pre-Alpine metamorphic event. In this framework, the observed abrupt Mn-enrichment in garnet rims could be interpreted as the onset of high-P overgrowth on a pre-existent pre-Alpine HT garnet, as reported in other units of the Alps in similar tectonic positions (Bucher et al., 2019).

The lower part of the Vallonetto section is made of Jd-bearing gneissic micaschist, followed upsection by a dark grey graphitic micaschist. At the contact between these two lithologies, discontinuous metric bodies of Tlc+Aeg-bearing impure marble locally occur. We suppose a magmatic protolith for the Jd-bearing gneissic micaschist, whereas the dark grey graphitic micaschist likely derived from an original sedimentary sequence mostly consisting of pelite ± rich in organic matter. The uppermost part of the Vallonetto section is made of Cld-bearing micaschist with detrital allanite and metric bodies of glaucophanite, suggesting a volcano-clastic origin for this sequence.

Both sequences containing some intrusive bodies were involved in the Alpine subduction and in the following exhumation, preserving their original lithostratigraphic configuration in spite of the intense deformation and metamorphic re-equilibration.

Alpine evolution

The Alpine tectono-metamorphic evolution of the Monte Banchetta succession of the BRU was reconstructed by applying the isochemical phase diagram modeling approach. The P-T path from peak conditions to the final exhumation was constrained, and related to the different deformation stages recognized in the study area.

The D1 tectono-metamorphic event − defined by phengite + paragonite + glaucophane I + chloritoid I + epidote I assemblage − occurred at the metamorphic peak, which has been constrained at 20-23 kbar and 440-500 °C. These P-T peak conditions have been constrained based on the overlap of the P-T conditions (ellipses) inferred from the three modelled samples (Figure 51 and Figure 52). During the D1 event, jadeite developed in magmatic bodies with felsic composition

of the Vallonetto Section. These P-T peak conditions are remarkably consistent among the investigated samples, which are representative of different chemical systems, and point to peak metamorphism within the eclogite-facies field (Figure 52).

Based on minero-chemical composition of the metamorphic phases, similar P-T conditions (470-520 °C, at 17-19 Kbar) were inferred for the oceanic succession of the Monte Banchetta-Punta Rognosa unit based on conventional thermobarometry (see previous Chapter from Corno et al., 2019). These data suggest a common metamorphic evolution for the oceanic and continental successions of the BRU, in agreement with the reconstructed tectono-stratigraphy and implying their pre-orogenic juxtaposition.

The D2 tectono-metamorphic event is testified by the development of the main foliation at the regional scale, defined by upper blueschist-facies assemblages: phengite ± paragonite + glaucophane II+ chloritoid II + epidote II ± chlorite, and by the replacement of jadeite by albite + quartz in the gneissic micaschist of the Vallonetto section (sample AC74). Considering the reaction curves limiting the stability fields of the D2 assemblage (i.e. reactions 4 and 6 in Figure 52), this event is qualitatively constrained at around 11-13 kbar and 450-500°C. The D3 tectono-metamorphic event was responsible for the widespread retrogression of the HP mineral assemblages and the development of greenschist-facies assemblages (chlorite + albite + muscovite). Taking into account the fact that the oceanic succession of the BRU is tectonically juxtaposed with the continental succession since the first deformation stages, it is possible to suppose a common D3 event in the pumpellyite and stilpnomelane stability fields at about 350°C and P <5-7 kbar (Corno et al., 2019).

The exhumation path is characterized by an early decompression of at least 10 kbar, which was either isothermal or associated to a little T decrease, during which the Jd-out decompression reaction was crossed, leading to the development of the main regional foliation (D2 event). This event developed in the glaucophane + paragonite stability field according to the reaction 4 in Figure 52 and at lower T with respect to the amphibole + paragonite out/ garnet + albite in (reaction 6 in Figure 52). Therefore, the S2 foliation was equilibrated at an apparent geothermal gradient of about 10–12 °C/km, corresponding to the upper blueschist-facies (UBS), and this suggests a subduction channel environment. The subsequent exhumation stage is marked by a further decompression of almost 7-8 kbar associated with a significant temperature decrease (cooling down to 350–400°C), in the pumpellyite and stilpnomelane stability fields: this implies an increase in the geothermal gradient to ~25°C/km, compatible with continental collision regime (D3 event).

6.3.2 Comparison between the BRU and neighboring units

In the investigated sector of the Alpine chain, both eclogitic and blueschist-facies units are exposed (see Malusà et al., 2002, and Agard, 2021, for a detailed review). Six of these units have been selected for a comparison with the BRU (Figure 52 for locations of each unit), due to their proximity to the BRU and because their P-T paths have been already constrained in the literature. The selected units include: (i) the eclogite-facies, oceanic derived, Susa-Lanzo-Orsiera unit (Zermatt-Saas type; Servizio Geologico d'Italia, 2002) exposed in the Susa Valley (location A in Figure 52b), the blueschist-facies, oceanic units exposed in (ii) the Beth-Ghinivert area, (iii) the Albergian area, (iv) the Fraiteve area (locations B, C and D in Figure 52b), and the blueschist-facies, continental units exposed in (v) the Ambin-Vanoise Massif, and (vi) the Acceglio-Col Longet nappe (locations E-F and G-H in Figure 52b). It is important to note that the P-T evolution of these units were constrained with different methods, ranging from the pseudosection approach (i.e. for the Susa-Lanzo-Orsiera unit and the Ambin-Vanoise Massif), to multi-equilibrium thermobarometry (average P-T method of THERMOCALC; Holland & Powell, 1998) (i.e. for the Beth-Ghinivert, Albergian and Fraiteve area), to conventional thermobarometry and/or the analysis of the position of relevant reactions in the P-T space (i.e. for the Albergian and Fraiteve zones and the Acceglio-Col Longet nappe).

For the oceanic-derived, eclogitic rocks of the Susa-Lanzo-Orsiera unit (i.e. the Internal Piedmont Zone), exposed in the Susa Valley (A in Figure 52a), Ghignone et al. (2020) estimated peak P-T conditions of 25-29 kbar, 460-510°C. The observed peak assemblages in metapelites include chloritoid + garnet + phengite + lawsonite, whereas those observed in metabasic rocks consist of garnet + omphacite + glaucophane + phengite + minor talc ± lawsonite.

The oceanic-derived blueschist units (i.e. External Piedmont Zone) exposed in the proximity of the BRU registered different peak P-T conditions, ranging from the greenschist-amphibolite-facies transition to the blueschist-eclogite-facies transition. In the Beth-Ghinivert area (D in Figure 52a, just a few kilometers to the east from the BRU), Giacometti & Rebay (2013) estimated peak P-T conditions of 10 kbar, 492 ±35°C (peak assemblage in metapelites: phengite + chloritoid + chlorite ± epidote ± lawsonite; peak assemblage in metabasic rocks: Na-amphiboles + phengite + epidote ± chlorite). In the Albergian area (B in Figure 52a, 5-7 kilometers to the North-East with respect to the BRU), Agard et al. (2001) estimated peak P-T conditions of 18-21 kbar, 390-450°C (peak assemblage in metapelites: carpholite + chloritoid + phengite + paragonite + chlorite ± lawsonite; peak assemblage in metabasic rocks: phengite + paragonite + chlorite + glaucophane ± lawsonite). For the Fraiteve area (C in Figure 52a, 5-7 kilometers to the North-West with respect to the BRU), the same authors estimated peak P-T conditions of 16.5-18.5 kbar, 300-

390°C (peak assemblage in metapelites: carpholite ± chloritoid + phengite + paragonite + chlorite + lawsonite; peak assemblage in metabasic rocks: glaucophane + epidote + chlorite + lawsonite).

Peak P-T conditions registered by the continental-derived, blueschist-facies units adjacent to the BRU are also variable. In the Ambin-Vanoise massif, Strzerzynski et al. (2012) estimated minimum eclogite-facies peak P-T conditions of 17.5 kbar, 470° C for the Clarea Unit (E in Figure 52a) (peak assemblage: glaucophane + garnet + paragonite + phengite) and blueschist-facies conditions of 6.5-9 kbar, 350° C for the Ambin Unit (F in Figure 52a) (peak assemblage: chlorite + phengite). In the Acceglio-Col Longet nappe, Schwartz et al. (2000) (G in Figure 52a) and Michard et al. (2004) (H in Figure 52a) estimated average P-T peak conditions of about 12-15 kbar, 400-450 °C (peak assemblage: quartz + jadeite + garnet + phengite + zoisite + paragonite + glaucophane) at the blueschist-eclogite-facies transition.

From this comparison, it appears that the BRU experienced a metamorphic peak within the eclogite-facies field, at P-T conditions intermediate between those registered by the eclogite-facies of the Internal Piedmont Zone (Ghignone et al., 2020) and those registered by the oceanic and continental-derived units classically ascribed to the blueschist-facies metamorphic domain. Our results thus suggest that the BRU could be one of the westernmost eclogite-facies unit in the Western Alps, therefore extending the eclogite-facies metamorphic domain toward the west. Although in the literature a correspondence between the continental-derived rocks of BRU and those of the Col Longet nappe (Ultrabriançonnais domain) has been proposed based on the occurrence of jadeite in the pre-Triassic basement and to the lithostratigraphic features of its overlying Mesozoic sedimentary cover (Caron & Saliot, 1969; Caron, 1971), the two continental units recorded significantly different peak P-T conditions: the BRU registered peak pressures 12-15 kbar higher than those of the Col Longet nappe. The difference in peak P-T conditions is less marked between the BRU and the neighboring oceanic-derived units of the Beth-Ghinivert and Albergian-Fraiteve area; in this context a re-evaluation of their metamorphic evolution using the isochemical phase diagram approach is advisable, in order to test whether the apparent different peak metamorphic conditions could be imputable to different thermobarometric approaches.

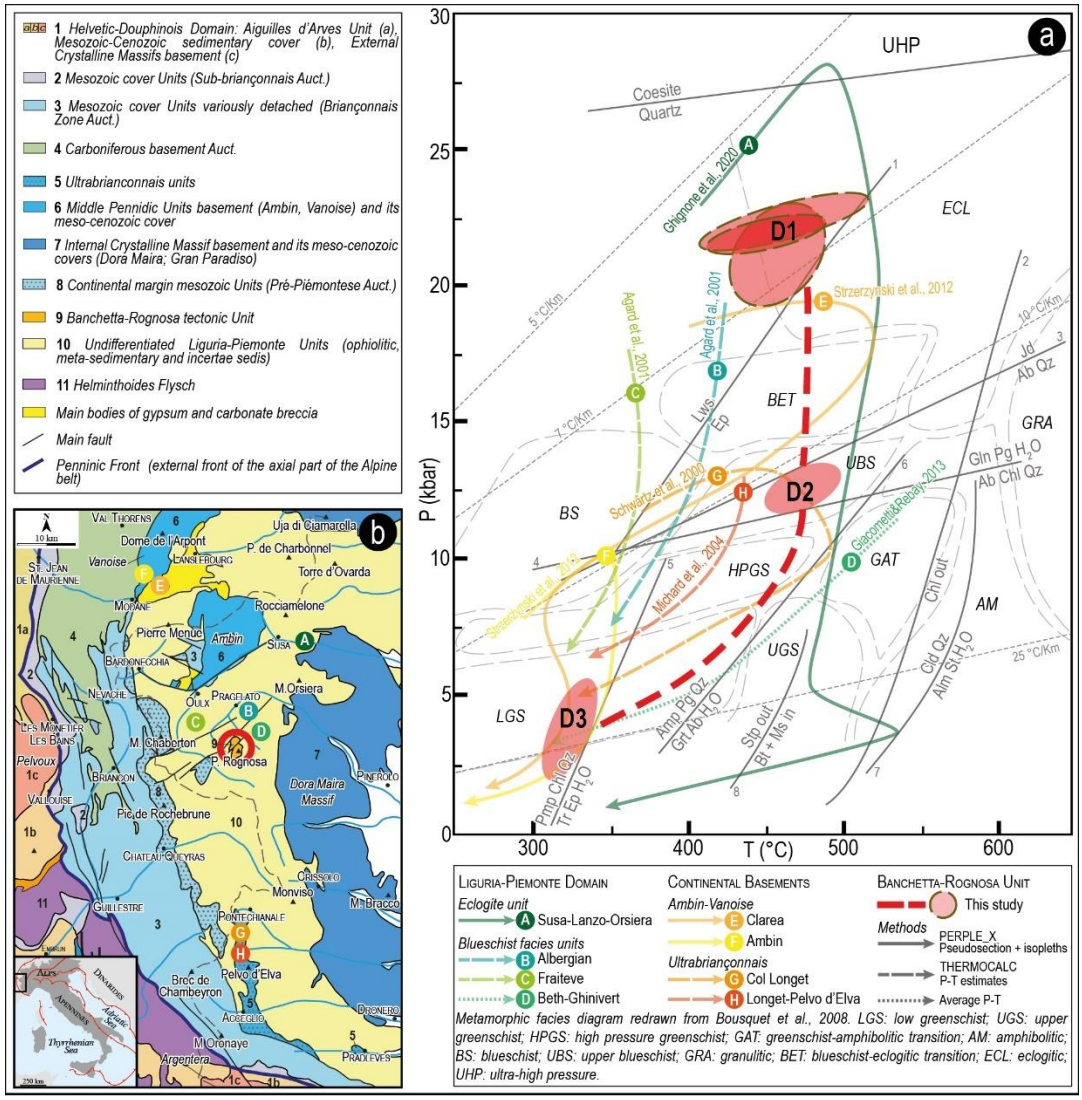

Figure 52 from Corno et al., 2021b. a) Compilation of P–T trajectories of different units of the Western Alps for comparison with the studied area. Whereas the D1 P–T estimates for the Banchetta-Rognosa unit were obtained by isochemical phase diagram modelling, the retrograde tectono-metamorphic events (i.e. D2 and D3) have been qualitatively inferred on the basis of mineral assemblages only. Different line patterns indicate different thermobarometric methods as reported in the legend. Reactions 1 to 8 are from: 1–2: Poli & Schmidt, 1995; 3: Holland, 1980; 4: Guiraud et al., 1990; 5: Evans, 1990; 6: Powell & Holland, 1990; 7: Rao & Johannes, 1979; 8: Nitsch, 1971; b Simplified tectonic map of the Western Alps (redrawn from the Structural Model of Italy, Bigi et al., 1990) and approximate location of units considered for comparison.

CHAPTER 7

The Albergian unit

Figure 53 Landscape on the Monte Albergian – Gran Mioul area from the summit of P.Rognosa.

7.1. Introduction

The Albergian unit (AU hereafter) crops out extensively from the Chisone valley, to the north, to the Pellice valley, to the south (Piana et al., 2017). In the investigated area, the AU is comprised between other units of the Ligurian-Piedmont zone and hence it belongs to the Middle meta-sedimentary units of the Ligurian-Piedmont zone (See Agard, 2021).

In the area investigated during this PhD (Figure 18), the AU is juxtaposed to the Lago Nero and Cerogne-Ciantiplagna units by a NE-SW high angle fault system to the north-west and embeds the Banchetta-Rognosa tectonic unit in the Troncea Valley (see Chapter 4).

In its general features (Caron, 1977; Servizio Geologico d'Italia, 2002, 2020; Agard, 2021), the AU is made of a thick succession of Cretaceous calcschist wrapping scattered blocks of oceanic lithosphere (i.e. serpentinite, meta-gabbro and metabasite), locally covered by a thin supra-ophiolitic sequence.

The largest bodies of serpentinite and serpentine schist occur widespread in the Argentera valley, in the lower Thuras valley, in the lower Troncea valley, and in the Col Clapis area (Figure 54a). Usually, these serpentinite blocks fade up section to ophicarbonate rocks. The contact with the overlying gabbro is locally marked by layers of talc-schist (e.g. Col Clapis area). Gabbro bodies crop out in the Col Clapis (Figure 54a-b) area and on the right slopes of the Troncea valley, above the village of Troncea near the Colle del Beth (Figure 54c). They occur as hm-size bodies embedded in the metasedimentary cover. Metabasite and greenstone crop out extensively as metric to km bodies in the studied area (Figure 54d). While smaller bodies are widespread throughout the whole area, the largest bodies occur in the Albergian-Gran Mioul mountain ridge, in the Colle Beth area, in the upper Troncea valley floor and in the Marin-Pelvo area. These bodies are often characterized by brecciated textures, with clasts and blocks from cm- to m- in size within a mafic matrix. Historically, these bodies have been exploited in the late XIX and early XX centuries for the collection of chalcopyrite (Colle del Beth area, Figure 54e). Locally, gabbro clasts and blocks occur within the meta-mafic breccia (Albergian-Gran Mioul area). Up section, thin layers of quartzite can occur, usually displaying fading boundaries with the underlying rocks. Quartzite layers crop out in the Col del Pis area, in the Colle Beth area and in the Albergian-Gran Mioul mountain ridge and are often followed by black micaschist, with low content of carbonate. The upper part of the metasedimentary cover is made of heterogeneous alternations of intensively folded calcschist (Figure 54f), impure marble, and micaschist, comprising the majority of the outcrops in the area and enveloping the other lithologies.

In order to investigate thoroughly the AU and in particular to attempt a reconstruction of the pre-collisional evolution of the oceanic sectors sampled by this units, this study detailed the lithostratigraphic successions exposed along the Albergian-Gran Mioul mountain ridge (Figure 55), located to East with respect to the village of Pragelato (upper Chisone valley).

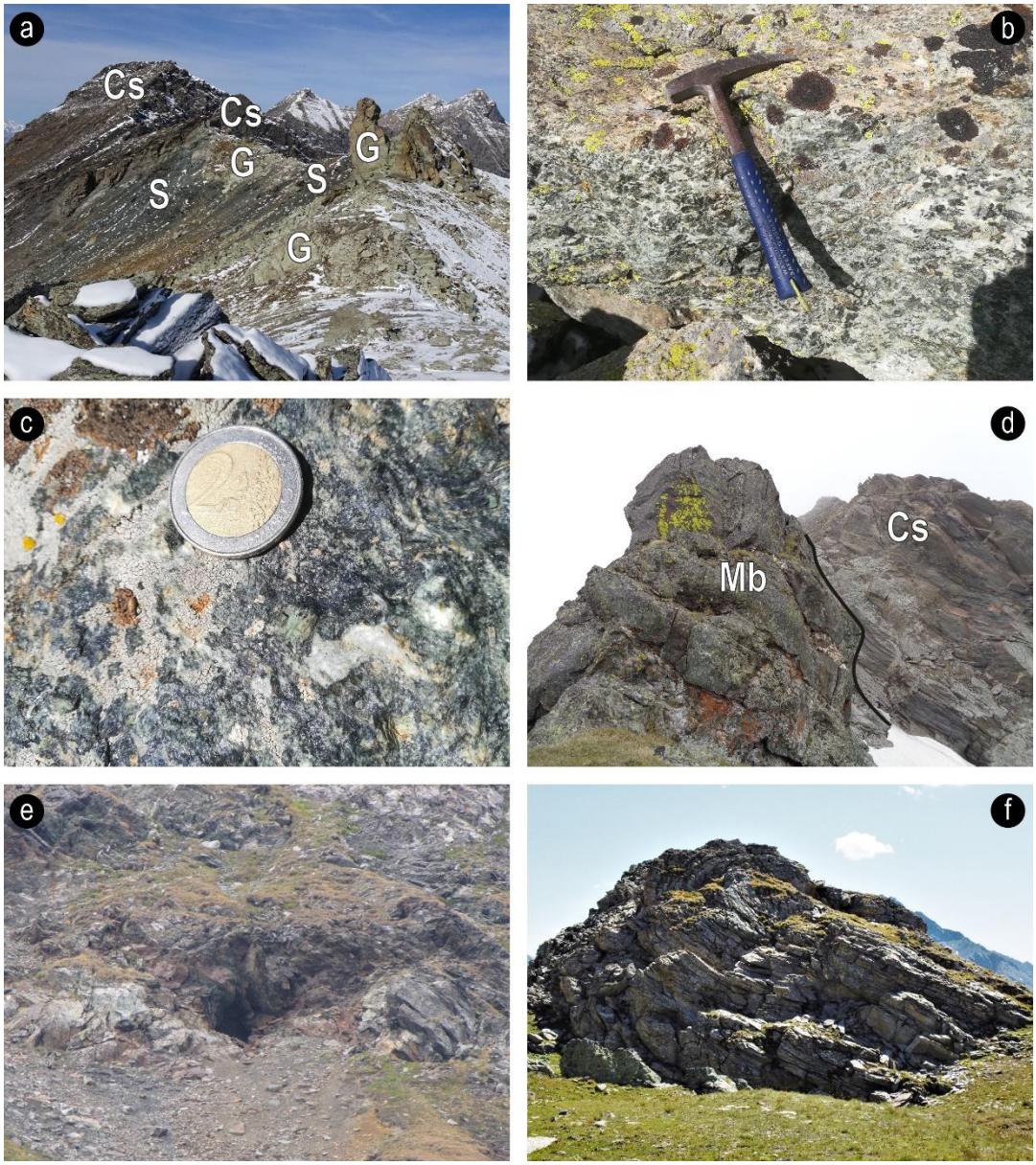

Figure 54 Main geological features of the Albergian unit. a) Col Clapis area, characterized by large meta-gabbro body (G) and serpentinite (S) bodies, embedded in calcschist (Cs); b) Mg-Al meta-gabbro body of the Col Clapis, characterized by a very coarse-grained texture; c) Fe-Ti meta-gabbro body from the Colle del Beth, characterized by preserved magmatic clinopyroxenes; d) large metabasite body embedded in calcschist of the Albergian unit in the Vallone dell'Albergian area (E of Monte Albergian); e) old chalcopyrite gallery in the metabasite North of Colle del Beth; f) large pluri-metric fold in the calcschist of the Albergian unit (Colle del Morefreddo).

Figure 55 (next page) from Corno et al., 2022. a) General and schematic map of the Western Alps. The Liguria-Piemonte oceanic domain (LP) is subdivided according to Agard (2021), u: blueschist- to subgreenschist-facies units; m: epidote- and lawsonite blueschist-facies units; l:- blueschist-eclogite to eclogite-facies units; b) Geological map of the Albergian - Gran Mioul area, (upper Chisone Valley, Italian Western Alps). c) schematic lithostratigraphic log of the mafic body of the Albergian - Gran Mioul area within the AU. Abbreviations are according to map legend. Blocks with different internal patterns in Mb refer to metric or plurimetric clasts and blocks of different lithologies; a: Mg-Al metagabbro; b: Fe-Ti metagabbro; c: metaplagiogranite. Red squares

show the location of samples used for thermodynamic modeling; d) view on the southern side of Monte Gran Mioul. Acronyms and color lines are according to the legend of the geological map. Note the high frequency of faults and major fractures in the metamafic rocks and the “klippe-like” structure capping the summit of Monte Albergian (photo courtesy of M. Giovo).

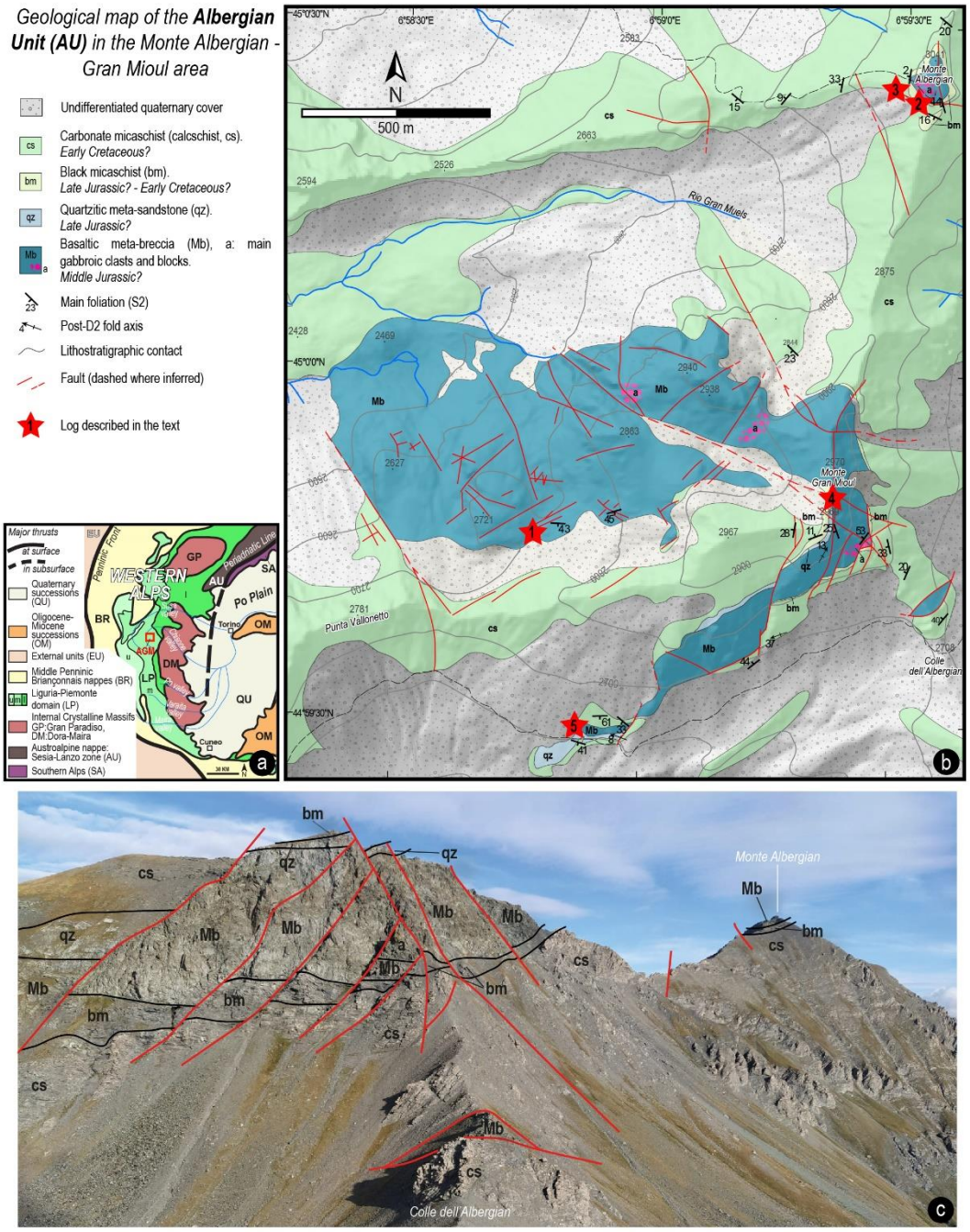

7.2 Lithostratigraphy of the Albergian unit in the M. Albergian-Gran Mioul area

The Albergian-Gran Mioul mountain ridge comprises a sector of the drainage divide reaching 3041 m a.s.l. on the summit of Monte Albergian. In this area, a pluri-hm body of meta-mafic rocks (gabbro apophysis and their volcanic and volcano-sedimentary cover) is embedded by heterogenous calcschist (Figure 55). In order to show the complex relationships between different lithologies, five lithostratigraphic logs from different localities will be described (Figure 56a).

Log 1- the central part of the Albergian – Gran Mioul block is mainly made of clast-supported basaltic meta-breccia (Figure 56a-b), reaching in thickness 200-300m in thickness. It is mainly a monomictic breccia made of basalt-diabase clasts and blocks (and minor doleritic elements, Figure 59b), from cm to pluri-m in size, within a minor mafic matrix. The composition of the matrix is similar to that of the mafic scree enclosed. Among basaltic blocks, rare plagiogranitic clasts have been found, wrapped by the same mafic matrix. In this thick sequence of meta-mafic rocks no evidence of (meta-)pillow lavas and (meta-)hyaloclastites have been found, suggesting for these mafic rocks a deep source close to the upper layers of an isotropic gabbro body. At a macroscale, larger blocks tend to be preserved in the lower part of the sequence, whilst the main upper part is made of clast-supported meta-breccia, with pluri-cm clasts of homogeneous meta-mafic composition. Hence, a rough fining-upward sequence can tentatively be inferred.

Log 2- close to the summit of Monte Albergian, coarse-grained, isotropic Mg-Al meta-gabbro clasts and blocks, up to pluri-metric in size occur (Figure 56a and Figure 56c-d). Locally, thinner scree levels of Fe-Ti meta-gabbro and meta-dolerite are intermingled within their volcanic and volcaniclastic cover, as described in log 1.

Log 3- just a few meters to the south-east with respect to log 2, larger Mg-Al meta-gabbro pods and lenses display primary contact with the meta-diabase, characterized by transitional and fading edges often highlighted by fine-grained, leucocratic meta-gabbro (Figure 56a-c). The magmatic coarse-grained texture is well preserved and unaffected by Alpine deformation, with the original sites of magmatic clinopyroxene and of plagioclase still perfectly recognizable (Figure 56c).

Log 4- on the southern summit of Monte Gran Mioul (2969m, Figure 55), the syn-rift meta-sedimentary sequence crops out. It comprises discontinuous bodies of quartzitic meta-sandstone (Figure 56a-f), usually a few meters thick, and discontinuous levels of micaschist (locally characterized by discontinuous impure marble). The whole succession is capped by a thick sequence of calcschists, characterized in the lower part by levels and lenses of impure marble, about ten cm

thick. In this sector, the contact between meta-mafic rocks and their meta-sedimentary cover is affected by Alpine tectonics and highlighted by copper sulfides and epidote-enriched faults and fractures.

Log 5- on the southern face of Monte Gran Mioul a preserved contact between meta-mafic breccia and quartzitic meta-sandstone can be observed (Figure 56a-e). In this location, discontinuous quartzitic meta-sandstone is characterized by a "detrital pollution" from the meta-mafic rocks, inferred by the occurrence of Na-amphibole, lawsonite, ilmenite and allanite crystals, decreasing in volume from the transitional contact with the meta-mafic rocks towards the upper meta-sedimentary sequence. The quartzitic meta-sandstone is followed up-section by a thick sequence of calcschist (Figure 56a-g), and minor micaschist.

Figure 56 (next page) Main lithostratigraphic features and relationships of the AU in the Albergian-Gran Mioul area. a) Lithostratigraphic logs of the AU. Red stars indicate the position of lithostratigraphic logs, see Figure 55 for their locations. Black circles with white letters inside each log show indicative position of corresponding pictures; b) basaltic meta-breccia texture, with cm clasts, cropping out in the north-western side of Monte Gran Mioul (log 1; q. 2650m a.s.l.); c) shaded boundary between meta-gabbro pod (a) and diabase sill? (Mb), note the fine-grained rim at the contact between lithologies (log 3; Monte Albergian south-west face, 3000m a.s.l.); d) stretched clast of meta-gabbro (a), pinched between diabase clasts (Mb). Note epidote + albite white-greenish veins cross-cutting both clasts (log 2; Monte Albergian, west side 2980m a.s.l.); e) lithostratigraphic contact between quartzitic meta-sandstone (qz) and basaltic meta-breccia (Mb), dashed black lines highlight pluri-cm clasts (log 5; Monte Gran Mioul south face, 2600m); f) stratigraphic contact between black micaschist and quarzitic meta-sandstone (log 4; Monte Gran Mioul, southern side 2960m a.s.l.); g) calcschist (Cs) characterized by differential erosion between pluri-cm dark levels of impure marble and pluri-cm discontinuous layers of carbonate micaschist (log 5; south face of Monte Gran Mioul, 25500m a.s.l.).

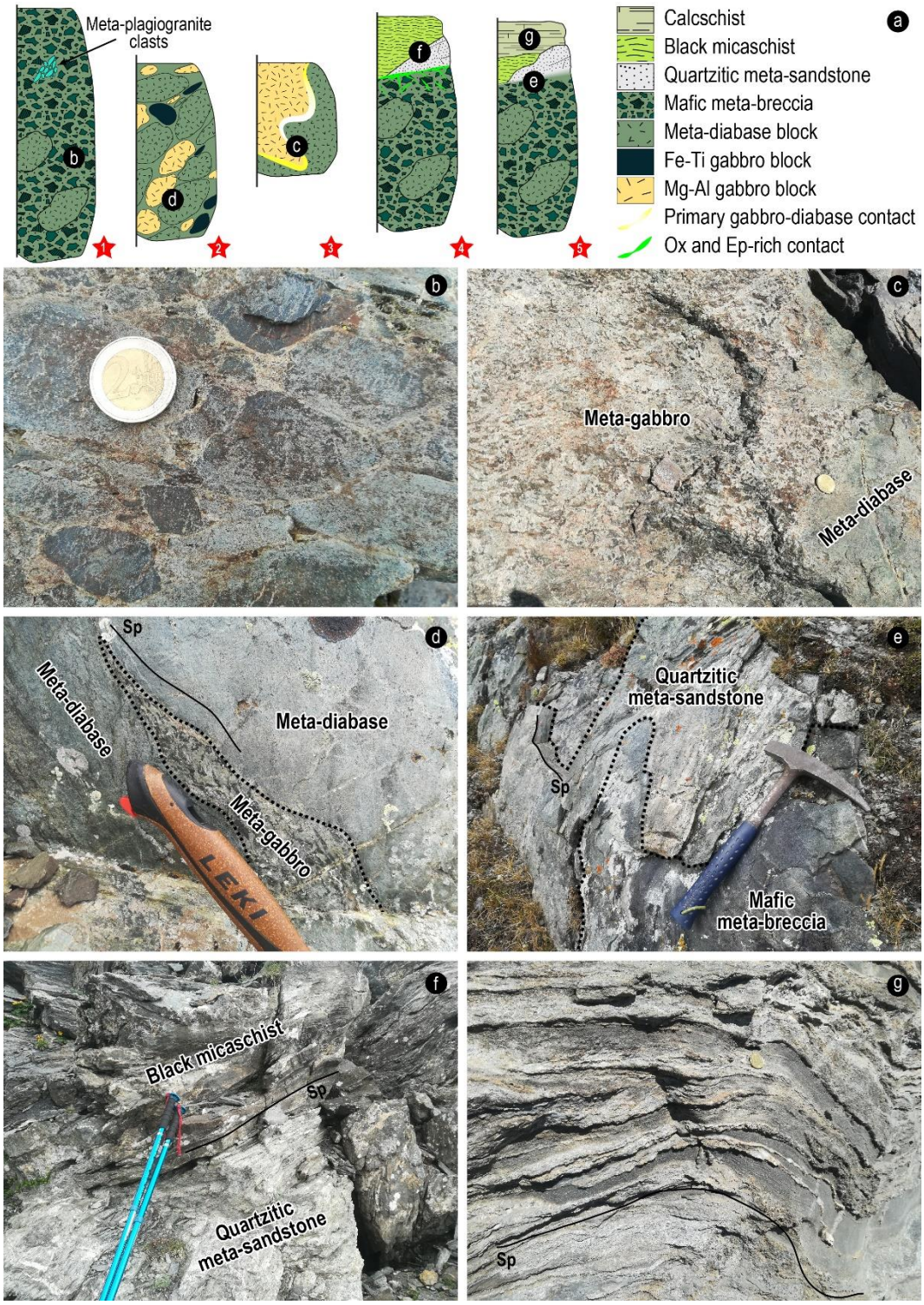
Meta-plagiogranite clasts
b
d
c
f
g
e
1
2
3
4
5
Calcschist
Black micaschist
Quartzitic meta-sandstone
Mafic meta-breccia
Meta-diabase block
Fe-Ti gabbro block
Mg-Al gabbro block
Primary gabbro-diabase contact
Ox and Ep-rich contact
a
b
c
Meta-gabbro
Meta-diabase
d
Sp
Meta-diabase
Meta-gabbro
LEKI
e
Quartzitic meta-sandstone
Sp
Mafic meta-breccia
f
Black micaschist
Sp
Quartzitic meta-sandstone
g
Sp

7.2.1 Structural evolution

Three main tectono-metamorphic events have been recognized in the area: i) the older D1 event is recorded by the oldest metamorphic foliation (S1), defined by peak mineral assemblages, mainly preserved in the meta-sedimentary rocks; ii) the D2 event is related to the development of the regional schistosity in the area (S2, Sp in Figure 56), which represents the axial plane of isoclinal folds (with N-S trending axis), generally dipping towards W-NW. This event is responsible for strain slip cleavage, mechanic re-orientation and recrystallization/retrogression of minerals of D1 event; iii) the D3 event, occurred during greenschist-facies requilibration, is responsible for the development of open folds (with E-W trending axis; Figure 56g) and for the reactivation/reorientation of older structures.

Intense faulting characterizes the meta-mafic block of the AU in the Albergian-Gran Mioul area, with two main systems: i) a N-S normal faults, generally dipping at high-angle towards the West, and ii) NE-SW trans-tensional high-angle faults (Figure 55).

7.3 Main remarks of the Mesozoic evolution of the Albergian unit

The current setting of the AU is the product of a polyphasic deformation history, both Alpine and rifting-related (hence Jurassic in age).

The most simplistic model describing the actual setting of the meta-mafic rocks of the AU, foresees a 4-steps scenario describing the evolution from a magmatic stage, in a slow-spreading ridge setting, followed by an OCC evolution and a polyphasic Alpine deformation. This model is inspired to that described for other blueschist-facies meta-ophiolitic bodies of the Western Alps and Alpine Corsica (e.g. Lagabrielle et al., 2014 and references therein). This model can account only for the possible succession of events that lead to the present-day setting of the hectometric meta-mafic body of the M. Albergian – Gran Mioul area, and it is not intended to be inferred to the evolution of the other meta-mafic bodies occurring in the Albergian unit, since their complex evolution and tectono-metamorphic history must be investigated on a case-by-case basis.

In this framework, the meta-mafic rocks of the AU sample a portion of a Jurassic isotropic gabbro body and its relationships with the volcanic and volcaniclastic rocks above (Figure 57a). The coarse grain-size, found in the present day meta-gabbro, is typical of a deep magmatic body intruded in the Jurassic oceanic crust. Hence, the transient contacts between meta-gabbro and meta-basaltic rocks (log 3) can be inferred as original magmatic contacts occurring at the gabbro-dyke transition. At modern OCCs, it has been found that volcanic activity usually predates the faulting, hence the occurrence of basaltic-rich hanging walls and basaltic rider blocks.

According to Tucholke et al. (2008) and Olive et al. (2010), a certain amount of magmatic activity and products are essential to the development of large detachment faults, occurring at the axis of slow-spreading ridges. Thus, it can be inferred that the lithological interface between massive and dense gabbro and basaltic rocks, acting as a surface of weakness, has been affected by a detachment surface typical of oceanic core complex, responsible for the progressive exhumation of the gabbroic body (Figure 57b). A petrographic witness of the fast exhumation of this gabbroic body is the occurrence of pigeonite relicts: pigeonite is in fact a typical clinopyroxene of volcanic Ca-poor rocks, only rarely observed in blueschist-facies gabbroic rocks worldwide (Nakayama et al., 1973). However, the coarse grain-size of these gabbros contrasts the idea of a fast, superficial emplacement of these rocks. Hence, a deep plutonic emplacement followed by a fast exhumation, leading to clinopyroxene exsolution, can be tentatively inferred for these rocks. In this setting of complex interactions between faulting and magmatism, volcanic activity at the seafloor does not have to necessarily occur (Godard et al., 2009), hence justifying the absence of meta-pillow lavas and meta-hyaloclastites.

The next step foresees the formation of a highly heterogenous seafloor, characterized, in Jurassic times, by structural highs and lows (Figure 57b). In one of these structural lows, tectonic breccias from the OCC detachment fault, reworked as sedimentary breccias, must have been accumulated as scree, mainly made by mafic rocks (former dykes and gabbro-dikes transitions) and minor gabbros and plagiogranitic clasts (logs A and B). Hence for the AU we can infer the occurrence of a block in the hanging wall of a detachment fault, as witnessed by the occurrence of carbonate in the matrix of the meta-breccia (Figure 57b). The active tectonic setting of Late Jurassic was then responsible for the emplacement of oceanic debris flows in morphological lows, discontinuously capping the basaltic-gabbroic meta-breccia. Hence, well-sorted siliciclastic turbidites (i.e. quartzitic meta-sandstone, logs 4 and 5), characterized by detrital allanite and ilmenite crystals, imply a storage area far from a continental margin and long-distance flows (Figure 57c). During the first stages of subduction, Alpine deformation was responsible for the reactivation of the OCC detachment that must have uprooted the AU block from its original oceanic basement, and subsequently enveloped it in the trench sediments (i.e. carbonate micaschist/calcschists) of the newly forming accretionary wedge (Figure 57d).

Due to the strong rheological contrast between the AU meta-mafic block and the embedding calcschists, extensional and shear veins began to form since the first stages of exhumation, in epidote-bearing blueschist-facies conditions (log 4). While in this phase calcschists adjusted ductile deformation (non-cylindrical folds and thrusts), brittle deformation already occurred in the AU meta-mafic block as witnessed by the formation of glaucophane+epidote veins in the meta-breccia (both

in the matrix, in the clasts and cross-cutting them both) and epidote-veins, mainly at the contact between quartzitic meta-sandstones and meta-breccias (see insets of Figure 57d). A similar type of deformation, strongly influenced by rheological contrast among different lithologies, has been already reported and widely investigated in the Central Alps in the Cima Lunga unit (see Maino et al., 2021, for a review), where non-cylindrical folding developed in weaker rocks surrounding stronger mega-lithons.

Figure 57 (next page) Tectono-stratigraphic sketch on the evolution of the AU in the M. Albergian – Gran Mioul area. a) Modified Penrose model according to Dick (1989). This model for slow-spreading ridges is based on the abundance of peridotite and frequent absence of gabbros (Dick et al., 2006), as seen widespread through the Western Alps. Data collected in present day oceanic ridges (such as the SW Indian Ridge and the Mid-Atlantic Ridge) suggests that oceanic crust generated in spreading centers at slow- and ultraslow mid-ocean ridge (such as the Alps) can consist of gabbro massifs. These gabbro intrusions are usually centered beneath a magmatic ridge overlain by pillow lavas and dikes that extend into mantle peridotite (Dick, 1989). In this scenario, a focused melt flow in the mantle towards ridge segment-midpoints can be envisaged (Whitehead et al., 1984). On the right, sketched detail on the gabbro-dyke transition zone where future detachment faults develop; b) Gabbro body exhumed at the ocean floor by a intra-oceanic detachment fault, defining in the hanging wall a body of meta-mafic scree. In this setting, the majority of clasts are expected to come from the diabase – basalt zone, however gabbro clasts can occur in minor part (upper inset). The texture is clast-supported and the matrix is not abundant. Local post-detachment vulcanic effusions can occur; c) after submarine volcanic activity, the meta-mafic hanging wall is discontinuously covered by siliciclastic turbidites coming from the continent; d) during Alpine orogenesis, the AGM block suffers peak metamorphism at lawsonite-blueschist-facies conditions. While the embedding calcschist still suffer ductile deformation, during the first stages of exhumation the M. Albergian – Gran Mioul block already develops extensional and shear veins, witnessing a brittle deformation at blueschist-facies conditions. Orange inset shows intense non-cylindrical folding in calcschists of the Albergian unit surrounding the M. Albergian-Gran Mioul block (hammer for scale); green inset shows a polished metabasite sampled at the contact with quartzitic meta-sandstone (log 4), characterized by copper sulfides and epidote-enriched faults and fractures; blue inset shows a glaucophane + quartz vein in a basaltic meta-breccia of the AU.

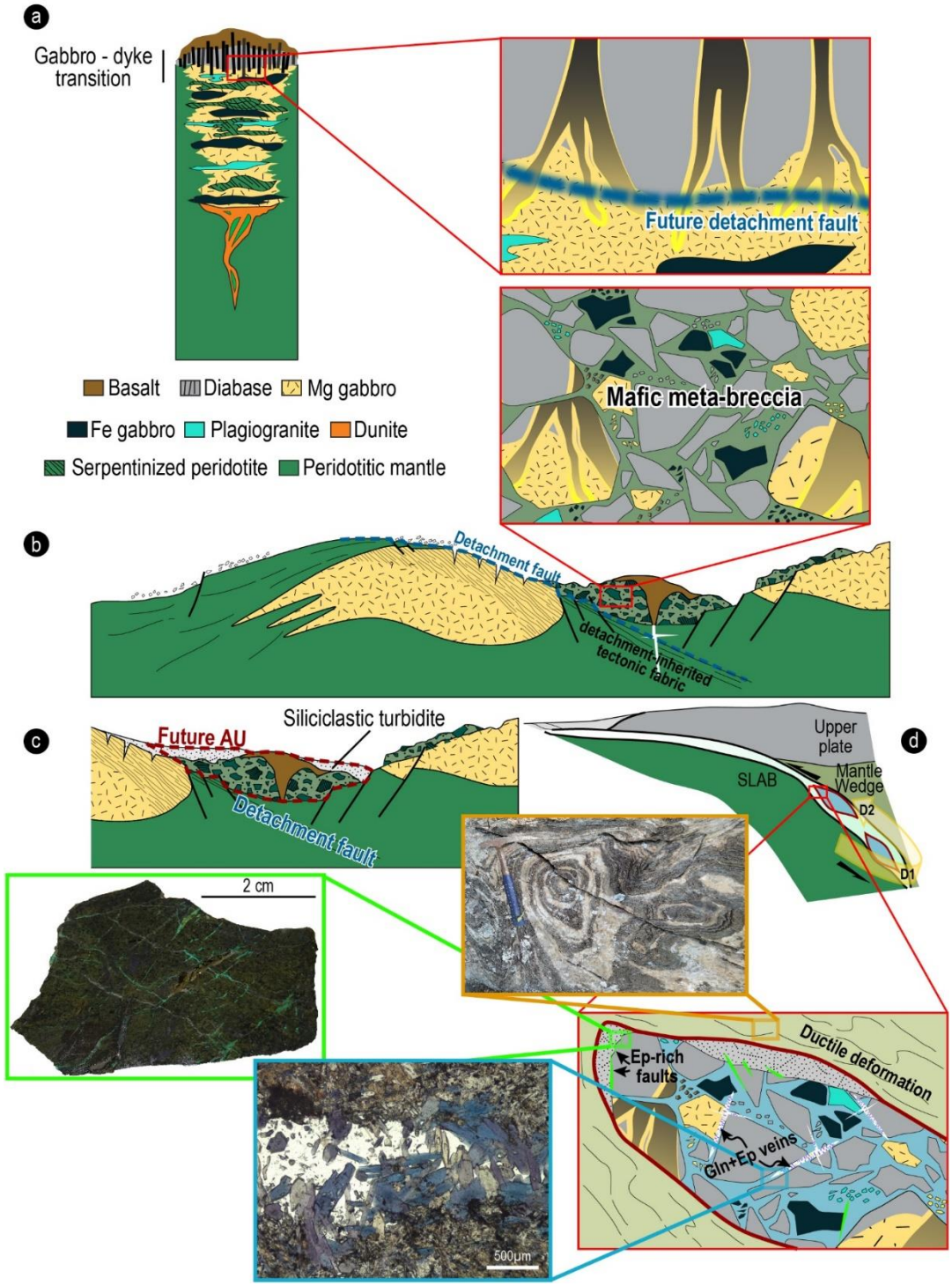
a
Gabbro - dyke transition
Future detachment fault
Mafic meta-breccia
Basalt
Diabase
Mg gabbro
Fe gabbro
Plagiogranite
Dunite
Serpentinized peridotite
Peridotitic mantle
b
Detachment fault
detachment-inherited tectonic fabric
c
Siliciclastic turbidite
Future AU
Detachment fault
d
Upper plate
SLAB
Mantle Wedge
D2
D1
2 cm
Ductile deformation
Ep-rich faults
Gln+Ep veins
500µm

CHAPTER 8

The lawsonite-bearing rocks and tectono-metamorphic evolution of the Albergian unit

Figure 58 Landscape view on the M. Gran Mioul southwestern slopes, the large, klippe-like meta-mafic body is roughly approximated by the snow covered area.

8.1. Introduction

The Albergian unit (AU) described in the previous Chapter 7 is characterized by occurrence of lawsonite-bearing rocks, known since the studies of Caron (1974, 1977) that described the occurrence of different generations of lawsonite mainly in the meta-sediments and locally in the meta-mafic rocks in the Argentera valley. The occurrence of preserved lawsonite was also confirmed by later studies (e.g. Malusà et al., 2002; Servizio Geologico d'Italia, 2002; Agard, 2021). In this frame, Corno et al. (2022) emphasized the abundance of fresh lawsonite in the meta-mafics rocks of this unit as well. Notably (see below), the accurate study on the lawsonite-bearing rocks provides fundamental constraints on the subduction and exhumation history of the units involved in the collisional zones.

Therefore, based on Corno et al. (2022), the aim of this Chapter 8 is i) to present petrography and mineral chemistry of the meta-mafic rocks of the AU, with emphasis on the preserved magmatic textures in the meta-mafic clasts, and on fresh

lawsonite occurrence and its replacement; and ii) to reconstruct the P-T tectono-metamophic evolution of the AU by phase equilibrium modeling.

Due to the purpose of this Chapter, a brief introduction to the significance of the lawsonite-bearing metamorphic rocks and their occurrence in the Western Alps is given in the following section.

8.1.1 Significance and importance of lawsonite-bearing rocks

Lawsonite-bearing metamorphic rocks, characteristics of eclogite- and blueschist-facies conditions, have been documented in many orogenic belts and are regarded as major markers of exhumed fossil subduction zones (e.g. Tsujimori and Ernst, 2014; Whitney et al., 2020). Lawsonite is a hydrous mineral retaining up to 12 wt% of H_2O; due to its stability up to depths of 300 km, it is one of the major H_2O carriers in cold subduction zones (Faccenda, 2014; Schmidt and Poli, 1994; Poli and Schmidt, 1998; van Keken et al., 2011). Moreover, the stability field of lawsonite-bearing assemblages in mafic rocks is strongly influenced by fluid composition, especially its $X_{(CO2)}$ [i.e. $CO_2/(H_2O+CO_2)$] (Goto et al., 2007; Poli et al., 2009), making lawsonite a key mineral in order to understand carbonation/decarbonation processes in subduction zones. Thus, lawsonite should be considered a crucial mineral both for defining metamorphic conditions and for understanding fluid-rock interaction processes during the evolution of orogenic belts. However, lawsonite is a mineral prone to be easily retrogressed during both prograde and retrograde metamorphism and it has been reported as a preserved mineral only in few eclogite- and blueschist-facies orogens worldwide (Whitney et al., 2020 for a review). Recognizing prograde and/or retrograde lawsonite is, therefore, crucial to correctly define burial/exhumation processes, (paleo)geothermal gradients, and geochemical processes in tectonic reconstructions of collisional orogen.

In the exhumed accretionary wedge of the Western Alps (Figure 1a), lawsonite-bearing rocks have been documented in the Liguria-Piemonte oceanic units and in the continental units of the Sesia-Lanzo zone since the late XIX century (among the numerous papers, e.g. Franchi 1895, 1897; Ellenberger, 1960; Compagnoni, 1977; Pognante et al., 1980, 1991; Mevel and Kienast, 1980; Martin and Tartarotti, 1989; Desmons, 1990; Groppo and Castelli, 2010; Zucali and Spalla, 2011; Lefeuvre et al., 2020). Focusing on the Liguria-Piemonte oceanic units (LP), preserved lawsonite relicts (and its pseudomorphs) have been reported in two eclogite-facies units: (i) the Voltri Unit (Scarsi et al., 2018 and references therein), and (ii) the Monviso Unit (Groppo and Castelli, 2010). In addition, fresh lawsonite-bearing meta-mafic (and meta-sedimentary) rocks are widespread in the eclogite- and blueschist-facies units of Alpine Corsica (Vitale Brovarone et al., 2011, 2013, 2014a). In the blueschist-

facies domain of the Western Alps, fresh lawsonite has been notably observed in the meta-sediments (e.g. Pognante, 1991; Lefeuvre et al., 2020; Agard, 2021): the abundance of lawsonite in meta-sediments has been generally linked to decarbonation processes, which mobilize Ca from calcium carbonate making it available for the lawsonite growth (Cook-Kollars et al., 2014; Nitsch, 1972). However, fresh lawsonite in mafic bodies associated with these blueschist-facies meta-sediments is scarcely documented in the literature (Caron, 1977; Vitale Brovarone et al., 2020; Agard, 2021 and references therein).

8.2. Petrographic and petrological features of the meta-ophiolitic bodies above the village of Pragelato and widespread lawsonite occurrence

8.2.1 The sampling site in the Albergian-Gran Mioul area

Lawsonite-bearing rocks of the AU discussed in this Chapter were collected in the Albergian Unit along the Albergian-Gran Mioul mountain ridge (E of the Pragelato village, upper Chisone Valley; Figure 55 and Figure 58), characterized by calcschists embedding a km-scale body of meta-mafic rocks (see details on previous Chapter 7).

Briefly, the meta-mafic body mostly consists of a clast-supported basaltic meta-breccia exposed with a thickness of about 200-300 m (Figure 55). This is mainly a monomictic breccia, dominated by basalt/diabase clasts (Figure 59a) and blocks, with minor doleritic clasts (Figure 59b). The clasts range from few a centimeters to several meters in size and are hosted within a fine-grained mafic matrix. Clasts and blocks of coarse-grained, isotropic Mg-Al meta-gabbro, up to several meters in size, occur close to the top of Monte Albergian. Some of these blocks display the primary contact between the diabase/basalt and the gabbro, characterized by transitional and fading edges. The magmatic coarse-grained ophitic texture of the gabbroic protolith is well preserved, with the original sites of the magmatic pyroxene and plagioclase still perfectly recognizable (Figure 59c). Locally, minor bodies of Fe-Ti meta-gabbro and meta-dolerite occur. In addition, rare plagiogranitic clasts have been found, wrapped by the same basaltic matrix.

The whole meta-mafic body is covered by: (i) discontinuous levels of quartzitic meta-sandstone (Figure 59d), usually a few meters thick, and (ii) discontinuous levels of black micaschist locally intercalated with impure marble layers. These are followed by a thick sequence of calcschists, containing levels and lenses of impure marbles, about ten cm thick, in the lowermost part. Clasts of impure marbles, up to pluri-cm in size, can be found in the upper part of the calcschists.

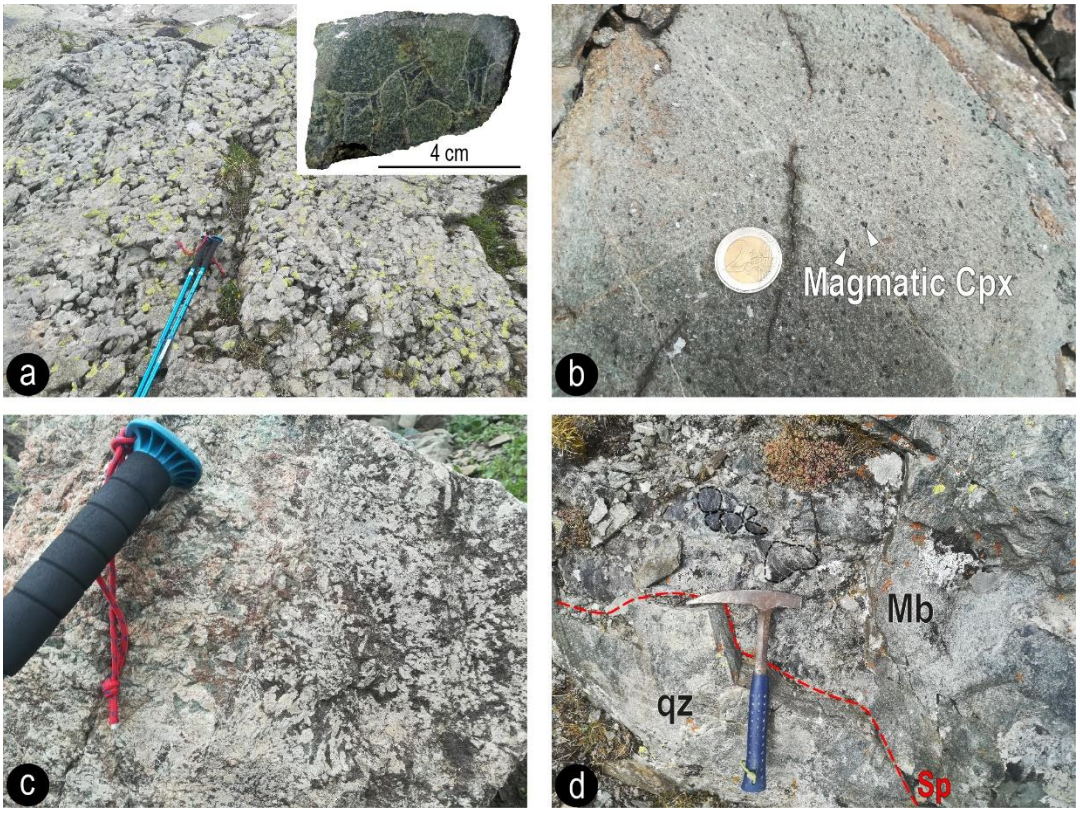

Figure 59 Field photographs of the Albergian - Gran Mioul area from Corno et al., 2022. a- differential erosion between (meta)diabase clasts, centimetric in size, and the fine-grained mafic matrix, highlighting the brecciated structure of the metamafic rocks (Monte Gran Mioul west side, 2700 m a.s.l.). The detail in the inset shows a polished sample of basaltic meta-breccia with a clast-supported texture. b- Decimetric clast of meta-dolerite consisting of mm-sized clinopyroxene crystals, weakly isoriented, within a fine-grained green matrix (Monte Gran Mioul northwest couloir, 2800 m a.s.l.). c- detail of a coarse-grained metagabbro, with magmatic ophitic texture still perfectly preserved but replaced by metamorphic minerals. Note the absence of metamorphic structures (Monte Albergian south-west face, 2990 m a.s.l.). d- lithostratigraphic contact between quartzitic metasandstone (qz), with well-developed layering (Sp main foliation) defined by alternating pluri-cm-thick quartzite layers and cm thick micaceous layers, and basaltic metabreccia (Mb). The dashed black lines highlight pluri-cm clasts within the meta-breccia (Monte Gran Mioul south face, 2600 m a.s.l.).

8.2.2 Petrography and mineral chemistry

More than 50 thin sections representative of all the lithologies distinguished in the studied section of AU were observed under optical microscope. In this section microstructures and petrographic features are described, with emphasis on the occurrence of lawsonite.

Basaltic meta-breccia

Clasts and blocks of meta-diabase and meta-basalt consist of lawsonite ± clinopyroxene + white mica + Na-amphibole + Ca-amphibole + quartz + epidote + chlorite + pumpellyite + albite + titanite. The fine-grained matrix is usually made of

the same assemblage but lacks clinopyroxene relicts and it contains scattered calcite. Both clasts and matrix display a poorly developed S2 foliation, defined by phengite + Na-amphibole + epidote + quartz + titanite ± chlorite ± pumpellyite. Magmatic Ca-clinopyroxene relicts are only locally preserved within the clasts; they are mostly retrogressed by actinolite + chlorite + albite. Lawsonite occurs both in the clasts and in the matrix (Figure 60a) after the magmatic plagioclase, mainly preserved fresh (i.e. metastable) and locally replaced by two events of retrogression: a first one, characterized by blastesis of zoisite ± pumpellyite, and a second one, characterized by more extensive growth of muscovite and epidote (± quartz) (Figure 61a). Lawsonite is locally wrapped by patches of Na-amphibole + Ca-amphibole. Na-amphibole crystals are locally overgrown by poikiloblastic albite, chlorite, and Ca-amphibole. Basaltic meta-breccias are locally crosscut by a network of veins at variable angles with respect to the main S2 foliation, resulting syn to post- D2 event. These veins, filled by quartz + idioblastic Na-amphibole + epidote, crosscut both the clasts and the matrix (Figure 60a).

Lawsonite is characterized by a significant Ti + Cr + Fe substitution of the Al site (Figure 62a). Three different generations of white mica have been recognized: the syn-D1 phengite displays the highest Si content (Si up to 3.71 a.p.f.u.), the syn-D2 phengite have Si in the range 3.35-3.50 a.p.f.u., whereas a marked decrease in Si is observed in the syn-D3 muscovite flakes (Si < 3.30 a.p.f.u; Figure 62b). The relict magmatic Ca-clinopyroxenes have augitic and pigeonitic compositions (Figure 62c). Na-amphiboles plot in the glaucophane and crossite fields, while Ca-amphiboles plot in the actinolite field (Figure 62e-f) (Leak, 1978; Hawthorne et al., 2012). Na-amphiboles occurring in the second deformation event display shifting compositions, from glaucophane to crossite. X_{Mg} of Na-amphiboles ranges from 0.62 to 0.77, while X_{Mg} of actinolite ranges from 0.34 to 0.83. Epidote-group minerals grow as zoisite during the D2 event and as epidote during the D3 event (Figure 62d).

Figure 60 (next page) Representative microstructures and mineral assemblages under optical microscope from Corno et al., 2022. a) Detail of a Gln + Ep + Qz vein in a basaltic meta-breccia. The inset shows the same vein at a lower magnification: note that the vein cross-cuts both clasts and matrix (Plain Polarized Light, PPL). b) Preserved ophitic texture within a Mg-Al metagabbro consisting of idioblastic (interstitial) magmatic plagioclase sites, now replaced by an aggregate of idioblastic lawsonite + interstitial omphacite and chlorite, and by the intercumulus clinopyroxene domains (lower right), in which the magmatic clinopyroxene is partially replaced at rims by glaucophane (left-side Crossed Polarized Light, XPL, right-side PPL). c) Fe-Ti meta-gabbro characterized by a magmatic clinopyroxene core (Cpx), partially retrogressed by Na-amphibole. In detail, an inner coronitic texture of glaucophane grows on clinopyroxene core and it is itself replaced by a thin outer mantle of Fe-glaucophane and a widespread rim of crossite. Note lawsonite crystals dispersed within the outer edge of crossite (left-side PPL, right-side XPL). d) Quartzitic metasandstone characterized by iso-oriented white mica, lawsonite, and Na-amphibole. Crossite (lavender in color) overgrows Fe-glaucophane crystals (bluish). The inset shows a detail of epidote with a detrital allanitic core (PPL). e) Black micaschist characterized by mm crystals of lawsonite, only partially retrogressed by zoisite and quartz (left-side PPL, right-side XPL). f) Calcschist characterized by cloudy lawsonite crystals wrapped by the main foliation (S2). A relict pre-S2 foliation is preserved in the cores of lawsonite crystals, highlighted by quartz + pyrite (PPL).

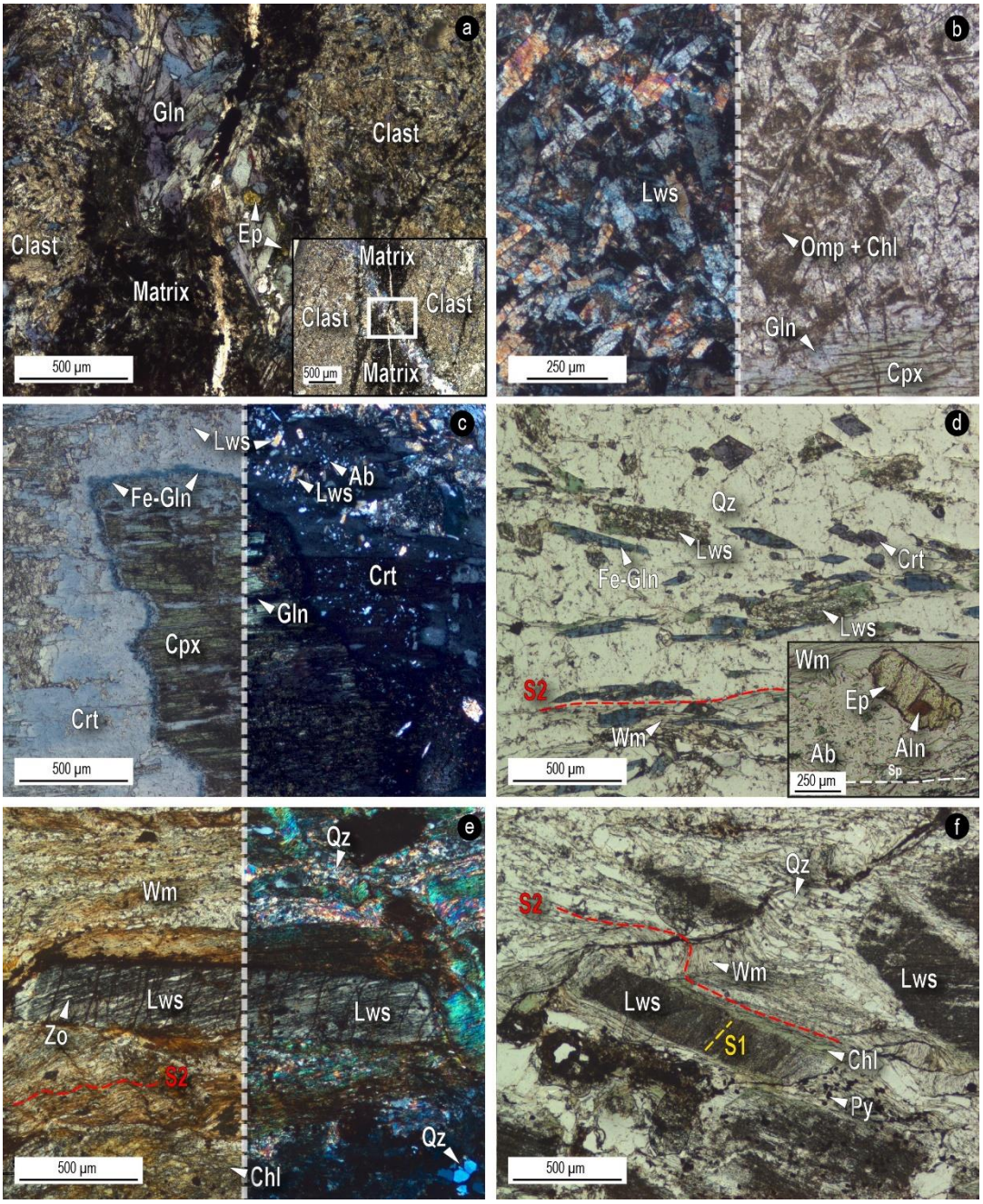
a
Gln
Clast
Ep
Clast
Matrix
Matrix
Clast
Clast
500 µm
500 µm
Matrix
b
Lws
Omp + Chl
Gln
250 µm
Cpx
c
Lws
Fe-Gln
Ab
Lws
Crt
Gln
Cpx
Crt
500 µm
d
Qz
Lws
Crt
Fe-Gln
Lws
Wm
S2
Ep
Wm
Ab
Aln
Sp
500 µm
250 µm
e
Qz
Wm
Lws
Lws
Zo
S2
Qz
500 µm
Chl
f
Qz
S2
Wm
Lws
Lws
S1
Chl
Py
500 µm

Meta-gabbros bodies

Meta-gabbro clasts, pods, and lenses still preserve their original coarse-grained magmatic texture. They can be classified as Mg-Al meta-gabbros (better developing and preserving the peak assemblage) and Fe-Ti meta-gabbros.

Mg-Al meta-gabbros are made of lawsonite + Ca-clinopyroxene + omphacite + white mica + Na-amphibole + Ca-amphibole + epidote + chlorite + albite + rutile + titanite and rare quartz. Small subhedral crystals of garnet have been occasionally found only in rare fine-grained meta-gabbros (e.g. sample 5482). Mg-Al meta-gabbros are often characterized by a perfectly preserved ophitic structure, with the idiomorphic sites of magmatic plagioclase now completely replaced by aggregates of idioblastic lawsonite, up to 500 μm in size, and the intercumulus domains originally consisting of clinopyroxene still recognizable (Figure 60b). Lawsonite crystals include small patches of quartz, suggesting they grew in SiO2-saturated domains (Figure 61b). Although generally perfectly preserved, lawsonite is locally replaced by two distinct retrograde assemblages, the first consisting of zoisite + paragonite, and the second of muscovite + epidote ± pumpellyite. The plagioclase sites as a whole are locally replaced at rims by white mica + albite + pumpellyite aggregates. The intercumulus magmatic Ca-clinopyroxene is often still preserved; it is only locally replaced, along fractures and rims, by Na- and Ca-amphiboles (Figure 60b) and by minor omphacite. Few veins crosscut the Mg-Al meta-gabbros, usually consisting of quartz and albite.

In Mg-Al meta-gabbros three different generations of white mica have been identified: syn-D1 phengite (Si up to 3.67 a.p.f.u.), minor syn-D2 phengite (Si from 3.35 to 3.45 a.p.f.u.), and syn-D3 muscovite (Si < 3.25 a.p.f.u.; Figure 62b), which is the most widespread white mica. Clinopyroxene composition ranges from Ca-pyroxene to Ca-Na-pyroxene (Figure 62c). It is worth noting that the large relicts of "magmatic" clinopyroxenes already contain low amounts of Na, whose abundance increases gradually in fine-grained clinopyroxenes occurring in the matrix. "Magmatic" clinopyroxenes plot in the diopside, augite, and pigeonite fields, whilst D1 metamorphic clinopyroxenes plot in the omphacite field (Morimoto, 1988). A first generation of Na-amphibole plots in the glaucophane field, while a second one, related to the late stages of the D2 event, plots in the crossite field (Figure 62f). Both these generations of Na-amphibole are often overgrown by actinolite (Figure 62e). X_{Mg} of Na-amphiboles ranges from 0.67 to 0.83, while for actinolite it ranges from 0.61 to 0.85. Epidote-group minerals occur as a first generation of zoisite and a second generation of epidote (Figure 62d).

Fe-Ti meta-gabbros consist of Na-amphiboles + Ca-clinopyroxene relicts + Ca-Na clinopyroxene + lawsonite + white mica + epidote + albite + chlorite + titanite + rutile (Figure 60c). The magmatic Ca-clinopyroxene is locally still preserved, but it is mostly replaced by metamorphic Ca-Na pyroxenes and by different types of Na-

amphiboles + minor zoisite and chlorite. The metamorphic Ca-Na clinopyroxenes occur in two generations (Figure 62c): earlier exsolution lamellae with acmite/aegirine-augite composition (Figure 62d) occur at a high angle with respect to the main cleavages, whereas a later omphacite generation grew along the main cleavages within larger magmatic clinopyroxenes (Figure 61d). At least three generations of Na-amphibole occur in different domains of the magmatic clinopyroxene sites (Figure 62f): glaucophane is concentrated in the core, Fe-glaucophane forms a thin mantle and crossite forms a thick rim (Figure 60c and Figure 61c). The magmatic plagioclase domains are more difficult to be recognized, because pervasively retrogressed. Lawsonite usually occurs in patches, partially or completely retrogressed by chlorite + albite or by muscovite + epidote, or as µm relicts in Na-amphibole (Figure 61c). White mica is usually not abundant and occurs as syn-D3 muscovite patches with epidote, retrogressing previous lawsonite crystals (Figure 62b).

Plagiogranites

Plagiogranite clasts consist almost exclusively of Na-pyroxene, lawsonite, and quartz with minor white mica + Na-amphibole + zoisite + albite + chlorite and titanite (Figure 63e). The plagiogranite clasts are embedded in a matrix similar to that of basaltic meta-breccia and made of Na-amphibole + white mica + epidote + quartz + chlorite + albite and minor lawsonite. A weak S2 foliation is defined by Na-amphibole + white mica + epidote + quartz. Lawsonite is usually well preserved and only locally replaced by zoisite and quartz. White mica is often associated with titanite, suggesting it replaced magmatic biotite. Clinopyroxenes plot both in the jadeite field and in the acmite field (Morimoto, 1988; Figure 62c and Figure 63f) and are only seldom replaced by Na-amphiboles and chlorite. Na-amphibole compositions plot at the transition between glaucophane and crossite fields (Figure 62f).

The S2 foliation is cross-cut by quartz + albite and quartz + albite + Na-amphibole veins.

Figure 61 (next page) Representative microstructures and mineral assemblages under SEM (backscattered electron images, BSE), from Corno et al., 2022. a) Lawsonite crystals almost completely replaced by phengite, zoisite, and pumpellyite in a basaltic metabreccia. Note the widespread occurrence of epidote, retrogressing both lawsonite and zoisite; b) Detail of the plagioclase domain reported in Fig. 3b. Lawsonite crystals include µm-sized "drops" of quartz; omphacite + chlorite growing in the intercumulus matrix do not display any preferential orientation. c) Clinopyroxene domain in a Fe-Ti metagabbro: the magmatic clinopyroxene, still preserved in the core, is mostly replaced by three different types of Na-amphiboles: glaucophane in the core, Fe-glaucophane in the thin mantle, and crossite in the thick rim. Crossite includes sub-idioblastic crystals of lawsonite and is partially retrogressed by albite at the rim. d) detail of a magmatic clinopyroxene domain from a Fe-Ti meta-gabbro: the magmatic Cpx is replaced by two generations of metamorphic clinopyroxene. An earlier generation

of acmite (developed at a high angle with respect to the main cleavages in the crystals) is overgrown by later omphacite (light gray). e) Lawsonite crystals of a quartzitic metasandstone replaced by zoisite at rims and including quartz in the core. Epidote, often with an allanitic core, occurs both over lawsonite and Fe-glaucophane. f) Lawsonite porphyroblast from a calcschist, preserving an early pre-S2 foliation, defined by quartz and pyrite. The core of the lawsonite is slightly enriched in Ti + Fe and it appears brighter. The main foliation S2 (see full image in the inset) wraps around the lawsonite crystal and is defined by muscovite and paragonite, growing at rims of the lawsonite.

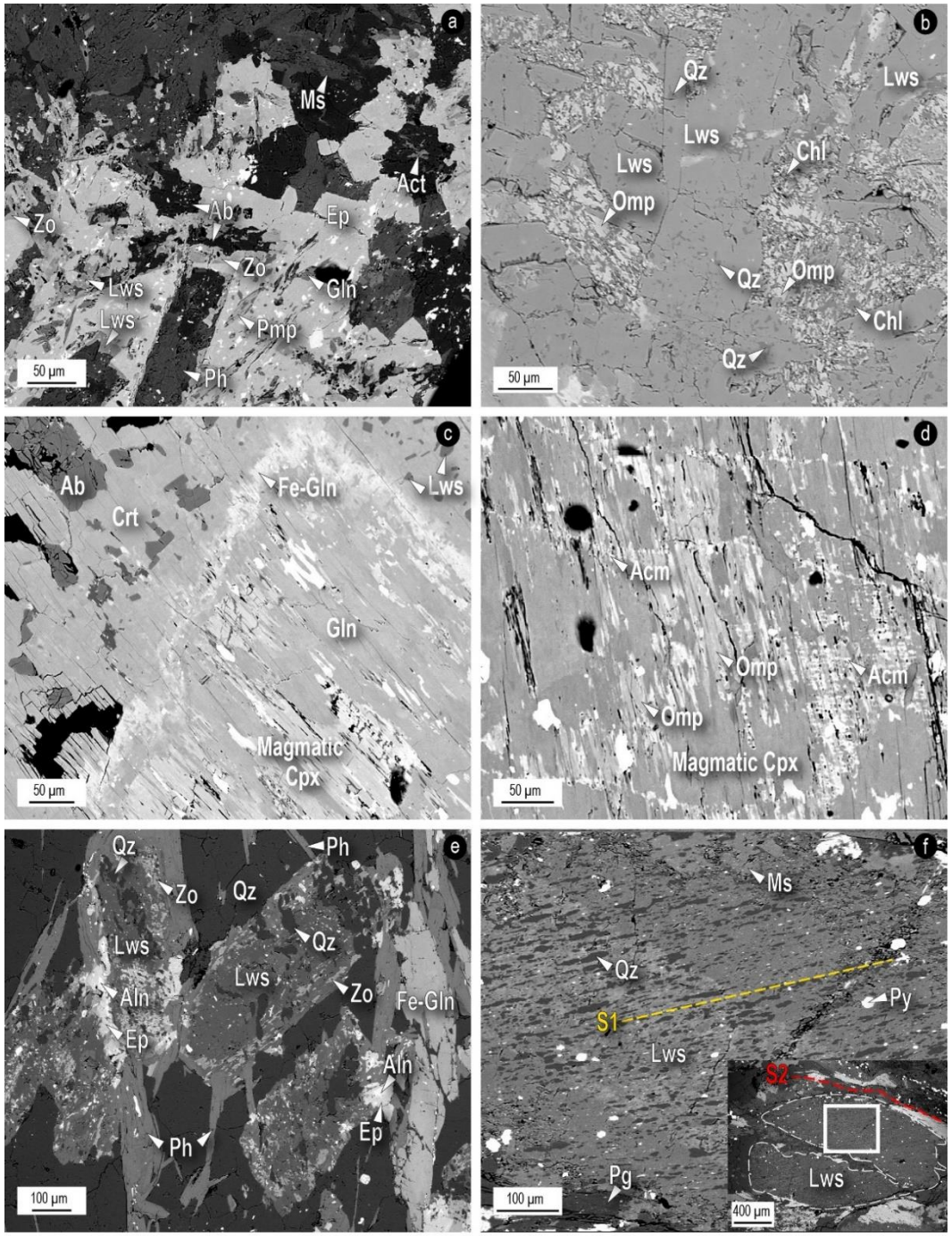

Quarzitic meta-sandstones

Quarzitic meta-sandstones consist of quartz + white mica + Na-amphibole + epidote + lawsonite + chlorite + albite + detrital allanite and ilmenite. The main foliation (S2) is defined by mm-thick white mica + Na-amphibole + lawsonite discontinuous layers alternated with pluri-mm thick discontinuous quartz domains (Figure 60d). Lawsonite is preserved as euhedral to subhedral crystals, variably overgrown by zoisite + quartz (Figure 61e). A late retrogression rarely occurs, linked to muscovite + epidote blastesis. Na-amphibole crystals are locally replaced by poikiloblastic albite and epidote + chlorite assemblages. Allanite occurs as relict crystals overgrown by epidote (Figure 60d).

The first generation of Na-amphibole can be classified as Fe-glaucophane, while a second generation has a crossitic composition (Figure 62f). Three generations of white mica occur in different microstructural positions: syn-D1 phengite flakes (Si up to 3.71 a.p.f.u.) are often found in poikiloblastic albite, syn-D2 phengite (Si from 3.47 to 3.35 a.p.f.u.) defines the main foliation that wraps pre-kinematic crystals of lawsonite; both syn-D1 and -D2 flakes are partially replaced by syn-D3 muscovite (Si < 3.27 a.p.f.u.), which only locally develops an incipient syn-D3 micro-crenulation cleavage (Figure 62b). Epidote-group minerals occur as zoisite, overgrowing lawsonite, and epidote, overgrowing allanite relicts (Figure 62d).

The S2 foliation is cross-cut by veins filled by epidote (near the contact with meta-mafic rocks) and by albite + quartz.

Figure 62 (next page) Mineral chemistry and classification diagrams from Corno et al., 2022. a) Lawsonite Al-site composition, showing that the transition metals (i.e. Fe + Ti + Cr) slightly substitute Al in the lawsonite structure. b) White mica composition in the Si vs (AlIV + AlVI) diagram, showing three distinct generations of white mica in most of the investigated lithologies. Muscovitic compositions are systematically related to the D3 event; phengitic compositions are related to the D1 and D2 events and define two distinct clusters in most of the investigated samples (with a partial overlap for a few of them). c) Morimoto (1988) pyroxene diagram; the Q vertex for magmatic clinopyroxene is reported in grey on the right. The arrows highlight changes in compositions between different generations of clinopyroxene, as suggested by microstructural evidence; each clinopyroxene generation has been related to a specific tectono-metamorphic stage (mag: magmatic relicts; D1: first deformation stage). Note the gradual Na-enrichment in the clinopyroxenes from meta-gabbros and the occurrence of three different magmatic clinopyroxenes. d) Epidote-group minerals diagram highlighting the occurrence of two generations of epidote minerals: D2 zoisite and D3 epidote. e- Amphibole composition in the Hawthorne et al. (2012) diagram Na vs AlIV. D1 and D2 amphiboles plot in the Glaucophane (Na-amphibole) field, while D3 Ca-amphibole rarely enters in the tremolite field. f- Na-amphibole classification according to the $Fe^{3+}/(Fe^{3+} + Al_{VI} + Ti)$ vs. $Fe^{2+}/(Fe^{2+} + Mg + Mn)$ diagram. While amphiboles from metamafic rocks (i.e. metagabbros and metabasites) generally plot in the Mg-rich glaucophane field, amphiboles form the metasedimentary lithologies usually plot in the Fe-rich glaucophane field. A general trend towards Fe^{3+}-enriched compositions (Crossite) is generally observed through all samples and is highlighted by dashed arrows and labels (D1: first deformation stage; D2: second deformation stage).

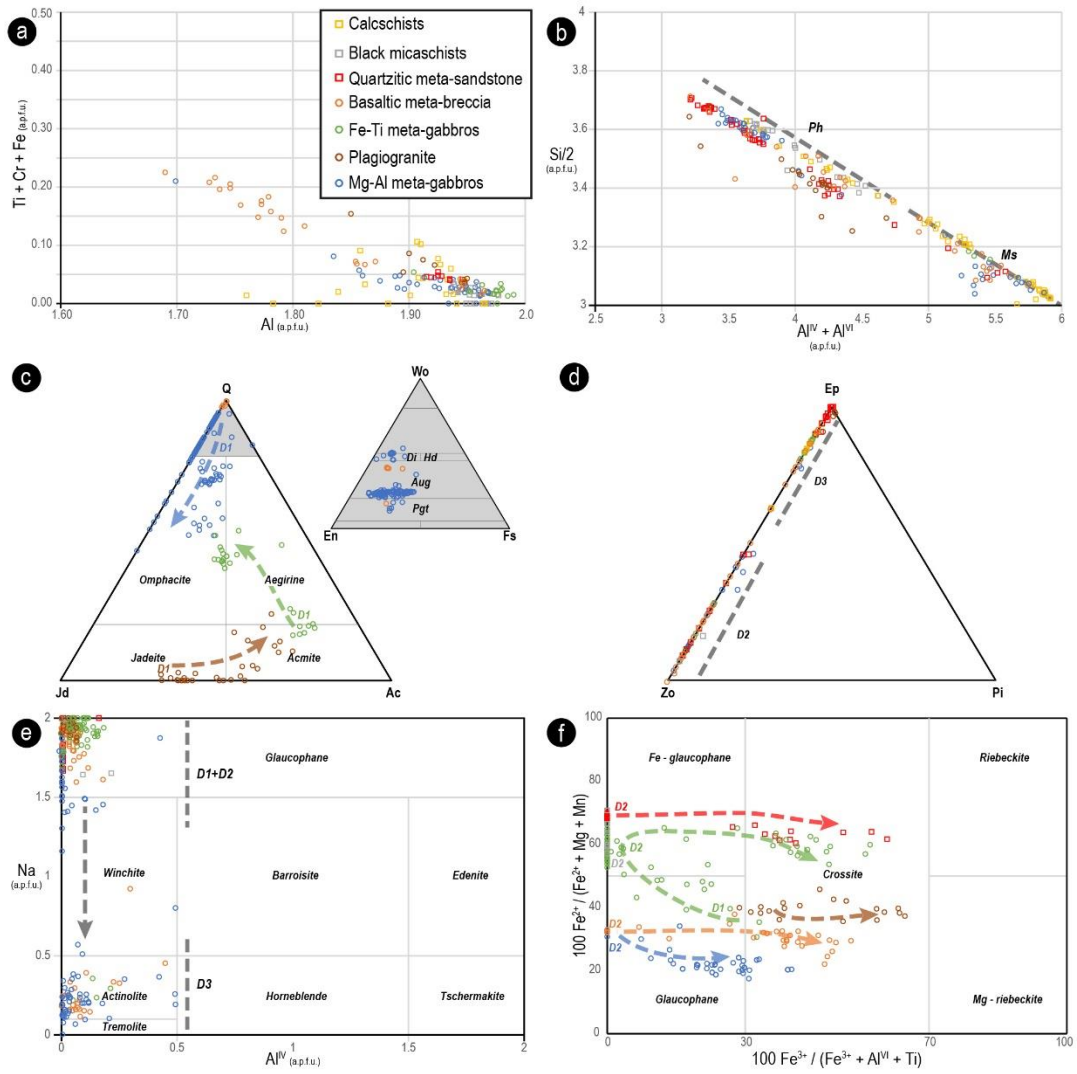

Black micaschists

Black micaschists consist of white mica + quartz + lawsonite + Na-amphibole + chlorite + epidote + albite + calcite + graphite and accessory rutile and titanite. They are characterized by a compositional banding defined by white mica + lawsonite + Na-amphibole + chlorite domains alternated with quartz ± calcite domains.

Lawsonite occurs as large, pluri-mm porphyroblasts (Figure 60e), pre-kinematic with respect to the main S2 foliation defined by white mica + Na-amphibole + epidote.

Lawsonite is only locally retrogressed at rims by chlorite and quartz. Na-amphibole occurs in large subhedral crystals often replaced by chlorite + quartz + albite. Na-amphibole has a Fe-glaucophane composition (Figure 62f). White mica occurs in different microstructural sites: syn-D1 phengite has the highest Si content (up to 3.66

a.p.f.u.), whereas syn-D2 phengite has Si content ranging between 3.50 and 3.38 a.p.f.u. (Figure 62b). Syn-D3 µm-sized crystals of epidote partially replace lawsonite, together with quartz. Epidote + Na-amphibole + quartz veins are observed at variable angle with respect to the S2 foliation.

Calcschists

Calcschists consist of calcite + quartz + white mica + lawsonite + chlorite + graphite and accessory phases (i.e. tourmaline, pyrite, titanite). The main foliation S2 is defined by white mica + quartz + carbonate ± chlorite. Lawsonite occurs as large euhedral to subhedral pre-kinematic porphyroblasts (with respect to the S2). They locally include an internal schistosity (S1), discordant with respect to the external S2 and defined by white mica + quartz + pyrite ± graphite (Figure 60f and Figure 61f). Lawsonite porphyroblasts are weakly zoned; the zoning is marked by Ti- and Fe enrichments in the core, which is also characterized by higher amounts of inclusions (apatite + pyrite + quartz; Figure 61f). Lawsonite crystals are only locally retrogressed by fine-grained quartz + white mica + calcite ± chlorite assemblages growing at rims. Three types of white mica have been recognized: phengite, muscovite, and paragonite. The three micas occur in several generations and microstructural positions. Syn-D1 phengite (Si up to 3.63 a.p.f.u.) mainly occurs as relicts inside large lawsonite porphyroblasts along with a first generation of paragonite, generally at a high angle with respect to the main foliation. The S2 foliation is defined by a second generation of phengite (Si from 3.35 to 3.50 a.p.f.u.) and of paragonite, while muscovite (Si < 3.30 a.p.f.u.) replaces lawsonite crystals at rims and defines an incipient syn-D3 crenulation cleavage, at a high angle with respect of S2 schistosity (Figure 62b). Chlorite occurs both dispersed in the rock and along lawsonite rims.

8.2.3 Petrography of samples selected for the P-T modeling

Based on their textural features and mineral assemblages, two samples (i.e. 5482: Mg-Al meta-gabbro; 5681: plagiogranite meta-breccia, see Figure 59c) have been selected from the main meta-mafic body for further petrological investigations, aimed at constraining the HP tectono-metamorphic evolution of the Albergian Unit in the upper Chisone Valley. Their petrographic features and mineral chemistry data are briefly summarized here. Modal proportions (vol.%) of the main minerals have been estimated using high-resolution multispectral maps processed using the MultiSpec© software (Figure 63a-b). The anhydrous bulk rock compositions used for the phase diagram modeling are reported in Table 4, together with the calculated

normative minerals. The blastesis-deformation relationships of the selected samples are summarized in Table 5.

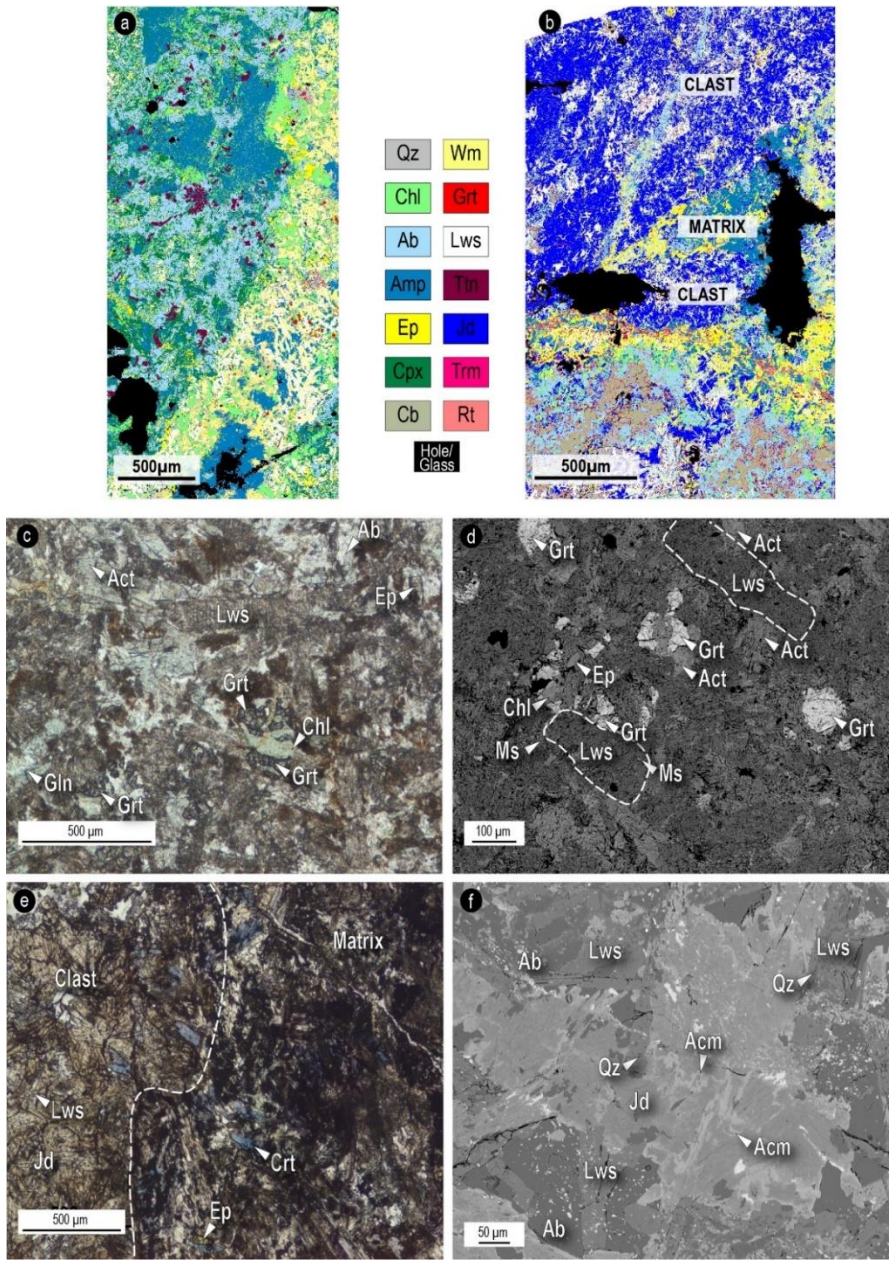

Figure 63 (previous page) X-ray maps and representative microstructures for samples used for thermodynamic modeling, from Corno et al., 2022. a) X-ray map of the Mg-Al metagabbro, sample 5482. b) X-ray map of the plagiogranite meta-breccia, sample 5681, with well recognizable clast and matrix relationships. c) Anhedral garnet crystals, partially retrogressed by chlorite and epidote, in sample 5482 (PPL). d) BSE detail of the sialic domain in sample 5482, showing small garnet crystals replaced by epidote and chlorite. Lawsonite is fresh and only locally replaced at rims by muscovite. e) Clast-matrix boundary in the plagiogranite metabreccia. The clast (on the left) is characterized by the widespread occurrence of jadeite crystals, lawsonite, and minor Fe-glaucophane, this last decreasing in amount away from the boundary zone. The matrix has a more retrogressed paragenesis, with a widespread occurrence of epidote-group minerals and crossite (PPL). f) BSE detail of a

jadeite crystal from the plagiogranitic clast in sample 5681. Note rims and edges of acmitic composition, with albite growing both on jadeite + acmite and on lawsonite.

Sample 5482: Mg-Al meta-gabbro

Sample 5482 is a fine-grained Mg-Al meta-gabbro characterized by a banded structure at the micro-scale (Figure 63a). It consists of white mica (10%), albite (18%), amphibole (16%), clinopyroxene (19%), lawsonite (10.5%), garnet (1%), quartz (8%), epidote (4%), chlorite (11%), titanite (2.5%). Two types of layers can be distinguished (not thicker than 1 mm), likely deriving from mafic vs. sialic–rich levels in the gabbroic protolith. The mafic layers now consist of clinopyroxene + actinolite + chlorite + albite + titanite ± epidote, whereas the sialic layers consist of white mica + actinolite + epidote + chlorite + lawsonite + garnet (Figure 63a). Representative analyses of mineral composition for this sample are reported in the Supplementary material (see Appendix IV). Garnet occurs in crystals from 100 to 200 μm in size and has an almandine – spessartine-rich composition (Alm28-52Sps14-38Prp1.5-4Grs22-34). It is partially retrogressed by epidote and chlorite + white mica pseudomorphs (Figure 63c). Lawsonite is partially retrogressed by muscovite and epidote (Figure 63d). Relicts of Ca-clinopyroxene (from 300 to 500 μm) are still preserved in the mafic layer, within an actinolite, albite, and chlorite matrix. The "magmatic" Ca-clinopyroxene has an augitic composition, but it contains relatively high amounts of Na (X_{Na} up to 0.20), thus suggesting that it was chemically re-equilibrated during Alpine metamorphism; it is partially replaced by omphacite and actinolite at rims. Epidote is partially retrogressed by actinolite and Mg-chlorite.

Sample 5681: Plagiogranite meta-breccia

Sample 5681 meta-breccia is made of plagiogranitic clasts within a mafic matrix (Figure 63b). Clasts consist of jadeite (47%), lawsonite (23%), albite (19%), epidote (2.5%), white mica (1%), quartz (1.5%), Na-amphiboles (1%), chlorite (0.5%), rutile (1.5%) and titanite (3%). Representative analyses of mineral composition for this sample are reported in the Supplementary material (see Appendix IV). Clasts, from mm to cm in size, are weakly foliated. Jadeite crystals, up to 500 μm in size, are set in a matrix consisting of poikiloblastic albite, quartz, and lawsonite (Figure 63f). Jadeite is locally overgrown by Na-amphiboles, while lawsonite is retrogressed by syn-D2 zoisite + quartz and/or syn-D3 muscovite + epidote assemblages. The mafic matrix is made of albite (27%), Na-amphiboles (26.5%), white mica (14.5%), epidote (13%), quartz (4%), chlorite (7%), lawsonite (2.5%), rutile (2%) and titanite (3.5%). It is mainly made of the assemblage phengite + Na-amphiboles, partially retrogressed

by albite + chlorite. Lawsonite occurs in lower amounts and is extensively retrogressed by the muscovite + epidote assemblage.

Table 4 Bulk rock compositions of the two samples (5482 and 5681) used for thermodynamic modeling from Corno et al. (2022), calculated by combining the mineral proportions obtained from the quantitative modal estimate of SEM-EDS multispectral maps, with singlepoint analyses. Lower part: normative minerals calculated for these bulk-compositions.

Oxide (wt%)	SiO_2	Al_2O_3	FeO	Fe_2O_3	MgO	MnO	CaO	Na_2O	K_2O	TiO_2	*Total*		
5482	59.41	8.76	5.2	---	11.98	0.14	10.03	2.96	0.66	0.86	100		
5681 clasts	61.81	12.19	0.2	3.97	0.86	---	7.67	10.3	0.08	2.92	100		
5681 matrix	59.22	12.2	4.43	---	7.59	---	6.35	5.42	1	3.8	100		
Normative minerals	Quartz	Pl	Or	Di	Hy	Wo	Acm	Ilm	Hem	Ttn	Mag	Ap	Na_2SiO_3*
5482	6.05	33.59	3.9	30.95	22.82	---	---	1.63	---	---	0.29	---	---
5681 clasts	2.29	63.85	0.47	1.88	---	8.76	8.54	0.42	---	6.6	---	0.76	2.76
5681 matrix	3.59	51.87	5.91	20.05	11.36	---	---	7.22	---	---	---	---	---

*= sodium metasilicate

Table 5 Blastesis-deformation relationships for the two rock samples used for thermodynamic modeling (samples 5482 and 5681), from Corno et al., 2022.

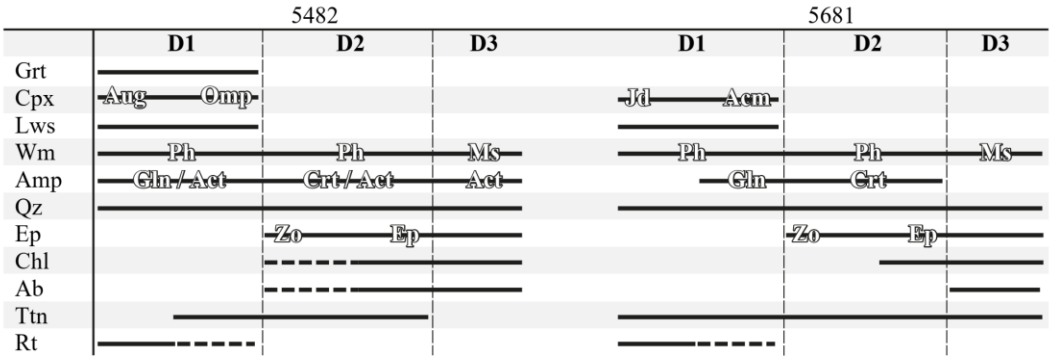

8.2.4 Thermodynamic modeling

The peak P-T conditions of the selected samples were constrained using the isochemical phase diagram approach, based on the predicted stability field of the observed assemblages, combined with the intersection of compositional isopleths modeled for white mica and clinopyroxene (for both samples), and for garnet (for sample 5482). P-T isochemical phase diagrams were calculated for a garnet +

omphacite Mg-Al meta-gabbro (sample 5482) and a plagiogranitic meta-breccia (sample 5681). For this second sample, two distinct phase diagrams have been calculated, one for the plagiogranitic clasts, and one for the mafic matrix, due to the significant difference in mineral assemblages and bulk compositions between the two domains. Bulk rock compositions of these samples (Table 4) were calculated by combining the mineral proportions obtained from the quantitative modal estimate of SEM-EDS multispectral maps, with single-point analyses. For these bulk-compositions, normative minerals have been also calculated (Table 4).

The coarse-grained relicts of "magmatic" clinopyroxenes have not been fractionated in the calculation of the bulk composition of sample 5482, because they were involved in the Alpine metamorphic re-equilibration, as witnessed by their relatively high Na contents.

The P-T pseudosection for sample 5482 was calculated in the system MnNCFMASTH (MnO-Na_2O-CaO-FeO-MgO-Al_2O_3-SiO_2-TiO_2-H_2O). For sample 5681, the P-T pseudosection of the plagiogranitic clasts was calculated in the system NCKFMASTOH (Na_2O-CaO-K_2O-FeO-MgO-Al_2O_3-SiO_2-TiO_2-O_2-H_2O), while that for the mafic matrix was calculated in the system NCKFMASTH (Na_2O-CaO-K_2O-FeO-MgO-Al_2O_3-SiO_2-TiO_2-H_2O). All the isochemical phase diagrams were calculated using Perple_X 6.9.0 (Connolly, 1990, 2005, 2009), the internally consistent thermodynamic database of Holland and Powell (2011) (ds62), and the equation of state for H2O of Holland and Powell (1998). Fluid saturated conditions were assumed, and the fluid was considered as pure H_2O (a_{H2O}=1). This last assumption is realistic for the studied samples, because of the large occurrence of hydrous phases and the absence of primary carbonates and sulfides.

MnO was neglected in the pseudosection calculated for sample 5681 (both for clasts and matrix) because Mn-bearing phases are lacking. Fe^{3+} was neglected in pseudosections of samples 5482 and the matrix of sample 5681, because Fe^{3+}-rich oxides are absent and the amount of Fe^{3+} in the analyzed minerals is very low. On the opposite, Fe^{3+} was considered for the clasts of sample 5681, due to the occurrence of acmitic-rich clinopyroxenes. The following solid solution models were used: biotite, chlorite, garnet, white mica (White et al., 2014), clinopyroxene (Green et al., 2007), amphibole (Green et al., 2016), feldspar (Fuhrman and Lindsley, 1988), and epidote (Holland and Powell, 1998). Quartz, lawsonite, talc, and kyanite were considered as pure phases.

In all the calculated phase diagrams, lawsonite is predicted to be stable at lower T and high-P conditions with respect to epidote; the lawsonite-to-epidote transition is marked by a (nearly) discontinuous reaction with a positive slope, ranging from about 450°C, 14 kbar to 550°C, 20 kbar. White mica and quartz are predicted to be stable in almost the whole P-T region of interest in sample 5482; jadeite and quartz

are modeled in all the fields of the pseudosection calculated for the plagiogranitic clasts of sample 5681, whereas white mica, Na-amphibole, jadeite, and quartz are predicted to be stable in all the fields of the pseudosection calculated for the matrix of sample 5681.

Sample 5482

The modeled isochemical phase diagram is dominated by large trivariant fields and minor di- and four-variant fields (Figure 64a). The diagram is crossed by a thin but extended divariant field marking the miscibility gap between two types of clinopyroxenes: Cpx1 is a Ca- and Mg-rich clinopyroxene, with low X_{Na} values (X_{Na} = Na/(Na+Ca)) and it is predicted to be stable at lower-T and higher-P conditions, whereas Cpx2 is an omphacite (Ca-Na clinopyroxene) and it is predicted to occur at higher-T and lower-P conditions. In this sample, the microstructural relicts of the coarse-grained magmatic clinopyroxene are mostly Ca-rich clinopyroxenes containing low amounts of Na (X_{Na}= 0.09-0.20), whereas omphacitic compositions are observed for the fine-grained clinopyroxenes in the matrix. The microstructural relicts of "magmatic" clinopyroxene do not preserve their original composition, but they were instead re-equilibrated during the HP metamorphic peak. Although not commonly reported, a similar change in composition from Ca-rich clinopyroxenes with low X_{Na} content, to Ca-Na clinopyroxenes (i.e. omphacite, with X_{Na} >0.20), has been observed in other low-grade lawsonite blueschist-facies units, including Alpine Corsica (Piccoli et al., 2018) and Chugoku mountains of south-western Japan (Tsujimori and Liou, 2007). These clinopyroxenes have not been fractioned in the calculation of the bulk rock, because their compositions changed during Alpine metamorphism, as witnessed by Na content. On the other hand, the fine-grained omphacite in the matrix grew during a first stage of moderate heating and decompression related to the first tectono-metamorphic event (D1, see Table 5).

The observed peak assemblage (Na-amphibole + Ca-amphibole + Grt + Cpx1 + Lws + Qz + Wm + Ttn) is modelled by a large tri-variant field at T < 480 °C and P = 16-22 kbar; this field is bounded by the appearance of Cpx2 at higher temperatures (T > 470°C), and by the appearance of zoisite and talc at lower (P<16 kbar) and higher (P>22 kbar) pressures, respectively. It is also worth noticing that titanite is the Ti-rich mineral predicted to be stable in this field, in agreement with the petrographic observations. The modeled garnet (Alm28-52Sps14-38Prp1.5-4Grs22-34) and clinopyroxene (Cpx1: X_{Na} =0.09-0.20) compositional isopleths allow to further constrain the peak P-T conditions of this sample at 21 ± 1.5 kbar and 450 ±30 °C.

Sample 5681

The pseudosection modeled for the matrix of this sample is characterized by large tri-variant fields and minor narrow di-variant fields (Figure 64b). The observed peak assemblage (Qz + Jd + Wm + Na-amp + Lws + Ttn + Rt) is predicted by a tri-variant field at T < 450 °C, limited toward lower pressures by the appearance of paragonitic mica, and toward higher pressures by the appearance of an omphacitic clinopyroxene. The modeled compositional isopleths of jadeite corresponding to its measured composition in the matrix (X_{Na} = 0.87-0.94) are consistent with the predicted mineral assemblage. The modeled compositional isopleths for syn-D1 phengite flakes (Si = 3.67 - 3.40 a.p.f.u) allow to better constrain the P-T conditions at 18 ± 2 kbar and 410 ± 20 °C.

The phase diagram modeled for the plagiogranitic clast is characterized by large quadri-variant fields and minor narrow tri-variant fields (Figure 64c). The observed mineral assemblage (Jd + Qz + Wm + Lws + Ttn + Rt) encompasses a large quadri-variant field. It is worth noticing that, in agreement with the petrographic observations, titanite is predicted to occur in the modeled assemblage. A tighter constrain of the P-T conditions is possible thanks to modeled compositional isopleths for jadeite (X_{Na}) and white mica (Si a.p.f.u.). The measured Si values for the syn-D1 phengite flakes (Si = 3.40-3.67 a.p.f.u.) better constrain temperatures at T<450 °C. At the same time, the lowest X_{Na} values of modeled isopleths for peak-related jadeite (X_{Na} = 0.87) fit well in the range of T < 430 °C and P of 21-24 kbar. The intersection of the estimated P-T conditions for matrix and clasts plots in a relatively small field at 400 ± 20 °C and 19 ±1 kbar.

Figure 64 (next page) P-T isochemical phase diagrams for the modeled samples, using the measured bulk compositions reported in *Table 4*. The black ellipses show the constrained P-T conditions, based on the mineral assemblages and the intersection of compositional isopleths, as indicated in each legend. Pie-charts in the insets show the predicted volume % for each phase at peak P-T conditions a) sample 5482 Mg-Al metagabbro; b) sample 5681, matrix of plagiogranite metabreccia; c) sample 5681, clasts of plagiogranite metabreccia; d) Summary P-T diagram for the AU, constraining the metamorphic peak at lawsonite-blueschist-facies conditions, at approximately 20 kbar and 400-430°C. These conditions are given by the intersection of ellipses of the previous phase diagrams.

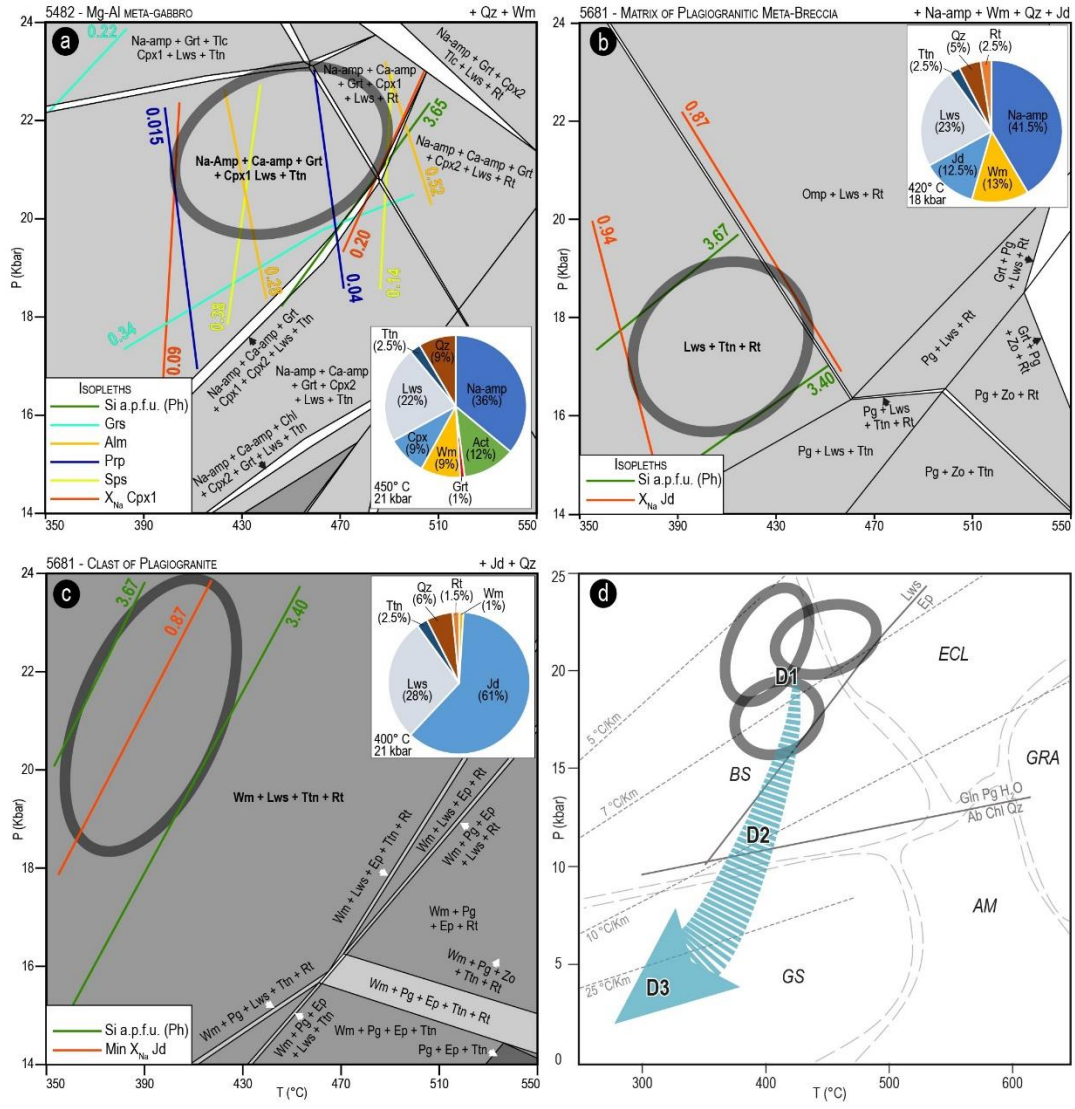

8.2.5 Metamorphic evolution

P-T estimates for the Albergian Unit

The isochemical phase diagram approach allowed to constrain the Alpine peak metamorphic conditions experienced by the Albergian Unit and to qualitatively infer its exhumation history (Figure 64d). The D1 tectono-metamorphic event, occurred at the metamorphic peak, is constrained at 19 ±1 kbar and 400 ± 20 °C in the lawsonite stability field, where the ellipses show the constrained P–T conditions, based on the mineral assemblages and the intersection of compositional isopleths, as indicated in each legend (Figure 64a-b-c). For this area, Agard et al. (2001) and Beyssac et al. (2002) predicted P-T conditions of 18-21 kbar and 380-430 °C,

estimated using the Si-in-Phe barometer and the RSCM thermometer (Raman spectroscopy on carbonaceous material) applied on the meta-sedimentary cover. Our results are, therefore, in very good agreement with these authors (for a detailed review see Vitale Brovarone et al., 2014a).

Widespread through the AU rocks, two sets of compositions for clinopyroxenes of the D1 event can be observed. In fact, clinopyroxenes' compositions shift from jadeite to acmite in plagiogranitic clasts, from acmite to aegirine-augite in Fe-Ti meta-gabbros, and from Na-bearing augite to omphacite in Mg-Al meta-gabbros. The D2 tectono-metamorphic event marks a decompression and heating stage, in the epidote stability field. This event is recorded by the development of the main foliation (S2) at the regional scale, defined in most lithologies by the blueschist-facies assemblage white mica + Na-amphibole + zoisite ± paragonite ± chlorite. At this stage, chlorite + paragonite ± potassium white mica and/or zoisite + Na-amphibole overgrow lawsonite crystals (Forneris and Holloway, 2003), documenting lawsonite breakdown in the epidote blueschist-facies. As reported by Shelley and Bossiere (1999) these types of lawsonite retrogression do not imply the release of significant amounts of water, hence no widespread retrogression occurred and Na-amphibole + epidote assemblages are still well preserved in the main S2 foliation. A geothermal gradient of about 10-12°C/km can be inferred for the development of this schistosity, at 11-13 kbar and 450-500 °C, well within the glaucophane + paragonite stability field (see Figure 64d). Widespread retrogression occurring in the D3 event developed at P< 5 kbar and T<350 °C along a 25°C/km geothermal gradient, as suggested by the occurrence of the later albite + chlorite + quartz assemblage.

The P-T path reconstructed describes a clockwise trajectory, from the D2 event consistent with other trajectories recently constrained with similar methods in adjacent areas (Ghignone et al., 2020; Corno et al., 2021). Furthermore, the estimated peak P-T conditions and the preservation of abundant fresh lawsonite imply that the Albergian Unit experienced a cold subduction (Martin et al., 2014).

Widespread lawsonite occurrence in the AU meta-mafic rocks

The HP/LT to LP/LT Alpine tectono-metamorphic evolution was responsible for intense transpositions and overprinting of folding in the AU (such as in its adjacent units, e.g. Caron, 1977; Malusà et al., 2002). The highly stiff meta-mafic bodies embedded in the calcschists were low-strain domains, which preserved pre-metamorphic and peak metamorphic assemblages. Abundant lawsonite has been preserved in those lithologies, such as meta-gabbros, where the original magmatic texture is still preserved.

In these meta-mafic rocks (where deformation is not enhanced by pervasive fluid circulation as in the embedding calcschists), equilibrium conditions were not achieved during retrogression: this allowed the preservation of metastable phases such as lawsonite, even though the exhumation trajectory of AU (Figure 64d) plots in the stability field of epidote. Thus, the meta-mafic rocks are considerably more useful than calcschists in unraveling the peak metamorphic history of AU (i.e. a segment of the Liguria-Piemonte ocean).

Usually, the development of lawsonite in cold subduction zones has been linked to fluids coming from the down going slab (see Tsujimori and Ernst, 2014, for a review). Specifically, the abundance of lawsonite in calcschists has been explained in the blueschist-facies of the Western Alps through mass transfer of H_2O and decarbonation processes (Lefeuvre et al., 2020; Vitale Brovarone et al., 2014a). These fluid-rock interaction processes, testified by abundant lawsonite crystallization in HP/LT veins as well as in metasomatic rocks, has been observed worldwide from the Alpine Corsica (Vitale Brovarone, 2014b; Piccoli et al., 2018) to the Zagros orogen in southeastern Iran (Munoz-Montecinos et al., 2021). However, bulk rock composition is of primary importance to explain lawsonite crystallization in meta-mafic rocks (Tsujimori and Ernst, 2014; Wei and Clark, 2011). The normative minerals predicted from the measured bulk rock compositions are in agreement with the assumed protoliths' nature (see Table 3), thus suggesting that the chemical systems remained closed during the whole metamorphic evolution. Hence, the widespread crystallization of lawsonite in meta-mafic rocks can be related to the breakdown of magmatic Ca-rich plagioclase and its hydration (anorthite *sensu lato*) and/or to the large carbon content, as noticed also by other authors (Pognante, 1989; Martin et al., 2014, for a review). To preserve metastable lawsonite in such amounts, Clarke et al. (2006) envisaged a cold geothermal gradient and exhumation processes accompanied by substantial cooling. However, an alternative exhumation process can be inferred to justify the incomplete retrogression of lawsonite in the epidote stability field. Wei and Clark (2011) in fact suggested the occurrence of an exhumation sufficiently fast for lawsonite to be preserved in favorable structural and textural domains.

8.3 Main remarks

- Lawsonite is preserved in meta-mafic rocks as well as in meta-sediments of the AU. Since major veins, witnessing mass transfer of fluids, developed after the D2 event and lawsonite is linked to the prograde metamorphic stages (D1 event), the observed lawsonite in the AU did not grow in relation to decarbonation processes and mass transfer of fluids but might be connected to favorable Ca-rich bulk compositions in meta-mafic rocks. The weak D3 retrogressive event permitted widespread preservation of fresh metastable lawsonite.

- The abundance of metastable lawsonite in the AU, and its minor occurrence in the surrounding units, could be linked to fast exhumation processes rather than different tectonic conditions (as suggested by Zack et al., 2004). In fact, fast exhumation hampered lawsonite-epidote substitution and favored the preservation of a large amount of metastable lawsonite.

- Due their different rheologies and responses to strain, meta-sedimentary lithologies and oceanic meta-mafic rocks may record differently the Alpine metamorphic peak. Hence, metamorphic assemblages preserved by rock successions with bulk compositions less prone to a good conservation of peak mineral assemblages, could lead to a misunderstanding of the true peak P-T conditions.

CHAPTER 9

The Lago Nero unit

Figure 65 Landscape view from the Lago Nero, in the distance a freshly snowed Ambin massif.

9.1. Introduction

The Lago Nero unit (LNU hereafter) crops out extensively from the mountains above the village of Cesana Torinese (Figure 65), up to the Assietta mountain ridge (Susa-Chisone watershed), and up to the mountains above the village of Bardonecchia (Figure 18; Piana et al., 2017). The LNU rests in the upper part of the tectonic pile exposed in the investigated area and belongs to the Upper meta-sedimentary dominated units of the Ligurian-Piedmont zone (*sensu* Agard, 2021). The LNU is tectonically juxtaposed to a large number of units: i) in the upper Chisone and upper Susa valleys, it lies geometrically above the Cerogne-Ciantiplagna unit, from which it is separated by a low angle shear zone (almost never detectable on the field); ii) in its representative locality above the villages of Cesana T.se and Claviere, the LNU geometrically lies beneath the Chenaillet Ophiolite; iii) in the sector comprised between the villages of Cesana T.se and Bardonecchia (hence on the left slopes of the upper Susa valley), the LNU lies between the Chaberton-Grand Hoche and Gondran pre-Piedmont units above (Polino et al., 1983) and the Puy-Venaus unit

below; iv) in the Rochemolles and Frejus secondary valleys (upper Susa valley), the LNU lies above the Roche de l'Aigle unit.

The LNU is made of oceanic lithosphere covered by a meta-sedimentary sequence similar to the ones of the non-metamorphic Ligurian units of the Apennines. In its typical localities (above the village of Cesana T.se; Figure 66), the southern portion of the unit is characterized by a pretty continuous oceanic basement, from the serpentinized exhumed mantle, meta-basalts and syn- and post-rift covers. On the other hand, in the northern portion of the unit (above the village of Bardonecchia), only scattered blocks of oceanic lithosphere occur and the vast majority of the unit is made of post- and minor syn-rift meta-sedimentary rocks. The thick meta-sedimentary cover is mainly made of meta-radiolarite formation (Late Jurassic in age; Martin & Polino, 1984; Cordey & Bailly; 2007), a meta-limestone formation (associated to the Titonian-Valanginian Calpionella limestone of the Ligurian units in the Apennines; Burroni et al., 2003), the Replatte formation (associated to the Valanginian-Santonian Palombini shale of the Apennines), the Gondran flysch and the Rocher Renard complex.

The first studies on this unit intermingle with the works on the overlying Chenaillet Ophiolite, since in the first part of the XX century the units were not differentiated (Koehn & Vuagnat, 1970). Nowadays, the two units are distinguished on the based of i) lower P-T conditions recorded by the Chenaillet Ophiolite (see next Chapter) and ii) the completely absence of a meta-sedimentary cover in the Chenaillet Ophiolite (see Chapter 11 in De Graciansy et al., 2011). The first accurate studies on the lithostratigraphy of the LNU are Polino (1984) and Polino & Lemoine (1984). Lately, Burroni et al. (2003) focused their research on the Late Cretaceous lithologies of the meta-sedimentary cover of the LNU, attributing the Rocher Renard complex to a formation related to frontal erosion in the accretionary wedge, whereas the Gondran Flysch is interpreted as deposits supplied by the faulted continental margin of the European plate.

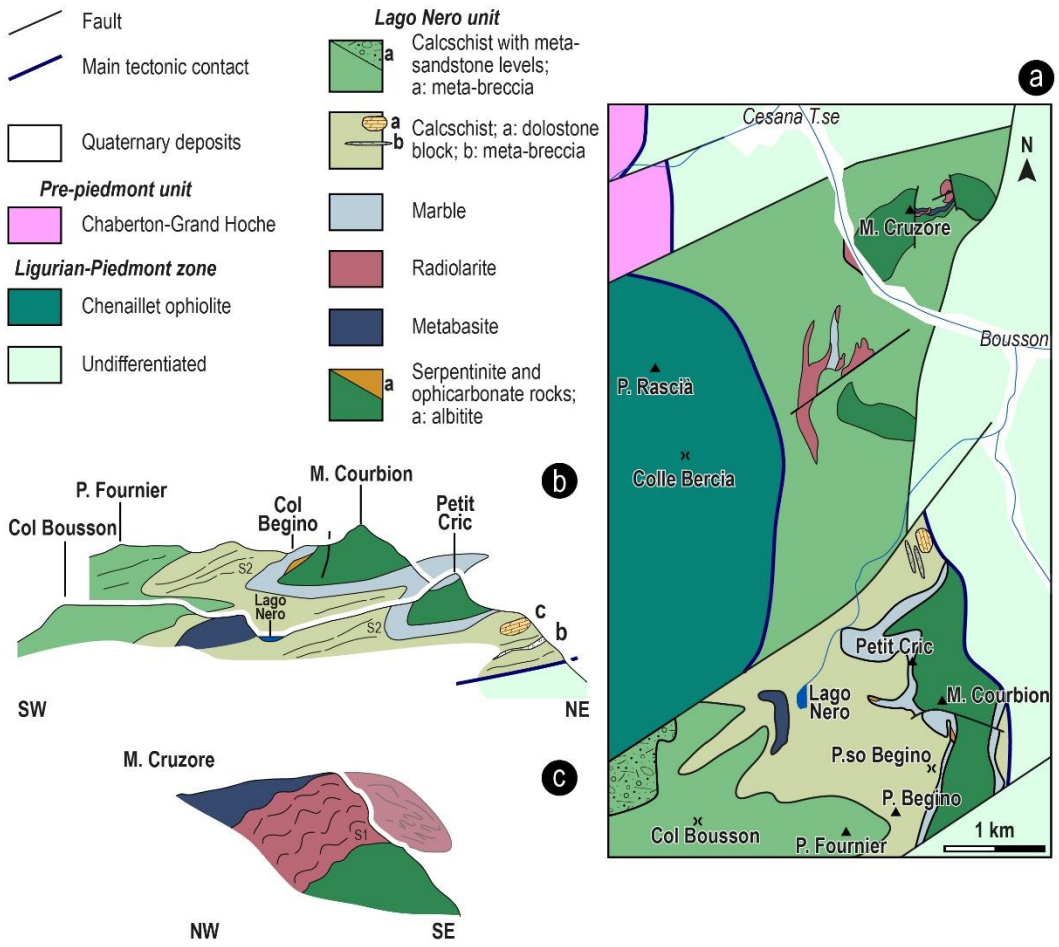

Figure 66 a. Schematic geological map of the Lago Nero unit in the Cesana T.se area; b. Schematic cross-sections of the Lago Nero section; c. Schematic cross-section of the M. Cruzore section. S1 schistosity is sub-parallel to lithostratigraphic contacts.

9.2. Lithostratigraphic, structural and petrographic features of the Lago Nero unit

The complex lithostratigraphy of the LNU has been studied mainly in two typical sections (Figure 67), i.e. the area around the Lago Nero (orographic left, to the South with respect to Cesana T.se, Figure 68a; Polino, 1984; Polino & Lemoine, 1984) and the M. Cruzore area (orographic right, to the North with respect to Cesana T.se, Figure 69a; Polino, 1984; Polino & Lemoine, 1984; Martin & Polino, 1984). The details on the lithostratigraphic of these sections will be described below (9.2.1 and 9.2.2). From the structural point of view, in both sections three main tectono-metamorphic events have been recognized: i) the older D1 event is recorded by the

oldest metamorphic foliation (S1), sub-parallel to stratigraphic boundaries (Figure 66 and Figure 70) and defined by peak mineral assemblages (Figure 71); ii) the D2 event is responsible for the development of the regional schistosity in the area (S2, Sp in Figure 68 and Figure 69), which represents the axial plane of isoclinal folds (with NE-SW trending axis, Figure 66), generally dipping towards W-SW. This event is responsible for strain slip cleavage, mechanic re-orientation and recrystallization/retrogression of D1 minerals; iii) the D3 event is responsible for the development of open folds (with ENE-WSW trending axis; Figure 66c, Figure 68f, Figure 70c) and for the reactivation/reorientation of older structures occurred during greenschist-facies conditions.

Two main faulting systems have been distinguished: i) a N-S high-angle normal faults, and ii) NE-SW trans-tensional high-angle faults (Figure 66).

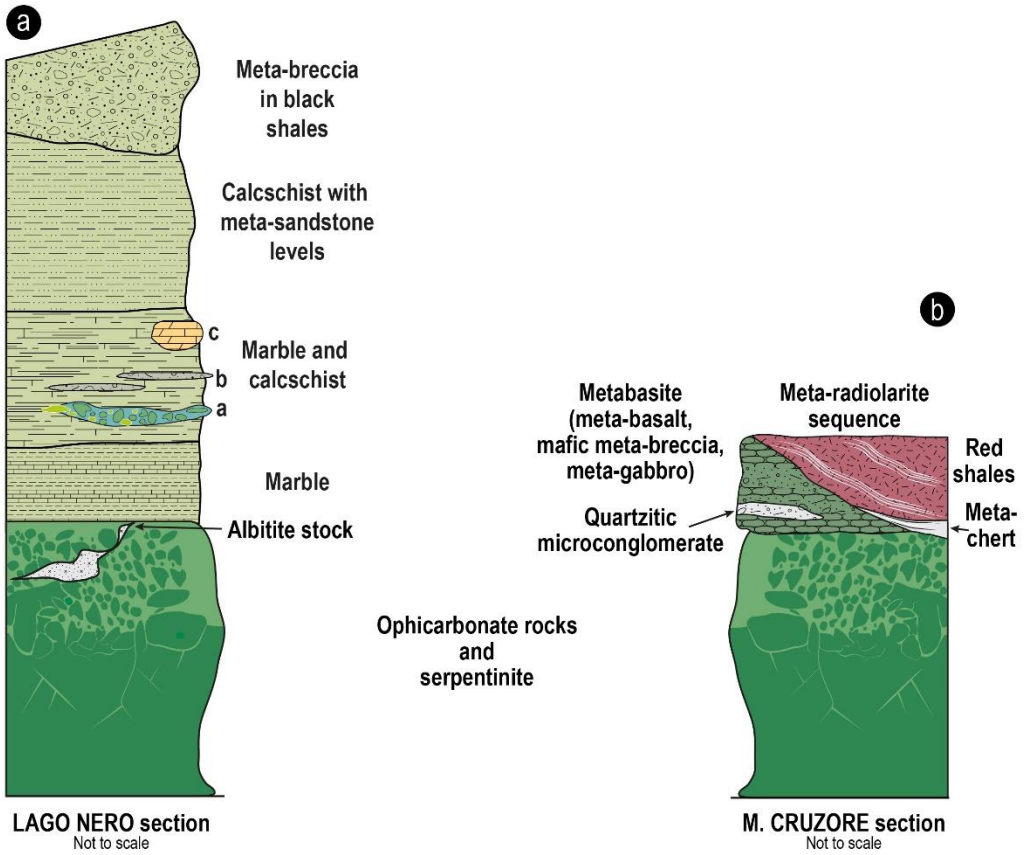

Figure 67 The two representative sections from the Lago Nero unit: the Lago Nero section, cropping out South of the village of Cesana T.se, and the M. Cruzore section, cropping out to the North with respect to Cesana T.se.

9.2.1 Lago Nero section

The lowest part of the LNU in the Lago Nero section is made of serpentinite, heterogeneously covered by ophicarbonate rocks (Figure 68b). Serpentinite usually displays a massive, isotropic texture but where it is affected by intense deformation it develops a very pervasive foliation (serpentinite-schist). Ophicarbonate rocks represent the first syn-rift lithology; they display a brecciated texture (Figure 68b), with serpentinite clasts and blocks within a carbonate matrix, with widespread talc and serpentine veins. On the south face of the M. Courbion, a level of albitite, up to 3-4 meters in thickness, is characterized by a brecciated texture (Figure 68c and Figure 72a). The rock is made of albite, quartz, muscovite flakes with thin phengite rims (Figure 73b), epidote, chlorite, titanite and minor Mg-riebeckitic amphibole (Figure 73d). Accessory zircon and allanite also occur. The matrix of the rock is made of the same mineral assemblage but with a very fine-grained texture (Figure 72). This breccia could be the product of Alpine deformation on an albitite/alkali syenite body.

In the Lago Nero section the exhumed mantle (i.e. serpentinite) is covered by meta-limestone (i.e. marble), ascribed to the Calpionella formation of the Apennines and characterized by thick pluri-decimetric bedding (Figure 68a). This marble formation displays gradual transition to the Replatte formation (Lemoine, 1971), made of an alternance of calcschist and marble levels attributed to the Palombini shales of Cretaceous age. The Replatte formation at different lithostratigraphic levels envelopes both oceanic- and continental-derived clasts and blocks (Figure 67 and Figure 68e-f). Oceanic blocks are made of metabasite s.l. (meta-basalt, greenstone, mafic meta-breccia, meta-gabbro, etc.) and ophicarbonate rocks. Such blocks can be up to pluri-decametric in size, e.g. the cliff of meta-basalt above the Lago Nero which has been interpreted (Polino & Lemoine, 1984) as a large olistolith embedded in calcschist of the Replatte formation (a in Figure 67, Figure 68d). Continental-derived clasts and blocks occur in smaller dimension, from centimetric to pluri-metric, and usually towards the stratigraphic lows of the Replatte formation. They are mainly made of marble and dolostone blocks, and minor clasts of crystalline basement rocks (i.e. micaschist and quartzite; b in Figure 68f). A typical outcrop is represented by the Petit Cric ridge (see Figure 66, Figure 68e), in this section the lowest level is made of mixed detritism (both continental and oceanic), then a level of carbonate breccia occurs, with centimetric clasts of Triassic dolostone and limestone. Up section, a poorly delimited level is made of scattered decametric blocks of dolostone (c in Figure 67, Figure 68e). The last level, a few meters in thickness, is made of a polygenic meta-breccia (b in Figure 67) with micaschist, chloriteschist, quartzite and marble clasts within a matrix made of quartz, white mica, albite and carbonate (c in Figure 68f). The Gondran flysch follows upwards, made by an alternance of calcschist and meta-sandstone. In area around the Cima Fournier the transition

between Replatte formation and Gondran flysch is marked by grey to black schists (black shales according to Barfety et al., 1996). The Gondran flysch, up to 20m in thickness, is mainly made of thin calcschist layers alternated with minor coarse-grained meta-sandstone layers. Meta-sandstone layers display arkosic composition, with quartz, feldspar and minor rock fragments, i.e. mainly continental crystalline rocks and limestone with original sedimentary textures still preserved (see Burroni et al., 2003, for a complete description). The following Rocher Renard complex is made by scattered blocks, up to decametric in size, embedded by dark schist. Blocks and clasts come from an oceanic lithosphere and its meta-sedimentary cover. Meta-ophiolitic blocks are made of meta-basalt, ophicarbonate rocks, serpentinite and meta-gabbro. Blocks from the meta-sedimentary cover are made of marble and calcschist, presumably from the Replatte formation. Locally, smaller blocks and clasts of meta-chert has been observed.

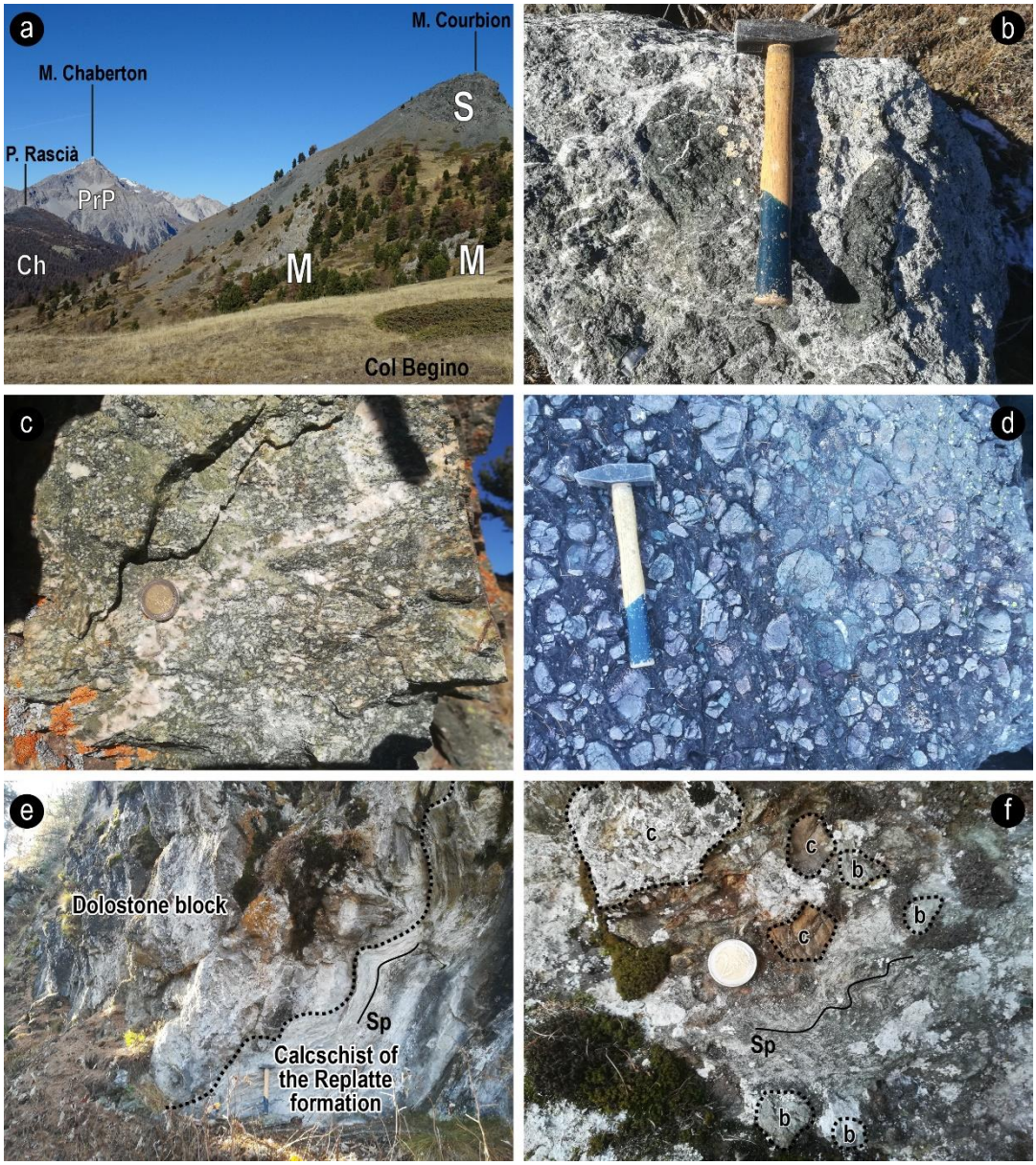

Figure 68 Representative lithologies of the Lago Nero section. a) View from the Col Begino: in the foreground the serpentinite (S) and marble (M) of the Lago Nero section. In the background, the Chenaillet ophiolite (Ch) and the Chaberton-Grand Hoche unit of the Pre-Piedmont zone (PrP); b) typical brecciated texture of the ophicarbonate rocks at the expense of serpentinite (i.e. exhumed mantle); c) brecciated albitite cropping out between serpentinite and marble, near Col Begino; d) brecciated texture of the metabasite from the outcrop above the Lago Nero, in the same area also relict pillows structures occur; e) pluri-metric dolostone block wrapped by calschist of the Replatte formation, cropping out on the Petit Cric northern ridge; f) polygenic meta-breccia with continental basement clasts (b) and cover rocks clasts (c) within a calcschist matrix made of quartz, white mica, albite and carbonate.

9.2.2 Monte Cruzore section

The lowest part of the M. Cruzore section is made of serpentinite, representing a portion of exhumed mantle (Figure 69a). In addition, the oceanic crust comprises scattered meta-basalt and meta-gabbro bodies, from plurimetric to pluridecametric in size. The original contacts with the underlying, above mentioned, serpentinized exhumed mantle are often reactivated by Alpine deformation and often occur sheared, while the contacts with overlying syn-rift meta-sediments are often well preserved. Within the meta-mafic rocks a partial lithostratigraphic sequence can be provided, with pillow-like structures (Figure 69b) observable in the lowermost stratigraphic levels and rimmed by local hyaloclastite and variolite (Figure 69d), while brecciated structures with variolite occur in the uppermost levels (Figure 69c-d). Under a petrographic point of view, meta-mafic rocks are made of 3 kinds of clinopyroxene (Figure 73a), one magmatic (Ca-Mg rich) and two of which metamorphic (Ca-Na- and Na-clinopyroxenes, Figure 71a), Na amphiboles (glaucophane and Mg-riebeckite, Figure 71b and Figure 73c-d), and of albite, chlorite, lawsonite and minor quartz and phengite (Figure 72b and Figure 73b). Locally talc can occur in very small crystals (20-50 μm; Figure 71a) growing with Ca-Na clinopyroxenes over magmatic Ca-Mg-clinopyroxene. Titanite, rutile and apatite occur as accessory minerals. Locally, in the upper part of this mafic sequence, where meta-mafic breccias occur, clasts of plagiogranitic compositions have been found made of Na-clinopyroxene (Figure 71b and Figure 73a), albite and minor white mica, chlorite and titanite. Variolite are usually made of very fine-grained white mica, albite and chlorite (Figure 72c).

Scarce, decimetric meta-microconglomeratic levels occur in these meta-mafic rocks, for example on the southern slopes of the M. Cruzore (Figure 72d-e). These levels broadly represent the transition between the underlying preserved pillow meta-basalts and the overlying mafic meta-breccia (made of reworked pillow basalts). These levels display a brecciated, matrix-supported texture, with mm to pluri-mm clasts dispersed in a fine-grained matrix. Clasts are usually angular fragments poorly rounded, with poor preferential orientation (Figure 72d). Matrix is mainly made of abundant albite, quartz and apatite, and minor Mg-chlorite, chlorite and detrital K-feldspar. Clasts on the other hand are chiefly made of quartz and albite, with preserved lawsonite crystals (up to 200 μm) and minor pumpellyite and detrital zircon (Figure 72e). Titanite and minor rutile occurs both in matrix and in clasts.

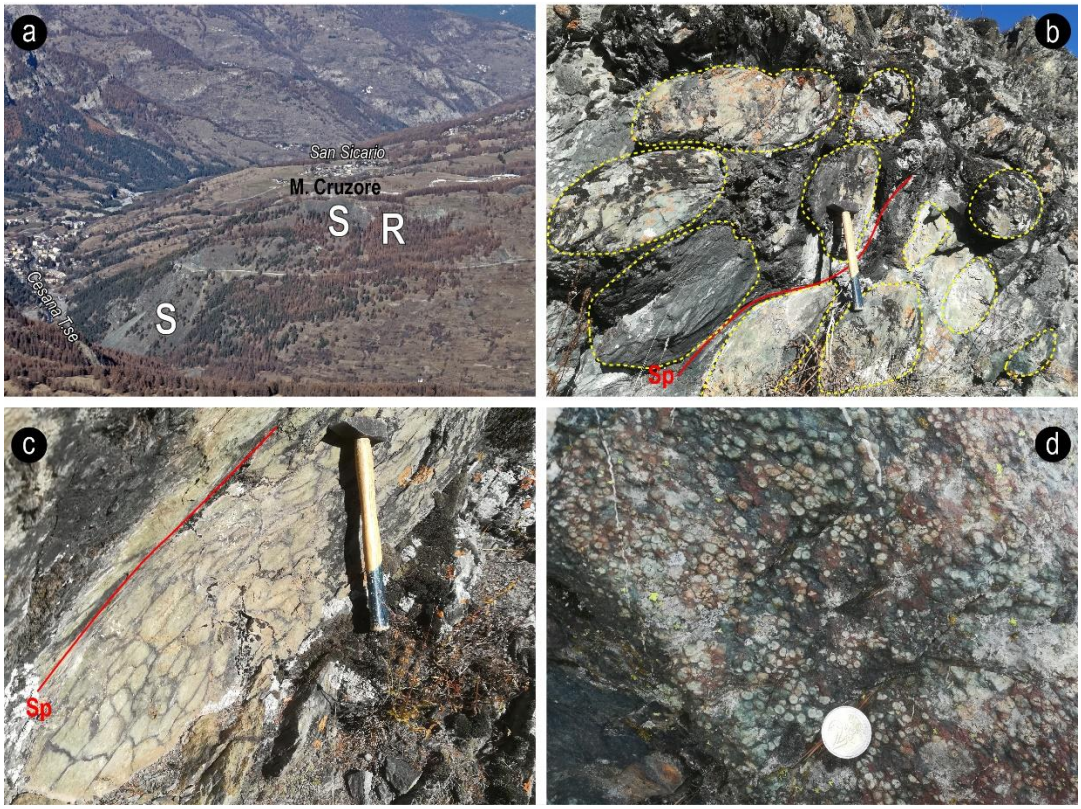

Figure 69 Representative lithologies from the mafic rocks of the M. Cruzore section. a) Landscape view on the M. Cruzore, were serpentinite (S) and meta-radiolarite (R) occur; b) pillow relicts in the metabasite from the M. Cruzore section; c) typical brecciated texture of the metabasite; d) variolite texture locally occurring in some metabasite layer, generally on the outer rim of relict pillows.

The transition between meta-mafic rocks and the first syn-rift meta-sediments is well observable on the southern slopes of the M. Cruzore. In this sector, reworked fragments of pillow meta-basalt (Figure 70a) are intercalated with thin layers of meta-chert. This level is then topped by the lower part of the meta-radiolarite formation, showing in turn thin intercalations of mafic debris. This meta-radiolarite sequence is made by two main terms (Figure 72and Figure 72f): a lower part of grey and/or green quartzite, gradually fading into an upper red fine-grained meta-shale. Locally, the meta-radiolaritic sequence hosts Si, Fe, S and Mn mineralizations (W of Cesana T.se, see Martin & Polino, 1984). These quartz-rich deposits are generally characterized by a banded texture, with greenish or reddish thicker layers alternated to thinner white layers of quartz. The lower grey/green layers (Figure 70b) are mainly made of quartz and clastic white mica grains, and represent the actual radiolarian meta-chert, that is the silica-rich sediment made of radiolarians fragments within a siliceous cement or groundmass (Figure 70b and Figure 72f). Locally, ghosts of the original radiolarians can still be found as small round shapes forming the rocks.

Figure 70 The meta-radiolarite sequence of the M. Cruzore section. a) Southern slope of the M. Cruzore displaying the complete meta-radiolarite section (inversed due to Alpine folding). Meta-breccia with both metabasite and grey meta-chert is capped by a thin layer (hammer for scale in the far left) of grey meta-chert. Then, a thick sequence of red meta-radiolarite follows; b) detail on a grey meta-chert; c) detail on folded red meta-radiolarite with typical ribbon-like texture.

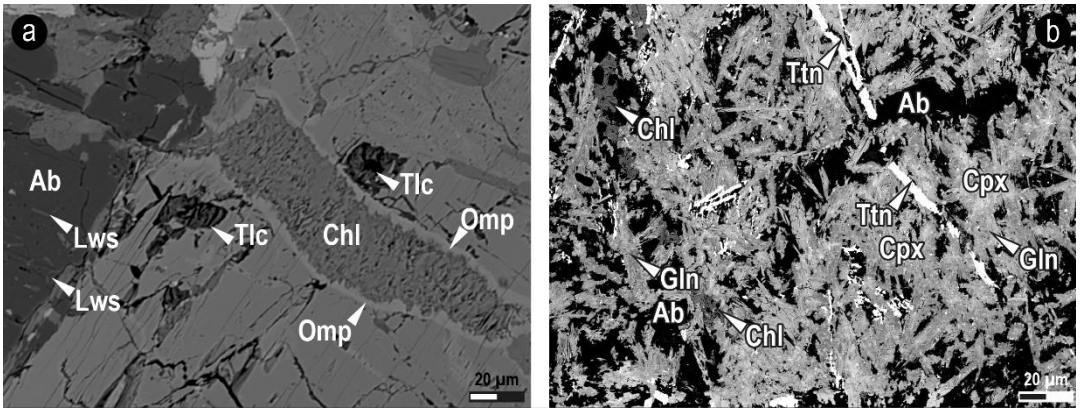

Figure 71 Representative microstructures and mineral assemblages under SEM (backscattered electron images, BSE). a) Meta-gabbro characterized by omphacite rims on former magmatic clinopyroxene (now completely retrogressed by chlorite), very small talc and lawsonite crystals occur; b) detail on ophitic texture in a metabasite, characterized by elongated clinopyroxene crystals almost completely retrogressed by glaucophane and interstitial albite.

On the other hand, the reddish upper portion represents the original fine-grained muds forming the upper part of this formation, typical of pelagic conditions. These red meta-radiolarites are characterized by a ribbon-like layering (Figure 70 and Figure 72f), that usually develops during diagenesis and whose distribution in the rock depends on the original clay/silica/carbonate ratio. These ribbon-like layers are very good relicts of the original stratification of the rock. These rocks, cropping out widespread in the Cesana T.se area, have historically been ascribed to the silica-rich sediments of Callovian-Kimmeridgian age, widespread in the non-metamorphic units of the Apennines (Conti et al., 1985; Schaaf, 1985; De Wever; 1995).

Figure 72 (next page) Representative microstructures and mineral assemblages under optical microscope; acronyms are PPL: Plain Polarized Light, and XPL: Crossed Polarized Light . a) sample of breccitated albitite from the Lago Nero section. Clasts are usually homogeneous and made of albite, white mica, quartz and chlorite, while the thin matrix layers within clasts are made of very fine-grained chlorite and epidote. Locally, allanite and zircon crystals occur (upper part XPL, lower part PPL); b) typical blueschist-facies assemblage from the meta-mafic rocks of the M. Cruzore section, characterized by omphacite, glaucophane, phengite, lawsonite, and late albite and chlorite (PPL); c) variolite texture from the M. Cruzore section. The variolites are usually concetric, with a core and a rim made of very fine-grained chlorite and white mica (muscovite) and a mantle of albite and white mica. The matrix, extremely fine-grained, is made of chlorite and widespread rutile crystals (PPL); d) brecciated texture from one of the meta-microconglomeratic levels occurring in the M. Cruzore section. Clasts are poorly rounded and wrapped by a fine-grained Mg-chlorite matrix. Lawsonite crystals seldomly occur, partially retrogressed by pumpellyite (upper left XPL, lower right PPL); e) rounded clast of the meta-microconglomeratic levels occurring in the M. Cruzore section. This clast is characterized by widespread occurrence of fresh lawsonite, dispersed within albite, white mica and quartz. Ex-amphibole crystals are now completely retrogressed by chlorite (PPL); f) meta-radiolarite characterized by typical ribbon-like texrture. Yellow arrows point to ghosts of the original radiolarians (PPL).

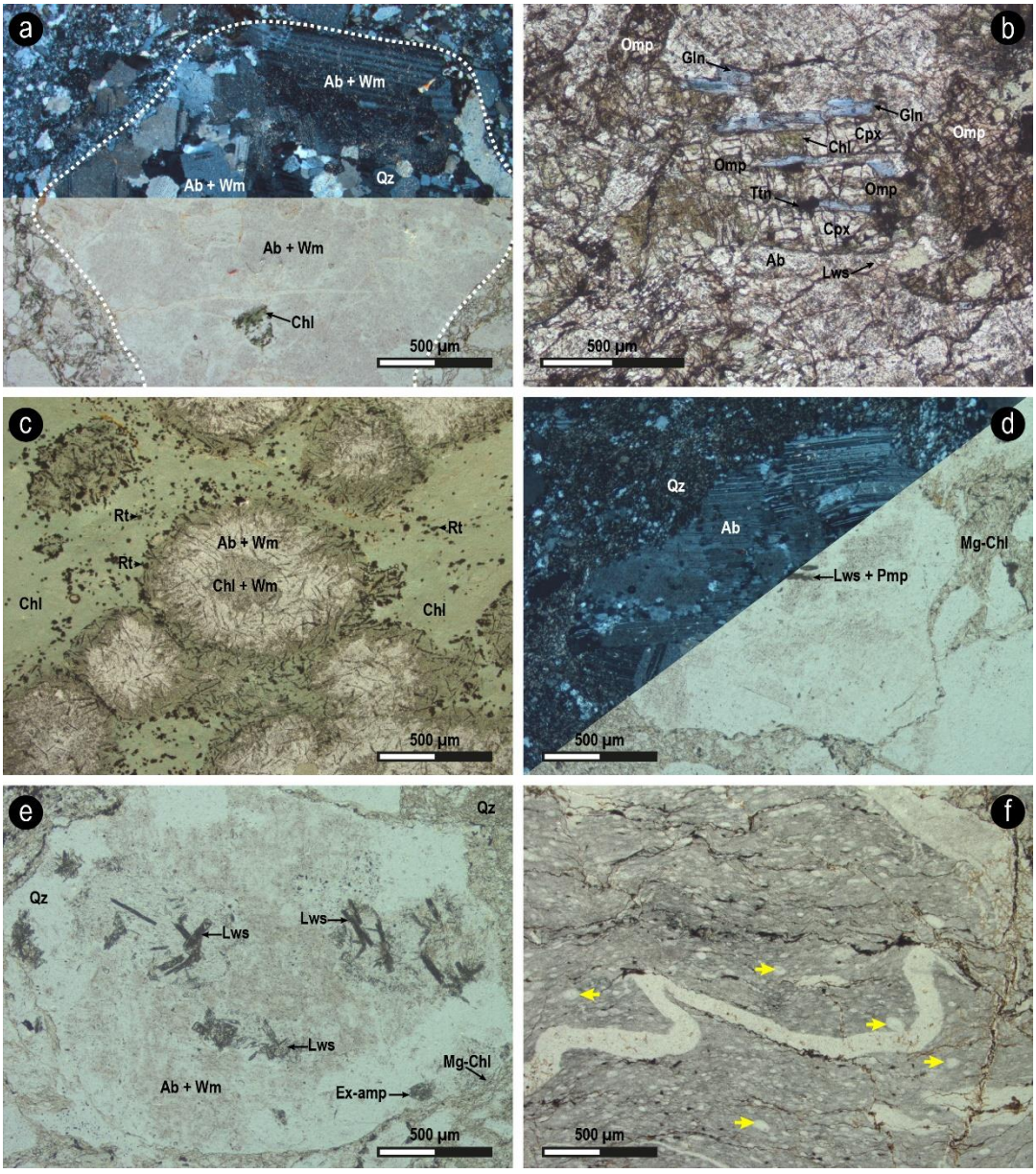
a
Ab + Wm
Ab + Wm
Qz
Ab + Wm
Chl
500 µm
b
Omp
Gln
Gln
Cpx
Omp
Chl
Omp
Omp
Tin
Cpx
Ab
Lws
500 µm
c
Rt
Rt
Ab + Wm
Rt
Chl + Wm
Chl
Chl
500 µm
d
Qz
Ab
Mg-Chl
Lws + Pmp
500 µm
e
Qz
Qz
Lws
Lws
Lws
Mg-Chl
Ab + Wm
Ex-amp
500 µm
f
500 µm

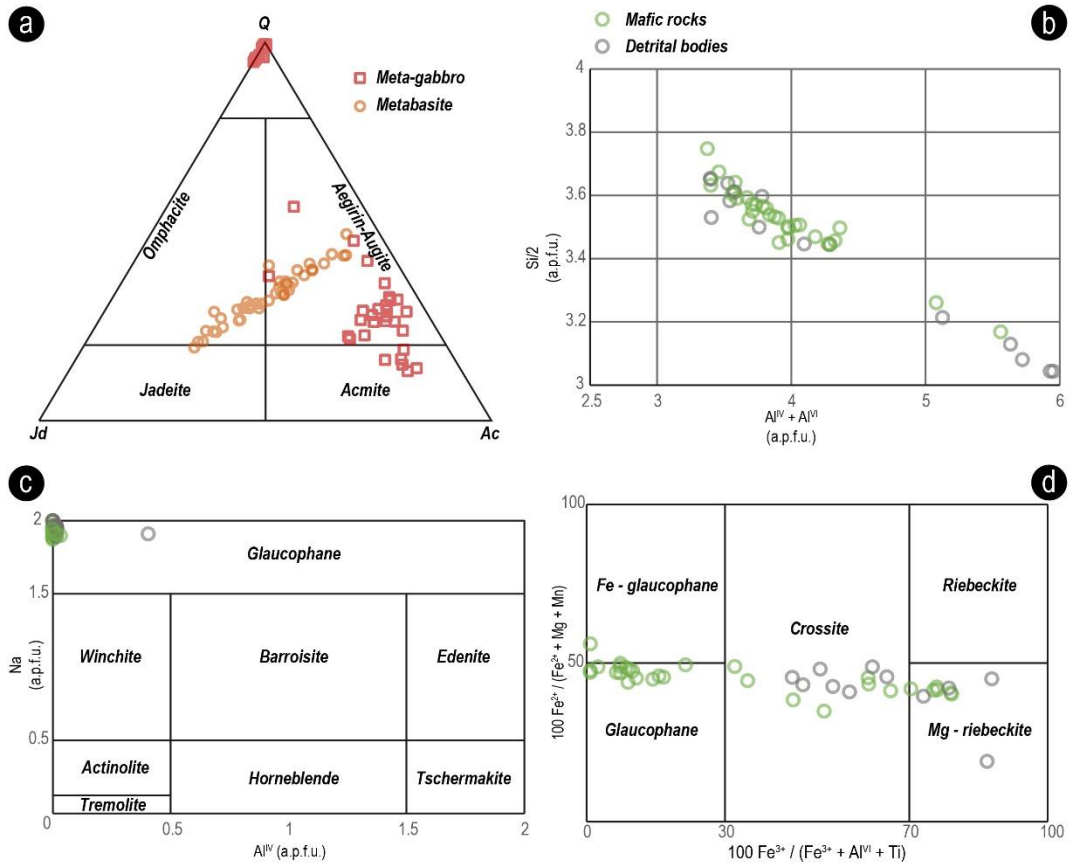

Figure 73 Mineral chemistry and classification diagrams from the Lago Nero unit. a) Morimoto (1988) pyroxene diagram; Q vertex (magmatic clinopyroxene)= En+Fs+Wo; b) White mica composition in the Si vs (Al^{IV} + Al^{VI}) diagram, showing two distinct generations of white mica. Muscovitic compositions (Si < 3.30 a.p.f.u.) are systematically related to the D3 event; phengitic compositions (Si > 3.30 a.p.f.u.) are related to the D1 and D2 events; c) Amphibole composition in the Hawthorne et al. (2012) diagram Na vs Al^{IV}. Amphiboles from both detrital and mafic rocks plot in the Glaucophane (Na-amphibole) field; d) Na-amphibole classification according to the $Fe^{3+}/(Fe^{3+} + Al^{VI} + Ti)$ vs. $Fe^{2+}/(Fe^{2+} + Mg + Mn)$ diagram. While amphiboles from mafic rocks (i.e. metagabbros and metabasites) generally display shifting compositions from glaucophane towards crossite, amphiboles form the detrital rocks generally display a shifting composition from Mg-riebeckite to crossite.

9.2.3. Metamorphic evolution

Metamorphic conditions of the LNU have been constrained with the conventional thermobarometry approach, combined with microstructural observations and chemical analyses (Figure 74). As for the other units, mainly the mafic rocks of the LNU have been used to constrain the Alpine peak conditions. However, also the detrital bodies (meta-microconglomerate, etc.) have provided useful constrains. The D1 event is defined by the Na-clinopyroxene + lawsonite ± Na-amphibole ± talc ± white mica + rutile mineral assemblage. Na-clinopyroxene occurs as jadeite shifting to aegirine-augite in metabasite and as acmite shifting to aegirine-augite in meta-

gabbro (Figure 73a). The widespread occurrence of fresh lawsonite constrains P-T peak conditions at minimum ~17 kbar and maximum of 400-450 °C. The occurrence of rare talc + acmite assemblage in metagabbro confirms this estimation (as reported by Corona et al., 2013). These conditions are in agreement with the high Si content of phengite occurring both in basic and detrital rocks (Si up to 3.70 a.p.f.u.; Figure 73b), as suggested by the phengite barometry of Massonne & Schreyer (1987). The maximum extension of the stability field of the talc + jadeite association (as reported by Corona et al., 2013) can sensibly be influenced by Fe^{3+} ratio, clinopyroxene composition and the peculiar occurrence of Na-amphibole.

The second metamorphic event (D2), identified as the main tectono-metamorphic event, is defined by the epidote + Na-amphibole + chlorite + titanite. The occurrence of widespread Na-amphibole (Fe/glaucophane shifting to crossite in mafic rocks and Mg-riebeckite shifting to crossite in detrital bodies; Figure 73c-d) implies conditions above the glaucophane stability field as reported by Guiraud et al. (2003). These conditions are in agreement with the Si content (> 3.40 a.p.f.u.) of phengite growth that according to Massonne & Schreyer (1987) implies minimum P of 10 kbar and T around 400 °C. The absence of Na-clinopyroxene constrains the upper limit of the D2 event to 12 kbar (as suggested by Holland, 1983). The late D3 event is characterized by typical greenschist-facies mineral assemblage, made of chlorite + albite + muscovite + clinozoisite + pumpellyite. Na-amphibole is often retrogressed by chlorite, while albite and chlorite grow over D1 clinopyroxenes. (Scarce) white mica related to the D3 is characterized by low Si content, usually under 3.20 a.p.f.u. (Figure 73b). While P is difficult to constrain, T can be constrained under 350 °C (Figure 74).

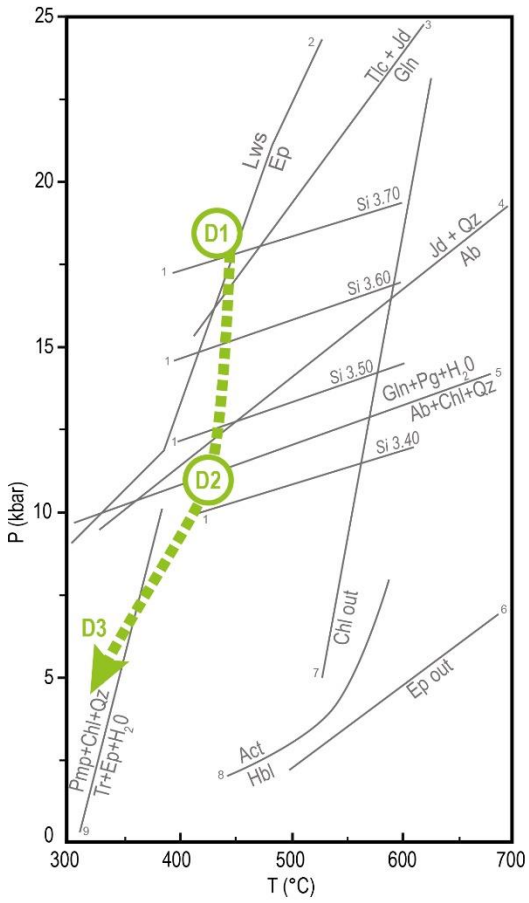

Figure 74 Petrogenetic grid. The dashed arrow shows the average P-T conditions for the LNU, from lawsonite-blueschist peak (D1), to epidote-blueschist facies D2 event, and greenschist-facies (D3) metamorphic retrogression. Curve 1: isopleths of Si4+ content in phengite (Massonne and Schreyer, 1987); curves 2, 6, and 7: lawsonite, epidote and chlorite stability curves according to Poli & Schmidt (1995); curve 3: talc + 2 jadeite stabily field according to Corona et al. (2013); Na-clinopyroxene stability curve 4 of Holland (1983); curve 5 according to Guiraud et al. (1990); curve 7 of Ernst (1979); curve 9 of Evans (1990).

9.3. Main remarks

- The Lago Nero section is ideal to investigate the lower part of the oceanic lithosphere and the extensive post-rift meta-sedimentary cover. On the other hand, the M. Cruzore area is ideal to investigate the meta-mafic rocks of the LNU and their relationships with the up-section syn-rift cover.

- Polino & Lemoine (1984) described the local occurrence of a granitic breccia on top of the exhumed mantle, mainly in the M. Courbion area. This rock was thoroughly studied but no evidence of an original granitic protolith has been found since no biotite or K-feldspar have been found in all the numerous collected samples. Due to the characteristic lithostratigraphic position (towards the uppermost part of the exhumed mantle close to the meta-sedimentary cover) and its very fine-grained matrix, we suggest for this breccia a different interpretation. This breccia could be the product of Alpine deformation on an albitite/alkali syenite body. Such rock crops out in the same stratigraphic position in the less-deformed, overlying Chenaillet Ophiolite. The brecciated structure could be linked to intense Alpine deformation along the lithostratigraphic boundary (exhumed mantle – meta-sedimentary cover) and not to an original, hereditary and primary texture. Another evidence supporting this hypothesis is the extensive retrogression affecting the rock and the mineral assemblage typical of LT/LP conditions (coherent with faulting/shearing). The same intense Alpine deformation has been found in the same position (i.e. at the top of the exhumed mantle) in the M. Cruzore section.

- The occurrence of widespread continental-derived clasts and blocks both within the mafic sequence (i.e. meta-microconglomeratic levels in metabasite) and in the meta-sedimentary cover (i.e. Replatte formation), permits to infer for the LNU a position close to the continent. Moreover, the occurrence of these continental detrital bodies at different levels within the same lithology, implies a continuous supply from the source. Hence, a position proximal to the continental margin can be tentatively be inferred for the LNU.

- Taking into account the complex and different lithostratigraphic settings displayed by the two described sections, the occurrence of a heterogenous oceanic basin must be envisaged. In this framework, the LNU samples different sectors of the Alpine Tethys, here characterized by structural highs and lows. This model can account only for the two studied successions, and

it is not intended to be inferred to the evolution of the other meta-ophiolitic bodies of the Lago Nero unit, since their complex evolution and tectono-metamorphic history must be investigated on a case-by-case basis.

- Based on conventional thermobarometry and mineral chemistry of the occurring mineral phases, this study confirms the occurrence of HP/LT blueschist metamorphism in the LNU, as already reported by previous authors (Agard et al., 2001a, b; Beyssac et al., 2002; Agard, 2021; Lefeuvre et al,. 2021). Moreover, P-T conditions can be constrained at P > 17 kbar and T < 400-450 °C.

CHAPTER 10

The Chenaillet ophiolite

Figure 75 Dolerite dyke cutting through a gabbroic body of Le Chenaillet, in the distance the Mesozoic carbonate rocks of Le Janus (belonging to the Briançonnais domain).

10.1. Introduction

The Chenaillet Ophiolite represents a very well preserved portion of Ligurian-Piedmont ocean in the Western Alps. It is made of an oceanic lithospheric succession comprising exhumed mantle, various mafic intrusives (i.e. gabbro *sensu lato*; Figure 75) and a world renown sequence of pillow basalts (Thiéblemont & Thiéblemont, 2017). Apart from scarce breccias closely related to oceanic lithosphere (Bertrand et al., 1980), no sedimentary cover is exposed. Historically, the Chenaillet Ophiolite has been known for its very low temperature - low pressure (LT-LP) Alpine metamorphism, ascribed to obduction processes. However, studies aimed at constraining the peak P-T conditions of Alpine metamorphism are virtually lacking, the general focus having been so far on its high temperature (HT) metamorphism and geochemical features.

This Chapter 10 investigates and details two kinds of rocks: gabbro and albitite/alkali syenite, whose petrographic features shed light on the complex metamorphic history of the Chenaillet Ophiolite.

Present Chapter 10 is based on a paper recently submitted by Corno and co-authors on a peer review journal.

10.2. Main features and previous studies of the Chenaillet ophiolite

The Chenaillet Ophiolite (CO hereafter) is a remnant of the Ligurian-Piedmont oceanic domain (i.e. Alpine Tethys ocean), developed in Middle to Late Jurassic between the European and Apulian plates. It crops out as a thin (i.e. less than 1 km) klippe-like unit at the uppermost structural levels of the tectonic pile, above blueschist-facies units of the Ligurian-Piedmont ocean. It consists of serpentinized peridotites, ophicarbonate rocks, various intrusive bodies (Mg-gabbro, Fe-gabbro, and alkali syenite/albitite), and large amount of pillow basalts and their related breccias and dolerites. This succession was widely studied and investigated by many generations of geologists (e.g. Buffon, 1786; Delesse, 1848; Michel-Lévy, 1877; Vuagnat, 1946, 1966, 1975; Vuagnat & Pusztaszeri, 1965; Mével, 1975; Mével & Velde, 1976; Lewis & Smewing, 1980; Chalot-Prat, 2005).

The ophiolite sequence is overprinted by weak (static) Alpine metamorphism and deformation so that primary contacts and relationships among different lithologies, as well as original magmatic textures are well persevered (Manatschal et al., 2011). In addition, this ophiolitic sequence preserves syn-magmatic shear zones, exhumation detachment faults developed along the ocean floor, and high-angle faults related to the extrusion of volcanic rocks (Manatschal et al., 2011; Balestro et al., 2019). Therefore, the CO has been largely regarded by the alpine literature as a key sector to refine genetic models for the Ligurian-Piedmont ocean, often considering geochemistry, isotope geochronology, magma genesis, and evolution of the oceanic crust (Martin, 1984; Costa & Caby, 2001; Chalot-Pra et al., 2006; Li et al., 2013; Lafay et al., 2017; Tribuzio et al., 2019; Nicollet et al., 2022).

Numerous researchers have investigated the tectono-metamorphic evolution of the Ligurian-Piedmont units of the Western Alps, however only a few studies focus on the petrologic and metamorphic features of the CO, and in particular on its alpine evolution. Pusztaszeri (1966) first described the occurrence of the prehnite + pumpellyite + albite + epidote + actinolite assemblage, which was interpreted as related to a weak (i.e. LP/LT) Alpine metamorphic event. Also, Mével et al. (1978), focusing on the amphibolitized gabbro, attributed the same mineral assemblage to low-grade Alpine metamorphism. On the other hand, Lewis & Smewing (1980) and

Bertrand et al. (1982) related this low-grade mineral assemblage to late-stage crystallization of the intrusive bodies.

Nicollet et al. (2021) recently dated these intrusive bodies. U-Pb dating on zircons dated the magmatic event to 161 ± 0.8 Ma in gabbro and 161.8 ± 1.7 Ma in albitite veins. U-Pb dating on monazite, xenotime and titanite allowed to constrain HT-metamorphism to 161.3 ± 4.0 Ma, 161.5 ± 2.4 Ma and 158.4 ± 2.3 Ma. Previously, similar ages were constrained with U-Pb on zircons by Li et al. (2013) for the troctolite and albitite stocks (~165 Ma).

According to these authors, the intrusive rocks of CO were hydrothermally metamorphosed in two stages, at prehnite-pumpellyite and greenschist -facies metamorphic conditions, respectively, hence sub-seafloor recrystallization pre-dates the Alpine metamorphic event. Since then, few studies aimed at constraining the Alpine metamorphic peak of this ophiolitic body, which was thought to have escaped most of the Alpine tectono-metamorphic history due to obduction processes (Mével et al., 1978; Lemoine, 1980; Chalot-Prat, 2005). On the other hand, Mével et al. (1978) first reported also evidence of high-temperature (HT)-metamorphism in the CO. Different authors variably interpreted this metamorphic event. Mével et al. (1978) tentatively attributed HT-metamorphism to syn-magmatic deformation, later partially obliterated by amphibolite-facies to low-grade metamorphism that occurred proximal to the sea floor. Caby (1995) associated amphibole-rich deformed gabbros and amphibole-bearing felsic veins to the interaction with migrating seawater-derived fluids, also responsible for triggering shear zones formation in the gabbro. According to this hypothesis, the syn-kinematic partial melting of the sheared gabbro would have generated SiO2-rich hydrous melts that fed the felsic veins. Tribuzio et al. (2019) conducted different chemical analyses on the sheared gabbro and the felsic veins, combining major and trace elements of both major minerals and whole rocks. They infer that the chemically evolved melts that formed such veins were responsible for the HT-metamorphism, and that reactions between melt and gabbro led to metasomatism of the deformed gabbro. Noteworthy, they did not find any clear evidence of seawater-derived fluids triggering either the ductile shear zones or partial melting of the gabbro. However, recently Nicollet et al. (2022) proposed two origins for the hydrous SiO2-rich melts: both pervasive seawater-derived fluids and local exsolved magmatic fluids, derived from evolved hydrous silicate melts (infiltrated into already cooled gabbro body).

With the aim of providing new data on the metamorphic evolution of the CO, this Chapter 10 focuses on the HP-LT metamorphic assemblages attributed to Alpine orogeny. New data have been collected in gabbroic samples from Rocca Remolon (eastern side of the CO) and the south-western ridge of Le Chenaillet, and in alkali syenite (i.e. albitite) samples from the Col du Gondran (both in the southwestern

portion of the massif, Figure 76). Particular attention is given to thermodynamic modeling of the Alpine pressure-temperature (P-T) evolution through isochemical phase diagrams, and to the distinction of the HT metamorphism vs. Alpine metamorphism.

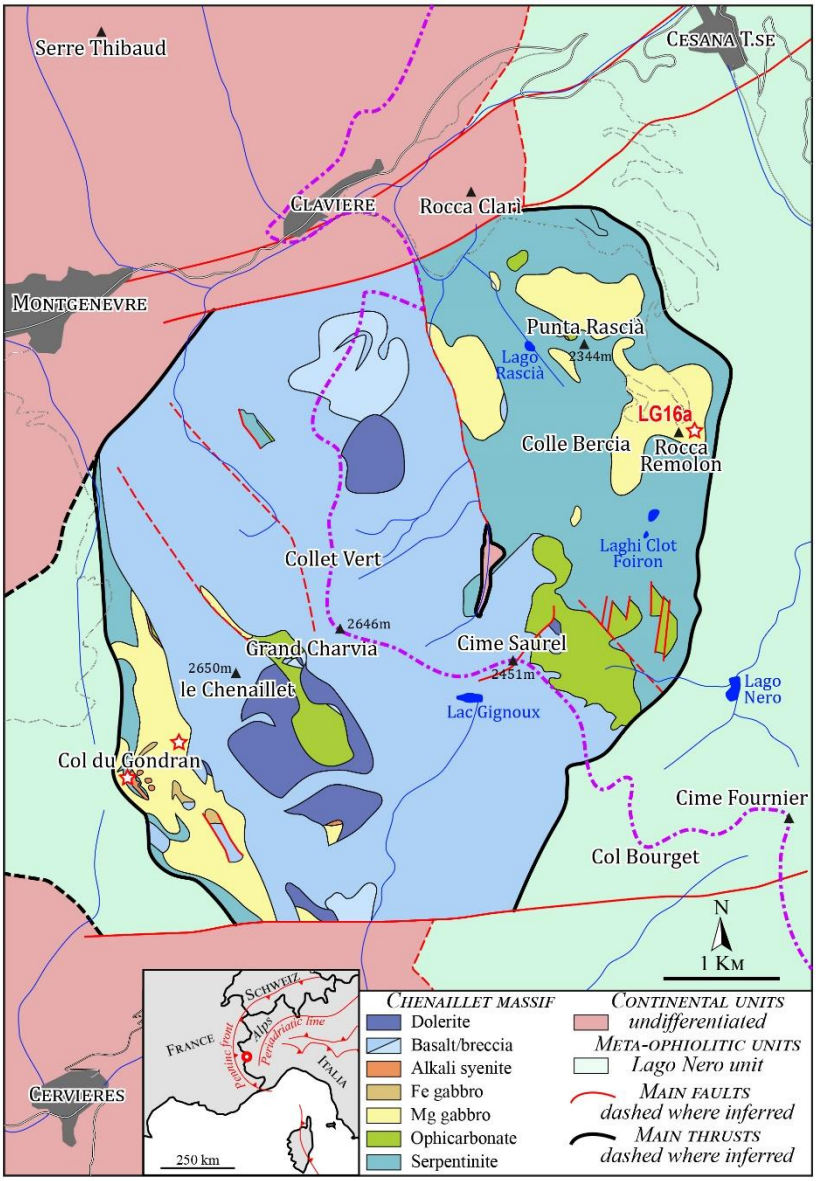

Figure 76 Schematic geological map of the Chenaillet Ophiolite, redrawn after Manatschal et al. (2011) and Chalot-Prat (2005). The red-white dot in the inset shows the position of the CO in the Western Alps, while the red-white stars in the geological map show the positions of the samples used for petrographic and mineral chemistry analyses; LG16a is the gabbroic sample used for thermodynamic modeling.

The CO is delimited to the north and to the south by late, high-angle faults which separate it from continental margin units (Polino et al., 1983; Lagabrielle & Polino,

1988; Barféty et al., 1995). It forms a klippe-like unit above the ophiolite-bearing blueschist-facies Lago Nero unit (e.g. Polino & Lemoine, 1984; Burroni et al., 2003), from which it is separated by a low-angle Alpine thrust fault. According to recent studies (Manatschal et al., 2011), this basal contact is deformed by large-scale west-vergent folds and Alpine reactivation of high-angle normal faults.

Opposite to the other surrounding meta-ophiolitic units of the Western Alps, the CO is believed to have never exceeded greenschist- to prehnite-pumpellyite facies conditions during the Alpine metamorphism (Pusztaszeri, 1966; Mével et al., 1978; Lewis & Smewing, 1980; Bertrand et al., 1982).

The CO is mainly made of serpentinized peridotite (generally exposed in the eastern sector), mafic plutonic rocks, and overlying pillow lavas (in the western sector of the massif). Sedimentary rocks are scarce and comprise mainly breccias, originated by reworking of mafic and ultramafic rocks. Post-rift Late Jurassic to Cretaceous sedimentary rocks are absent, in contrast with the neighboring oceanic units which comprise a large amount of post-rift meta-sedimentary rocks.

Mantle peridotite consists of strongly serpentinized lherzolite and harzburgite, with minor pyroxenite, dunite and wehrlite (Bertrand et al., 1987; Figure 77a). Within the highly serpentinized mantle rocks, a thin sequence of layered troctolite and olivine-bearing gabbro less than 1 km in diameter occurs, cross-cut by diorite, dolerite, and basalt dykes (Figure 77a-b). For this sequence various hypotheses have been inferred: according to Costa & Caby (2001), the gabbroic rocks represent remnants of the oceanic lower crust, preserving a paleo-Moho with the mantle peridotite. On the other hand, Manatschal et al. (2011) proved that the mafic rocks are intrusive with respect to the mantle rocks, and Li et al. (2013) described these rocks as small magmatic bodies, while Chalot-Prat (2005) interpreted the gabbros as sill-like intrusions. Dolerite, diorite, and basalt dykes usually occur within sheared gabbro, close to high-angle normal faults. Albitite/alkali syenite bodies occur as dikes and sills at the serpentinized peridotite-gabbro boundary throughout the massif (Caby, 1995; Chalot-Prat, 2005; Figure 77a-c). The well-known volcanic sequence of the CO consists of lava flows, pillow basalts, pillow breccias, and hyaloclastites, with strong affinities with MORB (Mid-Oceanic Ridge Basalt) series. Authors still do not agree on whether this volcanic sequence is linked to a single (Chalot-Prat, 2005) or several magmatic events (Manatschal et al., 2011; Li et al., 2013).

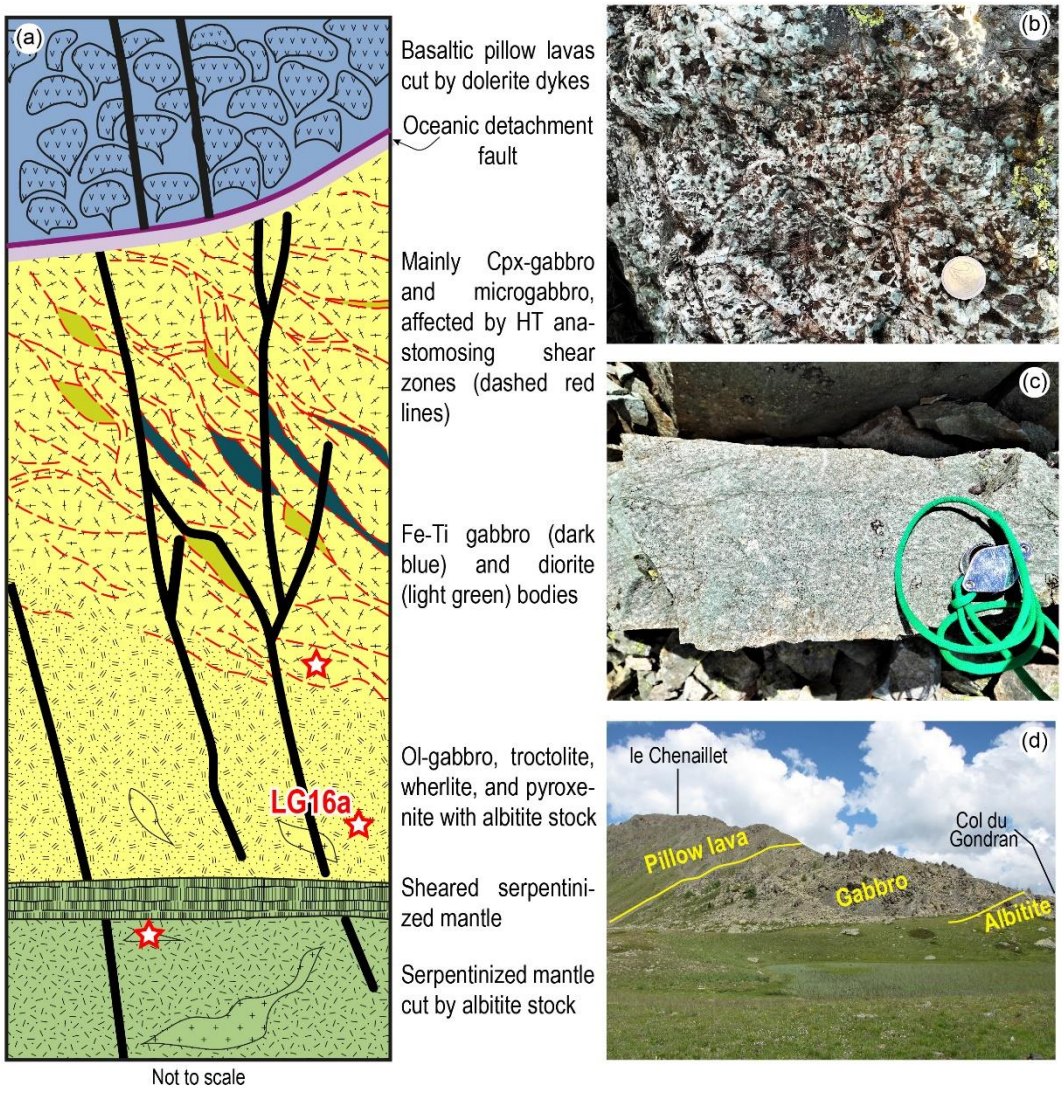

Figure 77 a. Simplified stratigraphic section of the Chenaillet ophiolite, redrawn after Costa & Caby (2001); the red-white stars show the lithologies sampled for analyses. LG16a is the gabbroic sample used for thermodynamic modeling; b. gabbro outcrop of Rocca Remolon, characterized by coarse-grained texture and minor sheared flaser gabbro; c. albitite/alkali syenite outcrop at the Col du Gondran; d. landscape picture of the Col du Gondran area and its geology.

10.3. Petrographic features of gabbro and albitite bodies

10.3.1 Sampled rocks

The petrological and petrographic investigation performed by the Author was focused on two lithologies: gabbro and albitite/alkali syenite (Figure 77b-c). Although we sampled a large number of lithologies from the area and observed them

under both optical and scanning electron microscopes, these two kinds of rocks proved to be the most interesting and the ones with the most representative mineral assemblages for the investigation of the Alpine metamorphic evolution. On the opposite, the basalt and pillow-lava of the Chenaillet massif did not prove to be useful for this kind of investigation, since they do not display either shreds of evidence of the HT-deformation event occurring in the gabbro bodies, or impressive Alpine metamorphic peak mineral assemblages. Their main petrographic features are reported in the Supplementary Material of Appendix V.

Gabbro is coarse-grained (Figure 77b) and has been subdivided into two types (according to Chalot-Prat, 2005): i) olivine-bearing gabbro, with Mg-chlorite after pseudomorphosed olivine, albite over magmatic plagioclase and minor preserved augite and, ii) amphibole-bearing gabbro, with albite over magmatic plagioclase, and abundant augite, partially replaced by different generations of late-magmatic amphiboles. Each gabbro body is made of smaller bodies (from 1 to 10m), surrounded by mylonitic, sheared boundaries (i.e. flaser gabbros) related to HT deformation during a late- to post-magmatic stage at granulite- and/or amphibolite-facies conditions (Mével et al., 1978; Caby, 1995; Tribuzio et al., 2019; Nicollet et al., 2022). Gabbros have been sampled both on the eastern and western sides of the Chenaillet Ophiolite; among them, the gabbro from Rocca Remolon (south-east of Punta Rascià) proved to be the most interesting (44°55’14.62”N 6°47’22.42”E). Albitite has been thoroughly studied by Martin (1984) and displays an apparent trivial composition with a large amount of albite (up to 90%), minor LT-amphiboles and fine-grained omphacite (responsible for the light-green and whitish color, Figure 77c), large zircon crystals, allanite, and apatite. Albitite has been sampled at the Col du Gondran (Figure 77d), where a large albitite sill is exposed at the peridotite-gabbro boundary (44°53’40.03”N 6°43’42.35”E).

10.3.2 Petrographic features and mineral chemistry

This section summarizes the petrographic and mineral chemical features of two types of rocks: gabbro and albitite (i.e. alkali syenite). Although only a gabbro sample has been used for thermodynamic modeling, also the main features of the albitite are reported, because this lithology proves to be useful to constrain the Alpine metamorphism experienced by this unit. Other lithologies from the area (e.g. basalts, diorites, etc.) were sampled and analyzed, but they proved to be less explicative and less reactive during the Alpine metamorphic evolution. A brief petrographic description of the basalt and pillow lava is provided in the Supplementary Material of Appendix V.

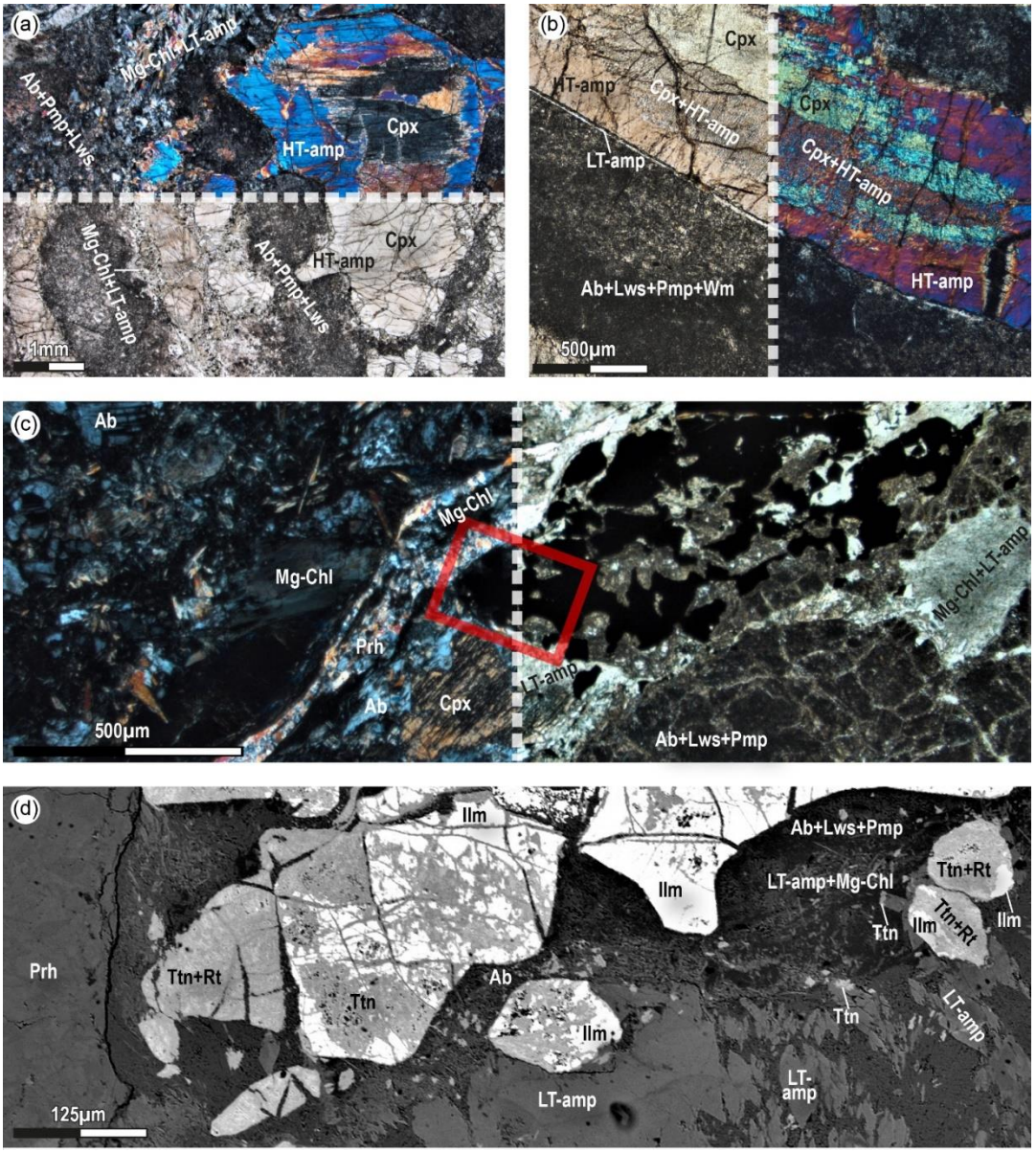

Figure 78 Representative microstructures and mineral assemblages of the gabbro from the CO. a. Typical coarse-grained texture of the gabbro, characterized by two main micro-structural domains: (ex-)plagioclase sites (now made of lawsonite+albite+pumpellyite) and clinopyroxene sites (with magmatic clinopyroxene preserved, and rims and patches of HT-amphiboles). Locally, Mg-chlorite+LT-amphibole completely replace retrogressed olivine (upper-part Crossed Polarized Light, XPL, lower part Plain Polarized Light, PPL); b. large clinopyroxene crystals characterized by HT-amphibole growing both at rims and in patches inside the clinopyroxene, while LT-amphibole grows as thin rims all around clinopyroxene and HT-amphiboles. Locally, the ex-plagioclase sites can be characterized by fine-grained white mica (left-side PPL, right-side XPL); c. complex fine-grained microstructure characterized by ex-olivine crystals (now completely replaced by Mg-chlorite+LT-amphibole), small clinopyroxene crystals, fine-grained ex-plagioclase sites (now made of albite+lawsonite+pumpellyite), and a prehnite vein (right-side PPL, left-side XPL). The red polygon shows the position of the inset in (d); d. inset of *Figure 78*c seen under SEM (backscattered electron image, BSE). Note the prehnite vein on the left-side of the figure and the idiomorph, small, LT-amphibole crystals on the right-side. Titanite crystals overgrow both magmatic ilmenite and the very small metamorphic rutile (<10 µm).

Gabbro

Gabbro still preserves the original, coarse-grained, magmatic texture (Figure 77). Mg-gabbros are characterized by two main micro-structural domains: (ex-)plagioclase sites and clinopyroxene sites (Figure 78 and Figure 79). They are made of Ca-clinopyroxene (32-36%) + albite (23-26%) + HT Ca-amphiboles (11-15%) + Mg-chlorite (7-8%) + pumpellyite (4-9%) + LT Ca-amphiboles (4-5%) + lawsonite (1-6%) + epidote (0-5%) + titanite (0.5%) + prehnite (0-5%) ± white mica (0.5-6%) and minor quartz, rutile and ilmenite (<0.5% in total).

Plagioclase sites, usually rounded in shape, are now completely replaced by fine-grained aggregates (pseudomorphoses) of albite, pumpellyite, and lawsonite, with the local occurrence of sericitic white mica and epidote (Figure 78a-b). Albite represents the majority of the site, while lawsonite occurs in small (up to 100 µm) anhedral crystals, (Figure 79a) without any preferential orientation (Figure 79e-f). Pumpellyite, 50 µm in length, usually grows over (or in association with) lawsonite, wrapped by albite and oligoclase (Figure 79e). White mica occurs only in some of the samples and seems to grow coeval with pumpellyite over lawsonite (Figure 79e). Locally, epidote grows together with white mica as saussurite aggregates after lawsonite. Prehnite can be associated with epidote in these sites, but more often it occurs in thin veins (Figure 78c-d), locally with epidote.

Figure 79 (next page) Representative microstructures and mineral assemblages under SEM (BSE images). a. Typical gabbro texture characterized by ex-plagioclase site and clinopyroxene site. Lawsonite, occurring in the plagioclase site, occurs in small crystals (up to 100 µm), partially replaced by pumpellyite. Clinopyroxenes are usually fractured with growth of Mg-chlorite and LT-amphibole along fractures; b. detail of the edge of a magmatic clinopyroxene, rimmed by HT-amphibole (approximately 50 µm) and then by thin LT-amphibole (10 µm); c. magmatic clinopyroxene rimmed by LT-amphibole, with Mg-chlorite growing in fractures and HT-amphibole patches. Note the aggregate of Mg-chlorite+LT-amphibole over completely replaced olivine; d. inset referred to the red polygon in figure c, showing the intergrowths of HT-amphibole inside the clinopyroxene; e. ex-plagioclase site made of small lawsonite crystals (<10 µm), partially overgrown by pumpellyite and small white mica flakes, within a plagioclase matrix partially preserving HT-plagioclase (Pl) and only locally albite replacement (inner and darker portion); f. ex-plagioclase crystal preserving its idioblastic shape (in the inset), now completely retrogressed by lawsonite, pumpellyite and albite. Note the pumpellyite crystals partially replacing earlier lawsonite.

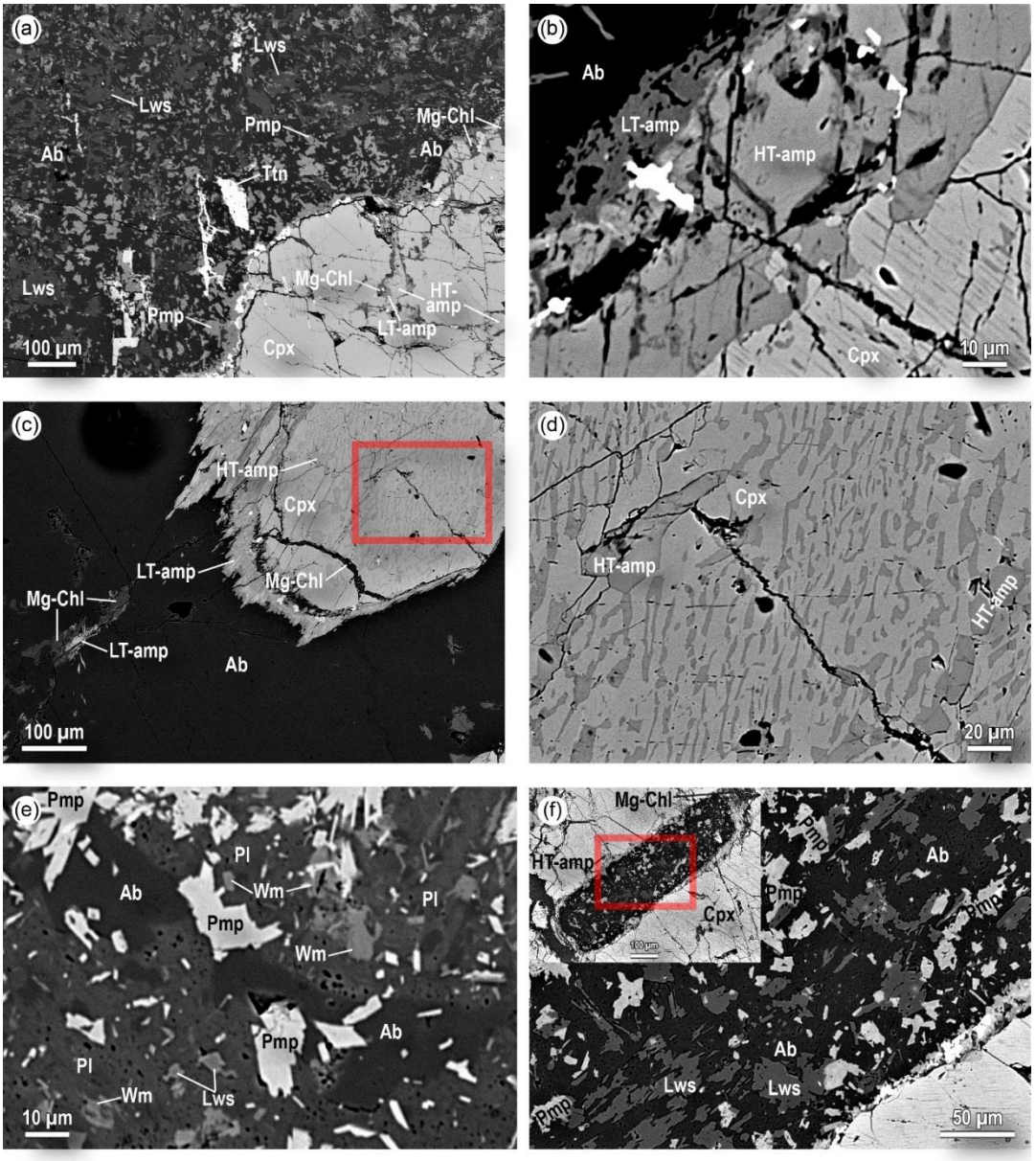

Clinopyroxene sites are made of preserved magmatic clinopyroxene, partially replaced by large HT Ca-amphiboles (Figure 78a-b). HT Ca-amphiboles grow in two micro-structural sites with respect to clinopyroxenes: they can form large rims, up to 200-300 µm (Figure 78a-b and Figure 79a-b), or can grow as exsolution inside clinopyroxenes crystals (Figure 78b and Figure 79c-d). The clinopyroxene is often rimmed by LT Ca-amphiboles and Mg-chlorite (Figure 78b and Figure 79a-b). This assemblage can also occur in thin veins (Figure 78c) and large pseudomorphs after

completely retrogressed olivine, as observed also by Chalot-Prat (2005) (Figure 78c-d and Figure 79c).

Titanite crystals (usually occurring in the proximity of clinopyroxene sites) grow over both magmatic ilmenite and metamorphic rutile, the last usually smaller than 10 µm (Figure 78d). Rutile, although very rare, has been ascribed to the peak mineral assemblage, since it is the Ti-bearing mineral phase stable at higher pressures (see Angiboust & Harlov, 2017). A summary of the blastesis/deformation relationships is presented in Table 6.

Table 6 Blastesis/deformation relationships of the gabbroic rocks from the Chenaillet Ophiolite. Black lines are for stable mineral phases at equilibrium with the mineral assemblage during a precise time in their evolution (dashed were inferred or very scarce). Grey lines are for metastable mineral phases still occurring in the rocks but no more at the equilibrium with the mineral assemblage.

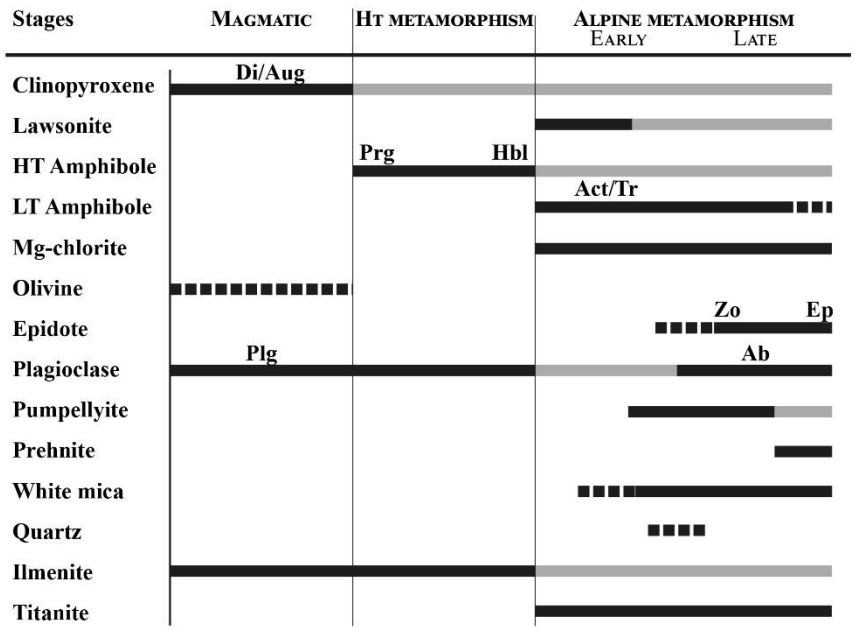

Figure 80 (next page) Mineral chemistry and classification diagrams for gabbro and albitite samples. a. Morimoto (1988) pyroxene diagram QUAD: Ca-Mg-Fe pyroxenes, J: 2Na, Q: Ca-Mg-Fe^{2+}; b. Morimoto (1988) pyroxene diagram; the Q vertex for magmatic clinopyroxene is also reported on the right. Note the occurrence of metamorphic Na-Ca clinopyroxene in the albitite and the shifting composition of magmatic clinopyroxene, between diopside and augite composition; c. Al amount (a.p.f.u.) in the M1 site vs. X_{Na} (Na/Na+Ca), showing a linear correlation both in the magmatic clinopyroxenes in the gabbro and in the albitite; d. Amphiboles composition plotted in the Hawthorne et al. (2012) diagram NaB vs. AlIV. Na-amphibole has not been found, while Ca-amphiboles can be distinguished between LT (low Al content) and HT (high Al content); e. Amphiboles composition in the Hawthorne et al. (2012) diagram Na+K vs. AlIV. While the amphiboles in the gabbro display variable compositions, from pargasite to hornblende and tremolite, the amphiboles in the albitite plot only in the tremolite (LT) field; f. X_{Mg} vs. Si (a.p.f.u.) diagram for amphiboles: while LT-amphiboles from the albitite plot in the actinolite-tremolite fields, both LT and HT amphiboles from the gabbro display higher X_{Mg} values.

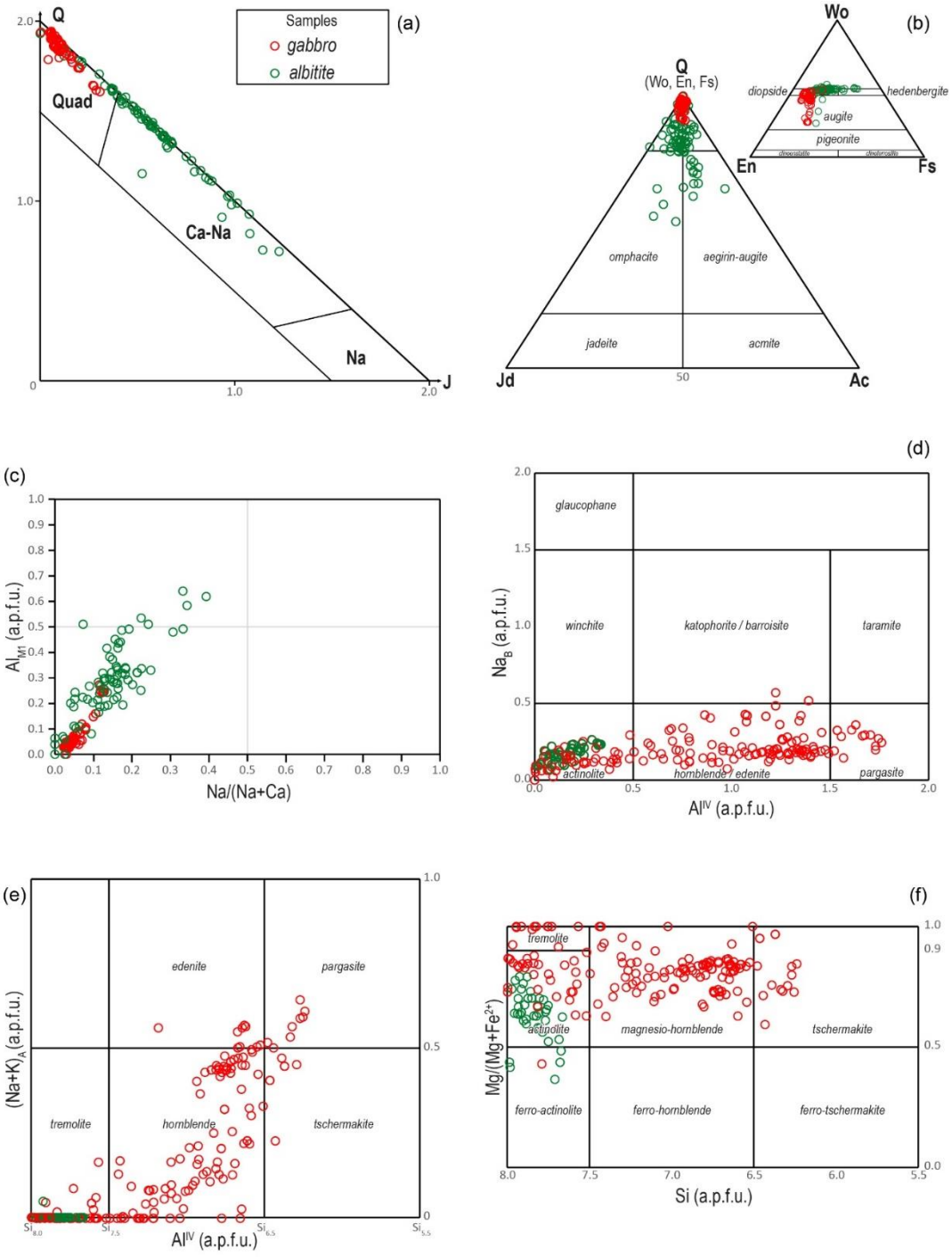

In Mg-gabbros, clinopyroxene plots in the Q vertex of the Morimoto diagram (1988), with augitic and diopsidic compositions (Figure 80a-b). A confined linear correlation between the amount of Al in the M1 site and the X_{Na}, defined as Na/(Na+Ca) is observed (Figure 80c). Ca-amphiboles have been classified based on Hawthorne et

al. (2012) and Leake et al. (1997). Based on Na (a.p.f.u.) occurrence in site B (Figure 80d), Na- and Ca/Na-amphiboles have not been found, while Ca-amphiboles (Figure 80d-e) occur as HT amphibole (with zoning composition from pargasite, to edenite/hornblende) and LT amphibole (actinolite s.l.). Na+K in site A vs AlIV diagram mostly points to compositions ranging from pargasite to hornblende, with only local edenite and tschermakite compositions (Figure 80e). X_{Mg} vs Si diagram (Figure 80f) permits constraining amphiboles to Mg-rich compositions. LT amphibole occurs both as actinolite (s.s.) and tremolite (X_{Mg} >0.90). White mica displays shifting (zoning) compositions (Figure 81a), from muscovite (Si<3.25 a.p.f.u.) up to phengite (Si from 3.25 to 3.40 a.p.f.u.). Pumpellyite, enriched in Al, has X_{Mg} ranging from 0.60 to 0.80 (Figure 81b). The original magmatic plagioclase is usually replaced by albite; however, rare relics of less retrogressed, Ca-richer plagioclase can still be found, with compositions up to labradorite (Figure 81c). Epidote group minerals display a very large range of compositions, from 100% zoisite to 85% epidote (s.s.; Figure 81d). Chlorite, occurring both in veins and after olivine crystals, has Mg-rich compositions with X_{Mg} values mostly in the range 0.73-0.75.

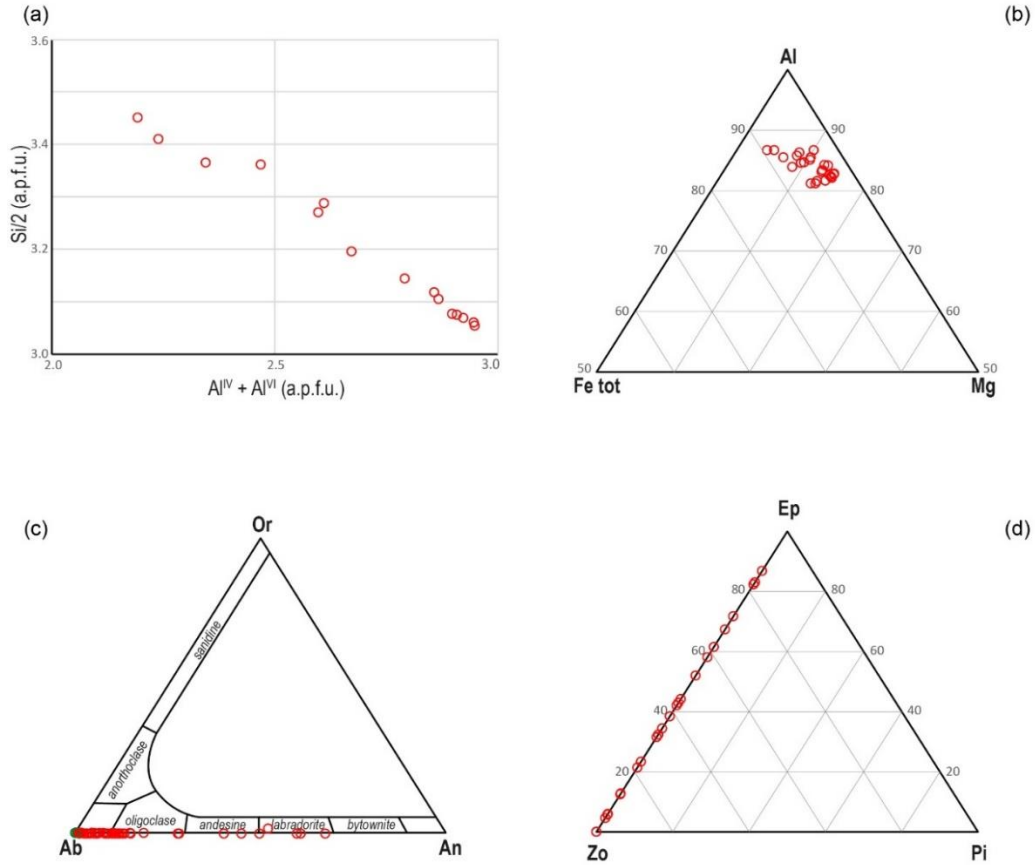

Figure 81 (previous page) Mineral chemistry and classification diagrams for gabbro and albitite samples. a. White mica composition plotted in the Si vs. (AlIV + AlVI) diagram. Even though no distinct generations can be distinguished, compositions shift from muscovite to phengite; b. Pumpellyite ternary diagram (Mg-Al-Fetot), showing a single generation of pumpellyite occurring in the gabbro samples; c. plagioclase classification diagram (after Deer et al., 1997). While plagioclase from albitite plots only in the albite field, plagioclase from the gabbro plots in a larger range from albite to labradorite; d. epidote group minerals occur only in the gabbro and display all kind of compositions, from 100% to 15% zoisite.

Albitite/alkali syenite

Albitite displays a typical ophitic texture, with large amounts of albite, intergrown with minor clinopyroxene and LT Ca-amphibole. It is made of albite (up to 90%), clinopyroxene, Ca-amphibole, titanite, large zircon crystals, allanite, and apatite. Clinopyroxene occurs in two micro-structural sites: as large crystals, up to 400 µm (Figure 82a), intergrown with large albite crystals, or as aggregates of small acicular crystals (Figure 82b), usually smaller than 100 µm, grown along the albite grain boundaries. Also, Ca-amphibole grows in two micro-structural sites: as rims around clinopyroxene or as large euhedral crystals, dispersed in the "albitic matrix" of the rock.

In the albitites, clinopyroxene crystals are zoned from Ca-rich to Ca-Na-rich compositions (Figure 80a). Magmatic relicts plot in the diopside-hedenbergite fields of Morimoto (1988, Figure 80b), while a second generation of clinopyroxene plots well within the Ca-Na clinopyroxene field, with compositions ranging from aegirine-augite to omphacite (Figure 80b). This second generation of clinopyroxene has X_{Na} values (i.e. Na/Na+Ca a.p.f.u.) ranging from 0.20 to 0.64, and Al in the M1 site linearly increasing with increasing X_{Na} (Figure 80c). Amphiboles plot in the Ca-amphiboles field of Hawthorne et al. (2012; Figure 80d-e), with low AlIV values. They show compositions in the actinolite (s.s.) field, with a large range of X_{Mg} from 0.4 to 0.7, increasing with the increasing amount of Si (Figure 80f). Albite is compositionally pure, with no Ca content (Figure 81c). These data highlight the complete absence of a HT metamorphic assemblage in these rocks, that appears to have suffered only an LT-HP event, referable to a subduction metamorphic event of inferred Alpine age.

Figure 82 (next page) Representative microstructures and mineral assemblage of albitite seen under optical microscope. a. large omphacite crystal intergrown with albite and titanite (upper part PPL, lower part XPL); b. small acicular crystals of omphacite growing along albite grain boundaries, partially replaced by LT-amphiboles.

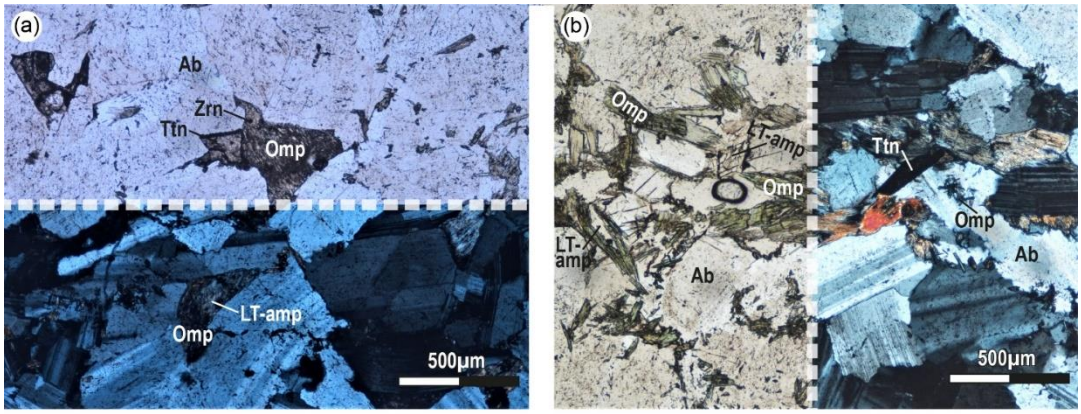

10.3.3 Thermodynamic modeling

A P-T isochemical phase diagram was calculated for the gabbro sample LG16a. This specific gabbro sample was selected for the thermodynamic modeling because it preserves very well the Alpine peak mineral assemblage (e.g. it contains 6% of lawsonite) and it is devoid of white mica and epidote (both <0.5%), thus allowing to simplify the system by neglecting K2O and Fe2O3. Isochemical phase diagrams have not been modeled for albitites because of their high variance mineral assemblage, although the newly reported occurrence of metamorphic Ca-Na clinopyroxenes provides important constraints on the metamorphic evolution of these rocks (see below). The bulk rock composition of sample LG16a was calculated by combining the mineral proportions obtained from the quantitative modal estimate of SEM-EDS multispectral maps, with single-point analyses acquired at SEM-EDS (all reported in Figure 83).

The P-T pseudosection was calculated in the system NCFMASTH (Na2O-CaO-FeO-MgO-Al2O3-SiO2-TiO2-H2O) using Perple_X 6.9.1 (Connolly, 1990, 2005, 2009), the internally consistent thermodynamic database of Holland and Powell (2011) (ds62), and the equation of state for H2O of Holland and Powell (1998). Fluid saturated conditions were assumed and the fluid was considered as pure H2O (aH2O=1). The fluid saturation assumption was validated by calculating two P-M(H2O) (mol%) isochemical phase diagrams at T= 300 °C and T=350 °C, available in the Supplementary Material (Appendix V). MnO and K2O were neglected because Mn- and K-bearing phases are lacking. Fe3+ was neglected because Fe3+-rich oxides are absent and the amount of Fe3+ in the analyzed minerals is very low. Nevertheless, the effects of Fe+3 on the stability of the observed peak mineral assemblage were investigated by calculating two P-X(Fe2O3) isochemical phase diagrams at T= 300 °C and T=350 °C, reported in the Supplementary Material (Appendix V). These calculations demonstrate that the observed peak assemblage is

limited to X(Fe2O3) < 0.5, and that its stability field is shifted toward progressively higher pressures with the increase of the oxidation state of the system. Hence, the assumption that all Fe is bivalent implies that the estimated peak pressures are minimum pressures.

The following solid solution models were used: biotite, chlorite, garnet (White et al., 2014), clinopyroxene (Green et al., 2007), amphibole (Green et al., 2016), feldspar (Fuhrman and Lindsley, 1988), and epidote (Holland and Powell, 1998). An ideal pumpellyite solution model has been used, assuming Fe-Mg occupies two octahedral (M1) sites and Al-Fe3 occupies 5 (M2) sites. Quartz, lawsonite, talc, and kyanite were considered as pure phases. The P-T evolution for the gabbro sample was constrained based on the predicted stability fields of the observed assemblages, as well as the predicted modal (vol%) amounts of each mineral phase.

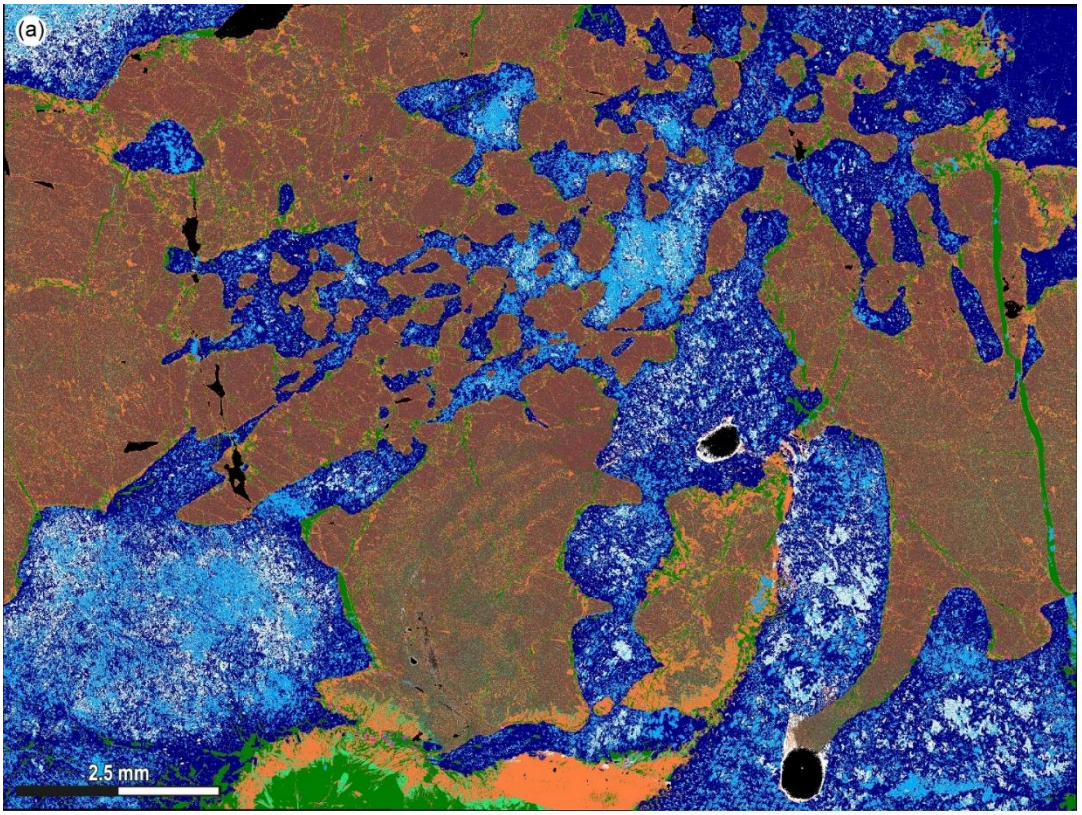

(b)

LG16a	SiO_2	Al_2O_3	MgO	FeO	CaO	Na_2O	K_2O	TiO_2	Total
Mol%	*52.36*	*5.58*	*17.16*	*3.73*	*18.80*	*2.22*	---	*0.15*	*100.00*
	Ab	Cpx	HT Amp	LT Amp	Pmp	Chl	Lws	Ttn	Total
Mode%	*26.05*	*35.78*	*11.49*	*4.27*	*8.92*	*6.97*	*5.64*	*0.56*	*99.68*

Figure 83 (previous page) Gabbro sample LG16a used for thermodynamic modeling. a. X-ray map of the modeled sample; b. bulk rock composition (mol %) and mode % of the main minerals of the modeled sample.

The isochemical phase diagram was modeled in a wide range of P-T conditions (250-700 °C and 1-15 kbar). The unfractionated bulk composition (i.e. the measured bulk composition of Figure 83b), was used for modeling, including both the magmatic and HT-related mineral relicts (i.e. clinopyroxene and HT Ca-amphibole respectively). The wt% bulk rock composition of the modeled sample (both the one acquired with SEM-EDS multispectral maps and the one acquired with geochemical analysis) was compared with other bulk rock compositions from (meta-)gabbro samples (Figure 84a-b) of the CO (Bertrand et al., 1982; Costa & Caby, 2001; Chalot-Prat, 2005) or from similar geological setting in the Alps (Bocchio et al., 2000; Bucher & Grapes, 2009) and beyond (Montanini et al., 2007; Shi et al., 2008).

The same approach was used in other studies (e.g. Bucher et al., 2005; Bucher & Grapes, 2009) on similar lithologies from other meta-ophiolitic sequences of the Western Alps. The results are shown inFigure 85a-b; geotherms typical of subduction settings (Agard et al., 2001; Agard, 2021), ranging from 7 to 25 °C/km, are shown because they are useful for a correct reading and understanding of the P-T evolution of the studied rocks. The isochemical phase diagrams inFigure 85a-b are matched with pie-charts (Figure 85c) for the predicted volume% of each mineral phase at specific P-T conditions (yellow dots in Figure 85a-b); Figure 85d, illustrates the variation in mineral modes along a hypothetical isothermal exhumation path (marked by yellow dots in Figure 85a-b). Isochemical phase diagrams with the predicted volume% of the main Alpine mineral phases are reported in the Supplementary Material of Appendix V.

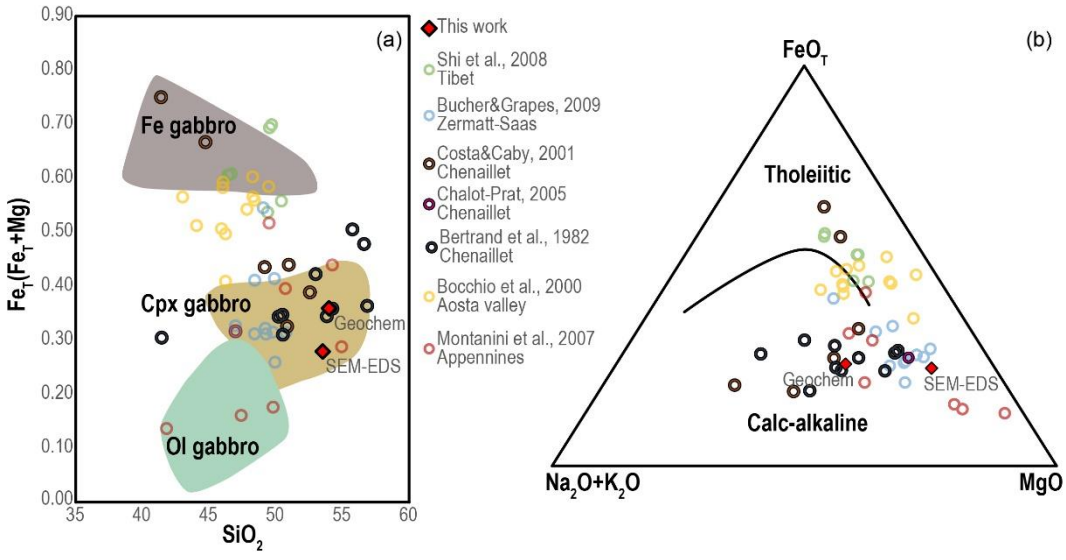

Figure 84 (previous page) Composition diagrams based on wt% bulk compositions from the studied sample (red diamonds) and other gabbros from other localities, both in the studied area and abroad.

The modeled isochemical phase diagram is dominated by tri- and quadri-variant fields (Figure 85a-b), with minor narrow divariant fields. The lawsonite-epidote transition is marked by a discontinuous reaction (yellow curve in Figure 85b) with a steep positive slope. Pumpellyite is predicted in a limited sector of the phase diagram, for T<400°C and P between 11 and 3 kbar (lilac curve). Magmatic clinopyroxene with diopsidic composition (Cpx) is predicted to be stable in all the investigated P-T range, while a second (metamorphic) clinopyroxene (Omp) is predicted at extremely low temperatures (T<300 °C and P>7 kbar). LT Ca-amphibole, mainly actinolite (Amp1), is predicted stable almost in every field of the phase diagram (green curve), whereas at T > 500 °C a second, pargasitic amphibole (Amp2) is predicted to occur (dark green curve).

The original magmatic mineral assemblage, already affected by HT metamorphism, is modeled by a small field at P < 2 kbar and T > 700 °C (lower right corner of Figure 85a-b), consistently with the results of previous studies, e.g. Nicollet et al., 2022). This field is characterized by diopsidic/augitic clinopyroxene, pargasitic amphibole, ilmenite, and plagioclase. The current mineral assemblage is the result of a complex sequence of metamorphic assemblages developed during decompression from P>11 kbar to P<3kbar at a nearly constant temperature of around 350-300 °C:

- At peak P-T conditions the studied gabbro still contained abundant magmatic clinopyroxene (Cpx: 60%), only partially replaced by actinolite (Amp1: 19.5%) + chlorite (3%); lawsonite (17%) grew at the expenses of magmatic plagioclase, and titanite (0.5%) completely replaced magmatic ilmenite. This assemblage (Cpx + Amp1 + Chl + Lws + Ttn) allows predicting a range of P-T conditions from a minimum of 9 kbar and 350 °C to a maximum of 15 kbar and 450 °C, which are compatible with a geothermal gradient of 8-10 °C/km (Figure 85a-b).
- During a first retrogression stage, at about 9 kbar and 350 °C (i.e. 12 °C/km geothermal gradient), the breakdown of lawsonite occurred, which was retrogressed mainly by pumpellyite (22%). At this stage, chlorite was no more stable and was partially replaced by very low amounts of quartz (1%) and mainly actinolite (30.5%), which grew also at the expense of HT Ca-amphibole and diopsidic clinopyroxene.
- At approximately 7 kbar, 350 °C (i.e. 15 °C/km geothermal gradient), albite grew (18%) in the plagioclase domains and partially replaced pumpellyite (16.5%). At this stage, chlorite started growing again (8%), partially over actinolite and clinopyroxene (48%).
- At 5 kbar (i.e. 20 °C/km geothermal gradient), pumpellyite was no more stable and was replaced by clinozoisite (11.5%), this last also overgrowing

the metastable preserved lawsonite relics. The amount of LT-amphibole sensibly decreased (4%), while albite and chlorite increased (20% and 10% respectively). At 3 kbar this trend continued, with decreasing amount of actinolite (2.5%) and (slightly) increasing amounts of albite (21%) and chlorite (11%), while clinozoisite amount remained unchanged (11%).

- A last decompression event, along a 25-30 °C/km gradient, was responsible for the appearance of prehnite, overgrowing epidote and actinolite, and growing inside veins.

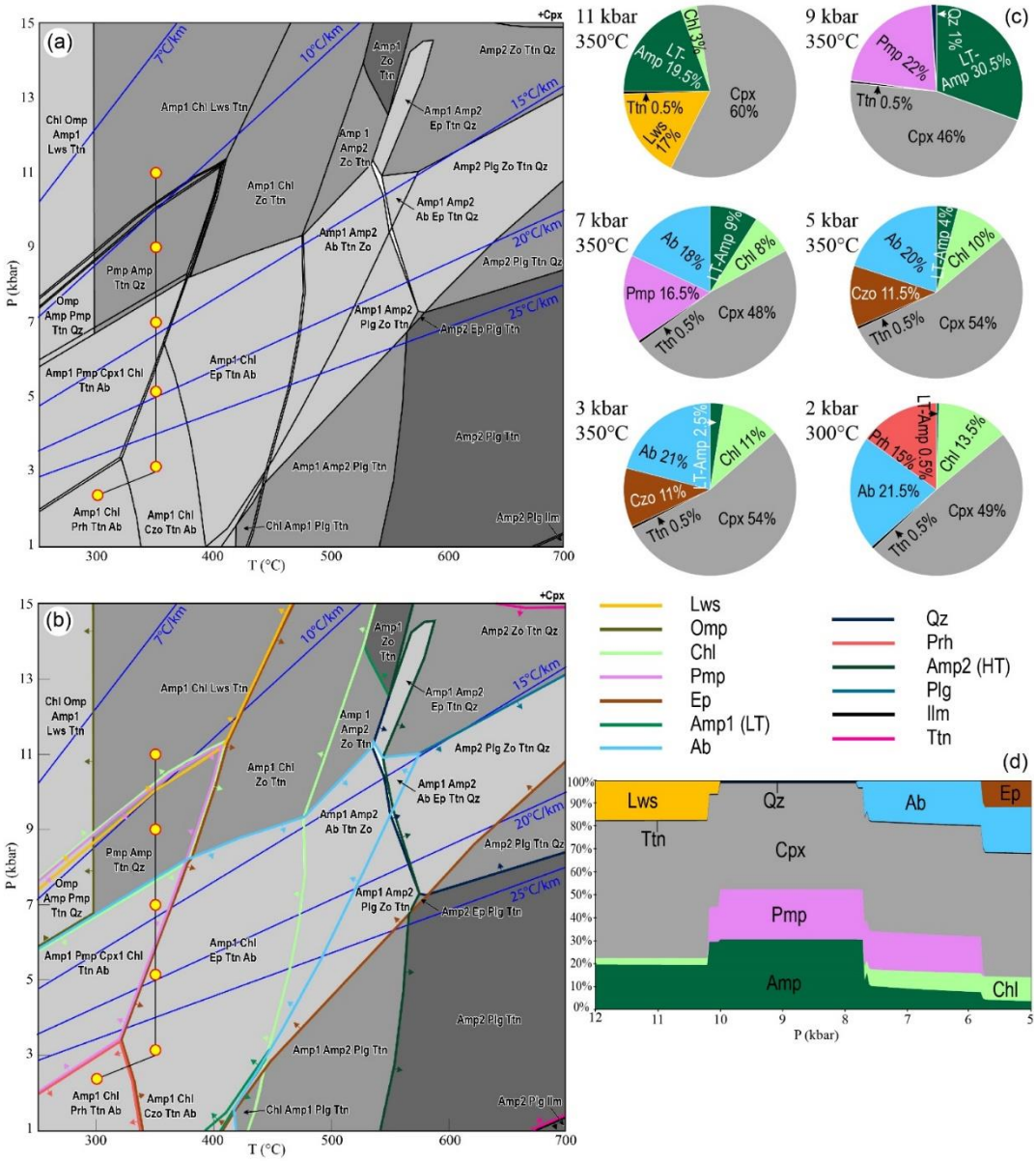

Figure 85 (previous page) a,b. P-T isochemical phase diagrams calculated for the modeled sample, using the bulk rock composition in *Figure 83*. Yellow dots correspond to P-T conditions at which pie-charts in Figure c

were calculated. The phase-in and phase-out boundaries for the main minerals are reported in (b); color coded according to legend on the right; c. pie-charts for predicted volume% of each mineral phase, calculated at the specific P-T conditions reported by the yellow dots in a. and b.; d. variation of mineral modes along an hypothetical isothermal exhumation path, marked by yellow dots in a. and b.

10.3.4 Discussion

The Chenaillet Ophiolite is a portion of the oceanic lithosphere exhumed at the seafloor of the Alpine Tethys (i.e. the Ligurian-Piedmont ocean) in the Late Jurassic. Studies based on mantle compositions through various units of the Alpine Tethys suggest that the CO could belong to the most oceanward part of the hyper-extended margin, rather than to a true ocean (Rampone & Piccardo, 2000; Picazo et al., 2016). The opening of the Alpine Tethys has been linked to the development of transform faults and oceanic core complexes along slow-spreading Mid Ocean Ridges (Chalot-Prat & Bourlier, 2005; Festa et al., 2015; Lagabrielle et al., 2015; Lagabrielle and Lemoine, 1997; Manatschal et al., 2011).

Figure 86(next page) Schematic evolution of the gabbro from the CO. a. Same isochemical phase diagram reported in Fig. 10a,b comprising both the HT-metamorphic event (HT mmp) and the Alpine evolution. The phase-in boundaries modelled for the gabbro sample studied in this work are reported with solid lines, while phase-in curves from other authors are reported with dashed lines. Stability curves for lawsonite, pumpellyite, omphacite and epidote are reported in colors for clearness. The red ellipse shows the constrained P-T conditions for the HT event, based on mineral assemblage. The large, red field in the upper left of the diagram shows the P-T peak conditions inferred for the gabbro sample LG16a based on the results of thermodynamic modeling. Alpine peak P-T conditions are further constrained by the overlap with the P-T peak conditions estimated for the albitite sample (blue field), delimited by the phase-in curves defined for the mafic system according to Harlow et al. (2015) (see text for further details). Letters from c to g in white circles represent the corresponding stages in the tectono-metamorphic evolution of the rock, reported in the correspondent figures on the right; b. schematic sketch for the original, magmatic texture of the studied gabbro; c. HT event in the gabbro, leading to the blastesis of HT-amphiboles over clinopyroxene and olivine; d. first stage of Alpine metamorphism, characterized by the development of the peak mineral assemblage. Lawsonite grows within the plagioclase sites, while Mg-chlorite and LT-amphibole completely replace olivine crystals and grow at the rim of clinopyroxene (+HT-amphibole) crystals; e. second stage of the Alpine event. Pumpellyite starts to overgrow lawsonite crystals inside plagioclase sites, while Mg-chlorite and LT-amphibole continue to grow at rims of clinopyroxene; f. third stage of the Alpine event. Albite replaces magmatic plagioclase and epidote and white mica starts to grow over lawsonite. In clinopyroxene sites, chlorite and LT-amphibole starts to grow also in fractures; g. fourth and last stage of the Alpine event, at the brittle-ductile transition, with blastesis of prehnite in veins cross-cutting the rock.

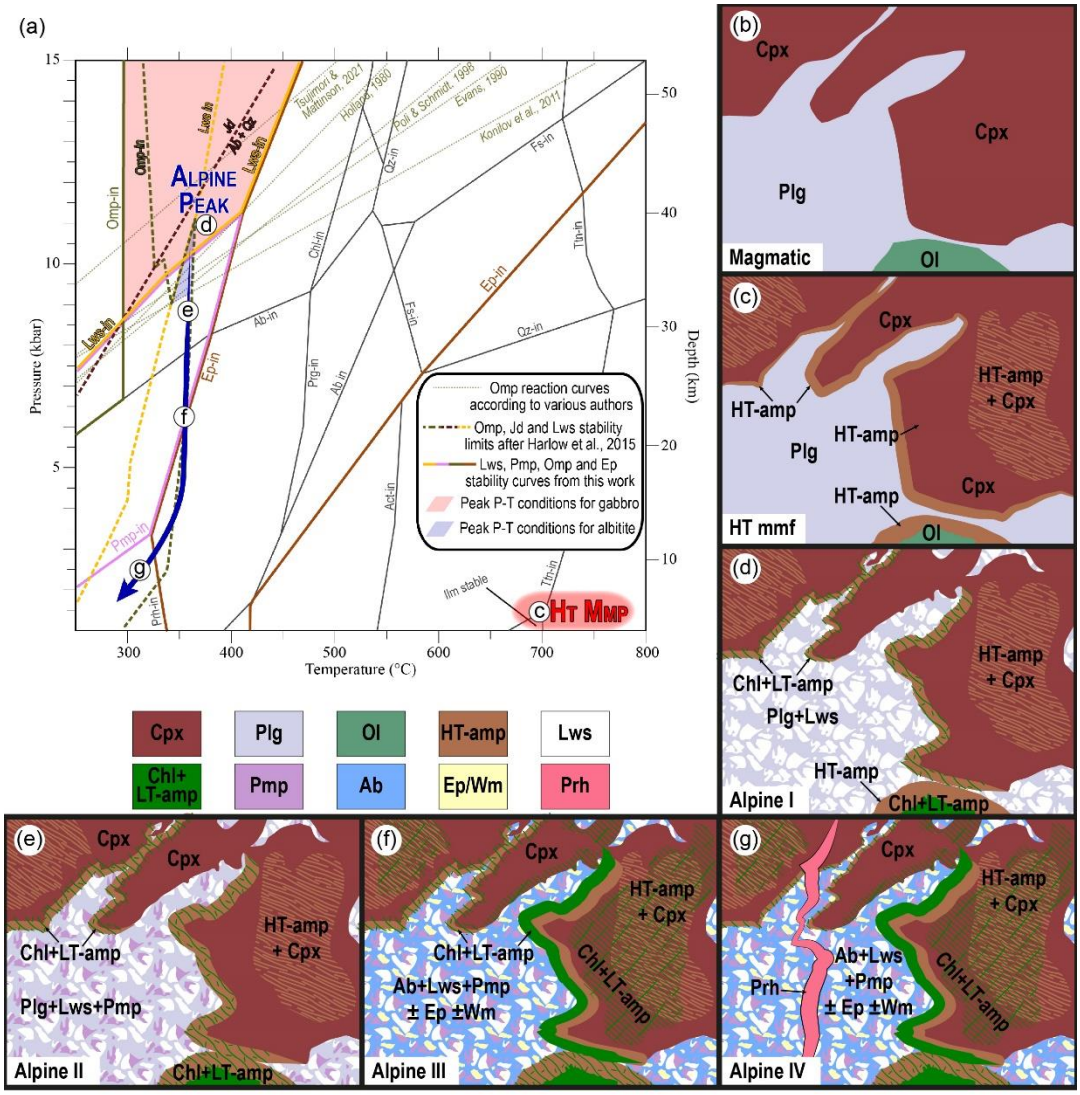

In the present tectonic nappe system of Ligurian-Piedmont units, the CO and its underlying Lago Nero unit have been distinguished on the basis of the Alpine mineral assemblages, that in the meta-mafic rocks of the Lago Nero unit comprise the occurrence of Na-clinopyroxene, phengite, glaucophane, and lawsonite (Koehn & Vuagnat, 1970; Polino et al., 2002). The peak Alpine P-T conditions of the units surrounding the CO have been constrained at 14-18 kbar and 300-400 °C for the Lago Nero unit (e.g. Agard et al., 2001; Beyssac et al, 2002) and 4.0-7.5 kbar and 250-300 °C for the adjacent continental units of the Houillère Zone (Briançonnais domain: e.g. Lanari et al., 2012). The common belief, reported in Manatschal et al. (2011), to explain the weak Alpine overprint and consequently the excellent preservation of oceanic contacts within the CO, is that it was not subducted during

Alpine convergence, but instead, it was thrusted (obducted) onto the proximal European margin and other meta-ophiolite-bearing units.

This study sheds light on two important aspects concerning the evolution of the Chenaillet Ophiolite recording both HT- and Alpine (LT-HP) metamorphism: i) the HT metamorphism and the LT-HP metamorphism are characterized by different micro-structures that developed in different times; ii) the CO experienced peak metamorphic conditions during the Alpine event at pressures significantly higher than those previously assumed.

HT vs. Alpine metamorphism

The here reported petrographic and mineral chemistry data demonstrate that HT metamorphism was recorded only by small bodies of gabbro and other minor plutonic rocks. No sign and/or evidence of HT micro-structures or mineral assemblages have been found neither in the volcanic rocks nor in the albitite (i.e. alkali syenite). Therefore, we argue that the HT metamorphism was localized in the small gabbroic bodies bordered by HT shear zones (Tribuzio et a., 2019; Nicollet et al., 2022) and that this HT metamorphic event preceded the volcanic activity, as evidenced by the interruption of shearing at the boundary with pillow lavas. Consequently, the complete absence of a HT metamorphic assemblage in these rocks, suggests that they suffered only an LT-HP event. In the Alpine setting in which the Chenaillet ophiolite is set, this LT-HP metamorphism can be linked only to subduction processes of inferred Alpine age.

Figure 86 shows the schematic evolution of the gabbro, from its magmatic origin (Figure 86b) to the HT (Figure 86c) and Alpine metamorphism (Figure 86d-g). The HT metamorphism in these rocks was responsible for the widespread blastesis of HT Ca-amphibole (pargasite to hornblende) (Figure 86a-c); further pieces of evidence of HT metamorphism, if any, have been presumably deleted by Alpine metamorphism.

Our detailed microstructural investigation implies that the low-grade metamorphic minerals pumpellyite, chlorite, actinolite, and prehnite, often interpreted as the product of oceanic seafloor metamorphism (Pusztaszeri, 1966; Mével et al., 1978; Lewis & Smewing, 1980; Bertrand et al., 1982), are instead related to an Alpine LP metamorphic event, because they overgrow and/or replace the diagnostic Alpine HP mineral phases (i.e. lawsonite). Although not preserved equally in all the lithologies, the Alpine-related mineral phases occur both in the plutonic and in the volcanic rocks of the CO.

Alpine event

In the CO, the Alpine event developed and was better preserved in the lithologies characterized by a low-variant mineral assemblage (i.e. gabbro). In these rocks, the presently observed mineral assemblage is the product of a complex history, consisting of i) the (partial) preservation of the magmatic mineral assemblage (Figure 86b), ii) a (presumably Late Jurassic) HT metamorphic event (Figure 86c) and iii) a multi-stage Alpine metamorphic history consisting of at least four evolutionary steps (Figure 86a and d-g).

The first stage of Alpine metamorphism (Figure 86a and d) is marked by the blastesis of lawsonite in the micro-structural sites of plagioclase in gabbroic rocks and chlorite + actinolite at the expense of HT-amphibole, as well as of magmatic clinopyroxene and olivine crystals. This stage represents the peak P-T conditions reached by the CO and can be constrained to a range of P-T conditions from a minimum of 9 kbar and 300 °C to a maximum of 15 kbar and 450 °C. These blueschist-facies conditions are further confirmed by the mineral assemblage observed in the albitite of the Col du Gondran, in which the coexistence of albite and omphacite is documented. As reported by Harlow et al. (2015) for the mafic system (Figure 86a), the coexistence of omphacite and albite is limited at P-T conditions lying below and to the left of the omphacite-in curve and below the jadeite-in curve. The absence of lawsonite in the albitite further constrains the P-T conditions on the right side of the lawsonite-in curve, defining a narrow T interval of 340-360 °C and P < 11 kbar. Overlapping the peak P-T conditions inferred for the albitite with the large stability field of the gabbro assemblage predicted by thermodynamic modeling, further constrains peak Alpine metamorphism at 10-11 kbar and 340-360 °C (Figure 86d). The predicted peak P-T conditions for the CO plot above the stability curve of omphacite (Figure 86a) as defined in the literature (different reactions: Holland, 1980; Evans, 1990; Poli & Schmid, 1998; Konilov et al., 2011; Tsujimori & Mattinson, 2021). Hence, based on an average geothermal gradient of 8-10 °C/km, we can infer that the Chenaillet Ophiolite reached a depth of 40-50 km, which cannot be related to any burial process but must be linked to subduction.

The second stage (Figure 86e) was mainly responsible for the breakdown of lawsonite, which was mostly overgrown by pumpellyite; this stage presumably occurred at around 9 (±1) kbar and 350 (±25) °C and approximately at 30 km of depth. The third stage of the Alpine evolution is marked by two important reactions (Figure 86a and f): the Ab-in and the Ep-in reactions. The clinopyroxene sites experienced the more pervasive retrogression, with the widespread growth of (Mg-)chlorite and actinolite. This event occurred at around 5 ±1 kbar and 350 ±25 °C, at 20 km of depth. The last Alpine event related to blastesis of metamorphic minerals occurred at the brittle-ductile transition, with the development of prehnite veins

cross-cutting through the rock, at T around 300 °C and P lower than 3 kbar (Figure 86g).

10.4 Main remarks and open questions

In this Chapter 10 were investigated two kinds of rocks (i.e. gabbro and albitite/alkali syenite) whose petrographic features shed light on the complex metamorphic history of the Chenaillet Ophiolite. Detailed analyses of mineral assemblages, blastesis/deformation relationships and mineral chemical data allowed distinguishing two metamorphic events: an earlier, HT event (already reported in the literature), and a second, later and composite low temperature, high pressure (LT-HP) event, recognized here for the first time. The LT-HP event is strikingly testified by the occurrence of lawsonite relicts in the gabbro, and of interstitial omphacite in the albitite. Thermodynamic modeling (i.e. isochemical phase diagram) performed on a gabbro sample suggests for this unit a minimum of 9 kbar and 300 °C and a maximum of 15 kbar and 450 °C. These P-T conditions point to a thickness of the overlying nappe stack of about 40-50 km, incompatible with obduction or burial processes, and instead compatible with subduction processes related to the Alpine orogeny. This study infers for the CO an Alpine metamorphic history at P-T conditions significantly higher than the (lower) greenschist-facies conditions suggested by a few previous authors (Pusztaszeri, 1966; Mével et al., 1978; Lewis & Smewing, 1980; Bertrand et al., 1982), reaching LT blueschist-facies conditions. Evidence of this assumption can still be tracked in those (few) rocks that better recorded and preserved subduction-related metamorphism. This finding opens to new challenging questions regarding both subduction and exhumation processes in complex orogens such as the Western Alps, whose answers require further studies:

i) Evidence of the Alpine HP metamorphism in the CO (marked by the lawsonite and omphacite occurrence) has been found only in the gabbroic and plutonic rocks occurring on top of the serpentinized mantle and below the volcanic cover. Hence, further studies are needed to understand whether these peak P-T conditions can be widened to the whole unit, or if the CO actually includes an upper less-metamorphic and a lower more-metamorphic portion.

ii) Alpine metamorphism in the CO seems to have occurred only as static blastesis of HP minerals, without the development of pervasive schistosity. This implies reconsidering relationships between metamorphic evolution and related deformation, possibly also in other external units of the Alpine chain.

iii) The HP Alpine metamorphic evolution of the CO (occurring on top of the nappe stack of Alpine units) opens also a series of implications in terms of models to explain and describe the subduction and exhumation processes of the oceanic units in this sector of the Western Alps.

CHAPTER 11

SYNTHESIS and DISCUSSION

The challenge of this PhD Thesis (see Chapter 1) was to provide new data to constrain the positions of different Ligurian-Piedmont units within the pre-collisional paleogeographic setting of the Alpine Tethys as well as their Alpine tectono-metamorphic evolution.

The obtained results, detailed in Chapter 4 to 10, are summarized and discussed in the present Chapter 11.

11.1 Paleogeographic restoration

In the investigated sector of the Western Alps, several segment of the Alpine Tethys can be identified based on their lithostratigraphic features and on the evolution of their tectono-stratigraphic successions. In Figure 87 the original location of these sampled segments is restored within a interpretative block diagram of the paleogeographic setting of the Alpine Tethys in the Upper Jurassic.

- The **Banchetta-Rognosa unit** (BRU, Figure 87) sampled a portion of the ocean-continent transition zone, were continental crust and exhumed mantle were adjacent in Mesozoic times. This assumption can be envisaged on the basis of:
    - occurrence of Cr-white mica (i.e. fuchsite) in the matrix of the syn-rift polymictic meta-breccia of the continental succession, indicative of pollution of mantle-derived elements and suggesting deposition in areas proximal to exhumed mantle;
    - widespread continental clasts and blocks in the syn-rift polymictic meta-breccia of the oceanic succession;
    - quartzitic meta-sandstone bodies with dolostone clasts and blocks, on top of both the continental and oceanic successions, in the same lithostratigraphic position, i.e. at the base of the common post-rift cover made of calcschist.

  Moreover, the two successions share a common tectono-metamorphic evolution since the earliest event, suggesting that they were already adjacent before (or during) the onset of subduction and Alpine deformation.

- The mafic, km-, meta-breccia body of the **Albergian unit** (AU, Figure 87) in the Albergian-Gran Mioul mountain ridge, sampled the hanging-wall of an OCC, close to a spreading axis of Alpine Tethys. This position is suggested by:

- the occurrence of the mafic meta-breccia, made only of oceanic crust-derived clasts and blocks. More specifically, only metabasite and minor meta-gabbro clasts and blocks occur, implying only local transport without external contamination;
- the preserved contacts between meta-gabbro and metabasite in some of the larger blocks of the meta-breccia, implying that the source of clasts and blocks for the mafic meta-breccia derives from the top of a gabbro body and its transitions to the overlying diabase and volcaniclastic cover;
- the absence of clasts and blocks from exhumed mantle, implying that the AU sampled very confined body;
- the occurrence of fine-grained quarzitic meta-sandstone bodies (i.e. siliciclastic turbidite) capping the mafic meta-breccia. These bodies (where untouched by Alpine deformation) display transitional contacts with the underlying mafic meta-breccia, consisting of gradual decrease of mafic-related minerals moving away from the mafic deposits. Moreover, quarzitic meta-sandstones contain very little continental scree (e.g. allanite relicts) and can be related to very mature meta-sediments, implying a strong amount of transportation and consequently quite a distance from the continental margin.

- The segment of oceanic lithosphere sampled by the **Lago Nero unit** (LNU in Figure 87) can be restored in an active spreading ridge, relatively close to the continental margin and characterized by a very complex and articulate paleo-topography. These considerations, can be inferred from:
  - the occurrence of preserved exhumed mantle in the Lago Nero section, characterized by ophicarbonate rocks and albitite stocks, similar to the peculiar ones reported in the adjacent Chenaillet ophiolite;
  - the occurrence of a well-preserved sequence of meta-basalts, with relict pillows and overlying meta-breccia in the M. Cruzore section;
  - the occurrence of levels of quarzitic meta-microconglomerate within the meta-basaltic sequence of the M. Cruzore section, representing debris material transported from the continental margin. This consideration implies that these levels can be interpreted as syn-extensional breccia (*sensu* Festa et al., 2021);
  - on the other hand, the meta-breccia levels completely embedded in the post-rift calcschist (i.e. Replatte formation), can be ascribed to syn-contractional deposits (*sensu* Festa et al., 2021), marking the onset of convergence.

In their general features, the Lago Nero unit and the Albergian unit consist of widespread and thick sequences of calcschist, embedding meta-ophiolite bodies. The syn- to lower post-rift deposits of the LNU are characterized by a more

abundant continental-derived scree in the detrital levels/bodies (with preserved K-feldspar and zircons) and a coarser grain with larger and angular clasts with respect to the fine-grained quarzitic meta-sandstones of the AU. These features suggest that the LNU includes continental-derived (meta-)sediments less mature than the AU ones. The meta-sediments of the LNU suffered less transportation than those of the AU and hence an original location of the Lago Nero unit closer to the continental margin can be envisaged.

- The **Chenaillet ophiolite** (CO in Figure 87), as reported by many authors (see Manatschal et al., 2011, and Balestro et al., 2019) sampled a portion of oceanic lithosphere, characterized by exhumed mantle, intruded by gabbroic stocks and overlain by basaltic lavas. Scarce sedimentary cover, represented only by local levels of monomictic mafic breccia (Bertrand et al., 1987; Chalot-Prat, 2005) characterizes the CO. As opposed to all the other units, no post-rift sequence occur in the CO. The CO has been interpreted as an oceanic core complex, in a slow-spreading ridge setting (Manatschal et al., 2011).

Based on these observations, it can be inferred as a major and general conclusion that during underplating different sectors of the Alpine Tethys were sampled, occurring in structural highs or in the hanging-wall of detachment faults. These rock bodies were uprooted from the oceanic lithosphere and currently occur embedded in the widespread post-rift meta-sediments within the meta-sedimentary dominated units of the Ligurian-Piedmont zone.

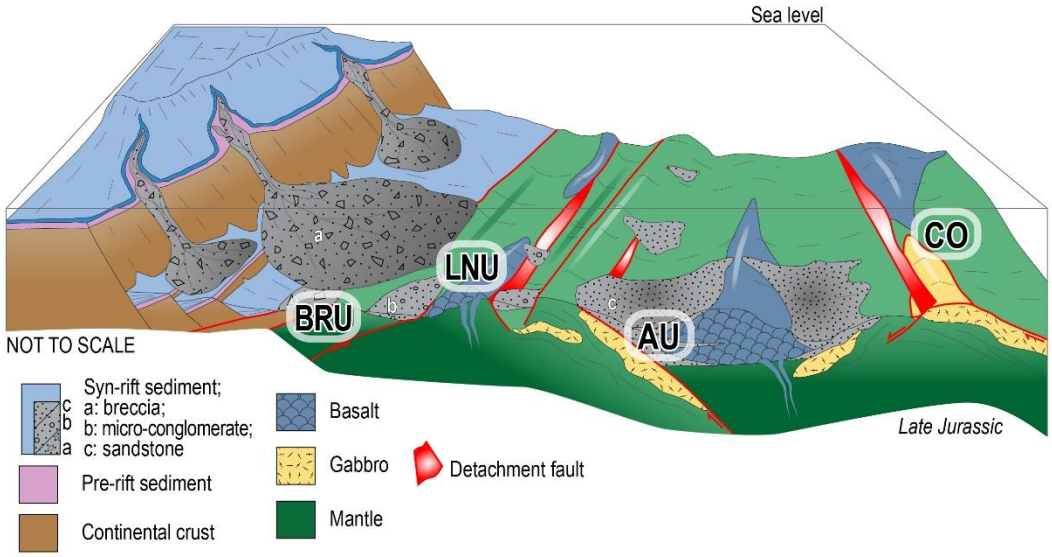

Figure 87 Interpretative block diagram showing the simplified paleogeographic setting of the Alpine Tethys in the Late Jurassic, before the deposition of the post-rift sediments. The studied units, reported as acronyms (BRU: Banchetta-Rognosa unit; LNU: Lago Nero unit; AU: Albergian unit; CO: Chenailllet ophiolite), are depicted in their presumed, relative location.

11.2 Tectono-metamorphic evolution

During this PhD project, for the first time the isochemical phase diagram approach was used to model and constrain the Alpine metamorphic evolution of units exposed in the investigated area of the Western Alps.

In particular, the constrained Alpine metamorphic peak conditions are:

- 20-23 kbar and 440-500 °C for the Banchetta-Rognosa unit;
- 18-20 kbar and 380-420 °C for the Albergian-Gran Mioul body of the Albergian unit;
- >9 kbar and >300 °C for the Chenaillet ophiolite.

In addition, based on conventional P-T thermobarometric estimates, the metamorphic peak conditions of the Lago Nero unit have been constrained at a minimum of 17 kbar and a maximum of 450 °C.

These data are reported in a schematic cross-section along the upper Susa and Chisone valleys (Figure 88), from the Dora-Maira internal crystalline massif to the pre-piemdont units, crossing the investigated sector of the Ligurian-Piemdont zone.

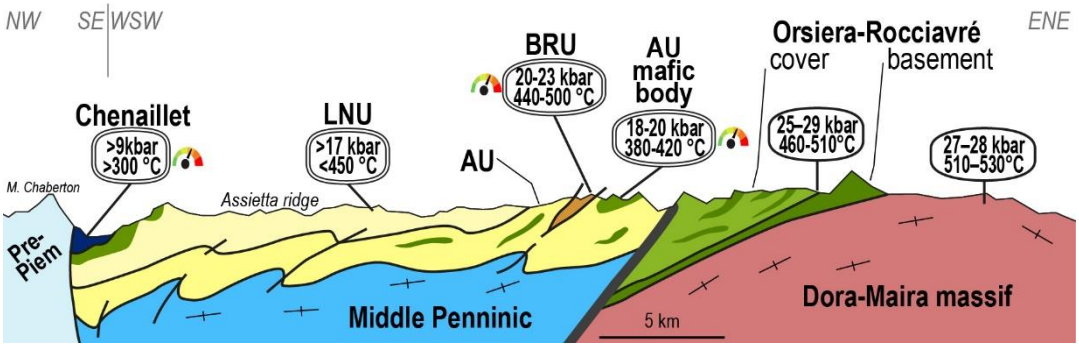

Figure 88 Schematized cross-section along the studied area in the upper Susa and Chisone vallyes (exaggerated vertical scale). Peak P-T estimates modeled by the Author and reported in this Thesis are highlighted small barometer icons (Chenaillet, BRU and AU mafic body). The estimations displayed for the other units are according to the most recent literature available: Manzotti et al., 2022, for Dora-Maira massif; Ghignone et al., 2021, for the Orsiera-Rocciavrè meta-ophiolite (i.e. Internal Piedmont Zone); Agard, 2001, for the Lago Nero unit.

Figure 89 is a compilation of P-T paths, from both the studied area (thicker lines) as well as the neighboring units with estimates from other authors. The Dora-Maira massif and the Internal Ligurian-Piedmont Zone occur to the East of the studied units (see Figure 88), while Ambin-Vanoise massif and the Ultrabriançonnais units occur to the North and to the South respectively.

Previous authors (see Agard, 2021 for a review) reported a progressive and constant westward decreasing gradient of metamorphic peak conditions. Although data

obtained by this PhD project fit with this general configuration (Figure 88 and Figure 89), it is worth stressing that:

- the BRU could represent one of the westernmost eclogitic unit of the Western Alps. This assumption derives from comparison of the peak metamorphic conditions of the BRU with respect to the ones of other eclogitic units on the Middle Penninic known in literature (i.e. Ambin-Vanoise massif, Strzerzynski et al. 2012, and Acceglio-Col Longet unit, Michard et al., 2004, and Schwartz et al., 2000);
- the general westward decrease in metamorphic peaks is abruptly interrupted by the eclogitic BRU, tectonically embedded within the lawsonite-blueschist AU (see also Figure 88). The present emplacement of the BRU within the (slightly) lower grade AU can be tentatively explained taking into account a trans-tensional tectonic regime during exhumation;
- in the blueschist-facies AU and LNU the good and widespread preservation of fresh lawsonite can be related to favorable Ca-rich bulk compositions and fast exhumation processes;
- the new and surprising data on the Alpine metamorphic evolution of the Chenaillet ophiolite (previously considered as anchi- or non-metamorphic) invoke for subduction related processes rather than obduction as suggested by previous authors (Bertrand et al., 1982; Caby, 1995). Therefore, the Chenaillet ophiolite must be considered in the description of the general westward decreasing of Alpine peak metamorphic conditions.
- this latter assumption brings with it the consequence that the geothermal gradient along the subduction channel, in this sector of the Western Alps (8°C/km according to Agard, 2021), could be revised and lowered to 6-7°C/km.

As general remark, it is worth noticing that the D2 events in the adjacent AU and BRU, responsible for development of the main foliation, are aligned along a ~10°C/km gradient together with the peak metamorphic conditions modeled for the Chenaillet ophiolite (Figure 89).

Based on the comparison with previous studies (e.g. Agard et al., 2001, and Beyssac et al., 2002) it can be inferred that i) generally, the isochemical phase diagram approach tends to model P-T conditions slightly higher than those previously constrained with other methods (i.e. Si-in-Phe barometer, Agard et al., 2001, and the RSCM thermometer, Beyssac et al. 2002); ii) a more complex tectonic setting for the studied area must be envisioned, taking into account a complex juxtaposition of bodies.

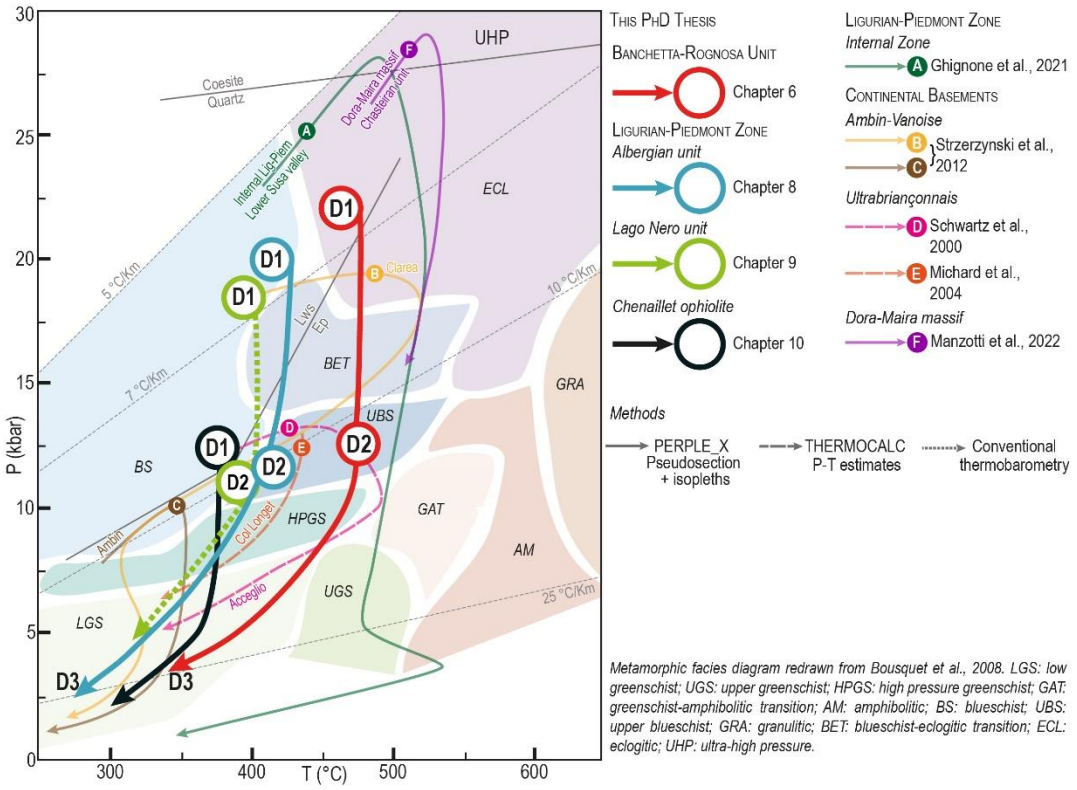

Metamorphic facies diagram redrawn from Bousquet et al., 2008. LGS: low greenschist; UGS: upper greenschist; HPGS: high pressure greenschist; GAT: greenschist-amphibolitic transition; AM: amphibolitic; BS: blueschist; UBS: upper blueschist; GRA: granulitic; BET: blueschist-eclogitic transition; ECL: eclogitic; UHP: ultra-high pressure.

Figure 89 Compilation of P-T paths of different units of the Western Alps, for comparison with the studied units from the upper Susa and Chisone valleys. Studied units (Banchetta-Rognosa unit, Albergian unit, Lago Nero unit, and Chenaillet ophiolite) are reported with thicker lines. Peak conditions were constrained with the isochemical phase diagram approach, while the retrograde exhumation part of the path was qualitatively inferred in the basis of mineral assemblages. Different line patterns indicate different thermobarometric methods, as reported in the legend. Lws-Ep reaction is from Poli & Schmidt (1995), modified below 10 kbar for the modeled bulk compositions.

11.3 CONCLUSIONS and FINAL REMARKS

To sum up, this Thesis aims to suggest new considerations and shed light on the Ligurian-Piedmont zone of the upper Susa and Chisone valleys. The units cropping out in this area (the Banchetta-Rognosa unit, the Albergian unit, the Lago Nero unit and the Chenaillet ophiolite) were already studied at the dawn of geology since the XIX century and then partially fell in oblivion. A multidisciplinary approach, based on lithostratigraphic and metamorphic investigations, proved to be essential to study these units in detail. Focusing on single, representative, geological bodies from each unit, this Thesis aimed to propose both paleogeographic and tectono-metamorphic constrains. Of course, the proposed models can account only for the studied successions, and they are not intended to be inferred to the evolution of the other meta-ophiolitic bodies occurring in these units or to similar units of the Western Alps, since their complex evolution and tectono-metamorphic history must be investigated on a case-by-case basis. However, this kind of approach could lead to a better understanding of the Alpine belt, both under a paleogeographic and metamorphic point of view.

REFERENCES

Agard, P., Vidal, O., & Goffé, B. (2001a). Interlayer and Si content of phengite in HP–LT carpholite-bearing metapelites. Journal of Metamorphic Geology, 19(5), 479-495.

Agard, P., Jolivet, L., & Goffe, B. (2001b). Tectonometamorphic evolution of the Schistes Lustres Complex; implications for the exhumation of HP and UHP rocks in the Western Alps. Bulletin de la Société géologique de France, 172(5), 617-636.

Agard, P., Monie, P., Jolivet, L. & Goffé, B. (2002). Exhumation of the Schistes Lustrés complex: in situ laser probe 40Ar/39Ar constraints and implications for the Western Alps. Journal of Metamorphic Geology, 20, 599-618.

Agard, P. & Lemoine, M. (2005). Faces of the Alps: structure and geodynamic evolution. Commission for the geological map of the World.

Agard, P., Yamato, P., Jolivet, L., & Burov, E. (2009). Exhumation of oceanic blueschists and eclogites in subduction zones: Timing and mechanisms. Earth-Science Reviews, 92(1-2), 53–79.

Agard, P. (2021). Subduction of oceanic lithosphere in the Alps: Selective and archetypal from (slow-spreading) oceans. Earth-Science Reviews, 103517.

Agard, P., & Handy, M. R. (2021). Ocean subduction dynamics in the Alps. Elements: An International Magazine of Mineralogy, Geochemistry, and Petrology, 17(1), 9-16.

Angiboust, S., Agard, P., Jolivet, L. & Beyssac, O. (2009). The Zermatt-Saas ophiolite: the largest (60-km wide) and deepest (c. 70-80km) continuous slice of oceanic lithosphere detached from a subduction zone? Terra Nova, 21, 171-180

Angiboust, S., Langdon, R., Agard, P., Waters, D. & Chopin, C. (2012). Eclogitization of the Monviso ophiolite (W. Alps) and implications on subduction dynamics. J. Metamorph. Geol., 30, 37-61.

Angiboust, S., & Harlov, D. (2017). Ilmenite breakdown and rutile-titanite stability in metagranitoids: Natural observations and experimental results. American Mineralogist: Journal of Earth and Planetary Materials, 102(8), 1696-1708.

Angiboust, S., & Glodny, J. (2020). Exhumation of eclogitic ophiolitic nappes in the W. Alps: New age data and implications for crustal wedge dynamics. Lithos, 356, 105374.

Aslanian, D., Moulin, M., Olivet, J. L., Unternehr, P., Matias, L., Bache, F., ... & Labails, C. (2009). Brazilian and African passive margins of the Central Segment of the South Atlantic Ocean: Kinematic constraints. Tectonophysics, 468(1-4), 98-112.

Assanelli, M., Luoni, P., Rebay, G., Roda, M., & Spalla, M. I. (2020). Tectono-metamorphic evolution of serpentinites from lanzo valleys subduction complex (Piemonte—Sesia-lanzo zone boundary, Western Italian Alps). Minerals, 10(11), 985.

Augenstein, C. (2012). The formation of the Lepontine gneiss dome. PhD thesis, Australian National University, 357 pp.

Babist, J., Handy, M. R., Konrad-Schmolke, M., & Hammerschmidt, K. (2006). Precollisional, multistage exhumation of subducted continental crust: The Sesia Zone, western Alps. Tectonics, 25(6).

Balestro, G., Fioraso, G., & Lombardo, B. (2013). Geological map of the Monviso massif (Western Alps). Journal of Maps, 9(4), 623-634.

Balestro, G., Lombardo, B., Vaggelli, G., Borghi, A., Festa, A. & Gattiglio, M. (2014). Tectonostratigraphy of the northern Monviso meta-ophiolite complex (Western Alps). Ital. J. Geosci., 133, 409-426.

Balestro, G., Festa, A. & Tartarotti, P. (2015). Tectonic significance of different block-in-matrix structures in exhumed convergent plate margins: Examples from oceanic and continental HP rocks in inner western Alps (northwest Italy). International Geology Review, 57, 581–605.

Balestro, G., Festa, A. & Dilek, Y. (2019). Structural architecture of the Western Alpine Ophiolites, and the Jurassic seafloor spreading tectonics of the Alpine Tethys. Journal of the Geological Society, 176(5), 913-930.

Balestro, G., Festa, A., De Caroli, S., Barbero, E., Borghi, A., & Gianotti, F. (2022). Multistage tectono-stratigraphic evolution of the Canavese Intracontinental Suture Zone: New constraints on the tectonics of the Inner Western Alps. Geoscience Frontiers, 13(6), 101448.

Balestro, G., Festa, A., Cadoppi, P., Groppo, C., & Roà, M. (2022). Pre-Orogenic Tectonostratigraphic Evolution of the European Distal Margin-Alpine Tethys Transition Zone in High-Pressure Units of the Southwestern Alps. Geosciences, 12(10), 358.

Ballevre, M., Manzotti, P., & Engi, M. (2014). From the highest (Dent-Blanche klippe) to the deepest unit (Money window): A kinematic model of the Western Alps. In 24 ème Réunion des sciences de la Terre 2014 (p. 191).

Ballèvre, M., Camonin, A., Manzotti, P. & Poujol, M. (2020). A step towards unraveling the paleogeographic attribution of pre-Mesozoic basement complexes in the Western Alps based on U-Pb geochronology of Permian magmatism. Swiss Journal of Geosciences, 113, 1-28.

Barale, L., Console, F., Corno, A., Frasca, G., Mosca, P., & Pantaloni, M. (2022). The geology of the Western Alps through the field notebooks of Secondo Franchi (1859-1932). Italian Journal of Geosciences, 141(1), 120-143.

Barféty, J. C., Gidon, M., & Mouterde, R. (1970). Observations stratigraphiques et structurales sur le Mézozoïque des environs de Bourg-d'Oisans (Isère). Géologie Alpine, 46, 23-28.

Barfety, J.C. (1972). Les variations du Trias médio-supérieur dolomitique et leur repartition dans la zone briançonnaise entre la vallée Étroite et le Guil (Hautes-Alpes). Comptes Rendus de l'Académie des Sciences, Paris, 287, 636-639.

Barfety, J.C., & Gidon, M. (1975). Longitudinal faulting and its place in structure of eastern Brianconnais. Comptes Rendus Hebdomadaires des Sciences de l'Academie des Sciences Serie D, 281(22), 1677-1680.

Barféty, J.C, Tricart, P., & Jeudy de Grissac, C. (1992). La Quatrième écaille près de Briançon (Alpes françaises) : un olistostrome précurseur de l'orogenèse pennique éocène. Comptes Rendus de l'Académie des Sciences, Paris, 314(1), 71-76.

Barfety, J. C., Lemoine, M., Graciansky, P. C. (de), Tricart, P. & Mercier, D. (1996). Notice explicative, carte géologique de la France (1/50 000), feuille Briançon (823). Bureau de Recherche Géologiques et Minières, Orléans.

Barfety, J.-C., Polino, R., Mercier, D., Caby, R., & Fourneaux, J. (2006). Notice de la carte géologique Névache-Bardonecchia-Modane, 799 (Bureau des Recherches Géologiques et Minières).

Baud, A. (1976). Les terriers de crustacés décapodes et l'origine de certains faciès du Trias carbonate. Eclogae Geologicae Helvetias, 69(2), 415-424.

Baud, A., & Megard-Galli, J. (1975). Évolution d'un bassin carbonate du domaine alpin Durant la phase pré-océanique : cycles et sequences dans le Trias de la zone briançonnaise des Alpes occidentales et des Préalpes. IXe congrès intern. sédim., Nice, 5, 45-50.

Baud, A., & Septfontaine, M. (1980). Présentation d'un profil palinspastique de la nappe des Préalpes médianes en Suisse occidentale. Eclogae Geologicae Helvetiae, 73(2), 651–660.

Bearth, P. (1967). Die Ophiolithe der Zone von Zermatt-Saas Fee. Beiträge zur Geologischen Karte der Schweiz, Neue Folge, 130 pp.

Beltrando, M., Compagnoni, R., & Lombardo, B. (2010a). (Ultra-) High-pressure metamorphism and orogenesis: An Alpine perspective. Gondwana reserch, 18, 147-166.

Beltrando, M., Rubatto, D. & Manatschal, G. (2010b). From passive margins to orogens: The link between ocean-continent transition zones and (ultra) high-pressure metamorphism. Geology, 38, 559-562.

Beltrando, M., Frasca, G., Compagnoni, R., & Vitale-Brovarone, A. (2012). The Valaisan controversy revisited: Multi-stage folding of a Mesozoic hyper-extended margin in the Petit St. Bernard pass area (Western Alps). Tectonophysics, 579, 17-36.

Beltrando, M., Manatschal, G., Mohn, G., Dal Piaz, G.V., Vitale Brovarone, A. & Masini, E. (2014). Recognizing remnants of magma-poor rifted margins in high-pressure orogenic belts: The Alpine case study. Earth-Science Reviews, 131, 88-115.

Berger, A., Thomsen, T. B., Ovtcharova, M., Kapferer, N., & Mercolli, I. (2012). Dating emplacement and evolution of the orogenic magmatism in the internal Western Alps: 1. The Miagliano Pluton. Swiss journal of geosciences, 105(1), 49-65.

Berra, F., Galli, M. T., Reghellin, F., Torricelli, S., & Fantoni, R. (2009). Stratigraphic evolution of the Triassic–Jurassic succession in the Western Southern Alps (Italy): the record of the two-stage rifting on the distal passive margin of Adria. Basin Research, 21(3), 335-353.

Bertrand, J., Steen, D. M., Tinkler, C., & Vuagnat, M. (1980). The melange zone of the col du Chenaillet (Montgenèvre ophiolite, Hautes-Alpes, France). Archives des sciences, 33(2-3), 117-138.

Bertrand, J., Courtin, B. & Vuagnat, M. (1982). Elaboration d'un secteur de lithosphère océanique Liguro-Piemontais d'après les données de l'ophiolite du Montgenèvre (Hautes-Alpes, France et province de Turin). Ofioliti, 7, 155-196.

Bertrand, J., Dietrich, V., Nievergelt, P. & Vuagnat, M. (1987). Comparative major and trace element geochemistry of gabbroic and volcanic rock sequences, Montgenèvre ophiolite, Western Alps. Schweiz. mineral. petrogr. Mitt., 67, 147-169.

Bertrand, J.M., Pidgeon, R.T., Leterrier, J., Guillot, F., Gasquet, D. & Gattiglio, M. (2000). SHRIMP and IDTIMS U-Pb zircon ages of the pre-Alpine basement in the internal western Alps (Savoy and Piemont). Schweizerische Mineralogische und Petrographische Mitteilungen, 80, 225-248.

Beyssac, O., Rouzaud, JN., Goffé, B., Brunet, F., & Chopin, C. (2002). Graphitization in a high-pressure, low-temperature metamorphic gradient: a Raman microspectroscopy and HRTEM study. Contributions to Mineralogy and Petrology, 143, 19–31.

Bigi, G., Castellarin, A., Coli, M., Dal Piaz, G.V., Sartori, R., Scandone, P. & Vai, G.B. (1990). Structural Model of Italy scale 1:500.000, sheet 1. C.N.R., Progetto Finalizzato Geodinamica, SELCA Firenze.

Bigioggero, B., Colombo, A., Del Moro, A., Gregnanin, A., Macera, P., & Tunesi, A. (1994). The Oligocene Valle del Cervo pluton: an example of shoshonitic magmatism in the Western Italian Alps.

Bocchio, R., Benciolini, L., Martin, S., & Tartarotti, P. (2000). Geochemistry of eclogitised Fe-Ti-gabbros from various lithological settings (Aosta Valley ophiolites, Italian western Alps). Protolith composition and eclogitic paragenesis. Period. Mineral, 69(3), 217-237.

Bolin, C., Mingguo, Z., Carswell, D. A., Wilson, R. N., Qingchen, W., Zhongyan, Z., & Windley, B. F. (1995). Petrogenesis of ultrahigh-pressure rocks and their country rocks at Shuanghe in Dabieshan, central China. European Journal of Mineralogy, 7(1), 119-138.

Borghi, A., Gattiglio, M., Mondino, F., & Zaccone, G. (1999). Structural and metamorphic evidences of pre-Alpine basement in the Ambin Nappe (Western Alps). Memorie di Scienze Geologiche, Padova, 51, 204-220.

Boriani, A., Origoni, E. G., Borghi, A., & Caironi, V. (1990). The evolution of the "Serie dei Laghi"(Strona-Ceneri and Scisti dei Laghi): the upper component of the Ivrea-Verbano crustal section; Southern Alps, north Italy and Ticino, Switzerland. Tectonophysics, 182(1-2), 103-118.

Bousquet, R., Oberhänsli, R., Goffé, B., Wiederkehr, M., Koller, F., Schmid, S. M., Schuster, R., Engi, M., Berger, A. & Martinotti, G. (2008). Metamorphism of metasediments at the scale of an orogen: a key to the Tertiary geodynamic evolution of the Alps. Geological Society, London, Special Publications, 298(1), 393-411.

Brune, S., Heine, C., Clift, P. D., & Pérez-Gussinyé, M. (2017). Rifted margin architecture and crustal rheology: reviewing Iberia-Newfoundland, central South Atlantic, and South China Sea. Marine and Petroleum Geology, 79, 257-281.

Bucher, K., Weisenberger, T. B., Klemm, O., & Weber, S. (2019). Decoding the complex internal chemical structure of garnet porphyroblasts from the Zermatt area, Western Alps. Journal of metamorphic Geology, 37(9), 1151-1169.

Bucher, K., Fazis, Y., De Capitani, C., & Grapes, R. (2005). Blueschists, eclogites, and decompression assemblages of the Zermatt-Saas ophiolite: High-pressure metamorphism of subducted Tethys lithosphere. American mineralogist, 90(5-6), 821-835.

Bucher, K., & Grapes, R. (2009). The eclogite-facies Allalin Gabbro of the Zermatt–Saas ophiolite, Western Alps: A record of subduction zone hydration. Journal of Petrology, 50(8), 1405-1442.

Buffon, G. (1786). Histoire naturelle des minéraux. T. iv., 395 p. Paris.

Burov, E., Francois, T., Yamato, P., & Wolf, S. (2014). Mechanisms of continental subduction and exhumation of HP and UHP rocks. Gondwana Research, 25(2), 464-493.

Burroni, A., Levi, N., Marroni, M. & Pandolfi, L. (2003). Lithostratigraphy and structure of the Lago Nero Unit (Chenaillet Massif, Western Alps): comparison with Internal Liguride units of Northern Apennines. Ofioliti, 28, 1-11.

Caby, R., & Galli, J. (1964). Existence de cinérites et de tufs volcaniques dans le Trias moyen de la zone briançonnaise. C.R. Acad. Sci., Paris, t. 259, 2, 417-420.

Caby, R., Michard, A. & Tricart, P. (1971). Decouverte d'une brèche polygenique à elements granitoïdes dans les ophiolites metamorphiques piemontaises (Schistes Lustrés du Queyras, Alpes françaises). Comptes Rendus de l'Académie des Sciences, Paris, 273, 999–1002.

Caby, R. (1995). Plastic deformation of gabbros in a slow-spreading Mesozoic ridge: example of the Montgenevre Ophiolite. In: Vissers, R.L.M. & Nicolas, A. (eds) Mantle and Lower Crust Exposed in Oceanic Ridges and in Ophiolites. Kluwer, Dordrecht, 123-145.

Cadoppi, P., Castelletto, M., Sacchi, R., Baggio, P., Carraro, F., & Giraud, V. (2002). Note illustrative della Carta Geologica d'Italia alla scala 1: 50.000–Foglio 154, Susa.

Cann, J. R., Blackman, D. K., Smith, D. K., McAllister, E., Janssen, B., Mello, S., ... & Escartin, J. (1997). Corrugated slip surfaces formed at ridge–transform intersections on the Mid-Atlantic Ridge. Nature, 385(6614), 329-332.

Caron, J. M., & Saliot, P. (1969). Nouveaux gisements de lawsonite et de jadeite dans les alpes franco-italiennes. Comptes Rendus de l'Académie des Sciences Paris, 268, 3153-3156.

Caron, J.M. (1970). Etude d'un stilpnomélane des Schistes lustres piemontais. Bulletin de la Société française de minéralogie et de cristallographie, 93, 133-136.

Caron, J. M. (1971). Contribution à l'étude lithostratigraphique et structurale de la région de Sestrière (Alpes Cottiennes, Italie). Trav. Lab. Géol. Grenoble, 21, 45-68.

Caron, J. M. (1974). Rapports entre diverses" generations" de lawsonite et les deformations dans les Schistes lustres des Alpes cottiennes septentrionales (France et Italie). Bulletin de la Société Géologique de France, 7(3), 255-263.

Caron, J.M. (1977). Lithostratigraphie et tectonique des Schistes lustrés dans les Alpes Cottiennes septentrionales et en Corse orientale. Thèse État, Strasbourg, 326 pp.

Caron, J. M., Polino, R., & Pognante, U. (1984). Ou sont les sutures majeures dans les Alpes internes? Transversale Briançon-Torino. Memorie della Società Geologica Italiana, 29, 71-78.

Caso, F., Nerone, S., Petroccia, A., & Bonasera, M. (2021). Geology of the southern Gran Paradiso Massif and Lower Piedmont Zone contact area (middle Ala Valley, Western Alps, Italy). Journal of Maps, 17(2), 237-246.

Castellarin, A., Cantelli, L., Fesce, A. M., Mercier, J. L., Picotti, V., Pini, G. A., ... & Selli, L. (1992). Alpine compressional tectonics in the Southern Alps. Relationships with the N-Apennines. In Annales tectonicae, 6(1), 62-94.

Castellarin, A., & Vai, G. B. (1986). Southalpine versus Po plain Apenninic arcs. In Developments in Geotectonics, 21, 253-280. Elsevier.

Castellarin, A. (2001). Alps-Apennines and Po Plain-frontal Apennines relations. In Anatomy of an Orogen: the Apennines and adjacent Mediterranean Basins. Springer, Dordrecht, 177-195.

Castellarin, A., Vai, G. B., & Cantelli, L. (2006). The Alpine evolution of the Southern Alps around the Giudicarie faults: A Late Cretaceous to Early Eocene transfer zone. Tectonophysics, 414(1-4), 203-223.

Chalot-Prat, F., Ganne, J., & Lombard, A. (2003). No significant element transfer from the oceanic plate to the mantle wedge during subduction and exhumation of the Tethys lithosphere (Western Alps). Lithos, 69(3-4), 69-103.

Chalot-Prat, F. (2005). An undeformed ophiolite in the Alps: Field and geochemical evidence for a link between volcanism and shallow plate tectonic processes. Special Papers-Geological Society of America, 388, 751.

Chalot-Prat, F. & Bourlier, E. C. Y. (2005). L'ophiolite du Chenaillet (Montgenèvre, Alpes franco-italiennes), témoin d'un segment de ride volcanique axiale d'un océan à croissance lente. Géol. Fr.

Chen, Y., Ye, K., Wu, T. F. & Guo, S. (2013). Exhumation of oceanic eclogites: thermodynamic constraints on pressure, temperature, bulk composition and density. Journal of Metamorphic Geology, 31(5), 549-570.

Choi, E., & Buck, W. R. (2012). Constraints on the strength of faults from the geometry of rider blocks in continental and oceanic core complexes. Journal of Geophysical Research: Solid Earth, 117(B4).

Chopin, C. (1984). Coesite and pure pyrope in high-grade blueschists of the Western Alps: a first record and some consequences. Contributions to Mineralogy and Petrology, 86(2), 107-118.

Chopin, C., Henry, C. & Michard, A. (1991). Geology and petrology of the coesite-bearing terrain, Dora Maira Massif, Western Alps. European Journal of Mineralogy, 3, 263–291.

Clarke, G.L., Powell, R. & Fitzherbert, J.A. (2006). The lawsonite paradox: a comparison of field evidence and mineral equilibria modelling. Journal of Metamorphic Geology, 24, 715–725.

Coltat, R., Branquet, Y., Gautier, P., Boulvais, P., & Manatschal, G. (2020). The nature of the interface between basalts and serpentinized mantle in oceanic domains: Insights from a geological section in the Alps. Tectonophysics, 797, 228646.

Compagnoni, R. (1977). The Sesia-Lanzo Zone: high pressure-low temperature metamorphism in the Austroalpine continental margin. Rendiconti Società Italiana di Mineralogia e Petrologia, 33(1), 335-374.

Compagnoni, R. (2003). HP metamorphic belt of the western Alps. Episodes, 26(3), 200-204.

Compagnoni, R., Rolfo, F., Groppo, C., Hirajima, T., & Turello, R. (2012). Geological map of the ultra-high pressure Brossasco-Isasca unit (Western Alps, Italy). Journal of Maps, 8(4), 465-472.

Compagnoni, R., Engi, M., & Regis, D. (2014). Valle d'Aosta section of the Sesia Zone: multi-stage HP metamorphism and assembly of a rifted continental margin. Geologial Field Trips, 6(1.2), 1-44.

Connolly, J.A.D. (1990). Multivariable phase diagrams: an algorithm based on generalized thermodynamics. American Journal of Science, 290, 666-718.

Connolly, J.A.D. (2005). Computation of phase equilibria by linear programming: a tool for geodynamic modeling and its application to subduction zone decarbonation. Earth and Planetary Science Letters, 236(1-2), 524-541.

Connolly, J.A.D. (2009). The geodynamic equation of state: what and how. Geochemistry, Geophysics, Geosystems, 10(10), 1-19.

Conti, M., Marcucci, M., & Passerini, P. (1985). Radiolarian cherts and ophiolites in the northern Apennine and Corsica: age, correlations and tectonic frame of siliceous deposition.

Contrucci, I., Matias, L., Moulin, M., Géli, L., Klingelhofer, F., Nouzé, H., ... & Sibuet, J. C. (2004). Deep structure of the West African continental margin

(Congo, Zaïre, Angola), between 5 S and 8 S, from reflection/refraction seismics and gravity data. Geophysical Journal International, 158(2), 529-553.

Cook-Kollars, J., Bebout, G. E., Collins, N. C., Angiboust, S. & Agard, P. (2014). Subduction zone metamorphic pathway for deep carbon cycling: I. Evidence from HP/UHP metasedimentary rocks, Italian Alps. Chemical Geology, 386, 31-48.

Cordey, F., & Bailly, A. (2007). Alpine ocean seafloor spreading and onset of pelagic sedimentation: new radiolarian data from the Chenaillet-Montgenèvre ophiolite (French-Italian Alps). Geodinamica Acta, 20(3), 131-138.

Corno, A., Mosca, P., Borghi, A., & Gattiglio, M. (2019). Lithostratigraphy and petrography of the Monte Banchetta-Punta Rognosa oceanic succession (Troncea and Chisonetto Valleys, Western Alps). Ofioliti, 44(2), 83-95.

Corno, A., Mosca, P., Gattiglio, M. & Borghi, A. (2021a). Geological map of the Monte Banchetta – Punta Rognosa area (Troncea valley, Western Alps). Journal of Maps, 17 (2), 150-160.

Corno, A., Groppo, C., Mosca, P., Borghi, & Gattiglio, M. (2021b). Eclogitic metamorphism in the Alpine far-west: petrological constraints on the Banchetta-Rognosa tectonic unit. Swiss Journal of Geosciences. 114:16.

Corno, A., Mosca, P., Groppo, C., Borghi, A., & Gattiglio, M. (2022). More widespread than supposed: preserved lawsonite in the blueschist-facies ophiolitic bodies from the Albergian unit (Liguria-Piemonte zone, Western Alps). Ofioliti, 47(2), 137-154.

Corona, J.C., Jenkins, D.M. & Holland, T.J.B. (2013). Constraints on the upper pressure stability of blueschist facies metamorphism along the reaction: glaucophane = talc + 2 jadeite in the Na_2O-MgO-Al_2O_3-SiO_2-H_2O system. American Journal of Science, 313, 967-995.

Costa, S. & Caby, R. (2001). Evolution of the Ligurian Tethys in the Western Alps: Sm/Nd and U/Pb geochronology and rare-earth element geochemistry of the Montgenèvre ophiolite (France). Chemical Geology, 175, 449–466.

Coward, M.P. & Dietrich, D. (1989). Alpine tectonics: an overview. In: Coward, M.P., Dietrich, D. & Park, R.G. (eds.), Alpine tectonics. Geological Society, London, Special Publications, 45, 1-29.

Cuthbert, S. J., Carswell, D. A., Krogh-Ravna, E. J., & Wain, A. (2000). Eclogites and eclogites in the Western Gneiss region, Norwegian Caledonides. Lithos, 52(1-4), 165-195.

D'Atri, A., Piana, F., Barale, L., Bertok, C., & Martire, L. (2016). Geological setting of the southern termination of Western Alps. International Journal of Earth Sciences, 105(6), 1831-1858.

Dal Piaz, G.V., Hunziker, J.C. & Martinotti, G. (1972). La Zona Sesia-Lanzo e l'evoluzione tettonico-metamorfica delle Alpi nordoccidentali interne. Memorie della Società Geologica Italiana, 11(4), 433-462.

Dal Piaz, G.V. (1974). Le mètamorphisme de haute et basse température dans l'évolution structurale du bassin ophiolitique alpino-appenninique. Ière partie. Bollettino della Società Geologica Italiana, 93, 437-468.

Dal Piaz, G. V., & Gosso, G. (1984). Le moderne interpretazioni tettoniche delle Alpi. Cento anni di geologia italiana. I Centenario SGI, Vol giub, 95-112.

Dal Piaz, G. V., & Polino, R. (1989). Evolution of the alpine Tethys. Atti dell'Accademia Nazionale dei Lincei, 80, 93-107,

Dal Piaz, G.V., Cortiana, G., Del Moro, A., Martin, S., Pennacchioni, G. & Tartarotti, P. (2001). Tertiary age and paleostructural inferences of the eclogitic imprint in the Austroalpine outliers and Zermatt-Saas ophiolite, Western Alps. Intern. J. Earth Sci., 90, 668-684.

Dal Piaz, G. V., Bistacchi, A., & Massironi, M. (2003). Geological outline of the Alps. Episodes Journal of International Geoscience, 26(3), 175-180.

Dal Piaz, G.V. (2010). The Italian Alps: a journey across two centuries of Alpine geology . In: Beltrando, M., Peccerillo, A., Mattei, M., Conticelli, S. and Doglioni, C. (Eds.), The Geology of Italy: tectonics and life along plate margins, Journal of the Virtual Explorer, Electronic Edition, 36, paper 8.

De Graciansky, P.-C., Roberts, D.G. & Tricart, P. (2011). The Western Alps, from Rift to Passive Margin to Orogenic Belt, Elsevier.

De Togni, M., Gattiglio, M., Ghignone, S., & Festa, A. (2021). Pre-Alpine Tectono-Stratigraphic Reconstruction of the Jurassic Tethys in the High-Pressure Internal Piedmont Zone (Stura di Viù Valley, Western Alps). Minerals, 11(4), 361.

De Wever, P., Baumgartner, P.O. & Polino, R. (1987). Précision sur les datations de la base des Schistes Lustrés post-ophiolitiques dans les Alpes Cottiennes. C.R. Acad. Sci., 305, 487-491.

De Wever, P. & Baumgartner, P.O. (1995). Radiolarians from the base of the Supra-ophiolitic Schistes Lustrés formation in the Alps (Saint-Véran, France and Traversiera Massif, Italy). In: Baumgartner, P.O., O'Dogerthy, L., Gorican, S., Urquhart, E., Pillevuit, A. & De Wever, P. (Eds.) Middle Jurassic to Lower Cretaceous Radiolaria of Tethys: occurrences, systematics, biochronology. Mém. Geol. Lausanne, 23, 725-730.

Debelmas, J., & Lemoine, M. (1966). Carte géologique du France (1/50 000), feuille Guillestre (847), Serv Carte geol France, Paris.

Decarlis, A., Manatschal, G., Haupert, I. & Masini, E. (2015). The tectono-stratigraphic evolution of distal, hyper-extended magma-poor conjugate rifted margins: Examples from the Alpine Tethys and Newfoundland-Iberia. Marine and petroleum geology, 68, 54-72.

Decarlis, A., Beltrando, M., Manatschal, G., Ferrando, S., & Carosi, R. (2017). Architecture of the distal Piedmont-Ligurian rifted margin in NW Italy: Hints for a flip of the rift system polarity. Tectonics, 36(11), 2388-2406.

Deer, W.A., Howie, R.A., & Zussman, J. (1997). Rock-Forming Minerals. Geol. Soc.Lond, U.K. Longmane, 528 p.

Delesse, (1848). Sur la variolite de la Durance. Bull. Soc. Géol. France, 2 (VII), 427-431.

Desmons, J. (1990). Sur quelques minéraux de la zone piémontaise (Zone du Combin) dans les Alpes françaises. Géologie Alpine, 66 pp.

Desmurs, L., Müntener, O., & Manatschal, G. (2002). Onset of magmatic accretion within a magma-poor rifted margin: a case study from the Platta ocean-continent transition, eastern Switzerland. Contributions to Mineralogy and Petrology, 144(3), 365-382.

Deville, E., Fudral, S., Lagabrielle, Y., Marthaler, M. & Sartori, M. (1992). From oceanic closure to continental collision: A synthesis of the 'Schistes lustrés' metamorphic complex of the Western Alps. Geol. Soc. Am. Bull., 104, 127-139.

Dick, H. J. B. (1989). Abyssal peridotites, very slow spreading ridges and ocean ridge magmatism. Geological Society, London, Special Publications, 42(1), 71-105.

Dumont, T. (1983). Le chaînon de Rochebrune au Sud-Est de Briançon : évolution paléogéographique et structurale d'un secteur de la zone piémontaise des Alpes occidentales. Thèse 3e cycle, Grenoble, 250 pp.

Dumont, T. (1984). Le Rhétien et le Lias inférieur prépiémontais: enregistrement sédimentaire du passage des carbonates de plateforme triasiques au Jurassique hémipélagique lors du début du rifting téthysien. Géologie alpine, 60, 13-25.199

Dumont, T., Lemoine, M., & Tricart, P. (1984a). Tectonique synsédimentaire triasico-liasique et rifting téthysien dans l'unité piémontaise de Rochebrune au Sud-Est de Briançon. Bulletin de la Société Géologique de France, (7), 26 (5), 921-933.

Dumont, T., Lemoine, M., & Tricart, P. (1984b). Pérennité de la sédimentation pélagique du Jurassique supérieur jusque dans le Crétacé supérieur au-dessus de la croûte océanique téthysienne ligure : la série supra-ophiolitique du lac des Cordes (zone piémontaise des Alpes occidentales au Sud-Est de Briançon). Comptes Rendus de l'Académie des Sciences, Paris, 299, 1069-1072.

Egli, D., & Mancktelow, N. (2013). The structural history of the Mont Blanc massif with regard to models for its recent exhumation. Swiss journal of geosciences, 106(3), 469-489.

Ellenberger, F. (1960). Sur une paragénèse éphémère à lawsonite et glaucophane dans le métamorphisme alpin en Haute-Maurienne (Savoie). Bulletin de la Societe Geologique de France, 7(2), 190-194.

Elter, G. (1971). Schistes Lustrès et ophiolites de la zone piémontaise entre Orco et Doire Baltée (Alpes Graies). Hypothèses sur l'origine des ophiolites. Géol. Alpine, 47, 147-169.

Engi, M., & Berger, A. (2003, April). Thermal evolution of the Lepontine Dome (central Alps). In EGS-AGU-EUG Joint Assembly (p. 12501).

Ernst, W. G. (1979). Coexisting sodic and calcic amphiboles from high-pressure metamorphic belts and the stability of barroisitic amphibole. Miner. Magazine, 43(326), 269-278.

Evans, B.W. (1990). Phase relations of epidote-blueschists. Lithos, 25, 3-23.

Faccenda, M. (2014). Water in the slab: A trilogy. Tectonophysics, 614, 1-30.

Ferrando, S., Bernoulli, D., & Compagnoni, R. (2004). The Canavese zone (internal Western Alps): a distal margin of Adria. Schweizerische Mineralogische und Petrographische Mitteilungen, 84(1-20).

Festa, A., Balestro, G., Dilek, Y., & Tartarotti, P. (2015). A Jurassic oceanic core complex in the high-pressure Monviso ophiolite (western Alps, NW Italy). Lithosphere, 7(6), 646-652.

Festa, A., Balestro, G., Borghi, A., De Caroli, S., & Succo, A. (2020). The role of structural inheritance in continental break-up and exhumation of Alpine Tethyan mantle (Canavese Zone, Western Alps). Geoscience Frontiers, 11(1), 167-188.

Festa, A., Meneghini, F., Balestro, G., Pandolfi, L., Tartarotti, P., Dilek, Y., & Marroni, M. (2021). Comparative analysis of the sedimentary cover units of the Jurassic Western Tethys ophiolites in the Northern Apennines and Western Alps (Italy): processes of the formation of mass-transport and chaotic deposits during seafloor spreading and subduction zone tectonics. The Journal of Geology, 129(5), 533-561.

Forneris, J. F. & Holloway, J. R. (2003). Phase equilibria in subducting basaltic crust: implications for H_2O release from the slab. Earth and Planetary Science Letters, 214(1-2), 187-201.

Fioraso, G. (2009). Carta Geologica della Val Troncea. CNR - Istituto di Geoscienze e Georisorse, Ente di Gestione Parco Val Troncea, Regione Piemonte. Litografia Geda–Nichelino.

Fioraso, G., Mosca, P., Corno, A., Bonadeo, L., Brunamonte, F., Baggio, P., Raco, B., Doveri M., Lelli, M., & Giacometti, F. (2021). Note Illustrative della Carta Geologica d'Italia alla scala 1:50.000. Foglio 171, Cesana Torinese. https://www.isprambiente.gov.it/Media/carg/note_illustrative/171_Cesana_Torinese.pdf

Florineth, D., & Froitzheim, N. (1994). Transition from continental to oceanic basement in the Tasna Nappe: evidence for Early Cretaceous opening of the Valais Ocean.

Franchi, S. (1895). Alcune metamorfosi di eufotidi e diabasi Alpi Occid. Boll. R. Com. geol., 181.

Franchi, S. (1897). Sopra alcuni nuovi giacimenti di roccie a lawsonite. Bollettino della Società geologica Italiana, 16, 73-76.

Franchi, S. (1899). Sull'eta'mesozoica della zona delle pietre verdi nelle Alpi occidentali. Bollettino del Regio Comitato Geologico Italiano, 29(3), 173-247.

Franchi, S. (1911). Il Retico quale zona di transizione fra la Dolomia principale ed il Lias a «faciès piemontese» - calscisti con Belemniti e pietre verdi - nell'Alta Valle di Susa. Bollettino del Regio Comitato Geologico Italiano, XLI, 306-340.

Franchi, S. (1929). Sulla tettonica delle Alpi Cozie franco-italiane.

Froitzheim, N., & Eberli, G. P. (1990). Extensional detachment faulting in the evolution of a Tethys passive continental margin, Eastern Alps, Switzerland. Geological society of America bulletin, 102(9), 1297-1308.

Froitzheim, N. & Manatschal, G. (1996). Kinematics of Jurassic rifting, mantle exhumation, and passive-margin formation in the Austroalpine and Penninic nappes (eastern Switzerland). Geol. Soc. Am. Bull., 108, 1120-1133.

Fudral, S., Deville, E., & Marthaler, M. (1987). Distinction de trois ensembles d'unités dans les «Schistes lustrés» compris entre la Vanoise et le Val de Suse (Alpes franco-italiennes septentrionales): aspects lithostratigraphiques, paléogéographiques et géodynamiques. Comptes rendus des séances de l'Académie des sciences. Série 2, Mécanique-physique, Chimie, Sciences de l'univers, Sciences de la Terre, 305, 467-472.

Fudral, S., Deville, E., Pognante, U., Gay, M., Fregolent, G., Lorenzoni, S., Robert, D., Nicoud, G., Blake, C., Jayko, A., Jaillard, E., Bertrand, J.M., Forno, M.G. & Massazza, G. (1994). Carte Géologique de la France à 1:50.000, feuille 776 Lanslebourg - Mont d'Ambin.

Fuhrman, M. L., & Lindsley, D. H. (1988). Ternary-feldspar modeling and thermometry. American mineralogist, 73(3-4), 201-215.

Gabalda, S., Beyssac, O., Jolivet, L., Agard, P., & Chopin, C. (2009). Thermal structure of a fossil subduction wedge in the Western Alps. Terra Nova, 21(1), 28-34.

Ganne, J., Bertrand, J. M., & Fudral, S. (2005). Fold interference pattern at the top of basement domes and apparent vertical extrusion of HP rocks (Ambin and South Vanoise massifs, Western Alps). Journal of Structural Geology, 27(3), 553-570.

Gasco, I., & Gattiglio, M. (2011). Geological map of the middle Orco valley, Western Italian Alps. Journal of Maps, 7(1), 463-477.

Gastaldi, B. (1878). Sui rilevamenti geologici fatti nelle Alpi piemontesi durante la compagna del 1877 (Vol. 2). Coi tipi del Salviucci.

Ghignone, S., Borghi, A., Balestro, G., Castelli, D., Gattiglio, M., & Groppo, C. (2021). HP tectono-metamorphic evolution of the Internal Piedmont Zone in Susa Valley (Western Alps): New petrologic insight from garnet+ chloritoid-bearing micaschists and Fe–Ti metagabbro. Journal of Metamorphic Geology.

Giacometti, F., & Rebay, G. (2013). Structural and petrological evolution of the Beth-Ghinivert zone (Schistes Lustres—Italian Western Alps). Rendiconti Online della Società Geologica Italiana, 29, 70-73.

Gillard, M., Manatschal, G., & Autin, J. (2016). How can asymmetric detachment faults generate symmetric Ocean Continent Transitions?. Terra Nova, 28(1), 27-34.

Godard, M., Awaji, S., Hansen, H., Hellebrand, E., Brunelli, D., Johnson, K., ... & Rosner, M. (2009). Geochemistry of a long in-situ section of intrusive slow-spread oceanic lithosphere: Results from IODP Site U1309 (Atlantis Massif, 30 N Mid-Atlantic-Ridge). Earth and Planetary Science Letters, 279(1-2), 110-122.

Goldstein, J. I., Newbury, D. E., Michael, J. R., Ritchie, N. W., Scott, J. H. J., & Joy, D. C. (2017). Scanning electron microscopy and X-ray microanalysis. Springer.

Goto, A., Kunugiza, K. & Omori, S. (2007). Evolving fluid composition during prograde metamorphism in subduction zones: A new approach using carbonate-bearing assemblages in the pelitic system. Gondwana Research, 11(1-2), 166-179.

Graciansky, P.C. (de), & Mercier, D. (1976). Séquences sédimentaires dans le «Dogger» briançonnais et ouverture téthysienne. Comptes Rendus de l'Académie des Sciences, Paris, 283, 475-478.

Green, E., Holland, T., & Powell, R. (2007). An order-disorder model for omphacitic pyroxenes in the system jadeite-diopside-hedenbergite-acmite, with applications to eclogitic rocks. American Mineralogist, 92(7), 1181-1189.

Green, E. C. R., White, R. W., Diener, J. F. A., Powell, R., Holland, T. J. B., & Palin, R. M. (2016). Activity–composition relations for the calculation of partial melting equilibria in metabasic rocks. Journal of Metamorphic Geology, 34(9), 845-869.

Groppo, C., Lombardo, B., Rolfo, F., & Pertusati, P. (2007). Clockwise exhumation path of granulitized eclogites from the Ama Drime range (Eastern Himalayas). Journal of Metamorphic Geology, 25(1), 51-75.

Groppo, C., Beltrando, M., & Compagnoni, R. (2009). P-T path of the UHP Lago di Cignana and adjoining HP meta-ophiolitic units: insights into the evolution of subducting tethyan slab. Journal of Metamorphic Geology, 27, 207-231.

Groppo, C. & Castelli, D. (2010). Prograde P–T evolution of a lawsonite eclogite from the Monviso meta-ophiolite (Western Alps): Dehydration and redox reactions during subduction of oceanic FeTi-oxide gabbro. J. Petrol., 51, 2489-2514.

Groppo, C., Rolfo, F., Sachan, H. K., & Rai, S. K. (2016). Petrology of blueschist from the Western Himalaya (Ladakh, NW India): exploring the complex behavior of a lawsonite-bearing system in a paleo-accretionary setting. Lithos, 252, 41-56.

Groppo, C., Ferrando, S., Gilio, M., Botta, S., Nosenzo, F., Balestro, G., Festa, A. & Rolfo, F. (2019). What's in the sandwich? New P–T constraints for the (U) HP nappe stack of southern Dora-Maira Massif (Western Alps). European Journal of Mineralogy, 31(4), 665-683.

Guillot, S., Hattori, K., Agard, P., Schwartz, S., & Vidal, O. (2009). Exhumation processes in oceanic and continental subduction contexts: a review. Subduction zone geodynamics, 175-205.

Guiraud, M., Holland, T.J.B. & Powell, R. (1990). Calculated mineral equilibria in the greenschist-blueschist-eclogite facies in Na_2O-FeO-MgO-Al_2O_3-SiO_2-H_2O: methods, results and geological applications. Contribution to Mineralogy and Petrology, 104, 85-98.

Hacker, B. R., Andersen, T. B., Johnston, S., Kylander-Clark, A. R., Peterman, E. M., Walsh, E. O., & Young, D. (2010). High-temperature deformation during continental-margin subduction & exhumation: The ultrahigh-pressure Western Gneiss Region of Norway. Tectonophysics, 480(1-4), 149-171.

Handy, M. & Oberhänsli, R. (2004). Explanatory notes to the map: metamorphic structure of the Alps–Age map of metamorphic structure of the Alps–Tectonic interpretation and outstanding problems. Mitteilungen der Österreichischen Mineralogischen Gesellschaft, 149, 201–225.

Harlow, G. E., Tsujimori, T., & Sorensen, S. S. (2015). Jadeitites and Plate Tectonics. Annual Review of Earth and Planetary Sciences, 43, 105–138.

Haupert, I., Manatschal, G., Decarlis, A., & Unternehr, P. (2016). Upper-plate magma-poor rifted margins: Stratigraphic architecture and structural evolution. Marine and petroleum geology, 69, 241-261.

Hawthorne, F. C., Oberti, R., Harlow, G. E., Maresch, W. V., Martin, R. F., Schumacher, J. C., & Welch, M. D. (2012). Nomenclature of the amphibole supergroup. American Mineralogist, 97(11-12), 2031-2048.

Holland, T.J.B. (1980). The reaction albite = jadeite + quartz determined experimentally in the range 600-1200°C. American Mineralogist, 65, 129-134.

Holland, T.J.B. & Powell, R. (1998). An internally consistent thermodynamic dataset for phases of petrological interest. Journal of Metamorphic Geology, 16, 309-343.

Holland, T.J.B. & Powell, R. (2011). An improved and extended internally consistent thermodynamic dataset for phases of petrological interest, involving a new equation of state for solids. Journal of Metamorphic Geology, 29, 333-383.

Ildefonse, B., Blackman, D. K., John, B. E., Ohara, Y., Miller, D. J., & MacLeod, C. J. (2007). Oceanic core complexes and crustal accretion at slow-spreading ridges. Geology, 35(7), 623-626.

Incerpi, N., Martire, L., Manatschal, G., & Bernasconi, S. M. (2017). Evidence of hydrothermal fluid flow in a hyperextended rifted margin: the case study of the Err nappe (SE Switzerland). Swiss Journal of Geosciences, 110(2), 439-456.

Inger, S., Ramsbotham, W., Cliff, R. A., & Rex, D. C. (1996). Metamorphic evolution of the Sesia-Lanzo Zone, Western Alps: time constraints from multi-system geochronology. Contributions to Mineralogy and Petrology, 126(1), 152-168.

Karner, G. D., & Driscoll, N. W. (1999). Style, timing and distribution of tectonic deformation across the Exmouth Plateau, northwest Australia, determined from stratal architecture and quantitative basin modelling. Geological Society, London, Special Publications, 164(1), 271-311.

Karson, J. A., & Winters, A. T. (1992). Along-axis variations in tectonic extension and accommodation zones in the MARK Area, Mid-Atlantic Ridge 23 N latitude. Geological Society, London, Special Publications, 60(1), 107-116.

Karson, J. A., Früh-Green, G. L., Kelley, D. S., Williams, E. A., Yoerger, D. R., & Jakuba, M. (2006). Detachment shear zone of the Atlantis Massif core complex, Mid-Atlantic Ridge, 30 N. Geochemistry, Geophysics, Geosystems, 7(6).

Koehn, P., & Vuagnat, M. (1970). Sur la présence du faciès "schistes à glaucophane" dans les roches du Mt. Cruzeau (Province de Turin, Italie). CR des Séances, SPHN, Genevé, 5, 59-64.

Konilov, A. N., Shchipansky, A. A., Mints, M. V., Dokukina, K. A., Kaulina, T. V., Bayanova, T. B., ... & O'Reilly, S. Y. (2011). The Salma eclogites of the Belomorian Province, Russia: HP/UHP metamorphism through the subduction of Mesoarchean oceanic crust. In Ultrahigh-pressure metamorphism (pp. 623-670). Elsevier.

Labrousse, L., Jolivet, L., Andersen, T. B., Agard, P., Hébert, R., Maluski, H., & Scharer, U. (2004). Pressure-temperature-time deformation history of the exhumation of ultra-high pressure rocks in the Western Gneiss Region, Norway. Special Papers-Geological Society of America, 155-184.

Lafay, R., Baumgartner, L. P., Stephane, S., Suzanne, P., German, M. H. & Torsten, V. (2017). Petrologic and stable isotopic studies of a fossil hydrothermal system in ultramafic environment (Chenaillet ophicalcites, Western Alps, France): Processes of carbonate cementation. Lithos, 294, 319–338.

Lagabrielle, Y. (1981). Les schistes lustrés à ophiolites du Queyras (Alpes franco-italiennes): données nouvelles et precisions lithostratigraphiques. C. R. Acad. Sc. Paris, II, 292, 1405-1408.

Lagabrielle, Y. (1982). Ophiolites et croute océanique: tectonique et environnement sédimentaire. Apports des données océaniques à l'interpretation géologique des series ophiolitifères du Queyras (Alpes franco-italiennes), Unpublished PhD Thesis, Université de Bretagne occidentale, Brest.

Lagabrielle, Y., Polino, R., Auzende, J.M., Blanchet, R., Caby, R., Fudral, S., Lemoine, M., Mevel, C., Ohnestetter, M., Robert, D. & Tricart, P. (1984). Les témoins d'une tectonique intraocéanique dans le domaine téthysien: analyse du rapport entre les ophiolites et leur couvertures métasédimentaires dans la zone piémontaise des Alpes franco-italiennes. Ofioliti, 9, 67-88.

Lagabrielle, Y. & Polino, R. (1985). Origine volcano-détritique de certaines prasinites des Schistes lustrés du Queyras (France): arguments texturaux et géochimiques. B. Soc. Géol. Fr., 4, 461-471.

Lagabrielle, Y. (1987). Les ophiolites: marqueurs de l'histoire tectonique des domaines océaniques: le cas des Alpes franco-italiennes (Queyras, Piémont): comparaison avec les ophiolites d'Antalya (Turquie) et du Coast Range de Californie (Doctoral dissertation, Brest).

Lagabrielle, Y. & Polino, R. (1988). Un schéma structural du domaine des Schistes lustrés ophiolitifères au nord-ouest du massif du Mont Viso (Alpes Sud-Occidentales) et ses implications (A structural map of the ophiolite-bearing 'Schistes lustrés' northwest of the Monte Viso massif (SW Alps) and its implications). Comptes Rendus de l'Académie des Sciences [Paris], Série 2 (306), 921–928.

Lagabrielle, Y., & Lemoine, M. (1997). Alpine, Corsican and Apennine ophiolites: the slow-spreading ridge model. Comptes Rendus de l'Académie des Sciences-Series IIA-Earth and Planetary Science, 325(12), 909-920.

Lagabrielle, Y., Brovarone, A. V., & Ildefonse, B. (2015). Fossil oceanic core complexes recognized in the blueschist metaophiolites of Western Alps and Corsica. Earth-Science Reviews, 141, 1-26.

Lanari, P., Guillot, S., Schwartz, S., Vidal, O., Tricart, P., Riel, N., & Beyssac, O. (2012). Diachronous evolution of the alpine continental subduction wedge: evidence from P–T estimates in the Briançonnais Zone houillère (France–Western Alps). Journal of Geodynamics, 56, 39-54.

Lanari, P., Riel, N., Guillot, S., Vidal, O., Schwartz, S., Pêcher, A., & Hattori, K. H. (2013). Deciphering high-pressure metamorphism in collisional context using microprobe mapping methods: Application to the Stak eclogitic massif (northwest Himalaya). Geology, 41(2), 111-114.

Lanari, P., Vho, A., Bovay, T., Airaghi, L., & Centrella, S., (2019). Quantitative compositional mapping of mineral phases by electron probe micro-analyser. Geological Society of London, Special Publications, 478, 39-63.

Laskowski, A. K., Kapp, P., Vervoort, J. D., & Ding, L. (2016). High-pressure Tethyan Himalaya rocks along the India-Asia suture zone in southern Tibet. Lithosphere, 8(5), 574-582.

Lavier, L. & Manatschal, G. (2006). A mechanism to thin the continental lithosphere at magma-poor margins. Nature, 440, 324-328.

Leake, B. E. (1978). Nomenclature of amphiboles. American Mineralogist, 63(11-12), 1023-1052.

Leake, B. E., Woolley, A. R., Arps, C., Birch, W. D., Gilbert, M. C., Grice, J. D., ... & Youzhi, G. (1997). Nomenclature of amphiboles. American Mineralogist, 82, 1019-1037.

Lefeuvre, B., Agard, P., Verlaguet, A., Dubacq, B. & Plunder, A. (2020). Massive formation of lawsonite in subducted sediments from the Schistes Lustrés (W. Alps): Implications for mass transfer and decarbonation in cold subduction zones. Lithos, 370; 105629.

Lefèvre, R., & Michard, A. (1976). Les nappes briançonnaises internes et ultra-briançonnaises de la Bande d'Acceglio (Alpes franco-italiennes): une étude structurale et pétrographique dans le faciès des Schistes bleus à jadéite. Sciences Géologiques, bulletins et mémoires, 29(3), 183-222.

Lemoine, M. (1951). Donnees nouvelles sur la geologie du Brianconnais oriental et sur le probleme de la quatrieme ecaille. Bulletin de la Société Géologique de France, 6(1-3), 191-204.

Lemoine, M. (1960). Présence de flyschs exotiques liés à la «4e écaille» près de Briançon (Hautes-Alpes). Comptes Rendus de l'Académie des Sciences, Paris, 250, 3684-3686.

Lemoine, M. (1961). Le Briançonnais interne et le bord de la zone des schistes lustrés dans les vallées du Guil et de l'Ubaye (Hautes et Basse-Alpes)(Schéma structural). Travaux du Laboratoire de Géologie de la Faculté des Sciences de Grenoble, 37, 97-119.

Lemoine, M. (1971). Données nouvelles sur la série du Gondran près Briançon (Alpes cottiennes). Réflexions sur les problemes stratigraphiques et paléogéographiques de la zone piémontaise. Géol. Alpine, 47, 181-201.

Lemoine, M., Bourbon, M. & Tricart, P. (1978). Le Jurassique et le Crétacé prépiémontais à l'Est de Briançon (Alpes occidentales) et l'évolution de la marge européenne de la Téthys: données Nouvelles et consequence. C.R. Acad. Sci. Paris, 286, 1655-1658.

Lemoine, M. (1980). Serpentinites, gabbros and ophicalcites in the Piemont-Ligurian domain of the Western Alps: possible indicators of oceanic fracture zones and of associated serpentinite protrusions in the Jurassic-Cretaceous Tethys. Archives des Sciences, 33(2-3), 103-115.

Lemoine, M., Bas, T., Arnaud-Vanneau, A., Arnaud, A., Dumont, T., Gidon, M., Bourbon, M., De Graciansky, P.C., Rudkiewicz, J.L., Mégard-Galli, J. & Tricart, P. (1986). The continental margin of the Mesozoic Tethys in the Western Alps. Marine and Petroleum Geology, 3, 179-199.

Lemoine, M. & Tricart, P. (1986). Les Schistes lustrés piémontais des Alpes Occidentales: Approche stratigraphique, structural et sédimentologique. Eclogae Geol. Helv., 79, 271-294.

Lemoine, M., Tricart, P. & Boillot, G. (1987). Ultramafic and gabbroic ocean floor of the Ligurian Tethys (Alps, Corsica, Apennines): in search of a genetic model. Geology, 15, 622-625.

Lemoine, M. & Trümpy, R. (1987). Pre-oceanic rifting in the Alps. Tectonophysics, 133, 305-320.

Lemoine, M., Tricart, P., Lagabrielle, Y., Deville, E., Fudral, S., Marthaler, M., & Sartori, M. (1993). From oceanic closure to continental collision: A synthesis of the" Schistes lustrés" metamorphic complex of the Western Alps: Alternative interpretation and reply. Geological Society of America Bulletin, 105(6), 845-849.

Lemoine, M., De Graciansky, P.C. & Tricart, P. (2000). De l'océan à la chaîne de montagnes. Tectonique Des Plaques Dans les Alpes. Gordon and Breach, Paris.

Lewis, A.D. & Snewing, J.D. (1980). The Montgenèvre ophiolite (Hautes-Alpes, France): metamorphism and trace element geochemistry of the volcanic sequence. Chemical Geology, 28, 291–306.

Li, X.H., Faure, M., Lin, W., Manatschal, G. (2013). New isotopic constraints on age and magma genesis of an embryonic oceanic crust: the Chenaillet Ophiolite in the Western Alps. Lithos 160-161, 283–291.

Locatelli, M., Federico, L., Agard, P., & Verlaguet, A. (2019). Geology of the southern Monviso metaophiolite complex (W-Alps, Italy). Journal of Maps, 15(2), 283-297.

Lombardo, B., Rubatto, D., & Castelli, D. (2002). Ion microprobe U-Pb dating of zircon from a Monviso metaplagiogranite: implications for the evolution of the Piedmont-Liguria Tethys in the Western Alps. Ofioliti, 27(2), 109-117.

Lory, C. (1863). Carte géologique du Briançonnais (Hautes Alpes), à l'échelle 1:250,000.

Maino, M., Adamuszek, M., Schenker, F. L., Seno, S., & Dabrowski, M. (2021). Sheath fold development around deformable inclusions: Integration of field-analysis (Cima Lunga unit, Central Alps) and 3D numerical models. Journal of Structural Geology, 144, 104255.

Malusà, M.G., Mosca, P., Borghi, A., Dela Pierre, F. and Polino, R. (2002). Approccio multidisciplinare per la ricostruzione dell'assetto tettono-stratigrafico e dell'evoluzione metamorfico-strutturale di un settore di catena orogenica: l'esempio dell'Alta Valle di Susa (Alpi Occidentali). Bollettino della Società Geologica Italiana, 57, 249-257.

Malusà, M. G., Faccenna, C., Garzanti, E., & Polino, R. (2011). Divergence in subduction zones and exhumation of high pressure rocks (Eocene Western Alps). Earth and Planetary Science Letters, 310(1-2), 21-32.

Manatschal, G. (2004). New models for evolution of magma-poor rifted margins based on a review of data and concepts from West Iberia and the Alps. International Journal of Earth Science, 93, 432-466.

Manatschal, G., Müntener, O., Lavier, L. L., Minshull, T. A., & Péron-Pinvidic, G. (2007). Observations from the Alpine Tethys and Iberia–Newfoundland margins pertinent to the interpretation of continental breakup. Geological Society, London, Special Publications, 282(1), 291-324.

Manatschal, M. & Müntener, O. (2009). A type sequence across an ancient magma-poor ocean–continent transition: the example of the western Alpine Tethys ophiolites. Tectonophysics, 473, 4-19.

Manatschal, G., Sauter, D., Karpoff, A. M., Masini, E., Mohn, G., & Lagabrielle, Y. (2011). The Chenaillet ophiolite in the French/Italian Alps: An ancient analogue for an oceanic core complex? Lithos, 124(3-4), 169–184.

Manzotti, P. (2011). Petro-structural map of the Dent Blanche tectonic system between Valpelline and Valtournenche valleys, Western Italian Alps. Journal of Maps, 7(1), 340-352.

Manzotti, P., Ballèvre, M., Zucali, M., Robyr, M. & Engi, M. (2014a). The tectonometamorphic evolution of the Sesia-Dent Blanche nappes (internal Western Alps): review and synthesis. Swiss Journal of Geosciences, 107(2), 309-336.

Manzotti, P., Pitra, P., Langlade, M. & Ballèvre, M. (2014b). Constraining P-T conditions during thrusting of a higher pressure unit over a lower pressure one (Gran Paradiso, Western Alps). Journal of Metamorphic Geology, 33, 981-1002.

Manzotti, P., Rubatto, D., Zucali, M., Korh, A. E., Cenki-Tok, B., Ballevre, M., & Engi, M. (2018). Permian magmatism and metamorphism in the Dent Blanche nappe: constraints from field observations and geochronology. Swiss journal of geosciences, 111(1), 79-97.

Manzotti, P., Bosse, V., Pitra, P., Robyr, M., Schiavi, F. & Ballèvre, M. (2018). Exhumation rates in the Gran Paradiso Massif (Western Alps) constrained by in situ U-Th-Pb dating of accessory phases (monazite, allanite and xenotime). Contributions to Mineralogy and Petrology, 173(3), 1-28.

Manzotti, P., Ballèvre, M., Pitra, P., Putlitz, B., Robyr, M., & Müntener, O. (2020). The growth of sodic amphibole at the greenschist-to blueschist-facies transition (Dent Blanche, Western Alps): bulk-rock chemical control and thermodynamic modelling. Journal of Petrology, 61(4), egaa044.

Marroni, M., Molli, G., Montanini, A., & Tribuzio, R. (1998). The association of continental crust rocks with ophiolites in the Northern Apennines (Italy): implications for the continent-ocean transition in the Western Tethys. Tectonophysics, 292(1-2), 43-66.

Marthaler, M., Fudral, S., Deville, E., & Rampnoux, J. P. (1986). Mise en évidence du Crétacé supérieur dans la couverture septentrionale de Dora Maira, région de Suse, Italie (Alpes occidentales). Conséquences paléogéographiques et structurales. Comptes rendus de l'Académie des sciences. Série 2, Mécanique, Physique, Chimie, Sciences de l'univers, Sciences de la Terre, 302(2), 91-96.

Marthaler, M., & Stampfli, G. M. (1989). Les Schistes lustrés à ophiolites de la nappe du Tsaté: un ancien prisme d'accrétion issu de la marge active apulienne?. Schweizerische mineralogische und petrographische Mitteilungen, 69(2), 211-216.

Martin, R. (1984). Patterns of albitization in the Montgenèvre ophiolite, Western Alps. Bulletin de minéralogie, 107(3), 345-356.

Martin, S., & Polino, R. (1984). Le metaradiolariti a Ferro di Cesana (Valle di Susa – Alpi Occidentali). Memorie della Società Geologica Italiana, 29, 107-125.

Martin, S. & Tartarotti, P. (1989). Polyphase HP metamorphism in the ophiolitic glaucophanites of the lower St. Marcel valley (Aosta valley).

Martin, S., Tartarotti, P. & Dal Piaz, G. V. (1994). The Mesozoic ophiolites of the Alps: a review. Boll. Geof. Teor. Appl.,36, (141-144), 175-216.

Martin, L. A. J., Hermann, J., Gauthiez-Putallaz, L., Whitney, D. L., Vitale Brovarone, A., Fornash, K. F. & Evans, N. J. (2014). Lawsonite geochemistry and stability–implication for trace element and water cycles in subduction zones. Journal of Metamorphic Geology, 32(5), 455-478.

Maruyama, S., Moonsup, C. & Liou, J.C. (1986). Experimental investigations of blueschist-greenschist transition equilibria: pressure dependence of Al2O3 contents in sodic amphiboles – a new geobarometer. Geological Society of America Memoirs, 146, 1-16.

Masini, E., Manatschal, G. & Mohn, G. (2013). The Alpine Tethys rifted margins: reconciling old and new ideas to understand the stratigraphic architecture of magma-poor rifted margins. Sedimentology, 60, 174-196.

Massonne, H.J. & Schreyer, W. (1987). Phengite geobarometry based on the limiting assemblage with K-feldspar, phlogopite and quartz. Contributions to Mineralogy and Petrology, 96, 212-224.

Mégard-Galli J. (1972a). Le Norien dans la zone briançonnaise: découverte d'un gisement fossilifère et considérations paléogéographiques. Comptes Rendus de l'Académie des Sciences, Paris, 274, 2443-2446.

Mégard-Galli, J. (1972b). Données nouvelles sur le Carnien dans la zone briançonnaise entre Briançon et la vallée du Guil : consé-quences tectoniques et paléogéographiques. Géologie alpine, 48,131-142.

Mégard-Galli, J. (1974). Âge et caractéristiques sédimentologiques du Trias dolomitique des unités piémontaises externes (zone du Gondran), entre Arc et Ubaye (Alpes occidentales). Géologie alpine, 50, 111-129.

Mégard-Galli, J., & Baud, A. (1977). Le Trias moyen et supérieur des Alpes nord-occidentales et occidentales : données nouvelles et corrélations stratigraphiques. Bull. BRGM, sect. IV, 3, 233-250.

Mégard-Galli, J., & Faure, J.L. (1988). Tectonique distensive et sédimentation au Ladinien supérieur-Carnien dans la zone briançonnaise. Bulletin de la Société Géologique de France, t. IV, 5, 705-715.

Mercier, D. (1977). Les modalités de la transgression jurassique dans la zone briançonnaise (région de Briançon, Hautes-Alpes). Étude stratigraphique et sédimentologique. Thèse 3e cycle, Paris, 351 pp.

Mercier, D., & Beaudoin, B. (1987). Revision du carbonifère briançonnais: Stratigraphie et évolution du bassin. Géologie Alpine, Mémoires, 13, 25-31.

Mevel, C. (1975). Les" pillow-lavas" spilitiques des massifs ophiolitiques du Chenaillet et des Gets (Alpes françaises). Structures et minéraux magmatiques reliques, étude chimique et zonations Comparaison avec les" pillow-lavas" métamorphisés du Queyras et de Hte Ubaye (Doctoral dissertation, Université Pierre et Marie Curie-Paris VI).

Mevel, C., & Velde, D. (1976). Clinopyroxenes in Mesozoic pillow lavas from the French Alps: influence of cooling rate on compositional trends. Earth and Planetary Science Letters, 32(2), 158-164.

Mével, C., Caby, R., & Kienast, J.-R. (1978). Amphibolite facies conditions in the oceanic crust: example of amphibolized flaser-gabbro and amphibolites from the Chenaillet ophiolite massif (Hautes Alpes, France). Earth and Planetary Science Letters, 39, 98–108.

Mevel, C. & Kienast, J. R. (1980). Chromian jadeite, phengite, pumpellyite, and lawsonite in a high–pressure metamorphosed gabbro from the French Alps. Mineralogical Magazine, 43(332): 979-984.

Michard, A. (1959). Contribution a l'etude geologique de la zone d'Acceglio-Longet dans la haute Varaita (Alpes cottiennes, Italie). Bulletin de la Société Géologique de France, 7(1), 52-61.

Michard, A., Goffe, B., Chopin, C. and Henry, C. (1996). Did the Western Alps develop through an Oman-type stage? The geotectonic setting of high-pressure metamorphism in two contrasting Tethyan transects. Eclogae Geologicae Helveticae, 89, 43-80.

Michard, A., Avigad, D., Goffé, B., & Chopin, C. (2004). The high-pressure metamorphic front of the south Western Alps (Ubaye-Maira transect, France, Italy). Schweizerische Mineralogische und Petrographische Mitteilungen, 84, 215–235.

Michard, A., Schmid, S. M., Lahfid, A., Ballèvre, M., Manzotti, P., Chopin, C., ... & Dana, D. (2022). The Maira-Sampeyre and Val Grana Allochthons (south Western Alps): review and new data on the tectonometamorphic evolution of the Briançonnais distal margin. Swiss Journal of Geosciences, 115(1), 1-43.

Michel-Lévy, A. (1877). Structure et composition minéralogique de la variolite de la Durance. C.R. LXXXIV, Soc. Géol. France., 264-266.

Minshull, T. A. (2009). Geophysical characterisation of the ocean–continent transition at magma-poor rifted margins. Comptes Rendus Geoscience, 341(5), 382-393.

Miranda, E. A., & Dilek, Y. (2010). Oceanic core complex development in modern and ancient oceanic lithosphere: Gabbro-localized versus peridotite-localized detachment models. The Journal of Geology, 118(1), 95-109.

Mohn, G., Manatschal, G., Muntener, O., Beltrando, M. & Masini, E. (2010). Unravelling the interaction between tectonic and sedimentary processes during lithospheric thinning in the Alpine Tethys Margins. International Journal of Earth Sciences, 99, 75-101.

Mohn, G., Manatschal, G., Masini, E., & Müntener, O. (2011). Rift-related inheritance in orogens: a case study from the Austroalpine nappes in Central Alps (SE-Switzerland and N-Italy). International Journal of Earth Sciences, 100(5), 937-961.

Mohn, G., Manatschal, G., Beltrando, M., Masini, E. & Kusznir, N. (2012). Necking of continental crust in magma-poor rifted margins: Evidence from the fossil Alpine Tethys margins. Tectonics, 31, TC1012.

Mohn, G., Manatschal, G., Beltrando, M. & Haupert, I. (2014). The role of rift-inherited hyper-extension in Alpine-type orogens. Terra Nova, 26, 347-353.

Molli, G., Crispini, L., Malusà, M. G., Mosca, P., Piana, F. & Federico, L. (2010). Geology of the Western Alps-Northern Apennine junction area: a regional review. Journal of the Virtual Explorer, 36, paper 9, 1-49.

Montanini A., Tribuzio, R., & Vernia, L. (2008). Petrogenesis of basalts and gabbros from an ancient continent–ocean transition (External Liguride ophiolites, Northern Italy). Lithos, 101(3-4), 453-479.

Morimoto, N. (1988). Nomenclature of pyroxenes. American Mineralogist, 7(3), 1133-1198.

Mosca, P., Polino, R., Rogledi, S., & Rossi, M. (2010). New data for the kinematic interpretation of the Alps–Apennines junction (Northwestern Italy). International Journal of Earth Sciences, 99(4), 833-849.

Mosca, P., Fioraso, G., Console, F., Pantaloni, M., & Tacchia, D. (2016). La Carta Geologica delle Alpi Occidentali in scala 1: 400.000 del Regio Ufficio Geologico: inestimabile documento della cartografia geologica italiana. La cartografia del Servizio Geologico d'Italia. Memorie descrittive della Carta Geologica d'Italia, 100, 61-72.

Muñoz-Montecinos, J., Angiboust, S., Garcia-Casco, A., Glodny, J. & Bebout, G. (2021). Episodic hydrofracturing and large-scale flushing along deep subduction interfaces: Implications for fluid transfer and carbon recycling (Zagros Orogen, southeastern Iran). Chemical Geology, 571, 120173.

Nakamura, D., & Hirajima, T. (2000). Granulite-facies overprinting of ultrahigh-pressure metamorphic rocks, northeastern Su-Lu region, eastern China. Journal of Petrology, 41(4), 563-582.

Nakayama, I., Kaji, A., Shioda, T., & Iwasaki, M. (1973). Finding of inverted pigeonite from the gabbro in the Mikabu zone at Kamiyama, eastern Shikoku, Japan. Memoirs of the Faculty of Science, Kyoto University. Series of geology and mineralogy, 40(1), 27-33.

Nicollet C., Paquette J.L., Bruand E., Bosse V., Pereira I. (2022). Crystallisation and fast cooling of the (meta)gabbro from the Chenaillet ophiolite (Western Alps): In-situ U–Pb dating of zircon, titanite, monazite and xenotime in textural context. Lithos, 414-415.

Nitsch, K.H. (1971). Stabilitatsbeziehungen von Prehnit- und Pumpellyit-haltiger Paragenesen. Contributions to Mineralogy and Petrology, 30, 240–260.

O'Brien, P. J. (2019). Eclogites and other high-pressure rocks in the Himalaya: a review. Geological Society, London, Special Publications, 483(1), 183-213.

Oberhansli, R., & Goffé, B. (2004). Explonatory notes to the Map: metamorphic structure of the Alps introduction. Mitteilungen der Osterreichischen ¨ Mineralogischen Gesellschaft 149, 115–123.

Okay, A. I., Xu, S., & Sengor, A. C. (1989). Coesite from the Dabie Shan eclogites, central China. European Journal of Mineralogy, 1(4), 595-598.

Olive, J. A., Behn, M. D., & Tucholke, B. E. (2010). The structure of oceanic core complexes controlled by the depth distribution of magma emplacement. Nature Geoscience, 3(7), 491-495.

Palin, R.M. & White, R.W. (2016). Emergence of blueschists on Earth linked to secular changes in oceanic crust composition. Nature Geosciences, 9, 60-65.

Péron-Pinvidic, G., & Manatschal, G. (2009). The final rifting evolution at deep magma-poor passive margins from Iberia-Newfoundland: a new point of view. International Journal of Earth Sciences, 98(7), 1581-1597.

Petrakakis, K. & Dietrich, H. (1985). MINSORT: A program for the processing and archivation of microprobe analysis of silicate and oxide minerals. Neues Jahrbuch für Mineralogie Abhandlungen, 8, 379-384.

Pfiffner, O.A., Lehner, P., Heitzmann, P., Mueller, St., & Steck, A. (1997). Deep structure of the Swiss Alps. Birkhäuser Verlag, Basel, 380 p.

Philippot, P. (1990). Opposite vergence of nappes and crustal extension in the French–Italian Western Alps. Tectonics, 9, 1143-1164.

Piana, F., Fioraso, G., Irace, A., Mosca, P., D'Atri, A., Barale, A., Falletti, P., Monegato, G., Morelli, M., Tallone, S. & Vigna, G. B. (2017). Geology of Piemonte region (NW Italy, Alps–Apennines interference zone). J. Maps, 13, 395–405.

Picazo, S., Müntener, O., Manatschal, G., Bauville, A., Karner, G., & Johnson, C. (2016). Mapping the nature of mantle domains in Western and Central Europe based on clinopyroxene and spinel chemistry: Evidence for mantle modification during an extensional cycle. Lithos, 266, 233-263.

Piccoli, F., Brovarone, A. V. & Ague, J. J. (2018). Field and petrological study of metasomatism and high-pressure carbonation from lawsonite eclogite-facies terrains, Alpine Corsica. Lithos, 304, 16-37.

Pieri, M., & Groppi, G. (1981). Subsurface geological structure of the Po Plain: CNR. Pubblicazione del Progetto Finalizzato Geodinamica, 414, 23.

Pinto, V.H.G., Manatschal, G., Karpoff, A.M. & Viana, A. (2015). Tracing mantle-reacted fluids in magma-poor rifted margins: The example of Alpine Tethyan rifted margins. Geochem. Geophys. Geosyst., 16, 3271-3308.

Plunder, A., Agard, P., Dubacq, B., Chopin, C., & Bellanger, M. (2012). How continuous and precise is the record of P–T paths? Insights from combined thermobarometry and thermodynamic modelling into subduction dynamics (Schistes Lustrés, W. Alps). Journal of Metamorphic Geology, 30(3), 323-346.

Pognante, U. (1979). The Orsiera-Rocciavrè metaophiolitic complex (Italian western Alps). Ofioliti, 4(2), 183-198.

Pognante, U., Compagnoni, R. & Gosso, G. (1980). Micro-Mesostructural relatinships in the continental eclogitic rocks of the Sesia-Lanzo Zone (Italian Western Alps): a record of subduction cycle. Rendiconti della Società Italiana di Mineralogia e Petrologia, 36(1), 169-186.

Pognante, U. & Kienast, J.R. (1987). Blueschist and Eclogite Transformations in Fe-Ti Gabbros: A Case from the Western Alps Ophiolites. Journal of Petrology, 28, 271-29.

Pognante, U, (1989). Lawsonite, blueschist and eclogite formation in the Southern Sesia Zone (western Alps, Italy). European Journal of Mineralogy, 1, 89-104.

Pognante, U., (1991). Petrological constraints on the eclogite-and blueschist facies metamorphism and P-T-t paths in the western Alps. Journal of Metamorphic Geology, 9(1), 5-17.

Poli, S. & Schmidt, M.W. (1995). H_2O transport and realase in subsuction zones: Experiemental constraints on basaltic and andesitic systems. Journal of Geophysical Research, 100, 22299-22314.

Poli, S. & Schmidt, M. W. (1998). The high-pressure stability of zoisite and phase relationships of zoisite-bearing assemblages. Contributions to Mineralogy and Petrology, 130(2), 162-175.

Poli, S., Franzolin, E., Fumagalli, P. & Crottini, A. (2009). The transport of carbon and hydrogen in subducted oceanic crust: An experimental study to 5 GPa. Earth and Planetary Science Letters, 278(3-4), 350-360.

Polino, R., Monticelli, F. & Vaccaro, D. (1983). L'unità piemontese Chaberton-Grand Hoche (Val Susa-Alpi Occidentali): evoluzione litostratigrafica, assetto strutturale e rapporti con i complessi circostanti. Mem. Soc. Geol. It., 26, 489-498.

Polino, R. (1984). Les séries océaniques du haut Val de Suse (Alpes Cottiennes): analyse des couvertures sédimentaires. Ofioliti, 9, 547-554.

Polino, R. & Lemoine, M. (1984). Détritisme mixte d'origine continentale et océanique dans les sédiments jurassico-crétacés supra-ophiolitiques de la Téthys ligure: la série du Lago Nero (Alpes Occidentales franco-italiennes). C.R. Acad. Sci., Série 2, 298, 359-364.

Polino, R., Dal Piaz, G.V. & Gosso, G. (1990). Tectonic erosion at the Adria margin and accretionary process for the Cretaceous orogeny of the Alps. Mémoires de la Société géologique de France, 165, 345-367.

Polino, R., Borghi, A., Carraro, F., Dela Pierre, F., Fioraso, G., and Giardino, M. (2002). Note illustrative della Carta Geologica d'Italia alla scala 1: 50.000, F. 132-152-153 "Bardonecchia". Regione Piemonte, Direzione Regionale dei servizi Tecnici di Prevenzione. Litografia Geda, Nichelino. Torino.

Powell, R. & Holland, T.J.B. (1990). An enlarged and updated internally consistent thermodynamic data-set with uncertainties and correlations: the system K_2O-Na_2O-CaO-MgOMnO-FeO-Fe_2O_3-Al_2O_3-TiO_2-C-H-O_2. Journal of Metamorphic Geology, 8, 89-124.

Proyer, A. (2003). Metamorphism of pelites in NKFMASH–a new petrogenetic grid with implications for the preservation of high-pressure mineral assemblages during exhumation. Journal of metamorphic Geology, 21(5), 493-509.

Pussenot, C. (1930). La nappe du Briançonnais et le bord de la zone des schistes lustrés entre l'Arc et le Guil. Imprimerie Allier.

Pusztaszeri, L. (1966). Etude pétrographique du massif du Chenaillet (Hautes-Alpes, France). Pétrographie. University of Genève, 468 p.

Quick, J. E., Sinigoi, S., & Mayer, A. (1995). Emplacement of mantle peridotite in the lower continental crust, Ivrea-Verbano zone, northwest Italy. Geology, 23(8), 739-742.

Rampone, E. & Piccardo, G.B., (2000). The ophiolite–oceanic lithosphere analogue: new insights from the Northern Apennines (Italy). In: Dilek, Y., Moores, E.M., Elthon, D., Nicolas, A. (Eds.), Ophiolites and Oceanic Crust: New Insights from Field Studies and the Oceanic Drilling Program. Geological Society of America Special Papers, 349, pp. 21–34.

Rao, B.B. & Johannes, W. (1979). Further data on the stability of staurolite + quartz and related assemblages. Neues Jahrbuch für Mineralogie Abhandlungen, 10, 437-447.

Reed, S. J. B. (2005). Electron microprobe analysis and scanning electron microscopy in geology. Cambridge university press.

Regio Ufficio Geologico (1908). Carta Geologica delle Alpi Occidentali in scala 1:400.000. R. Ufficio Geologico d'Italia, Roma.

Regis, D., Rubatto, D., Darling, J., Cenki-Tok, B., Zucali, M. & Engi, M. (2014). Multiple metamorphic stages within an eclogite-facies terrane (Sesia Zone, Western Alps) revealed by Th-U-Pb petrochronology. Journal of Petrology, 55, 1429-1456.

Regis, D., Venturini, G., & Engi, M. (2016). Geology of the Scalaro valley–Sesia Zone (Italian Western Alps). Journal of maps, 12(4), 621-629.

Reinecke, T. (1998). Prograde high-to ultrahigh-pressure metamorphism and exhumation of oceanic sediments at Lago di Cignana, Zermatt-Saas Zone, western Alps. Lithos, 42(3-4), 147-189.

Ribes, C., Manatschal, G., Ghienne, J. F., Karner, G. D., Johnson, C. A., Figueredo, P. H., ... & Epin, M. E. (2019). The syn-rift stratigraphic record across a fossil hyper-extended rifted margin: the example of the northwestern Adriatic margin exposed in the Central Alps. International Journal of Earth Sciences, 108(6), 2071-2095.

Ridley, J. (1989). Structural and metamorphic history of a segment of the Sesia-Lanzo zone, and its bearing on the kinematics of Alpine deformation in the western Alps. Geological Society, London, Special Publications, 45(1), 189-201.

Rivalenti, G., Rossi, A., Siena, F., & Sinigoi, S. (1984). The layered series of the Ivrea-Verbano igneous complex, we tern Alps, Italy. Tschermaks mineralogische und petrographische Mitteilungen, 33(2), 77-99.

Roda, M., & Zucali, M. (2008). Meso and microstructural evolution of the Mont Morion metaintrusive complex (Dent-Blanche nappe, Austroalpine domain, Valpelline, Western Italian Alps). Bollettino Societa Geologica Italiana, 127(1), 105.

Roure, F., Heitzmann, P. & Polino, R. (1990). Deep structure of the Alps. Mémoires de la Société géologique de France, 156; Mémoires de la Société géologique suisse, 1; Vol. spec. Società Geologica Italiana, 1, pp. 367.

Roure, F., Choukroune, P., & Polino, R. (1996). Deep seismic reflection data and new insights on the bulk geometry of mountain ranges. Comptes rendus de l'Académie des sciences. Série 2. Sciences de la terre et des planètes, 322(5), 345-359.

Rubatto, D. & Hermann, J. (2001). Exhumation as fast as subduction? Geology, 29, 3-6.

Saccani, E., Dilek, Y., Marroni, M. & Pandolfi, L. (2015). Continental margin ophiolites of Neotethys: remnants of ancient Ocean–Continent Transition Zone (OCTZ) lithosphere and their geochemistry, mantle sources and melt evolution patterns. Episodes, 38, 230-249.

Scambelluri, M., Müntener, O., Hermann, J., Piccardo, G. B., & Trommsdorff, V. (1995). Subduction of water into the mantle: history of an Alpine peridotite. Geology, 23(5), 459-462.

Scarsi, M., Malatesta, C. & Fornasaro, S. (2018). Lawsonite-bearing eclogite from a tectonic mélange in the Ligurian Alps: new constraints for the subduction plate-interface evolution. Geological Magazine, 155(2), 280-297.

Schaaf, A. (1985). Un nouveau canevas biochronologique du Crétacé Inférieur et moyen: les biozones à Radiolaires/A new biochronologic Radiolarian zonation for the Early and Middle Cretaceous. Sciences Géologiques, bulletins et mémoires, 38(3), 227-269.

Schmid, S. M., Aebli, H. R., Heller, F., & Zingg, A. (1989). The role of the Periadriatic Line in the tectonic evolution of the Alps. Geological Society, London, Special Publications, 45(1), 153-171.

Schmid, S.M., Fügenschuh, B., Kissling, E., & Schuster, R. (2004). Tectonic map and overall architecture of the Alpine orogen. Eclogae Geologicae Helvetiae, 97, 93-117.

Schmid, S.M. & Kissling, E. (2000). The arc of the western Alps in the light of geophysical data on deep crustal structure. Tectonics, 19, 62-85.

Schmidt, M. W. & Poli, S. (1994). The stability of lawsonite and zoisite at high pressures: Experiments in CASH to 92 kbar and implications for the presence of hydrous phases in subducted lithosphere. Earth and Planetary Science Letters, 124(1-4), 105-118.

Schneegans, D. (1933). Sur la découverte de nouveaux gisements de diplopores (Algues calcaires) dans le Trias de la zone du Briançonnais. Trav. lab. géol. Grenoble, 17, 59-73.

Schwartz, S., Lardeaux, J.M. & Tricart, P., (2000). La zone d'Acceglio (Alpes Cottiennes). Un nouvel exemple de croûte continentale éclogitisée dans les Alpes occidentales. Comptes Rendus de l'Académie des Sciences, 330, 859–866.

Schwartz, S., Guillot, S., Reynard, B., Lafay, R., Debret, B., Nicollet, C., Lanari, P., Auzende, A.L. (2013). Pressure–temperature estimates of the lizardite/antigorite transition in high pressure serpentinites. Lithos 178, 197–210.

SERVIZIO GEOLOGICO D'ITALIA (1911). Carta Geologica d'Italia alla scala 1:100.0000, F. 54 Oulx. Roma.

SERVIZIO GEOLOGICO D'ITALIA (1911). Carta Geologica d'Italia alla scala 1:100.0000, F. 66 Cesana T.se. Roma

SERVIZIO GEOLOGICO D'ITALIA (2002a). Carta Geologica d'Italia alla scala 1:50.0000, F. 154 Susa, Regione Piemonte, Direzione Regionale dei servizi Tecnici di Prevenzione. Litografia Geda, Nichelino. Torino.

SERVIZIO GEOLOGICO D'ITALIA (2002b). Carta Geologica d'Italia alla scala 1:50.0000, F. 132-152-153 Bardonecchia Regione Piemonte, Direzione Regionale dei servizi Tecnici di Prevenzione. Litografia Geda, Nichelino. Torino.

SERVIZIO GEOLOGICO D'ITALIA (2020). Carta Geologica d'Italia alla scala 1:50.0000, F. 171 Cesana.

http://www.isprambiente.gov.it/Media/carg/171_CESANA_TORINESE/Foglio.html

Shelley, D. & Bossière, G. (1999). Ile de Groix: retrogression and structural developments in an extensional régime. Journal of Structural Geology, 21(10), 1441-1455.

Shi, R., Yang. J., Xu, Z., & Qi, X. (2008). The Bangong Lake ophiolite (NW Tibet) and its bearing on the tectonic evolution of the Bangong–Nujiang suture zone. Journal of Asian Earth Sciences, 32(5-6), 438-457.

Sismonda, A. (1866). Carta geologica di Savoja, Piemonte e Liguria 1: 500.000. Pubblicata per cura del Governo di SM Vittorio Emanuele II, Re d'Italia.

Spear, F. S. & Cheney, J. T. (1989). A petrogenetic grid for pelitic schists in the system SiO 2-Al 2 O 3-FeO-MgO-K 2 OH 2 O. Contr. Min. and Petr., 101(2), 149-164.

Stampfli G.M. (1993). Le Briançonnais, terrain exotique dans les Alpes? Eclogae Geologicae Helvetiae, 86, 1-45.

Stampfli, G.M. & Marchant, R.H. (1997). Geodynamics evolution of the Tethyan margins of the Western Alps. In: Lehner, P., Heitzman, P., Frei, W., Horstmeyer, H., Mueller, S., Pfiffner, A. & Steck, A. (Eds.), Deep Structure of Switzerland. Results from NRP 20, Birkhaeuser-Verlag, Basel, 223-239.

Steinmann, M.C. (1994). Die noedpenninischen Bu¨ndnerschiefer der Zentralalpen Graubu¨ndens: Tektonik, Stratigraphie und Beckenentwicklung. PhD thesis, ETH Zurich, no. 10668.

Strzerzynski, P., Guillot, S., Leloup, P. H., Arnaud, N., Vidal, O., Ledru, P., Courrioux, G. & Darmendrail, X. (2012). Tectono-metamorphic evolution of

the Briançonnais zone (Modane-Aussois and southern Vanoise units, Lyon Turin transect, western alps). Journal of Geodynamics, 56, 55-75.

Tartarotti, P., Zucali, M., Panseri, M., Lissandrelli, S., Capelli, S., & Ouladdiaf, B. (2011). Mantle origin of the Antrona serpentinites (Antrona ophiolite, Pennine Alps) as inferred from microstructural, microchemical, and neutron diffraction quantitative texture analysis. Ofioliti, 36(2), 167-189.

Tartarotti, P., Festa, A., Benciolini, L. & Balestro, G. (2017). Record of Jurassic mass transport processes through the orogenic cycle: Understanding chaotic rock units in the high-pressure Zermatt-Saas ophiolite (Western Alps). Lithosphere, 9(3), 399-407.

Tartarotti, P., Guerini, S., Rotondo, F., Festa, A., Balestro, G., Bebout, G. E., ... & Scambelluri, M. (2019). Superposed sedimentary and tectonic block-in-matrix fabrics in a subducted serpentinite mélange (high-pressure Zermatt Saas Ophiolite, Western Alps). Geosciences, 9(8), 358.

Tartarotti, P., Martin, S., Festa, A., & Balestro, G. (2021). Metasediments Covering Ophiolites in the HP Internal Belt of the Western Alps: Review of Tectono-Stratigraphic Successions and Constraints for the Alpine Evolution. Minerals, 11(4), 411.

Termier, P. (1903). Les montagnes entre Briançon et Vallouise. Mém. expl. Carte géol. Fr., 182 pp.

Thiéblemont, D. & **Thiéblemont, V. (2017).** Le massif du Chenaillet (Briançonnais, HautesAlpes) : nouvelle perspective. Géologie de la France, 1, 11-26.

Tribuzio, R., Manatschal, G., Renna, M.R., Ottolini, L., Zanetti, A., (2019). Tectonomagmatic interplay and related metasomatism in gabbros from the Chenaillet ophiolite (Western Alps). Journal of Petrology, 60, 2483–2508.

Tricart P. (1984). From passive margin to continental collision; a tectonic scenario for the Western Alps. American Journal of Science, 284(2), 97-120.

Tricart, P. & Lemoine, M. (1991). The Queyras ophiolite west of Monte Viso (Western Alps): indicator of a peculiar ocean floor in the Mesozoic Tethys. J. Geodyn., 13, 163-181.

Tricart, P., Bourbon, M., & Lagabrielle, Y. (1982). Révision de la coupe Péouvou-Roche Noire (zone piémontaise, Alpes franco-italiennes): bréchification synsédimentaire d'un fond océanique ultrabasique. Géologie alpine, 58, 105-113.

Tricart, P., Dumont, T., & Lemoine M. (1985). Évolution d'une portion de marge continentale: blocs basculés alpins dans la nappe prépiémontaise de Rochebrune (Alpes occidentales). Revue de géographie physique et de géologie dynamique, 26(1), 3-17.

Tricart, P. & Schwartz, S. (2006). A north–south section across the Queyras Schistes lustrés (Piedmont zone, western Alps): Syn-collision refolding of a subduction wedge. Eclogae Geol. Helv., 99, 429-442.

Tsujimori, T. & Liou, J. G. (2007). Significance of the Ca-Na pyroxene-lawsonite-chlorite assemblage in blueschist-facies metabasalts: An example from the Renge

metamorphic rocks, southwest Japan. International Geology Review, 49(5), 416-430.

Tsujimori, T. & Ernst, W.G. (2014). Lawsonite blueschists and lawsonite eclogites as proxies for palaeo-subduction zone processes: a review. Journal of Metamorphic Geology, 32(5), 437–454.

Tsujimori, T., & Mattinson, C. (2021). Eclogites in different tectonic settings. In: Elias, S., & Alderton, D. Encyclopedia of Geology (2nd ed.), 561-568. Academic Press.

Tucholke, B. E., Behn, M. D., Buck, W. R., & Lin, J. (2008). Role of melt supply in oceanic detachment faulting and formation of megamullions. Geology, 36(6), 455-458.

van Keken, P. E., Hacker, B. R., Syracuse, E. M. & Abers, G. A. (2011). Subduction factory: 4. Depth-dependent flux of H_2O from subducting slabs worldwide. Journal of Geophysical Research: Solid Earth, 116(B1).

Villa, I.M., Bucher, S., Bousquet, R., Kleinhanns, I.C. & Schmid, S.M. (2014). Dating Polygenetic Metamorphic Assemblages along a Transect across the Western Alps. J. Petrol., 55 (4), 803-830.

Vissers, R.L.M., Van Hinsbergen, D.J.J., Meijer, P.T.H. & Piccardo, G.B. (2013). Kinematics of Jurassic ultra-slow spreading in the Piemonte Ligurian ocean. Earth Planet Sci. Lett., 380, 138-150.

Vitale Brovarone, A., Groppo, C., Hetényi, G., Compagnoni, R. & Malavieille, J. (2011). Coexistence of lawsonite-bearing eclogite and blueschist: phase equilibria modelling of Alpine Corsica metabasalts and petrological evolution of subducting slabs. Journal of Metamorphic Geology, 29(5): 583-600.

Vitale Brovarone, A., Beyssac, O., Malavieille, J., Molli, G., Beltrando, M. & Compagnoni, R. (2013). Stacking and metamorphism of continuous segments of subducted lithosphere in a high-pressure wedge: the example of Alpine Corsica (France). Earth-Science Reviews, 116, 35-56.

Vitale Brovarone, A., Picatto, M., Beyssac, O., Lagabrielle, Y. & Castelli, D. (2014a). The blueschist–eclogite transition in the Alpine chain: P–T paths and the role of slow-spreading extensional structures in the evolution of HP–LT mountain belts. Tectonophysics, 615, 96-121.

Vitale Brovarone, A., Alard, O., Beyssac, O., Martin, L. & Picatto, M. (2014b). Lawsonite metasomatism and trace element recycling in subduction zones. Journal of Metamorphic Geology, 32(5), 489-514.

Vitale Brovarone, A., Tumiati, S., Piccoli, F., Ague, J. J., Connolly, J. A. & Beyssac, O. (2020). Fluid-mediated selective dissolution of subducting carbonaceous material: Implications for carbon recycling and fluid fluxes at forearc depths. Chemical geology, 549, 119682.

Vuagnat, M. (1946). Sur quelques diabases suisses. Contribution à l'étude des spillites et des pillows lavas. BSMP, 26, 116-128.

Vuagnat, M. (1966). Les coussins éclatés du Lago Nero (Massif du Montgenèvre, Prov. de Turin) et le problème des brèches ophiolitiques (note préliminaire). Compte rendu des séances de la Société de physique et d'histoire naturelle de Genève, (3), 163-167.

Vuagnat, M. (1975). Pillow lava flows: isolated sacks or connected tubes?. Bulletin volcanologique, 39(4), 581-589.

Vuagnat, M., & Pusztaszeri, L. (1965). Sur la presence de hyaloclastites dans le massif du Mont-Genèvre (H.-A.). Arch. Sci. Genève, 18 (1), 120-123.

Wain, A. (1997). New evidence for coesite in eclogite and gneisses: Defining an ultrahigh-pressure province in the Western Gneiss region of Norway. Geology, 25(10), 927-930.

Wei, C. J. & Clarke, G. L. (2011). Calculated phase equilibria for MORB compositions: a reappraisal of the metamorphic evolution of lawsonite eclogite. Journal of Metamorphic Geology, 29(9), 939-952.

White, R. W., Powell, R., Holland, T. J. B., Johnson, T. E., & Green, E. C. R. (2014). New mineral activity–composition relations for thermodynamic calculations in metapelitic systems. Journal of Metamorphic Geology, 32(3), 261-286.

Whitney, D. L., & Evans, B. W. (2010). Abbreviations for names of rock-forming minerals. American mineralogist, 95(1), 185-187.

Whitney, D. L., Fornash, K. F., Kang, P., Ghent, E. D., Martin, L., Okay, A. I. & Brovarone, A. V. (2020). Lawsonite composition and zoning as tracers of subduction processes: A global review. Lithos, 370, 105636.

Zack, T., Rivers, T., Brumm, R. & Kronz, A. (2004). Cold subduction of oceanic crust: Implications from a lawsonite eclogite from the Dominican Republic. European Journal of Mineralogy, 16, 909–916.

Zhang, R. Y., Hirajima, T., Banno, S., Cong, B., & Liou, J. G. (1995). Petrology of ultrahigh-pressure rocks from the southern Su-Lu region, eastern China. Journal of Metamorphic Geology, 13(6), 659-675.

Zanoni, D., Iole Spalla, M., & Gosso, G. (2010). Structure and PT estimates across late-collisional plutons: constraints on the exhumation of western Alpine continental HP units. International Geology Review, 52(10-12), 1244-1267.

Zucali, M. & Spalla, M. I. (2011). Prograde lawsonite during the flow of continental crust in the Alpine subduction: Strain vs. metamorphism partitioning, a field-analysis approach to infer tectonometamorphic evolutions (Sesia-Lanzo Zone, Western Italian Alps). Journal of Structural Geology, 33(3), 381-398.